Analyzing Scaling Characteristics of Transport Properties
Using Particle-Tracking Based Techniques

by

Vikrant Vishal

A thesis submitted in partial fulfillment of the requirements for the degree of

Doctor of Philosophy

in

Petroleum Engineering

Department of Civil and Environmental Engineering
University of Alberta

Abstract

Appropriate scale-up provides a critical link between fine-scale heterogeneity descriptions and coarse-scale models used for transport modeling, which is essential for planning and management of subsurface reservoirs. A significant challenge in subsurface flow and transport modeling is to develop scale-appropriate parameters to represent physical heterogeneities that impact solute migration and flow response. Another challenge is to construct reservoir models that would capture the uncertainties stemming from incomplete data (often gathered over different scales) and loss of information or smoothing due to averaging.

Fine-scale models contain detailed descriptions of reservoir properties, but these models can be too computationally demanding and are not practically feasible for routine reservoir simulation. Coarse-scale models often offer a viable alternative that could decrease computational demand substantially. However, the increased grid-block size in the coarse scale model leads to an increase in numerical (or artificial) dispersion, which stems from the truncation error from most numerical discretization schemes and is directly proportional to grid-block size. The main issue with numerical dispersion when examining scale-up characteristics is that it tends to overwhelm the physical (or actual) dispersion.

Alternative transport modeling schemes, such as the Lagrangian (particle-tracking) methods, are widely adopted in simulating solute transport in porous media. Its primary advantage over typical numerical discretization methods (e.g., finite volume) is the absence of numerical dispersion and potential computational

efficiency. More importantly, certain particle-tracking methods are capable of modeling this type of anomalous behavior of transport.

In this research, a new particle-tracking method is developed for simulating probabilistic (or random) transition time steps and multi-phase immiscible flow. This is further integrated in a novel hierarchical framework for scale-up of reservoir and transport model parameters including porosity, dispersivity, and multi-phase flow functions (e.g., relative permeability and capillary pressure). A key feature of the developed particle-tracking formulation is the employment of kernel estimator for computing concentration and saturation distribution, which has greatly improved the overall computational efficiency by reducing the number of particles needed to achieve a consistent distribution.

The developed particle-tracking method for both probabilistic transition time steps and multi-phase immiscible flow is validated against the analytical solution and is demonstrated to alleviate numerical dispersion when compared against common numerical discretization (e.g., finite difference) methods. Predictions obtained from the coarse-scale models constructed according to the developed workflow are shown to be more consistent with the fine-scale model.

"Try and fail, but don't fail to try."

Stephen Kaggwa

"If you want to go fast, go alone. If you want to go far, go together."

African Proverb

"Certain things catch your eye, but pursue only those that capture the heart."

Ancient Indian Proverb

Dedicated to my parents and brothers, for their love,

endless support, and motivation.

Acknowledgments

I would like to express my gratitude to my supervisor, Dr. Juliana Y. Leung, for her continuous motivation, encouragement, guidance, and always open to discuss new ideas and thoughts. This enabled me to overcome over all obstacles smoothly and produce this valuable research work.

I am grateful to Dr. Daniel Fernàndez-Garcia, Universitat Politècnica de Catalunya, Spain, for providing the Random Walk Particle Tracking (RWPT) source code (RW3D-MRMT) and all the useful suggestions.

I highly appreciated the both Natural Sciences and Engineering Research Council of Canada (NSERC) and WestGrid and Compute/Calcul Canada for providing the financial support by the Discovery Grants Program and computing resources, respectively.

Also, I would like to express my sincerest love and gratitude to my parents and brothers, for their endless love and unflagging support, throughout my studies.

Last, but not the least, I thank all those who inspired and helped me throughout my research.

Table of Contents

List of Tables

List of Figures

List of Symbols

C	Mass concentration	ML^{-3}
f	Particle density distribution	
V	Interstitial or average pore velocity vector	LT^{-1}
h	Hydraulic head	L
D	Diffusion or dispersion coefficient	L^2T^{-1}
K	Hydraulic conductivity tensor	LT^{-1}
k	Permeability tensor	L^2
u	Darcy velocity vector	LT^{-1}
u	Laplace variable of time	
n	Arbitrary number	
t_1	Lower cut-off time	T
t_2	Upper cut-off time	T
t	Time	T
$\mathbf{x}$	Position vector	
$Z(\mathbf{x})$	Random variable	
m	Mass of particle	M
$\dot{m}$	Outlet mass rate	MT^{-1}
m_{o}	Total injectedmass	M
(v,v')	Point support within volume V and V'	
V	Averaging volume	L^3

Subscript symbols

b	Bin or block	

i, j	x- and y-directions	
L	Longitudinal or mean flow direction	
p	Particle's position	
s	Sub-grid realization/model	
T	Horizontal transverse or trend component	
R	Residual component	

Greek symbols

ρ_{corr}	Spatial autocorrelation function	
δ	Kronecker symbol	
σ^2	Variance	
ς	Tortuosity	
ϕ	Porosity	$L^3 L^{-3}$
μ	Fluid viscosity	$ML^{-1}T^{-1}$
τ	Time	T
α	Dispersivity	L
Δ	Difference operator	
ω	Exponent in a power average	
β	Exponent in a truncated power law	
$\gamma(\mathbf{h})$	Variogram or semi-variogram at lag distance $\mathbf{h}$	
ξ	Standard Gaussian random variable	
ψ	Probability density function	
∇	Differential operator	L^{-1}

$\bar{\gamma}(V,V')$ Average variogram or semi-variogram between averages

over volumes V and V'

ρ Fluid density ML^{-3}

Chapter 1: Introduction

Accurate predictions of flow and transport in natural porous media are crucial in management of valuable subsurface resources including water aquifers and hydrocarbon reservoirs. These predictions are usually assessed with uncertainty due to (1) underlying heterogeneity or spatial variation in rock and transport properties, (2) conditioning data, and (3) the sub-scale heterogeneity. This uncertainty, though, can be reduced by improved geophysical (e.g., seismic), core, well log, pressure test, and tracer test data, cannot be entirely eliminated. Reservoir models are typically constructed and subjected to flow and transport simulation to capture the aforementioned uncertainties. Although fine-scale models could capture detailed description of the heterogeneity, simulation with these models can be computationally demanding. A commonly-adopted alternative is to replace these fine-scale models with a coarser grid or asset of coarse-scale (scaled-up) models. During this process of coarsening, a number of transport properties (e.g., dispersivity and multiphase flow functions), along with reservoir properties (e.g., porosity and absolute permeability), must be scaled-up accordingly. Properly scaled-up models should not only honor the conditioning data, but they should retain the uncertainties due to large-scale and sub-scale heterogeneities.

For modeling solute transport in single-phase, one of the most important transport properties to be scaled-up is dispersivity. Transport of passive solute in porous media is generally controlled by one or more of the following physical

processes: (1) advection or convection, (2) diffusion, and (3) mechanical dispersion. Addition to these processes, capillary pressure also controls the transport in multiphase immiscible flow. In advection transport process, particles are simply carried by the average velocity of the fluid. Diffusion is a spreading process caused by the random molecular motion (Brownian motion) and collisions of the particles among themselves; this process occurs as long as a concentration gradient exists, even if the fluid is at rest, and is described by Fick's law. Third type of transport process is mechanical (kinetic) dispersion, which is a spreading or mixing phenomenon caused by the microscopic velocity variations in the pore spaces with respect to average pore fluid velocity. It is, therefore, dependent on the variation in the pore size/geometry distribution and is present only if there is flow. Macroscopically, mechanical dispersion process is similar to the diffusion process and is described mathematically in similar fashion as diffusion. It is practically impossible to separate the effects of mechanical dispersion and molecular diffusion. Hence the collective spreading due to both effects is usually referred to as hydrodynamic dispersion (Pickens and Grisak 1981a). In addition to mechanical dispersion and molecular diffusion, dispersion also occurs due to capillary pressure difference in multiphase immiscible flow. Dispersivity is a scale-dependent property of permeable media. It increases with increasing distance (or traveled distance) of investigation (Gelhar et al. 1979; Pickens and Grisak 1981a, 1981b), volume of sample (Arya et al. 1988; Gelhar et al. 1992; John et al. 2010), traveled time (Binning and Celia 2002) and heterogeneity (Adepoju et al. 2013). Heterogeneity is also a scale-dependent

property. Reservoir recovery performance depends on dispersion and heterogeneities; therefore, it is often observed that oil recovery decreases with increasing scale. The scale-dependent behavior of dispersivity is usually described as non-Fickian, anomalous, or non-Gaussian (Berkowitz et al. 2000; John 2008), characterized by early breakthrough and long (or heavy) tailed effluent histories at the late times. The advection-dispersion equation (ADE) is commonly adopted to model the solute transport in porous media at the representative elementary volume (REV) scale. However, several issues have been raised regarding the validity of the classical ADE in representing both Fickian and non-Fickian characteristics.

Dispersivity at the coarse scale can be computed by matching the recovery responses (e.g, breakthrough behavior) obtained from transport simulation between the coarse- and fine-scale models. The process of coarsening tends to homogenize the underlying heterogeneity; as a result, both local velocity variations and dispersion are reduced. Unfortunately, traditional numerical discretization techniques (finite volume and finite element) for transport simulation are prone to numerical dispersion, which tends to increase with grid-block size and would often overwhelm physical dispersion. Numerical dispersion also smears mixing fronts similar to physical dispersion and increases the apparent level of dispersion in the reservoir.

For flow involving multiphase immiscible phases, relationships between relative permeability, capillary pressure and saturation must be incorporated. These functions are often determined experimentally using core samples and

should be adjusted to the appropriate modeling scale. Scaling of these multiphase flow functions remains an ongoing research topic in the literature. Steady-state methods with the assumption of capillary equilibrium for small length-scales and slow rates and viscous-dominated flow for large length-scales or fast rates are commonly adopted. However, the main disadvantage associated with this method is that it is also prone to numerical dispersion (Pickup and Stephen 2000).

Lagrangian method such as random walk plus particle tracking (RW+PT), offers interesting solution alternative to Eulerian methods mainly due to grid-free approach and capability of eliminating numerical dispersion (Salamon et al. 2006; John et al. 2010; Jha et al. 2011). In contrast to Eulerian methods, the transport equation is not solved on a fixed grid but using a large number of representative particles to approximate both advection and dispersion. Its computational requirement is also less in comparison to numerical based simulators, since particles move independently and parallel computing formulation is favorable. Particle tracking can also be applied in the absence of diffusion (i.e., shock front) with no limits on the mesh size (Jha et al. 2009) and when flow is strongly advection dominant (Hoteit et al. 2002). It can be formulated to account for non-Fickian characteristics that are not captured in the ADE.

1.1 Physical and Numerical Modeling Aspects of Flow and Transport

In porous media, complex physical phenomena often occur over widely varying scales from the pore level (in the order of a few micro meters) to the field level (in

the order of kilometers). Below, physical and numerical modeling aspects of flow and transport at pore scale and Darcy or continuum scale are discussed.

1.1.1 Description of the Physical Processes at the Pore Scale

A porous medium is a two-phase disordered material in which one phase is solid and another phase is a connected void space (pore bodies and pore throats). Distribution of the solid and the void are critical for flow and transport. The pore structure is characterized by parameters such as specific surface area, tortuosity, surface asperity, pore size/geometry, and grain size.

1.1.1.1 Momentum Transport

Fluid flow in porous media is governed by the conservation of mass, momentum, and energy. When fluid flows through porous media, friction force is developed between solid interface and the fluid. The fundamental equation governing the motion of fluid in a porous medium at the pore scale is described by the momentum balance equation. Together with the mass balance equation, the system of equations is known as Navier-Stokes equations. It is defined as Eq. (1.1) for an incompressible fluid (Bird et al. 1960):

$$\underbrace{\rho \frac{\partial \boldsymbol{u}}{\partial t}}_{\substack{\text{Unsteady} \\ \text{acceleration}}} + \underbrace{\rho(\boldsymbol{u}\cdot\nabla)\boldsymbol{u}}_{\substack{\text{Convective} \\ \text{acceleration}}} = \underbrace{-\nabla p}_{\substack{\text{Pressure} \\ \text{gradient}}} + \underbrace{\mu\nabla^2\boldsymbol{u}}_{\substack{\text{Viscosity} \\ \text{force}}} + \underbrace{\rho\boldsymbol{g}}_{\substack{\text{Body} \\ \text{forces}}} \qquad (1.1)$$

where ρ is the density, u is the velocity, t is the time, p is the pressure, μ is the dynamic viscosity, and g is the gravitational acceleration. The Navier-Stokes equations can describe the temporal and spatial evolution of a viscous fluid in the

void space of a medium at the pore-scale. Other general forms of the equation can be used to describe the flow of a compressible fluid. These equations can be solved by applying the appropriate initial and boundary conditions at the solid interface (e.g. no-slip), and the velocity and pressure field in the pore-space can be determined. Modeling at this scale takes into account detailed geometry and connectivity in the pore spaces.

In case of two-phase immiscible flow, both fluids are governed by the Navier-Stokes equation with additional capillary force along the interface, that is:

$$\rho_i \frac{\partial \boldsymbol{u}}{\partial t} + \rho_i \boldsymbol{u} \cdot \nabla \boldsymbol{u} - \nabla \cdot (\mu_i (\nabla \boldsymbol{u} + (\nabla \boldsymbol{u})^T))) + \nabla p = \rho_i \boldsymbol{g} + \boldsymbol{f}_\Gamma; \ i = 1, 2 \qquad (1.2)$$

where $\boldsymbol{f}_\Gamma$ is the capillary force which is defined as:

$$\boldsymbol{f}_\Gamma = \tau \kappa \delta_\Gamma \boldsymbol{n}_\Gamma \qquad (1.3)$$

where τ is the tension coefficient between two fluids, κ is the local curvature of the interface, δ_Γ is the Dirac delta function that localizes the surface tension force to point load on the interface, and n_Γ as the unit normal to the interface.

1.1.1.2 Mass Transport

In porous media, solute is generally considered to be transported by one or more of the following physical processes:

- *Advection or Convection*

- *Molecular Diffusion*

- *Mechanical Dispersion*

Advection: Advection or convection is solute transport caused by the bulk movement of flowing fluid. If no other process exists, the solute particles are simply moved at average fluid velocity.

Diffusion: The transport of a solute from a region of higher concentration to a region of lower concentration is known as molecular diffusion. Diffusion takes place as long as a concentration gradient exists, even if the fluid is at rest. That is, it is independent of fluid velocity. This is a very slow process of solute transport. Diffusive flux is generally described by Fick's first law:

$$\boldsymbol{J} = -D_m \nabla C \tag{1.4}$$

where $\boldsymbol{J}$ is the solute flux, $\boldsymbol{C}$ is the concentration of the solute and D_m the coefficient of molecular diffusion. The mass transfer of a non-reactive solute is governed by the advection-diffusion equation (Saaltink et al. 1998):

$$\frac{\partial C(\boldsymbol{X},t)}{\partial t} + \nabla \cdot [\boldsymbol{V}(\boldsymbol{X})C(\boldsymbol{X},t) - D_m \nabla C(\boldsymbol{X},t)] = 0 \tag{1.5}$$

where D_m is molecular diffusion coefficient, $\boldsymbol{V}(\boldsymbol{X})$ is the pore-scale velocity, and $C(\boldsymbol{X}, t)$ is the solute concentration.

Mechanical Dispersion: Mechanical dispersion in porous media is a spreading or mixing phenomenon caused by variability in the microscopic velocities through pores (or pore-scale velocity gradients) in the medium (Taylor 1953). These velocity variations are the results of (1) velocity gradient in pore throats in the direction transverse to flow varying from zero velocity near the solid-void interface due to friction on pore walls to a maximum at the pore center, (2) variations in pore sizes, and (3) variations in path length (Fig. 1.1). Therefore, solute advances faster along the pore centre than the near-wall region; it also

moves through larger pores faster; finally, varying grain distribution also introduces tortuous flow paths for the solute particles.

Velocity variations in the pore space contribute to a difference in solute concentration along flow paths and across different flow paths, which, when combined with molecular diffusion, result in additional mixing termed mechanical dispersion. Mixing that occurs along the direction of fluid flow is termed longitudinal dispersion, whereas mixing that occurs normal to the direction of fluid flow is termed transverse dispersion. Transverse dispersion is considered to be the result of the split of flow paths (Fig. 1.2).

Hydrodynamic Dispersion: Since molecular diffusion cannot be separated from mechanical dispersion in flowing subsurface flow, the two are combined into a parameter called hydrodynamic dispersion coefficient, D. In a one-dimensional system, hydrodynamic dispersion is defined as (Fetter 2000):

$$D = \alpha_L v + D_m \tag{1.6}$$

where α_L is the longitudinal dispersivity, v is the average linear velocity, and D_m is the effective diffusion coefficient.

Peclet Number: The dimensionless measure of the degree of advective to dispersive transport is the Peclet number:

$$N_{Pe} = \frac{Advective\,flux}{Dispersive\,flux} = \frac{vL}{D} \tag{1.7}$$

where L is the characteristic length scale. N_{Pe} is typically greater than one when the system length scale is larger than the micrometer scale. At small scales, diffusion contributes much more effectively to solute transfer.

In multiphase immiscible flow, one of the important parameters is capillary pressure (P_c). It is inherently a pore-scale phenomenon and is defined at equilibrium as the difference in pressure across a curved interface separating two immiscible fluids, expressed as:

$$P_c = P_{nw} - P_w = \frac{2\sigma\cos\theta}{R_{eff}} \tag{1.8}$$

where P_{nw} is the non-wetting phase pressure at an interface, P_w is the wetting phase pressure at an interface, R_{eff} is the effective radius of the interface, σ is the surface tension between wetting and non-wetting fluid phases, and θ is the contact angle.

Pore-scale modeling directly accounts for the fundamental physical processes that govern the fluid flow and mass transport occurring at the smallest scale. It is often employed to simulate experimental set-up and to understand detailed microscopic processes and transport mechanisms. Despite its advantages, pore-level modeling remains challenging because of a number of limitations: (1) uncertainties in the detailed description of the complex pore geometries at the field scale and (2) high computational costs of simulating flow/transport at the pore-scale resolution for large-scale response prediction.

1.1.2 Modeling at the Darcy or Continuum Scale

Unlike the pore scale, the continuum or macroscopic (ranges from 10^{-2} to 10^{0}m) does not require microscopic details of pores. In other words, detailed descriptions of pores are ignored and employ the volume averaged laws such as Darcy's law where the porous medium is considered as macroscopically uniform

continuum. The scale of the continuum medium is defined by the concept of representative elementary volume (REV) (Bear 1972). From the statistical perspective, this is the scale at which the sub-scale variance of an effective (i.e., averaged) property becomes negligible. In other words, an effective macroscopic property can be defined by averaging its microscopic values below this REV. Most of the laboratory experiments are conducted at this scale to obtain required parameters and hence it is widely used for modeling in porous media.

1.1.2.1 Momentum Transport

Darcy's law describes the flow of a fluid through porous media at macroscopic scale. It was originally proposed as an empirical relation based on experimental observations; however, it can also be derived from the general momentum balance under certain conditions (e.g., near-zero Reynolds number flow). The Darcy's equation (Bear 1972) is described as:

$$q(X,t) = -\frac{K(X)}{\mu}(\nabla p(X,t) - \rho g) \tag{1.9}$$

where $q(X, t)$ is the specific discharge or volumetric flow rate per unit cross section area of porous medium perpendicular to the direction of flow, μ is the viscosity, and p is the fluid pressure along the flow path. The proportionality constant $K(X)$ is the coefficient of permeability. Here negative sign implies that flow is along the direction of decreasing gradient.

It is usually considered valid for sufficiently low flow where the Reynolds number (ratio of inertial forces to viscous forces) as defined for a porous medium is less than one, which is the case for most subsurface flows. Darcy's law is a

macroscopic approach to the study of flow in porous media and in this equation, all the interaction between the fluid and the porous structure is lumped into a single parameter permeability K. It is important to highlight that on a microscopic pore-scale level, there is no such thing as permeability exist. When there is multiphase flow, the most general form of the Darcy equation is described as:

$$\vec{u}_j = -\vec{\vec{\lambda}}_j (\nabla p_j + \rho_j \vec{g}) \tag{1.10}$$

where $\vec{u}_j$ is the Darcy velocity of phase j, $\vec{\vec{\lambda}}_j = \vec{\vec{K}} k_{rj} / \mu_j$ is the mobility, $\vec{g}$ is the acceleration due to gravity, k_r is the relative permeability, and ρ is the density of the fluid.

1.1.2.2 Mass Transport

In general, the transport of a solute in a porous medium is described by the advection-dispersion equation. Assuming a macroscopically homogeneous porous medium, the advection-dispersion equation on a representative elementary volume (REV) is described by a mass balance equation. Here the key assumption is that dispersion can be represented by an expression analogous to Fick's law of diffusion. At the macroscopic scale (or REV) the transport phenomena is governed by the advection-dispersion equation (Lichtner and Kang 2007):

$$\phi(X) \frac{\partial c(X,t)}{\partial t} + \nabla \cdot [q(X,t)c(X,t) - D(X,t)\nabla c(X,t)] = 0 \tag{1.11}$$

$$D_{ij} = \alpha_T |q| \delta_{ij} + (\alpha_L - \alpha_T) \frac{q_i q_j}{|q|} + D^d \varsigma_{ij} \tag{1.12}$$

where $\phi(X)$ is the porosity at position X, $c(X, t)$ is the bulk or macroscale concentration, $q(X, t)$ is the Darcy velocity, $D(X, t)$ is the macroscopic dispersion tensor, which integrates the impact of the heterogeneous pore structure and pore velocity on the dispersive solute flux, α_L and α_T represent the longitudinal and transverse dispersivity, respectively; $\delta_{i,j}$ is the Kronecker symbol; D^d is the molecular diffusion coefficient, and $\zeta_{i,j}$ is the tortuosity tensor. This equation (Eq. 1.11) is usually referred to as the classical or Fickian model of solute transport in porous media. Here effects of diffusion and dispersion are combined into a single tensor called hydrodynamic dispersion coefficient.

In multiphase immiscible flow, capillary pressure is defined at the macro-scale by the following empirical relationship:

$$P^{nw} - P^w = P^c(S^w) \tag{1.13}$$

where for a given elementary representative volume (REV), P^{nw} is the average non-wetting phase pressure, P^w is the average wetting phase pressure, P^c is the macroscopic capillary pressure, and S^w is wetting phase saturation. This approach assumes that P^c is a function of saturation only if rock-type is fixed; other pore-scale properties, such as interfacial configuration, interfacial curvature, contact angle, and pore morphology are ignored. All the pore-scale properties tend to be lumped into S^w without consideration of their individual effects.

The capillary pressure can also be described by the dimensionless Leverett J-function as:

$$J(S_w) = \frac{P_C(S_w)\sqrt{k/\phi}}{\gamma \cos\theta} \tag{1.14}$$

where P_c is the capillary pressure in pascal, S_w is the water saturation measured as a fraction, ϕ is the porosity, k is the permeability (m^2), θ is the contact angle, and γ is the surface tension (N/m). The Leverett J-function plays an important role because it is used to extrapolate the capillary pressure data for a given rock which is similar to other rocks but differing porosity, permeability, and wetting properties.

Darcy- or continuum-scale approach is widely used to model the flow and transport in porous media. However, the main difficulty with this approach is the requirement of accurate values of the macroscopic parameters such as permeability, dispersion coefficients, capillary pressure, relative permeability etc. which depend on the pore structure and pore-level physical processes. Furthermore, this approach does not take into account the pore geometries explicitly.

1.2 Problem Statement

It is often impractical to subject detailed fine-scale geological models to numerical flow and transport simulation due to its computational costs. Coarse-scale models should be constructed via proper scale-up of the relevant reservoir and transport properties. Scale-up of transport properties involve estimation of large-scale average quantities that capture the fine-scale (sub-grid unresolved) heterogeneities and their associated uncertainties.

Traditional numerical discretization schemes are prone to errors due to numerical dispersion, grid dependencies and orientation, and inaccuracy in flux

calculations in heterogeneous porous media with capillary pressure. Particle-tracking based approach, which is grid-free and capable of eliminating numerical dispersion (Jha et al. 2011), provides a viable alternative for detailed transport modeling. Its integration with a statistical scale-up workflow would allow fine-scale physics of single-phase transport and multi-phase flow in porous media to be translated into coarse-scale level (Tyagi et al. 2008) in a practical manner. It is assumed that Darcy-scale applies in this work.

The Fokker-Planck-Kolmogorov equation (FPKE) is basic equation to derive Particle-tracking based approach which is defined as:

$$\frac{\partial P(x,t)}{\partial t} = -\frac{\partial}{\partial x}\big[\mathbf{A}(x)P(x,t)\big] + \frac{1}{2}\frac{\partial^2}{\partial x^2}\big[\mathbf{B}(x)P(x,t)\big] \tag{1.15}$$

where $P(x, t)$ is the probability density for a particle to be at location x at time t. The similarity of the classical ADE and FPKE can be evident by replacing $P(x, t)$ = $C(x, t)$, $\mathbf{A}(x) = q(x, t)$, and ½ $\boldsymbol{B}(x) = D(x, t)$.

1.3 Research Objectives

In this thesis, scale-up/upscaling of flow and transport is addressed in porous media. For transport simulation, particle tracking techniques are employed. The principal objective of this work is to develop a particle-tracking approach to scale-up transport properties and multiphase flow function. To accomplish this objective, other sub-objectives are development of particle-tracking tool for probabilistic time step and multiphase immiscible flow.

In order to address the problems regarding scale-up/upscaling in single and multi-phase transport problems, the following objectives are completed in procedural order:

1. *Assessing the impact of subscale heterogeneities in 2- and 3-D heterogeneous reservoirs*

First, a multi-scale workflow is developed to scale-up effective dispersivities and reservoir attributes (porosity and permeability) to the transport modeling scale that takes into account of sub-scale variability. Next, effective transport parameters and reservoir attributes are populated in the coarse-scale model. A RWPT formulation RW3D-MRMT (Fernàndez-Garcia et al. 2005; Salamon et al. 2006; Fernàndez-Garcia and Sanchez-Vila 2011) is incorporated. The goal is to quantify the subscale heterogeneities and their associated uncertainties on transport during scale-up.

1.1 *Coupling with large-scale heterogeneities*

The effects of large-scale heterogeneity are studied. A combination of smaller-scale variability (residuals) and large-scale variability (deterministic trend), is considered.

1.2 *Modeling of sub-grid heterogeneities with probabilistic transit time distribution*

The RWPT formulation RW3D-MRMT is modified to account probabilistic transit time distribution. The results of modified code are validated against analytical solution.

2. *Stochastic modeling of multi-phase (two phase) flow*

The RWPT formulation RW3D-MRMT is modified to simulate phase saturations. This model is coupled with the continuity equation in an IMPES (implicit pressure, explicit saturation) fashion. To construct concentration from particles distribution, kernel functions are used. In addition, ideas of superposition adopted from the convolution-based particle tracking (CBPT) method are used to compute responses for a continuous injection from a single instantaneous point source.

3. *Scale-up of multi-phase flow functions (C_p and K_r functions) in heterogeneous reservoirs*

Scaling characteristics of capillary pressure and relative permeability functions with fluid saturations are studied. To scale-up multi-phase flow functions, a procedure similar to the one in objective (1) is implemented. To scale-up the functions, developed particle-tracking algorithm in objective (2) is used to avoid the numerical (or artificial) dispersion.

1.4 Thesis Outline

The thesis consists of seven chapters.

Chapter 1: A general introduction of the governing equations for flow and transport modeling at different scales are described. A problem statement is introduced. A set of research objectives pertinent to this thesis are explained.

Chapter 2: A workflow to scale-up reservoir attributes (porosity and permeability) and effective dispersivities is introduced. In particular, uncertainty due to sub-

scale heterogeneities (i.e., sub-scale variability) is quantified in the developed procedure.

Chapter 3: The workflow in Chapter 2 is extended such that large-scale variability (deterministic trend) is also considered.

Chapter 4: The workflow in Chapter 2 is extended to handle the modeling of residual variability, which occurs below the fine-scale model resolution, with probabilistic transit time distribution.

Chapter 5: It presents a multi-scale framework for solute transport which accounts for sub-scale variability, large-scale variability, and variability below the fine-scale. It essentially integrates the elements from Chapters to 4 into a single hierarchical framework.

Chapter 6: It presents a novel particle-tracking method to model multi-phase immiscible flow. Various new aspects, in comparison to existing works in the literature, are incorporated. Moreover, the method is also incorporated in a scale-up procedure (similar to that in Chapter 2) to compute effective multi-phase flow functions at the coarse scale.

Chapter 7: It summarizes the contributions of the thesis with conclusions, along with suggestions for future research on this topic.

References

Adepoju, O. O., Lake, L. W., & Johns, R. T. (2013). Investigation of anisotropic mixing in miscible displacements. *SPE Reservoir Evaluation & Engineering, 16(01)*, 85-96.

Arya, A., Hewett, T. A., Larson, R. L., & Lake, L. W. (1988). Dispersion and reservoir heterogeneity. *SPE Reservoir Eng, 3(1)*, (pp. 139-148).

Bear, J. (1972). *Dynamics of fluids in porous media.* New York: Elsevier.

Berkowitz, B., Scher, H., & Silliman, S. E. (2000). Anomalous transport in laboratory-scale, heterogeneous porous media. *Water Resour Res, 36(1)*, (pp. 149-158).

Binning, P., & Celia, M. A. (2002). A forward particle tracking Eulerian–Lagrangian localized adjoint method for solution of the contaminant transport equation in three dimensions. *Adv Water Resour, 25(2)*, (pp. 147-157).

Bird, R. B., Stewart, W. E., & Lightfoot, E. N. (1960). *Transport phenomena.* Madison, USA: John Wiley & Sons.

Fernàndez-Garcia, D., & Sanchez-Vila, X. (2011). Optimal reconstruction of concentrations, gradients and reaction rates from particle distributions. *J Contam Hydrol, (120-121)*, (pp. 99-114).

Fernàndez-Garcia, D., Illangasekare, T. H., & Rajaram, H. (2005). Differences in the scale-dependence of dispersivity estimated from temporal and spatial

moments in chemically and physically heterogeneous porous media. *Adv Water Resour, 28(7)*, (pp. 745-759).

Fetter, C. W. (2000). *Applied hydrogeology.* Prentice hall.

Gelhar, L. W., Gutjahr, A. L., & Naff, R. L. (1979). Stochastic analysis of macrodispersion in a stratified aquifer. *Water Resources Research, 15(6)*, 1387-1397.

Gelhar, L. W., Welty, C., & Rehfeldt, K. R. (1992). A critical review of data on field-scale dispersion in aquifers. *Water Resour Res, 28(7)*, (pp. 1955-1974).

Hoteit, H., Mose, R., Younes, A., Lehmann, F., & Ackerer, P. (2002). Three-dimensional modeling of mass transfer in porous media using the mixed hybrid finite elements and the random-walk methods. *Math Geol, 34(4)*, 435-456.

Jha, R. K., Bryant, S., & Lake, L. W. (2011). Effect of diffusion on dispersion. *SPE J, 16(1)*, (pp. 65-77).

Jha, R. K., John, A., Bryant, S. L., & Lake, L. W. (2009). Flow reversal and mixing. *SPE J, 14(1)*, (pp. 41-49).

John, A. K. (2008). *Dispersion in Large Scale Permeable Media (Dissertation).* University of Texas at Austin.

John, A. K., Lake, L. W., Bryant, S., & Jennings, J. W. (2010). Investigation of mixing in field-scale miscible displacements using particle-tracking

simulations of tracer floods with flow reversal. *SPE J, 15(3)*, (pp. 598-609).

Lichtner, P. C., & Kang, Q. (2007). Upscaling pore-scale reactive transport equations using a multiscale continuum formulation. *Water Resour. Res, 43*, W12S15.

Pickens, J. F., & Grisak, G. E. (1981a). Scale-dependent dispersion in a stratified granular aquifer. *Water Resources Research, 17(4)*, 1191-1211.

Pickens, J. F., & Grisak, G. E. (1981b). Modeling of scale-dependent dispersion in hydrogeologic systems. *Water Resources Research, 17(6)*, 1701-1711.

Pickup, G. E., & Stephen, K. D. (2000). An assessment of steady-state scale-up for small-scale geological models. *Pet Geosci, 6 (3)*, 203-210.

Saaltink, M. W., Ayora, C., & Carrera, J. (1998). A mathematical formulation for reactive transport that eliminates mineral concentrations. *Water Resour. Res, 34 (7)*, 1649–1657.

Salamon, P., Fernàndez-Garcia, D., & Gómez-Hernández, J. J. (2006). A review and numerical assessment of the random walk particle tracking method. *Journal of contaminant hydrology, 87(3)*, (pp. 277-305).

Taylor, G. (1953). Dispersion of soluble matter in solvent flowing slowly through a tube. *In Proceedings of the Royal Society of London A: Mathematical, Physical and Engineering Sciences*, (pp. 186-203).

Tyagi, M., Jenny, P., & Tchelepi, H. A. (2008). A Lagrangian, stochastic modeling framework for multi-phase flow in porous media. *J Comput Phys, 227(13)*, 6696-6714.
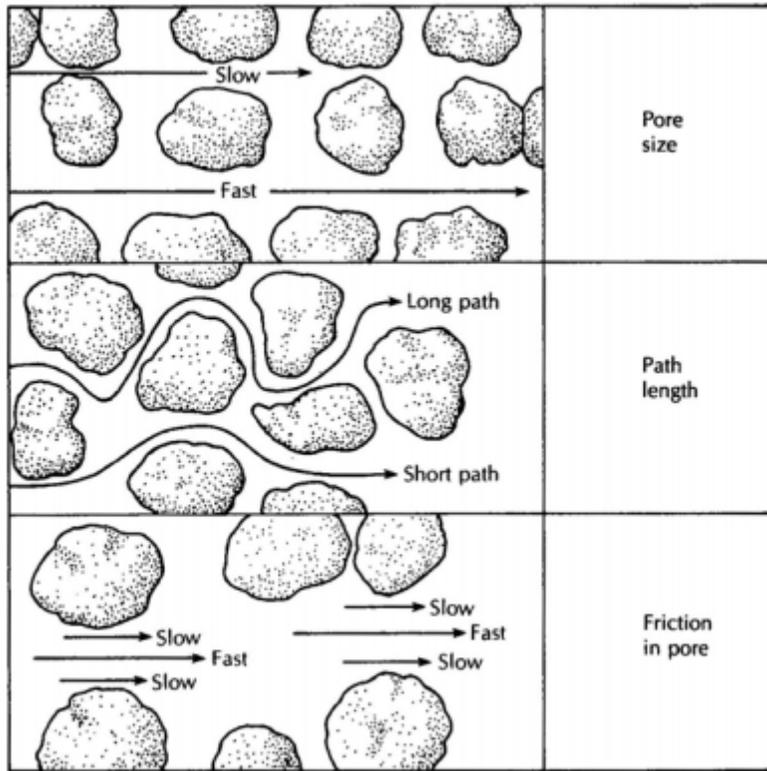
Figure 1.1: Factors causing pore-scale longitudinal dispersion (adopted from Fetter 2000).
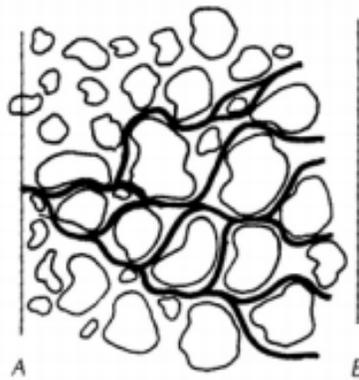
Figure 1.2: Flow paths in a porous medium that cause transverse dispersion (adopted from Fetter 2000).

Chapter 2: Modeling Impacts of Subscale Heterogeneities on Dispersive Solute Transport in Subsurface Systems[1]

2.1 Introduction

Dispersion in porous media results from the interplay between convective spreading and diffusion (Perkins and Johnston, 1963). Convective spreading occurs because of variations in path lengths and solute particles following different streamlines (Jha et al. 2011). Diffusion, on the other hand, is the process whereby random motion of solute particles involved in a net movement corresponding to the concentration gradient and is described by Fick's law. It is enhanced by additional mixing caused by concentration gradients as a result of uneven fluid velocities (Aronofsky and Heller 1957). Presence of local velocity gradients due to multi-scale heterogeneous rock properties can enhance mixing (Lake 1989).

It has been extensively reported in the literature that dispersivity increases with distance (Gelhar et al. 1992; Fleurant and Van Der Lee 2001) and time (Binning and Celia 2002). This scale-dependent behavior is usually described as non-Fickian, anomalous, or non-Gaussian (Berkowitz et al. 2000; John 2008), characterized by early breakthrough and long- or heavy-tailed effluent histories at the late times. Heavy-tailed nature of break through concentration profiles (BTCs)

has been also observed under convergent radial flow around injectors and producers (Pedretti et al. 2014). Under converging flow, heavy-tailed behavior of transport heavily depends on the vertical architecture and connectivity pattern between the injecting and producing locations. Jha et al. (2011) observed that diffusion is an important element in Fickian transport because it helps to ensure that movement of solute particles are independent and random (particles are moving from regions of low-velocity to high-velocity and vice versa). In case of realistic parabolic velocity profile in pore throat (similar to flow between two parallel plates), the velocities of particles near the porous material surface are not independent (due to no-slip boundary conditions at the solid surfaces) and in the absence of diffusion, solute particles near the low velocity region cannot move into main flow stream. In other words, without diffusion, each solute particle would follow the same streamline without interacting with particles from other stream lines. The randomness introduced by diffusion has allowed particles near the solid porous material with low velocity to switch between different streamlines and acquire independent velocity.

At the reservoir or field scale, non-Fickian behavior can be explained by both large-scale heterogeneity and unresolved sub-scale heterogeneities. Gylling et al. (1999), Becker and Shapiro (2003), and Gouze et al. (2008) attributed non-Fickian dispersion to long-range spatial correlation of geological features (e.g., increase in correlation in the permeability field), resulting in velocities to be correlated over large distances. A common example would be fractured formations with dual porous systems (Bijeljic et al. 2013). Non-Fickian dispersion

may also be explained by the temporal correlations of the solute motion due to mass transfers in small-scale geological structures (Dentz et al. 2004; Le Borgne and Gouze 2008). As noted by Le Borgne and Gouze (2008), it is most probable that both spatial correlations controlled by large-scale structures and temporal correlations controlled by small-scale structures lead to non-Fickian transport in some heterogeneous reservoirs. Since heterogeneity varies as a function of scales, description of dispersion must account for impacts of heterogeneity and scale (Arya et al. 1988; Gelhar et al. 1992; Mahadevan et al. 2003; Berkowitz et al. 2006; Jha et al. 2009; John et al. 2010; Jha et al. 2011).

Several studies (Aronofsky and Heller 1957; Scheidegger 1988; Berkowitz et al. 2006; Jha et al. 2011) discussed the specific issues about applicability of classical advection-dispersion equation (ADE) for modeling transport behavior of both Fickian and non-Fickian characteristics. The existence of preferential flow paths was clearly shown in laboratory-scale systems (Hoffman et al. 1996; Oswald et al.1997). Some experimental studies also revealed systematic deviation between experimental BTCs and ADE predictions. Levy and Berkowitz (2003) also measured the BTCs in homogeneous meter-length flow cells and observed non-Fickian dispersion behavior in terms of early-time and late-time arrivals (tails). The classical ADE formulation is not suitable for modeling non-Fickian transport because dispersion is modeled as a sum of diffusion and convective spreading, which act independently from each other, ignoring the mixing introduced by the interaction of these two mechanisms.

Another issue in the solute transport modeling is the numerical dispersion (artificial dispersion). Numerical dispersion is the result of truncation error and generally overwhelms physical dispersion (Lantz 1971; Fanchi 1983; Haajizadeh et al. 1999, Binning and Celia 2002). Many numerical schemes generate significant numerical dispersion and, therefore, lead to an overestimation of transverse mixing. Although numerical dispersion could be partially decreased by choosing proper discretization scheme (e.g., mesh size and time steps) and incorporating higher–order approximation, it still poses a significant challenge when used to analyze effects of physical dispersion. Advection dominated problems often suffer from numerical dispersion and numerical oscillations (instabilities) (Zheng and Bennett 2002; Salamon et al. 2006a, Hoteit et al. 2002, Fleurant and Van Der Lee 2001). These problems could be solved by selecting higher grid resolution and small time steps. These numerical problems can also be alleviated by choosing appropriate numerical scheme and better flux approximations, resulting in long executions times even with the CPUs available these days (Liu et al. 2004; Salamon et al. 2006a). Alternative method of solving partial differential equation (ADE) is particle tracking (Lagrangian method) based approach. Particle tracking is a grid-free approach capable of eliminating numerical dispersion (Salamon et al. 2006a; Jha et al. 2009; John et al. 2010). Its computational requirement is also less as compared to FD/FV/FE-based simulator, since particles move independently and parallel computing formulation is favorable.

Particle tracking formulations can be classified into a number of categories: (1) random walk particle tracking (RWPT) or classical random walk (CRW); and (2) continuous time random walk (CTRW). In RWPT, each transit time step $\tau = \Delta\tau$ is considered as discrete, constant, and deterministic whereas transition length vector ξ is independent and identically distributed (i.i.d) random variables with zero mean and unit variance (Salamon et al. 2006a). In CTRW, each τ and ξ are random variables following a probability density function $\psi(\tau, \xi) = \psi_\sigma(\xi)\psi_\tau(\tau)$, where both τ and ξ are independent, stationary stochastic processes (Srinivasan et al. 2010).

Different approaches were described in the literature for representing sub-scale effects in coarse-scale continuum flow simulations. Barker and Fayers (1994) introduced pseudo (effective) coefficients, referred to as α-factors, in the flux terms of the transport equation to relate compositions of fluids leaving a grid block to the average compositions within the grid block. Efendiev et al. (2000) derived expressions for calculating equivalent parameters two-phase dispersion tensor (D_{ij}) from volume-averaged equations. Berentsen et al. (2007) derives a pre-asymptotic one-dimensional upscaled model for the transverse averaged tracer concentration and generalizes dispersion tensors that may vary as a function of the transverse direction. The transverse mixing term in the two-dimensional governing equation is spectrally decomposed into its corresponding eigen values and eigen vectors, which are combined into an effective relaxation equation that describes both the short- and long-time behavior of dispersion for the Taylor flux, to model multi-scale dispersive flux.

Cortis et al. (2004) modeled the unresolved sub-scale heterogeneities using the memory functions in CTRW, while the large-scale behavior is treated deterministically. Parameters of the transition rate probability, β, t_1, t_2, are assigned to each facies (sub-region). Small-scale heterogeneities are mapped on the distribution of local transit times into a space-dependent memory term M(u; **x**), which gives rise to anomalous dispersion, while the effect of deterministic macroscopic heterogeneities are additionally included into the drift and flux terms: $\Delta_\psi(x)$ and $\theta_\psi(x)$ (Cortis et al. 2004; Berkowitz et al. 2006). Fernàndez-Garcia et al. (2009) studied the upscaling of mass transfer. Several formulations of the memory function are used in their multi-rate mass transfer model as the constitutive transport equation at the large scale.

The aforementioned works addressed the issue of upscaling, which involves computation of an equivalent parameter at the coarse scale by averaging response evaluated with a particular realization of fine-scale heterogeneity (Christie 2001). This process differs from scale-up, which refers to relating phenomena observable at one scale to another scale (Leung and Srinivasan 2011). Scale-up involves not only computing the equivalent parameter at the larger scale by upscaling, but it also entails transferring the uncertainty of sub-scale heterogeneity into the uncertainty (variability) in the large-scale equivalent parameters (Leung and Srinivasan 2012). In other words, parameters can be scaled-up, if we are able to upscale multiple realizations encompassing the uncertainty due to change in scale.

In this work, the term "fine-scale" refers to a length scale over which detailed description about heterogeneity is available. In particular, the discussion here focuses on heterogeneity description defined at the Darcy scale, or the representative elementary volume (REV) of the pore-scale. An example of a fine-scale model is one constructed from petrophysical log measurement available at a resolution of approximately 0.1m. A field-scale model at this resolution is generally impractical for numerical flow and transport modeling due to its large number of grid cells. A common alternative approach would be performing the numerical simulation over a coarser mesh (e.g., 5-10 m), which is referred to as the "coarse-scale" or the "transport-modeling-scale". Description of rock (e.g., porosity) and flow-related properties (e.g., dispersivities) at this coarse scale should be established through the aforementioned scale-up procedure. It is important that the fine-scale heterogeneity and its associated uncertainties be captured when scaling up models to the coarser, transport-modeling scale. In other words, "sub-scale" variability, which is occurring below the chosen transport-modeling scale, should be appropriately accounted for.

This work describes an approach to quantify the uncertainties in reservoir attributes and dispersivity introduced by scale-up. A new unified multi-scale workflow to scale-up effective dispersivities and reservoir attributes (porosity and permeability) in a consistent manner that takes into account sub-scale variability. It facilitates the construction of a suite of coarse-scale realizations using the transport modeling mesh that capture the fine-scale variability (at the sub-grid level) in rock properties (porosity and permeability) and transport properties

(longitudinal and transverse dispersivities). To scale-up rock properties, volume variance is computed corresponding to a given spatial correlation model inferred at the fine scale; volume variance refers to the uncertainty introduced when the volume support of the geo-modeling scale is less than the representative elementary volume scale of the attribute to be modeled (Lake and Srinivasan 2004; Leung and Srinivasan 2011); numerous sets of "conditioning data" are then sampled at the hard data (well) locations from probability distributions whose mean is the block average of the actual measured values and the variance is the variance of block mean. The term "conditioning data" refers to local data that is reproduced at the well locations in geostatistical simulations (Pyrcz and Deutsch 2014). Stochastic simulations are subsequently performed to generate multiple realizations at the transport modeling scale. Next, to scale-up dispersivities, multiple sub-grid geostatistical realizations depicting detailed fine-scale heterogeneities and of the same physical sizes as the transport modelling grid block is subjected to RWPT simulation. Effective longitudinal and transverse dispersivities are determined simultaneously by matching the corresponding breakthrough concentration history for each realization with an equivalent medium consisting of averaged homogeneous rock properties. Aggregating results derived with all realizations, we generate probability distributions of scaled-up dispersivities conditional to particular averaged rock properties, from which values representative of the transport modeling scale are randomly drawn.

The significance of capturing directly the sub-scale variability (uncertainty) in heterogeneity during scale-up of transport properties is

emphasized. A procedure is presented to model solute transport at coarse scale that is capable of capturing uncertainty in multi-scale heterogeneous models. Quantifying the uncertainty due to unresolved sub-grid heterogeneities would assist us in assessing the scaling characteristics of dispersion. Sub-scale variability in input dispersivities and rock properties are accounted for directly in the large-scale models.

This chapter is organized as the following: first, the governing equations for flow and transport modeling, as well as the particle-tracking formulation, are presented. Next, the proposed scale-up strategies are discussed in detail. Finally, application with a synthetic reservoir model is illustrated in a case study.

2.2 Flow and Transport Modeling in Porous Media

In this section, mathematical formulation of the flow and transport modeling equations are presented. This is followed by a discussion of the particle-tracking approach.

Conservation of mass for a solute component in a single-phase fluid system in a porous medium over the REV of the pore scale can be described by the continuum advection-dispersion equation (ADE) (Bear 1979)

$$\frac{\partial C}{\partial t} + \nabla \cdot \left(C \vec{u} \right) - \nabla \cdot \left(\vec{\vec{D}} \cdot \nabla C \right) = 0, \tag{2.1}$$

$$\nabla \cdot \left(\frac{\vec{\vec{k}}}{\mu} \vec{\nabla} P \right) = 0, \tag{2.2}$$

where $C(\mathbf{x},\,t)$ is solute concentration in mass per unit pore volume, which is a function of spatial coordinates ($\mathbf{x}$) and time (t), $\vec{u}$ is the Darcy velocity obtained from the solution of the steady-state flow Eq. (2.2), ∇ is the differential operator, and $\vec{\vec{D}}$ is the dispersion tensor (Bear 1979) that can be expressed in component notation (Binning and Celia 2002)

$$D_{ij}=\alpha_t\,|\,\vec{u}\,|\,\delta_{ij}+(\alpha_L-\alpha_T)\frac{u_iu_j}{|\,u\,|}+D^d\varsigma_{ij}, \tag{2.3}$$

where δ_{ij} is the Kronecker symbol, α_L and α_T represent the longitudinal and transverse dispersivity, respectively. D^d is the molecular diffusion coefficient, ς_{ij} is the tortuosity tensor, and u_i is component of the $\vec{u}$ along the ith direction. The velocity is calculated using Darcy equation as

$$\vec{u}=-\vec{\vec{K}}\vec{\nabla}h, where\,\vec{\vec{K}}=\frac{\vec{\vec{k}}\rho g}{\mu}; \tag{2.4}$$

$$\vec{V}=\frac{\vec{u}}{\phi}, \tag{2.5}$$

where $\vec{V}$ is the average pore or interstitial velocity, $\vec{\vec{k}}$ is the permeability tensor, μ is the fluid viscosity, h is the hydraulic head, $\vec{\vec{K}}$ is the hydraulic conductivity, and ϕ is the porosity.

The solute component can also be modeled discretely by representing it with a large number of small particles of mass Δm_i, where the summation over all particles re-establishes the total solute mass. The transport of these particles can be simulated using the particle tracking approaches such as RWPT. Over a given

time step or transit time, individual particles are advanced according to a drift term representing advection movement plus a random Brownian motion term representing diffusion/dispersion. Position of a particle at the new time level ($t+\Delta t$) can be written as (Tompson and Gelhar 1990; LaBolle et al. 1996; Hassan and Mohamed 2003)

$$X_p(t+\Delta t)=X_p(t)+\left(V_x(x_t,y_t z_t,t)+\frac{\partial D_{xx}}{\partial x}+\frac{\partial D_{xy}}{\partial y}+\frac{\partial D_{xz}}{\partial z}\right)\Delta t+$$
$$\sqrt{2D_{xx}\,\Delta t}\,z_1+\sqrt{2D_{xy}\,\Delta t}\,z_2+\sqrt{2D_{xz}\,\Delta t}\,z_3$$

$$Y_p(t+\Delta t)=Y_p(t)+\left(V_y(x_t,y_t z_t,t)+\frac{\partial D_{yx}}{\partial x}+\frac{\partial D_{yy}}{\partial y}+\frac{\partial D_{yz}}{\partial z}\right)\Delta t+$$
$$\sqrt{2D_{yx}\,\Delta t}\,z_1+\sqrt{2D_{yy}\,\Delta t}\,z_2+\sqrt{2D_{yz}\,\Delta t}\,z_3$$

$$Z_p(t+\Delta t)=Z_p(t)+\left(V_z(x_t,y_t z_t,t)+\frac{\partial D_{zx}}{\partial x}+\frac{\partial D_{zy}}{\partial y}+\frac{\partial D_{zz}}{\partial z}\right)\Delta t+$$
$$\sqrt{2D_{zx}\,\Delta t}\,z_1+\sqrt{2D_{zy}\,\Delta t}\,z_2+\sqrt{2D_{zz}\,\Delta t}\,z_3, \tag{2.6}$$

where X_p, Y_p, and Z_p are the position of a particle in x, y, and z coordinates, respectively. Δt is the time step, and z_i is a random number with zero mean and unit variance. V_i refers to the individual component of the velocity vector. Itô (1951) demonstrated that the particle density distribution $f(X_P,Y_P,Z_P,t)$, defined as the probability of finding a particle within a given interval $[(X_P,X_P+dX_P),(Y_P,Y_P+dY_P),(Z_P,Z_P+dZ_P)]$ at given time, obtained from Eq. (2.6) fulfills, in the limit of large number of particles and an infinitesimal step size, the Fokker-Planck equation

$$\frac{\partial f}{\partial t}+\nabla\cdot(\vec{u}f)\ =\ \nabla\nabla:\left(\vec{\vec{D}}f\right), \tag{2.7}$$

where f is particle density function; colon refers to the outer product resulting from multiplication of two tensors with dimension n

$$\nabla\nabla:\left(\vec{\vec{D}}f\right) = \sum_{i=1}^{n}\ \sum_{j=1}^{n}\frac{\partial^2 D_{ij}}{\partial x_i \partial x_j}f.$$

(2.8)

Eqs. 2.1 & 2.7 are identical. To establish the analogy between them, Kinzelbach (1986) modified the velocity as

$$u^*_{\,ij} = u_i + \sum_{j=1}^{3}\frac{\partial D_{ij}}{\partial x_j}.$$

(2.9)

and substitute Eq. (2.9) into Eq. (2.1) to give Eq. (2.10), which is equivalent to Eq. (2.7)

$$\frac{\partial C}{\partial t} + \nabla\cdot\left(u^*C\right) =\ \nabla\nabla:\left(\vec{\vec{D}}C\right).$$

(2.10)

In this work, a RWPT formulation called RW3D-MRMT (Fernàndez-Garcia et al. 2005; Salamon et al. 2006a, 2006b; Fernàndez-Garcia and Sanchez-Vila 2011) is applied. This formulation has been applied successfully to solve a number of field-scale transport problems (Salamon et al. 2007; Riva et al. 2008). It is capable of simulating advection, dispersion/diffusion, and simple first-order mass transfer as well as reactive multi-rate mass transfer with both regular or irregular grid geometry. It utilizes a hybrid scheme consisting of linear interpolation for velocities and tri/bilinear interpolation for the dispersion tensor. Readers should refer to the aforementioned references for additional details.

2.3 Scale-up Methodology

Theory and mathematical formulation of scale-up procedures are discussed. Procedures for constructing models of reservoir properties are presented followed by computation of effective dispersivities at the transport modeling (coarse) scale. Implementation details of the proposed multi-scale approach are also explained.

2.3.1 Scale-up of Reservoir Attributes

Scale-up of reservoir static properties is often performed for two reasons. First, measurements are usually available from different sources and scales; second, volume support for the transport modeling scale is typically much larger than that of the measured scale. These changes in scale or volume support lead to additional uncertainty in the scaled-up models due to averaging of sub-scale heterogeneity. This uncertainty is referred to as sub-scale variability (Fig. 2.1).

Most reservoir attributes are modeled as random variables because of the significant uncertainty associated with them. Since the average of a set of outcomes of a random variable is also a random variable, the spatial volume average of that attribute is also a random variable. The variance of mean of the attribute is a measure of the variability of the volume average (spatial average) at that particular volume support or scale V. Over short length scales, that variance is likely to be large and decreasing as V increases. This variance would eventually reach a constant negative unit slope on a log-log plot. A constant negative slope indicates that the volume support has reached the representative elementary volume (REV), a scale beyond which the sub-scale variability becomes

negligible. This negative slope can be derived from the law of large numbers: the sample variance is equal to the fine-scale variance divided by the number of samples; at scales larger than the REV, each sample is considered independent from each other (Leung and Srinivasan 2011). Let Z be a continuous Gaussian random variable with a variance of σ^2; for given autocorrelation model ρ_{corr}, the variance of its linear average ($\overline{Z}$) over a volume V can be computed according to Lake and Srinivasan (2004) by integrating over all possible lag distance η within V

$$Var(\overline{Z}) = \frac{2\sigma^2}{V^2} \left(\int_v \int_\eta \rho_{corr}(\eta) \, d\eta \, d\xi \right). \tag{2.11}$$

As V approaches zero, the variance of mean becomes the population mean at the point scale. It can be deduced from the above equation that (1) as the correlation length of heterogeneity increases, REV becomes larger and (2) for a given length scale, the variance of the mean increases with correlation length (Fig. 2.2).The general procedure for calculating the variance of the mean and the REV scale is to infer and model the variogram using data at the point support and then compute the variance of mean numerically by summing the model $\rho_{corr}(\eta)$ over all possible lag distances within V according to equation (2.11).

When the model length scale is smaller than the measurement REV, additional variance due to sub-scale variability must be accounted for when assigning data values to the model. First, the variance of mean is calculated corresponding to a particular length scale and for a particular spatial correlation length. This variance characterizes the uncertainty in property value for that particular length scale. When modeling is performed at a conditioning data

location using the support volume of the modeling grid, the uncertainty in the conditioning value is obtained by (1) sampling from probability distributions whose mean is the block-average of the actual measured values and the variance is the variance of block mean using spatially correlated probability values and (2) generating multiple sets of conditioning data. Uncertainty due to scale-up is accounted for by estimating a Gaussian-type likelihood function for the averaged conditioning data and performing parametric bootstrapping of this likelihood to assess uncertainty related to the conditioning data. Bootstrapping is a statistical resampling procedure for calculating uncertainty by using Monte Carlo simulation, where data is resampled from the same distribution with replacement (Pyrcz and Deutsch 2014). Using a linearly-averaged scaled-up semi-variogram $\bar{\gamma}$ (Journel and Hujbregts 1978), conditional simulation is performed on all sets of conditioning data in order to establish the uncertainty estimates at locations away from conditioning data (Leung and Srinivasan 2011). $\bar{\gamma}$ is defined mathematically as in Eq. (2.12), but it is often estimated numerically by discretizing the two volume supports (V, V'), respectively, into n and n' numbers of regularly-spaced points, and simply averaging the point-scale variogram values γ.

$$\bar{\gamma}(V, V') = \frac{1}{VV'} \int_V \int_{V'} \gamma(v, v') dv dv' \approx \frac{1}{nn'} \sum_{i=1}^{n} \sum_{j=1}^{n'} \gamma(\mathrm{h}_{ij}) \qquad (2.12)$$

The uncertainty in attribute value at any location away from the data location is compounded due to both sparse data and uncertainty in conditioning data. The work flow described in Leung and Srinivasan (2011) is followed:

1. Calculate γ using the fine-scale data.

2. Calculate variance of mean using the 3D point-scale variogram from Step #1 and Equation (2.11).

3. Compute scaled-up variogram $\bar{\gamma}$ at the coarse scale using Equation (2.12).

4. Sample multiple sets of scaled-up conditioning data values from distributions whose mean is the block-average of the actual measured values and the variance is the variance of the mean calculated in Step #2.

5. Perform conditional simulation at the coarse scale using the scaled-up variogram from Step #3 and scaled-up histogram (mean = fine-scale global mean; variance = variance of mean) using one sampled set of conditioning data.

6. Repeat Step #5 for other sets of conditioning data obtained in Step #4.

In this study, porosity ϕ and permeability k are the two rock properties to be modeled. The aforementioned procedure is used to compute scaled-up porosity values, which are assigned to individual grid blocks of the coarse-scale transport modeling mesh. Permeability is assumed to follow a log-normal distribution and can be related to the collocated porosity value as $k = a \times \phi^b$, where a and b are empirical constants. This assumption would imply that linearly averaging is also valid in the transformed space of $(k/a)^{1/b}$; therefore $\bar{k}$ is estimated from ϕ using the same empirical relation, assuming the transform relationship is invariant with scale (Leung and Srinivasan 2011). In principle, permeability can be scaled up in the same fashion as for the transport parameters, as explained in the next section, particularly if a simple correlation with porosity is unattainable.

2.3.2 Scale-up of Dispersivity

The procedure for constructing models of effective dispersivities at the modeling (coarse) scale is explained next. Variability at the sub-scale introduces uncertainty in transport-related attributes such as dispersivities at the coarse scale. It is this uncertainty that contributes to non-Fickian behavior. It is true that if all the fine-scale heterogeneities are modeled explicitly, any local (within grid cell) mixing would be represented by a Fickian model (John, 2008, Li et al. 2011). Although large-scale non-stationarities (trends) would also contribute to non-Fickian behavior, they can be modeled explicitly at the transport modeling scale and, hence, be readily combined with the proposed method. The underlying basis is that the temporal correlations of small-scale structures due to heterogeneities in the "sub-regions", as described by Dentz et al. (2004), can be represented by probability distributions of effective dispersivities calibrated using a series of fine-scale RWPT simulations. Therefore, by modeling the fine-scale heterogeneity explicitly, a single effective dispersivity value can be calibrated for that particular heterogeneity arrangement. Repeating this calibration process over numerous realizations would allow us to derive a distribution of effective dispersivities, and by sampling from these distributions, pre-asymptotic transport behavior (John 2008) due to uncertainty in small-scale structures can be modeled. It is important to point out that a Fickian model is employed here, as the effect of sub-scale variability is taken into account by sampling from the calibrated probability distributions of effective dispersivities.

Multiple sub-grid geostatistical realizations depicting the underlying fine-scale heterogeneity arrangements and of the same physical sizes of the transport modelling mesh are subjected to RWPT simulation. Effective longitudinal (α_{L}^{*}) and transverse dispersivities (α_{T}^{*}) are determined simultaneously by matching the corresponding breakthrough concentration history for each realization with an equivalent medium consisting of averaged homogeneous properties. In other words, for a particular fine-scale heterogeneity arrangement, its breakthrough concentration history (BTC) is compared against that of an equivalent homogeneous model based on the root mean square error or RMSE (Nash and Sutcliffe, 1970).

$$RMSE = \sqrt{\frac{1}{N-1} \sum_{i=1}^{N} \left[\left\langle C_{(\alpha_L|\phi, \alpha_T|\phi)} \right\rangle_{(t_{i-1} - t_i)} - \left\langle C_{(\alpha_L^{*}|\bar{\phi}, \alpha_T^{*}|\bar{\phi})} \right\rangle_{(t_{i-1} - t_i)} \right]^2}. \qquad (2.13)$$

The effective dispersivities α_{L}^{*} and α_{T}^{*} are obtained in an optimization procedure (e.g., simulated annealing) such that the RMSE is minimized. Aggregating results derived with all realizations, a conditional probability distribution of scaled-up dispersivities $P(\alpha_{L}^{*}|\bar{\phi})$ and $P(\alpha_{T}^{*}|\bar{\phi})$ are established.

For each coarse-scale model constructed in the previous section, effective dispersivity values are sampled from the probability distributions and assigned to individual grid blocks of the transport modeling mesh. However, it is expected that effective dispersivities should be correlated to porosity and/or permeability distribution; since permeability is computed directly from collocated porosity value, as discussed in the previous section, effective dispersivities should be sampled from the conditional probability distributions of $P(\alpha_{L}^{*}|\bar{\phi})$ and $P(\alpha_{T}^{*}|\bar{\phi})$.

These distributions are established by identifying a number of bins (n_b) to the histogram of $\bar{\phi}$; a set of n_s sub-grid realizations of $\phi \sim N(\bar{\phi}_b, \sigma^2)$ are generated using the fine-scale variogram γ, where the notation N denotes the Gaussian or normal distribution with $\bar{\phi}_b$ representing the porosity corresponding to a particular bin. Aggregating the results of α_L^* and α_T^* estimated from $n_s \times n_s$ models would yield the required $P(\alpha_L^* | \bar{\phi})$ and $P(\alpha_T^* | \bar{\phi})$.

The steps involved can be described as follow.

1. Assign n_b bins to the histogram of $\bar{\phi}$.

2. For a given bin, perform unconditional sequential Gaussian simulation to construct n_s sub-grid porosity models of $\phi \sim N(\bar{\phi}_b, \sigma^2)$ using fine-scale variogram γ. Permeability is computed from the collocated porosity value using the empirical relation $k = a \times \phi^b$.

3. Construct an equivalent homogeneous model corresponding to each of the n_s sub-grid porosity models obtained from #2. Since porosity is averaged linearly, it is postulated that linearly averaging is also valid in the transformed space of $(k/a)^{1/b}$; therefore $\bar{k}$ is estimated from $\bar{\phi}$ using the same empirical relation, assuming the transform relationship is invariant with scale (Leung and Srinivasan 2011).

4. Compute hydraulic head and velocity distributions with the appropriate boundary conditions at steady state using Eq. (2.2) and Eq. (2.4), respectively, for n_s heterogeneous models and n_s homogeneous models

generated in #2-3. Particle-based transport modeling is performed to simulate the solute transport.

5. The effective dispersivities α_L^* and α_T^* are obtained in an optimization scheme such that the mismatch in breakthrough concentration profile between the heterogeneous model and the equivalent homogeneous model (Eq. 2.13) is minimized.

6. Steps 1 to 5 are repeated for other bins in #1.

7. Probability distributions of $P(\alpha_L^*|\bar{\phi})$ and $P(\alpha_T^*|\bar{\phi})$ [i.e., $P(\alpha_L^*|\bar{\phi}_i)$ and $P(\alpha_T^*|\bar{\phi}_i)$ for $i = 1...n_b$] are obtained by aggregating the scaled-up values of α_L^* and α_T^* for all $n_b n_s$ models.

8. For each coarse-scale model constructed in the previous section, α_L^* and α_T^* are assigned to individual grid blocks by sampling from the probability distributions $P(\alpha_L^*|\bar{\phi})$ and $P(\alpha_T^*|\bar{\phi})$.

The scale-up procedures are implemented in a multi-scale based workflow shown in Fig. 2.3 to construct models of porosity, permeability, and effective dispersivities at the transport modeling scale. A case study is discussed in the next section to illustrate the impacts of incorporating sub-scale variability.

2.4 Case Study

Consider a synthetic 2D domain that is 500m×500m with two wells as shown in Fig. 2.4(A). In theory, the true model is always unknown; however, values of rock properties at wells can be inferred quantitatively from physical measurements. In this example, porosity values at a resolution of 1 m are extracted at the well

locations. A "true" 500 × 500 model with $\Delta x = \Delta y = 1$ m is assumed to be known. Porosity distribution follows the histogram and variogram model as shown in Fig. 2.5(A) and Fig. 2.6(A), respectively. Permeability (k in md) value is related to porosity as $25000 \times \phi^2$ and ranges from 81.0 to 3058.4 md (mean = 1566.1 md), while ϕ ranges from 0.05 to 0.35 (mean = 0.25). Longitudinal dispersivity α_L at 1-m volume support is set to be 0.5 m, with transverse dispersivity $\alpha_T = 0.1 \times \alpha_L$ (Perkins and Johnston 1963; Gelhar et al. 1992).

Instead of generating a suite of equi-probable realizations at a fine-scale of 1 m and subjecting each to transport modeling, which could be overwhelming because of the incurred computational costs, a suite of coarse-scale 50 × 50 models with $\Delta x = \Delta y = 10$ m (Fig. 2.4B). Therefore, the objectives of this study are to: (1) construct a suite of coarse-scale models of porosity and permeability that takes into account (a) uncertainty in reservoir heterogeneity at the modeling scale and (b) variability introduced by scale-up of reservoir attributes from fine-(measurement) scale to coarse-(modeling) scale; and (2) perform particle-tracking simulation using the entire suite of coarse-scale models to capture the response uncertainty.

Variance of mean is calculated corresponding to a volume support of 10 m ×10 m, and its value is approximately 0.9 based on γ and Eq. (2.11). The averaged variogram $\bar{\gamma}$ is calculated according to Eq. (2.12), and the results are shown in Fig. 2.6(B). Ten sets of conditioning data of ϕ are sampled at well locations from normal distributions whose mean is the block-average of the actual measured values and the variance is the variance of the mean using Monte Carlo simulation.

Conditional sequential Gaussian simulations (SGSIM), as implemented in GSLIB (Deutsch and Journel 1998), are performed according to $\bar{\gamma}$ and scaled-up histogram Fig. 2.5(B); ten realizations are simulated corresponding to each conditioning data set. Finally, a total of 100 realizations of scaled-up porosity distribution are obtained, and one of those realizations is shown in Fig. 2.7(B). Porosity distribution for the true model is also in Fig. 2.7(A).

To scale-up dispersivities, a fine-scale sub-grid 10×10 model with $\Delta x = \Delta y = 1$ m Fig. 2.4(C) is considered. Three ($n_b = 3$) bins corresponding to $\bar{\phi} = 0.1$, 0.2, and 0.3 are selected from the histogram in Fig. 2.5(B). Fifty ($n_s = 50$) sub-grid porosity models are simulated by unconditional sequential Gaussian simulation for each bin (Fig. 2.8), and one randomly selected model corresponding to $\bar{\phi} = 0.25$ is shown in Fig. 2.7(C). As expected, its corresponding histogram, as shown in Fig. 2.5(C), is the same as fine-scale histogram shown in Fig. 2.5(A). For each sub-grid model, a pair of injector and producer is placed diagonally across the domain (Fig. 2.4C). Steady-state hydraulic head and velocity distributions are computed based on finite difference approximation of Eqs. (2.2) and (2.4). Particle-tracking simulation is performed where effective dispersivities are estimated as described in the methodology section. The reduction in RMSE is shown in Fig. 2.9(A). The error is usually reduced below an acceptable tolerance level with fewer than 100 iterations with a very fast simulated annealing (VFSA) scheme (Li et al. 2004). Also shown in Fig. 2.9(B) is a comparison of breakthrough profiles obtained from sub-grid models. After the optimization procedure is performed, the response from the equivalent

homogeneous model matches well with the actual fine-scale heterogeneous model. Non-Fickian BTC is observable even in the homogeneous case; this is because the impacts of convergent radial flow around injectors and producers are particularly overwhelming in these small sub-grid models. This type of non-Fickian behavior is not observable in other 1D homogeneous model. A sensitivity analysis regarding boundary conditions with different configurations of the injector and producer placement, and the differences are negligible. Probability distributions of α_L^* and α_T^* corresponding to $\bar{\phi} = 0.25$ are shown in Fig. 2.10(A & B).

For each of the 100 coarse-scale models of porosity and permeability generated previously, values of α_L^* and α_T^* are drawn from these probability distributions, and they are subjected to particle-tracking simulation to predict solute (tracer) transport at the field scale and to assess the uncertainty due to sub-scale heterogeneity and variability. Results of cumulative mass ($\int \dot{m} dt / m_o$) flux at the outlet are shown in Fig. 2.11, where $\dot{m}$ and m_o refer to outlet mass flow rate and total mass injected, respectively. It is clear that the true fine-scale response (denoted by the red curve) is captured within the uncertainties exhibited by the coarse-scale models successfully. In addition, certain features that are commonly associated with non-Fickian transport, including heavy-tailed non-Gaussian breakthrough concentration profile and early breakthrough, are observed with the full scale-up scenario; the true fine-scale model, on the other hand, exhibits the more typical Fickian breakthrough characteristics.

In order to assess the impacts of the proposed scale-up procedure in uncertainties of coarse-scale recovery response, two additional scenarios are investigated. In the first case, neither scale-up of reservoir attribute nor scale-up of dispersivities is performed. In other words, fine-scale values (ϕ, k, α_L, and α_T) are used directly in the coarse-scale models, which are then subjected to particle-tracking modeling. The results are shown in Fig. 2.11. It is clear that the uncertainties demonstrated by the no scale-up scenarios are much more subdued. The fully scale-up models are more successful in approximating the true response in terms of the first and mean particle arrival times, despite the significant variability in the last particle arrival time (tailing behavior). It is observed in other cases where dispersivity values are increased from those used in this study, the coarse-scale models without scale-up would often fail to encompass the response from the true fine-scale model. In the second case, reservoir attributes are scaled up according to the prescribed method, while scale-up of dispersivities is ignored. In other words, properly scaled-up values of $\bar{\phi}$ and $\bar{k}$ are used together with fine-scale values of α_L, and α_T. Particle-tracking results are shown in Fig. 2.12. The standard deviations of particle arrival times for these two cases are much lower than the fully scale-up case.

Another case is considered, where scale-up values of porosity and permeability are used, and constant values of α_L^* and α_T^* drawn from the calibrated conditional probability distributions are assigned to the entire domain. Simulation results of the 100 coarse-scale models are shown in Fig. 2.13. It is interesting to note that the uncertainties exhibited by the coarse-scale models are

larger than the results shown in Fig. 2.11, where spatially-varying α_L^* and α_T^* values are assigned according to the proposed procedure, despite that both sets of coarse-scale models have successfully captured the response from the true fine-scale model. It appears that assigning constant α_L^* and α_T^* values everywhere would exaggerate the uncertainties (i.e., higher standard deviation in particle arrival times) in the ensuing coarse-scale transport response because the sub-scale uncertainty in α_L^* and α_T^* is not properly sampled. To verify this hypothesis, the corresponding particle distributions at a few snapshots of time for a randomly-selected coarse-scale model are compared with the true fine-scale response in Fig. 2.14. It is noted that the particle distribution for the fully scale-up models is more closely approximating the distribution obtained with the true fine-scale model. In particular, when only constant α_L^* and α_T^* are assigned, the particle plume is less dispersed, especially along the transverse direction, and this tendency becomes more pronounced with time; hence, the resultant BTC does not necessarily exhibit the long-tailed characteristics as observed in the spatially-varying α_L^* and α_T^* case. This is also supported by Fig. 2.13, which shows that the last particle arrives sooner in cases with constant α_L^* and α_T^*, exhibiting less tailing characteristics.

Finally, the computational requirement involved in this study is stated in Table 2.1. A high-performance computing (HPC) Linux-based computing environment (Jasper cluster provided by WestGrid and Compute/Calcul Canada), consisting of 240 nodes with Xeon X5675 processors, 12 cores (2 x 6) and 24 GB of memory, and 160 nodes with Xeon L5420 processors, 8 cores (2 x 4) and 16 GB of memory, was employed for the velocity and transport calculations. Jasper

uses an InfiniBand interconnect. The X5675 nodes are connected at 40 Gbit/s, with a 1:1 blocking factor, which is the fastest interconnect currently in WestGrid. The L5420 nodes are connected at 20 Gbit/s, with a 2:1 blocking factor. As shown in Table 1, the costs for transport calculations are much higher than that for the velocity calculations, despite that they are being carried out with the HPC platform with parallel computing capabilities. It is important to highlight that in real field applications, data is typically scarce and available at a volume support that differs from the modeling scale; therefore, capturing these uncertainties in a suite of fine-scale realizations and subjecting them to transport modeling are impractical due to the formidable computational costs. The ability to construct coarse-scale models that reflect the sub-grid heterogeneities is crucial.

2.5 Conclusions

1. In this chapter, we propose a new unified multi-scale workflow to scale-up effective dispersivities and reservoir attributes (porosity and permeability) in a consistent manner that takes into account of sub-scale variability. Conditional probability distributions of averaged (effective) quantities representative of the transport modeling scale are established; Monte Carlo simulations are performed to sample from these distributions.

2. Certain features commonly associated with non-Fickian transport including heavy-tailed non-Gaussian breakthrough concentration profile and early breakthrough, are observed with the ADE model where subscale variability is

integrated by assigning spatially-varying dispersivities that are sampled from the calibrated conditional probability distributions.

3. The fully scaled-up models, constructed based on the proposed procedure, are capable of capturing the fine-scale variability in transport modeling. Furthermore, ignoring the spatial variability in scaled-up effective dispersivities could not properly capture the effects of sub-scale variability, causing the overall uncertainty in the final recovery response to be overestimated.

4. The proposed method can be combined with large-scale trend model to integrate sub-scale heterogeneities and large-scale geologic structures that are both contributing to non-Fickian transport behavior at field scale.

References

Aronofsky, J. S., & Heller, J. P. (1957). A diffusion model to explain mixing of flowing miscible fluids in porous media. *Trans AIME, 210(12)*, (pp. 345-349).

Arya, A., Hewett, T. A., Larson, R. L., & Lake, L. W. (1988). Dispersion and reservoir heterogeneity. *SPE Reservoir Eng, 3(1)*, (pp. 139-148).

Barker, J. W., & Fayers, F. J. (1994). Transport coefficients for compositional simulation with coarse grids in heterogeneous media. *SPE Adv Technol Ser, 2(2)*, 103-112.

Bear, J. (1979). *Hydraulics of groundwater.* New York: McGraw-Hill.

Becker, M. W., & Shapiro, A. M. (2003). Interpreting tracer breakthrough tailing from different forced-gradient tracer experiment configurations in fractured bedrock. *Water Resour Res, 39(1)*, 1024.

Berentsen, C. W., Van Kruijsdijk, C. P., & Verlaan, M. L. (2007). Upscaling, relaxation and reversibility of dispersive flow in stratified porous media. *Transport Porous Med, 68(2)*, (pp. 187-218).

Berkowitz, B., Cortis, A., Dentz, M., & Scher, H. (2006). Modeling non-Fickian transport in geological formations as a continuous time random walk. *Reviews of Geophysics, 44(2)*.

Berkowitz, B., Scher, H., & Silliman, S. E. (2000). Anomalous transport in laboratory-scale, heterogeneous porous media. *Water Resour Res, 36(1)*, (pp. 149-158).

Bijeljic, B., Raeini, A., Mostaghimi, P., & Blunt, M. J. (2013). Predictions of non-Fickian solute transport in different classes of porous media using direct simulation on pore-scale images. *Physical Review E, 87(1)*, 013011.

Binning, P., & Celia, M. A. (2002). A forward particle tracking Eulerian–Lagrangian localized adjoint method for solution of the contaminant transport equation in three dimensions. *Adv Water Resour, 25(2)*, (pp. 147-157).

Christie, M. A. (2001). Flow in porous media — scale up of multiphase flow. *Current Opinion in Colloid & Interface Science, 6(3)*, (pp. 236-241).

Cortis, A., Gallo, C., Scher, H., & Berkowitz, B. (2004). Numerical simulation of non-Fickian transport in geological formations with multiple-scale heterogeneities. *Water Resour Res, 40(4)*.

Dentz, M., Cortis, A., Scher, H., & Berkowitz, B. (2004). Time behavior of solute transport in heterogeneous media: transition from anomalous to normal transport. *Advances in Water Resources, 27(2)*, (pp. 155-173).

Deutsch, C. V., & Journel, A. G. (1998). *Geostatistical software library and users guide.* New York: Oxford university press.

Efendiev, Y., Durlofsky, L. J., & Lee, S. H. (2000). Modeling of subgrid effects in coarse-scale simulations of transport in heterogeneous porous media. *Water Resour Res, 36(8)*, (pp. 2031-2041).

Fanchi, J. R. (1983). Multidimensional numerical dispersion. *SPE J, 23(1)*, (pp. 143-151).

Fernàndez-Garcia, D., & Sanchez-Vila, X. (2011). Optimal reconstruction of concentrations, gradients and reaction rates from particle distributions. *J Contam Hydrol, (120-121)*, (pp. 99-114).

Fernàndez-Garcia, D., Illangasekare, T. H., & Rajaram, H. (2005). Differences in the scale-dependence of dispersivity estimated from temporal and spatial moments in chemically and physically heterogeneous porous media. *Adv Water Resour, 28(7)*, (pp. 745-759).

Fernàndez-Garcia, D., Llerar-Meza, G., & Gómez-Hernández, J. J. (2009). Upscaling transport with mass transfer models: Mean behavior and propagation of uncertainty. *Water Resour Res, 45(10)*.

Fleurant, C., & Van Der Lee, J. (2001). A stochastic model of transport in three-dimensional porous media. *Math Geol, 33(4)*, (pp. 449-474).

Gelhar, L. W., Welty, C., & Rehfeldt, K. R. (1992). A critical review of data on field-scale dispersion in aquifers. *Water Resour Res, 28(7)*, (pp. 1955-1974).

Gouze, P., Le Borgne, T., Leprovost, R., Lods, G., Poidras, T., & Pezard, P. (2008). Non-Fickian dispersion in porous media: 1. multiscale measurements using single-well injection withdrawal tracer tests. *Water Resour Res, 44(6)*.

Gylling, B., Moreno, L., & Neretnieks, I. (1999). The channel network model—A tool for transport simulations in fractured media. *Ground Water, 37(3)*, (pp. 367-375).

Haajizadeh, M., Fayers, F. J., Cockin, A. P., Roffey, M., & Bond, D. J. (1999). On the importance of dispersion and heterogeneity in the compositional simulation of miscible gas processes. *In SPE Asia Pacific Improved Oil Recovery Conference.* Kuala Lumpur, Malaysia: Society of Petroleum Engineers.

Hassan, A. E., & Mohamed, M. M. (2003). On using particle tracking methods to simulate transport in single-continuum and dual continua porous media. *J Hydrol, 275(3)*, (pp. 242-260).

Hoffman, F., Ronen, D., & Pearl, Z. (1996). Evaluation of flow characteristics of a sand column using magnetic resonance imaging. *J Contam Hydrol, 22(1)*, 95-107.

Hoteit, H., Mose, R., Younes, A., Lehmann, F., & Ackerer, P. (2002). Three-dimensional modeling of mass transfer in porous media using the mixed hybrid finite elements and the random-walk methods. *Math Geol, 34(4)*, 435-456.

Itô, K. (1951). *On stochastic differential equations* (Vol. 4). Rhode Island, Rhode Island: Mem. Am. Math Soc.

Jha, R. K., Bryant, S., & Lake, L. W. (2011). Effect of diffusion on dispersion. *SPE J, 16(1)*, (pp. 65-77).

Jha, R. K., John, A., Bryant, S. L., & Lake, L. W. (2009). Flow reversal and mixing. *SPE J, 14(1)*, (pp. 41-49).

John, A. K. (2008). *Dispersion in Large Scale Permeable Media (Dissertation).* University of Texas at Austin.

John, A. K., Lake, L. W., Bryant, S., & Jennings, J. W. (2010). Investigation of mixing in field-scale miscible displacements using particle-tracking simulations of tracer floods with flow reversal. *SPE J, 15(3)*, (pp. 598-609).

Journel, A. G., & Huijbregts, C. J. (1978). *Mining geostatistics.* London: Academic press.

Kinzelbach, W. (1986). *Groundwater modelling: an introduction with sample programs in BASIC* (Vol. 25). New York: Elsevier.

LaBolle, E. M., Fogg, G. E., & Tompson, A. F. (1996). Random-walk simulation of transport in heterogeneous porous media: Local mass-conservation problem and implementation methods. *Water Resour Res, 32(3)*, (pp. 583-593).

Lake, L. W. (1989). *Enhanced oil recovery.* New Jersey: Prentice Hall.

Lake, L. W., & Srinivasan, S. (2004). Statistical scale-up of reservoir properties: Concepts and applications. *J Pet Sci Eng, 44(1)*, (pp. 27-39).

Lantz, R. B. (1971). Quantitative evaluation of numerical diffusion (truncation error). *Society of Petroleum Engineers Journal, 11(03)*, (pp. 315-320).

Le Borgne, T., & Gouze, P. (2008). Non-Fickian dispersion in porous media: 2. Model validation from measurements at different scales. *Water Resour Res, 44(6)*.

Leung, J. Y., & Srinivasan, S. (2011). Analysis of uncertainty introduced by scaleup of reservoir attributes and flow response in heterogeneous reservoirs. *SPE J, 16(3)*, (pp. 713-724).

Leung, J. Y., & Srinivasan, S. (2012). Scale-up of mass transfer and recovery performance in heterogeneous reservoirs. *J Pet Sci Eng, (86-87)*, (pp. 71-86).

Levy, M., & Berkowitz, B. (2003). Measurement and analysis of non-fickian dispersion in heterogeneous porous media. *J Contam Hydrol, 64(3)*, (pp. 203-226).

Li, L., Zhou, H., & Gómez-Hernández, J. J. (2011). A comparative study of three-dimensional hydraulic conductivity upscaling at the macro-dispersion experiment (MADE) site, Columbus Air Force Base, Mississippi (USA). *J Hydrol, 404(3)*, (pp. 278-293).

Li, X., Koike, T., & Pathmathevan, M. (2004). A very fast simulated re-annealing (VFSA) approach for land data assimilation. *Comput Geosci, 30(3)*, (pp. 239-248).

Mahadevan, J., Lake, L. W., & Johns, R. T. (2003). Estimation of true dispersivity in field-scale permeable media. *SPE J, 8(3)*, (pp. 272-279).

Nash, J., & Sutcliffe, J. V. (1970). River flow forecasting through conceptual models part I—A discussion of principles. *Journal of hydrology, 10(3)*, (pp. 282-290).

Oswald, S., Kinzelbach, W., Greiner, A., & Brix, G. (1997). Observation of flow and transport processes in artificial porous media via magnetic resonance imaging in three dimensions. *Geoderma, 80(3)*, 417-429.

Pedretti, D., Fernàndez-Garcia, D., Sanchez-Vila, X., Bolster, D., & Benson, D. A. (2014). Apparent directional mass-transfer capacity coefficients in

three-dimensional anisotropic heterogeneous aquifers under radial convergent transport. *Water Resour Res, 50(2)*, (pp. 1205-1224).

Perkins, T. K., & Johnston, O. C. (1963). A review of diffusion and dispersion in porous media. *SPE J, 3(01)*, (pp. 70-84).

Pyrcz, M. J., & Deutsch, C. V. (2014). *Geostatistical reservoir modeling.* New York: Oxford university press.

Riva, M., Guadagnini, A., Fernandez-Garcia, D., Sanchez-Vila, X., & Ptak, T. (2008). Relative importance of geostatistical and transport models in describing heavily tailed breakthrough curves at the Lauswiesen site. *J Contam Hydrol, 101(1)*, (pp. 1-13).

Salamon, P., Fernàndez-Garcia, D., & Gómez-Hernández, J. J. (2006a). A review and numerical assessment of the random walk particle tracking method. *Journal of contaminant hydrology, 87(3)*, (pp. 277-305).

Salamon, P., Fernàndez-Garcia, D., & Gómez-Hernández, J. J. (2006b). Modeling mass transfer processes using random walk particle tracking. *Water Resour Res, 42(11)*.

Salamon, P., Fernandez-Garcia, D., & Gómez-Hernández, J. J. (2007). Modeling tracer transport at the MADE site: the importance of heterogeneity. *Water resources research, 43(8)*.

Scheidegger, A. E. (1988). An evaluation of the accuracy of the diffusivity equation for describing miscible displacement in porous media. *Proc. Theory Fluid Flow Porous Media Conf* (pp. 101-116). Calgary: Imperial Oil Research Laboratory.

Srinivasan, G., Tartakovsky, D. M., Dentz, M., Viswanathan, H., Berkowitz, B., & Robinson, B. A. (2010). Random walk particle tracking simulations of non-Fickian transport in heterogeneous media. *Journal of Computational Physics, 229(11)*, (pp. 4304-4314).

Tompson, A. F., & Gelhar, L. W. (1990). Numerical simulation of solute transport in three-dimensional, randomly heterogeneous porous media. *Water Resour Res, 26(10)*, (pp. 2541-2562).

Zheng, C., & Bennett, G. D. (2002). *Applied contaminant transport modeling* (Vol. 2). New York: Wiley-Interscience.

Transport modeling scale

Fine-scale variability at
the sub-grid level

sub-scale variability
should be accounted
for during scaleup
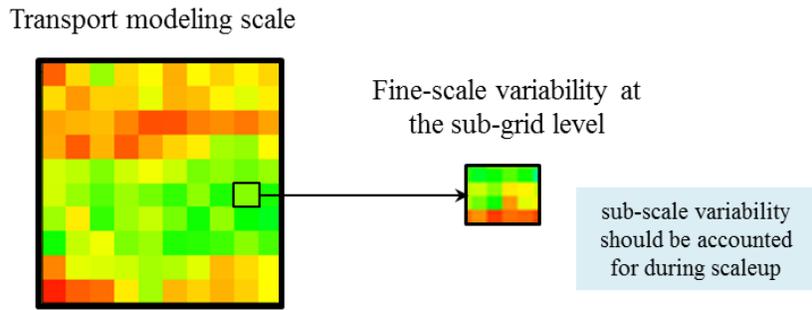
Figure 2.1: Illustration of concept of sub-scale variability.
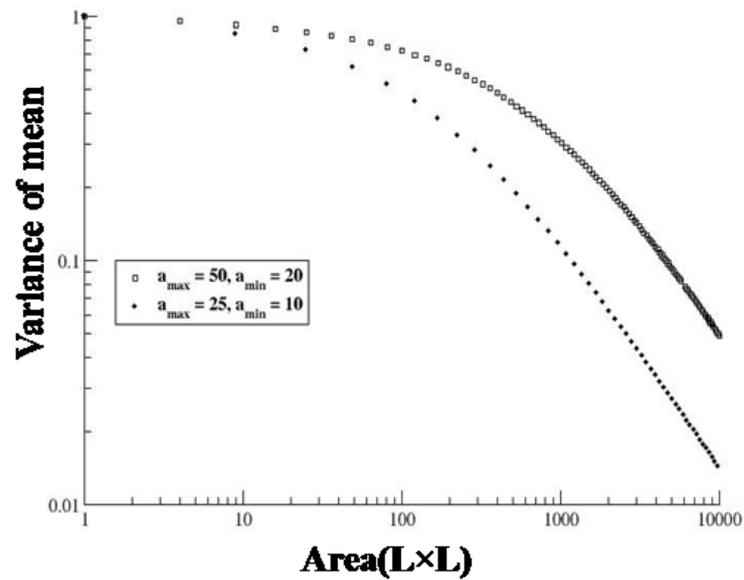
Figure 2.2: Variance of mean as a function of correlation length (a_{max} = maximum range of continuity and a_{min} = minimum range of continuity) and averaging scale.
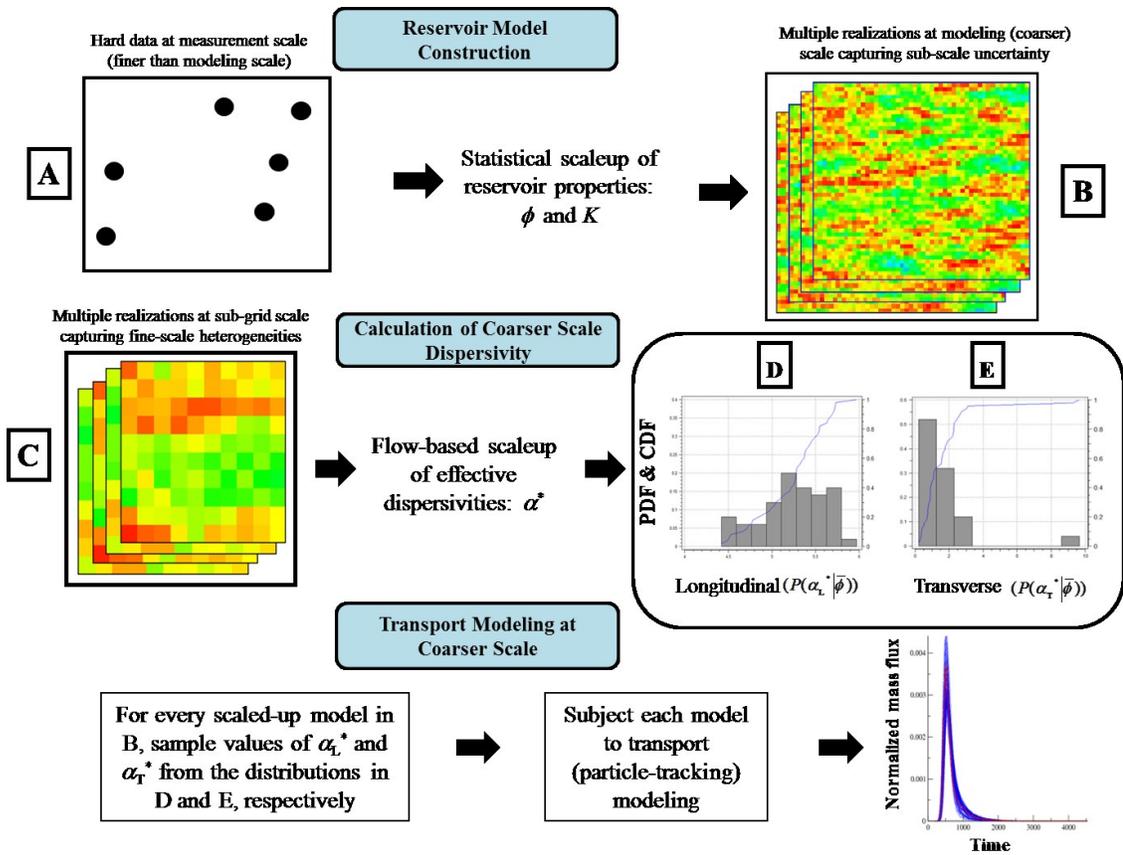
Figure 2.3: Workflow for scale-up of reservoir properties and effective dispersivities.
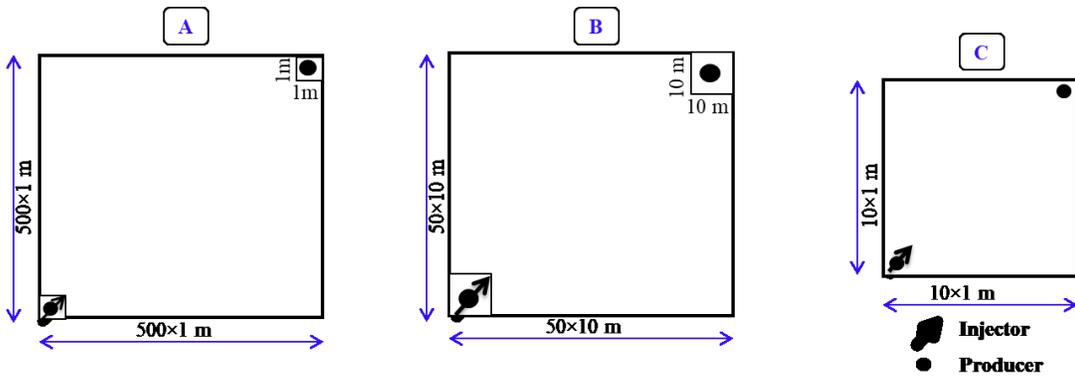
Figure 2.4: Setup for (A) fine-scale model, (B) coarse-scale model, and (C) sub-grid model.
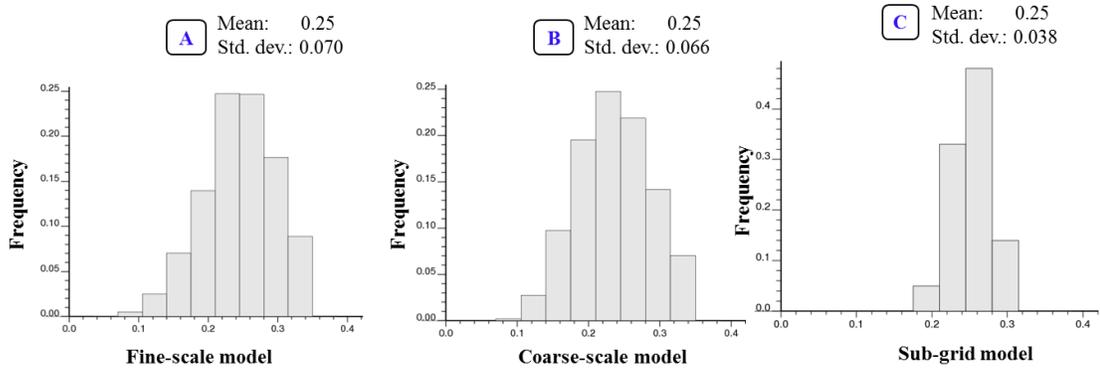
Figure 2.5: Histogram plot of Porosity of (A) fine-scale model, (B) coarse-scale model, and (C) sub-grid model.
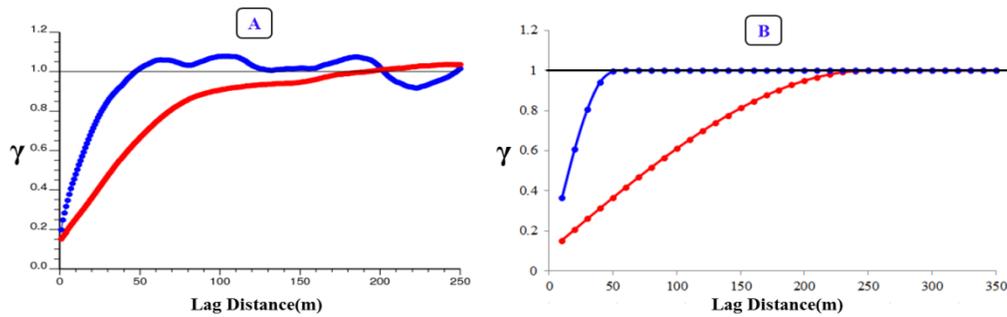
Figure 2.6: Variogram plot of (A) fine-scale model and (B) coarser-scale model. Blue: direction of minimum anisotropy; red: direction of maximum anisotropy.
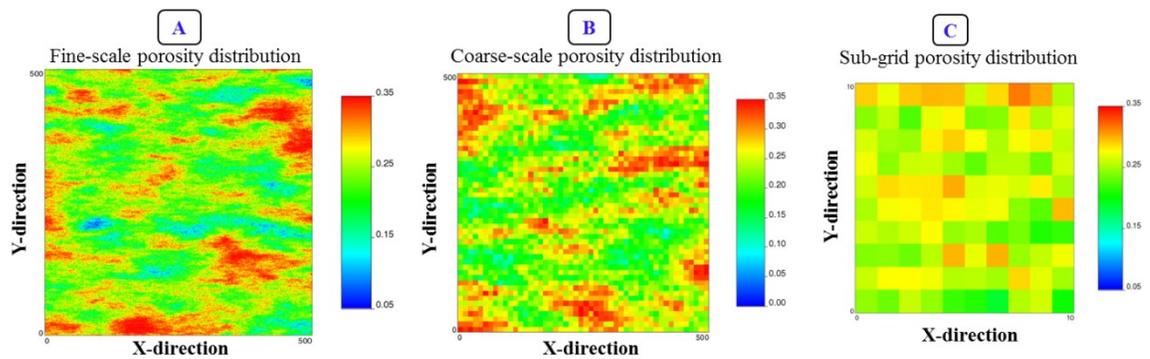
Figure 2.7: Porosity distribution at various scales: (A) fine-scale model, (B) coarse-scale model, and (C) sub-grid model.
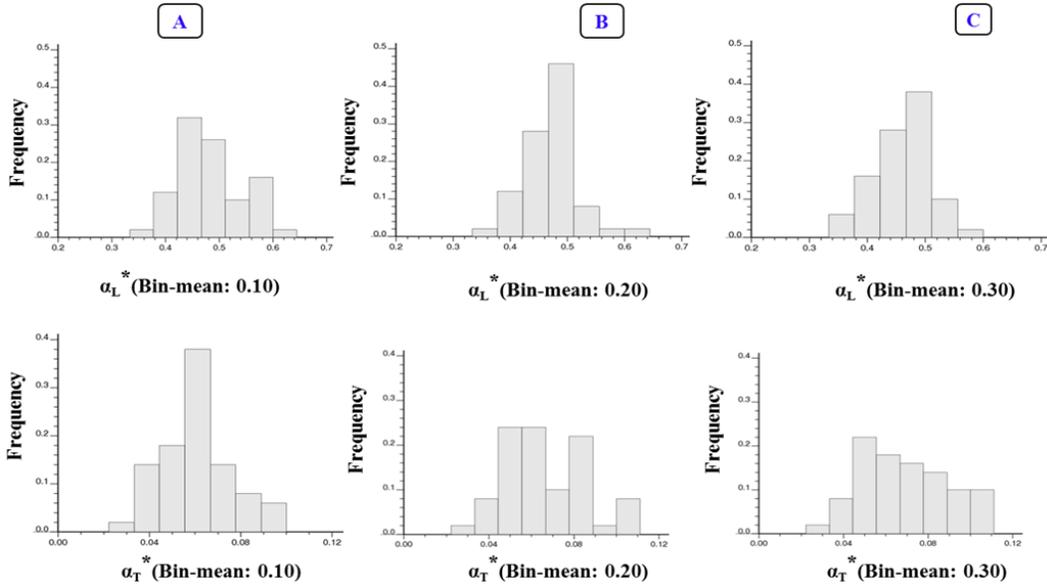
Figure 2.8: Distribution of effective dispersivities values with different bin-mean. ($\bar{\phi}$).
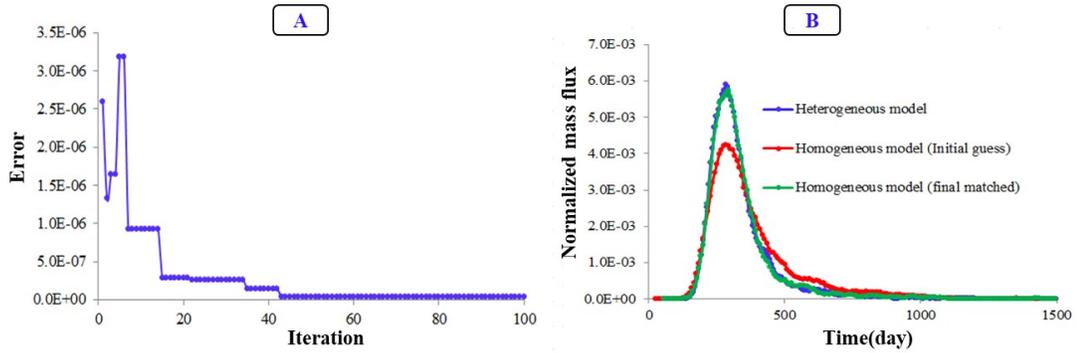
Figure 2.9: Left: Reduction in RMSE. Right: Comparison of breakthrough response obtained from the heterogeneous model and homogeneous models (before and after the minimization procedure).
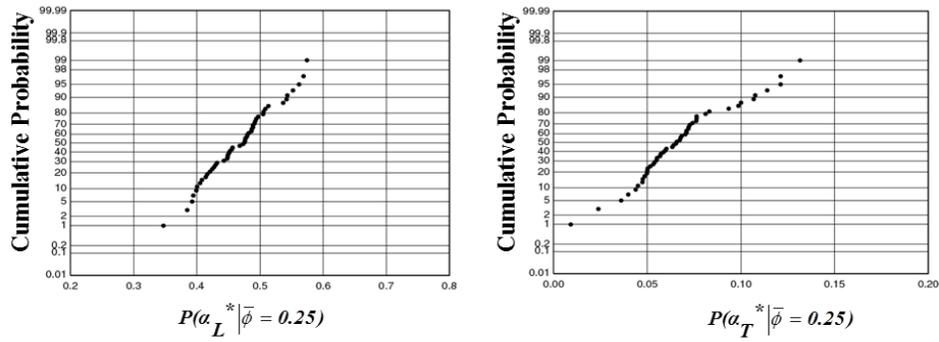
Figure 2.10: Conditional probability distribution $P(\alpha_L^*|\bar{\phi})$ and $P(\alpha_T^*|\bar{\phi})$ of effective dispersivities (α_L^* and α_T^*) corresponding to $\bar{\phi} = 0.25$.
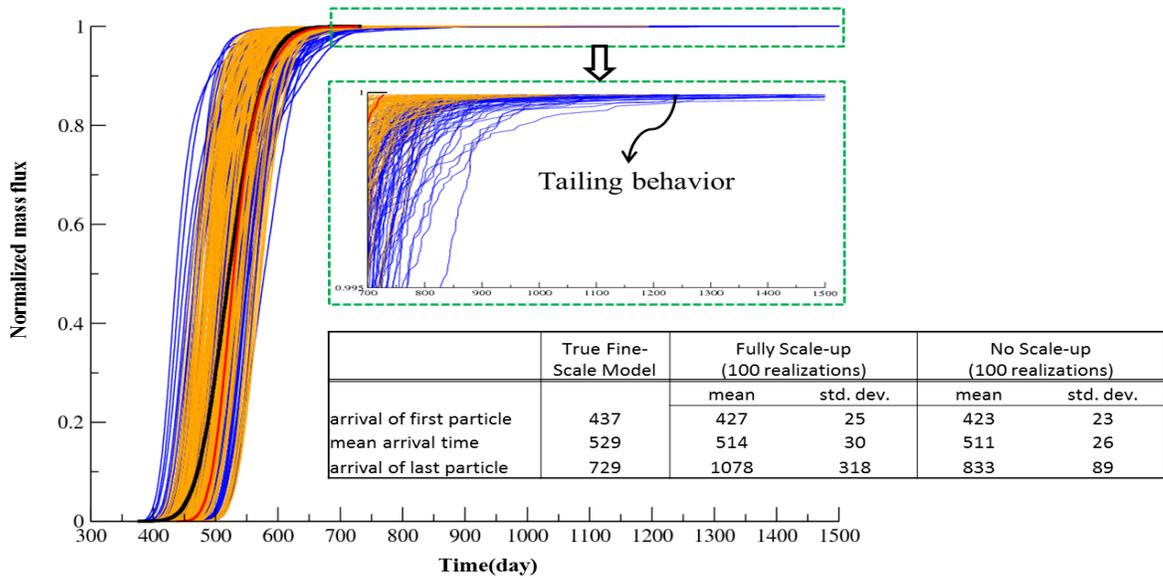
Figure 2.11: Normalized cumulative mass flux profiles for fully scaled-up models (blue) and models without scale-up of reservoir attributes and dispersivities (orange). Red and black curves correspond to the true fine-scale true model and the Gaussian plume, respectively.
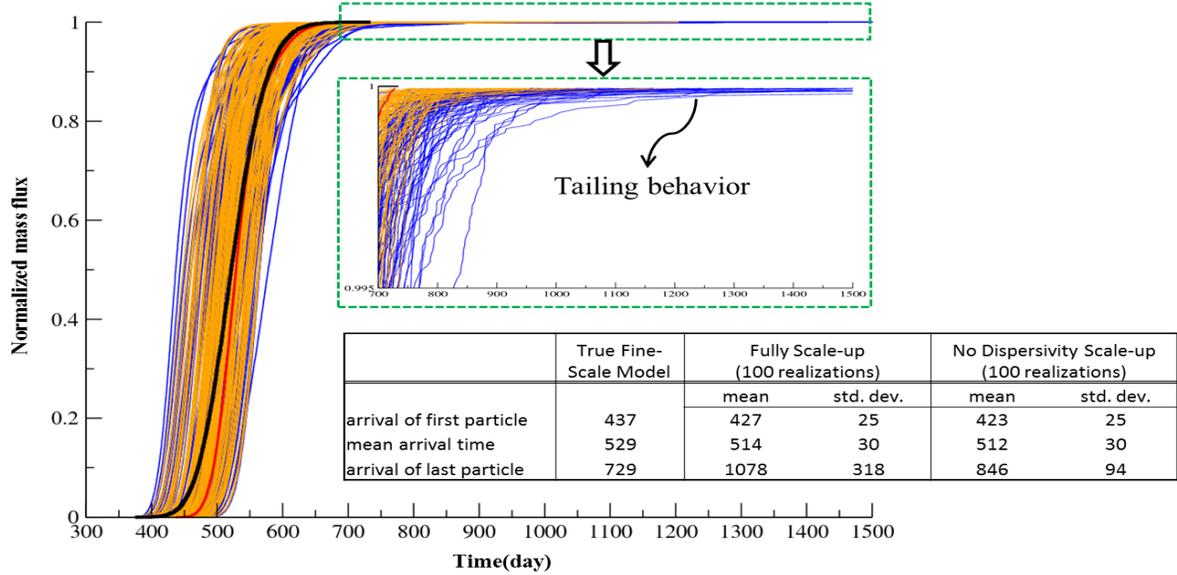
Figure 2.12: Normalized cumulative mass flux profiles for fully scaled-up models (blue) and the models where reservoir attributes are scaled up according to the prescribed method, while scale-up of dispersivities is ignored (orange). Red and black curves correspond to the true fine-scale model and the Gaussian plume, respectively.
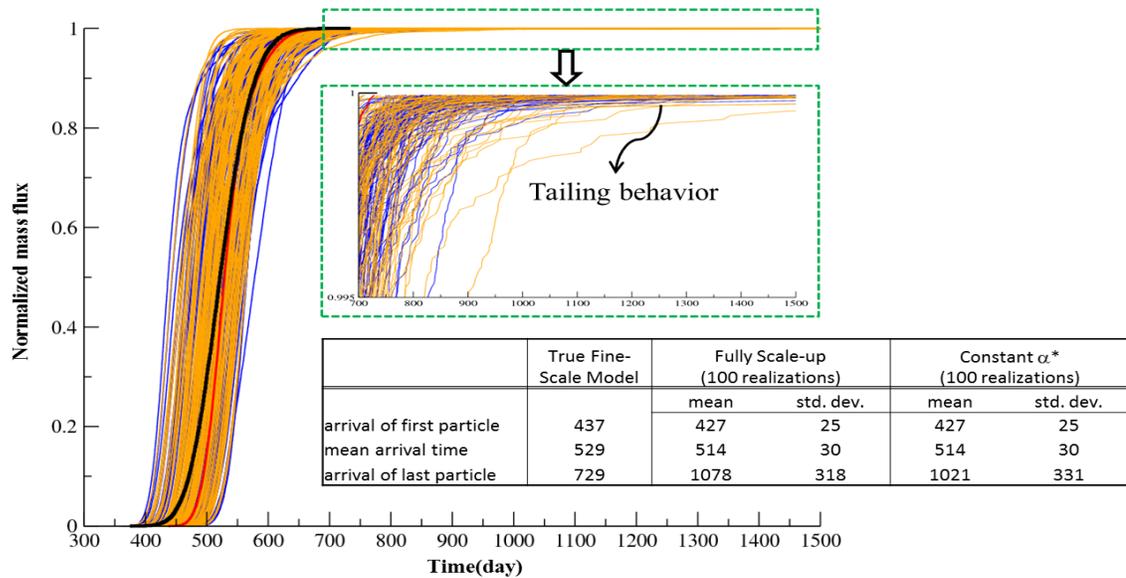
Figure 2.13: Normalized cumulative mass flux profiles for fully scaled-up models (blue) and fully scaled-up models but with constant α_L^* and α_T^* (orange). Red and black curves correspond to the true fine-scale model and the Gaussian plume, respectively.
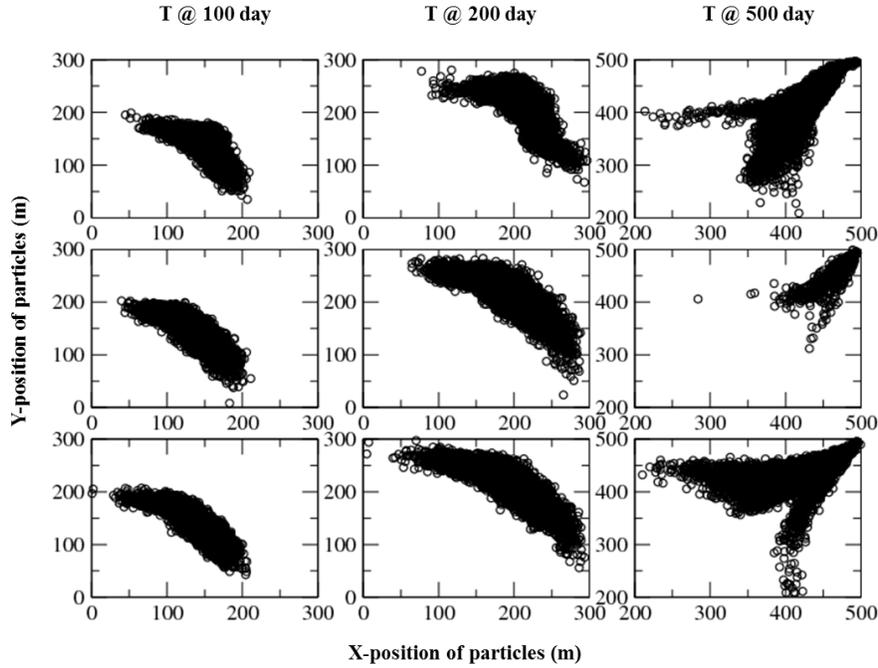
Figure 2.14: Particle distribution at various snapshots of time. 1st row: true fine-scale model; 2nd row: fully scaled-up model but with constant $\alpha_L{}^*$ and $\alpha_T{}^*$; and 3rd row: fully scaled-up model.

Table 2.1: Compilation of computational time

		Number of runs	Computational time using Jasper cluster (Velocity + Transport) Calculations	Remarks
1)	Fine-scale model (500×500 with 1×1m grid size)	1	(175 sec + 1800 sec) = 1975 sec	
2)	Sub-grid model (10×10 with 1×1m grid size)	(50 heterogeneous models + 50 homogeneous models) x 3 $\bar{\phi}$ levels	(300 sec + 180 sec) x 3 = 1440 sec	Calculation of P(α_L*| $\bar{\phi}$) and P(α_T*|$\bar{\phi}$) with100 iterations in VFSA using parallel computing scheme
3)	Coarse-scale model (50×50 with 10×10m grid size)	100	(200 sec + 1224 sec) x 100 = 14240 sec	Fully scaled-up model

Chapter 3: Statistical Framework for Scale-Up of

Dispersivity in Multi-Scale

Heterogeneous Media[2]

3.1 Introduction

Dispersion or mixing in subsurface flow stems from the interaction between convective spreading, diffusion and mechanical dispersion (Dullien 2012). It is well established that dispersivity or dispersion increases with scale, travelled distance (Gelhar et al. 1992; Fleurant and Van Der Lee 2001) and elapsed time (Binning and Celia 2002). This scale-dependent behavior is usually depicted as anomalous or non-Fickian (Berkowitz et al. 2000; John 2008), characterized by an invariant concentration peak, early breakthrough, and a long-tailed effluent profile. Though near wellbore flow may introduce anomalous behavior (Pedretti et al. 2014), most non-Fickian features originate from multi-scale heterogeneities (Le Borgne and Gouze 2008): large-scale trends (Gylling et al. 1999; Becker and Shapiro 2003; Gouze et al. 2008) and sub-scale variability (Dentz et al. 2004). Given heterogeneity varies with scales, it seems reasonable that dispersion would also be scale dependent (Mahadevan et al. 2003; Berkowitz et al. 2006; John et al. 2010; Jha et al. 2011; Bijeljic et al. 2013).

However, to capture non-Fickian characteristics is not trivial. First of all, fully isolating physical dispersion from numerical (artificial) dispersion is difficult (Lantz 1971; Fanchi 1983; Binning and Celia 2002), even by means of

---

[2]A version of this chapter is published in Environmental Earth Sciences Journal.

higher-order approximations. A viable alternative is the particle-tracking approach, which does not require discretization or a mesh and is free of numerical dispersion (Salamon et al. 2006a; John et al. 2010). Two classes of formulations are commonly adopted: random-walk particle-tracking (RWPT) and continuous-time random-walk (CTRW). In RWPT, each transit time step $\tau = \Delta t$ is considered as deterministic, constant and discrete, whereas transition length vector ξ is an i.i.d (independent and identically-distributed) random variable with unit variance and zero mean (Salamon et al. 2006a). RWPT predictions resemble those obtained with the classical advection-dispersion equation (ADE). Many early works, such as Aronofsky and Heller (1957) and Scheidegger (1959) have highlighted the problems of modeling both non-Fickian and Fickian characteristics with ADE. Systematic deviation between experimental breakthrough concentration (BTC) profiles and ADE predictions are observed by Levy and Berkowitz (2003). In case of the Fickian transport, incorrect spatial distribution of volume-averaged concentration is obtained for a Dirichlet boundary, if the resident concentration, C_r (**x**, t), form of the ADE is used for pulse injection. Instead, flux-averaged concentration can be correctly estimated using the flux-weighted concentration, C_f (x, t), form of the ADE for a Dirichlet boundary (Kreft and Zuber 1978; Parker 1984; Parker and Genuchten, 1984). In the case of non-Fickian transport, the classical ADE formulation fails to model the scale-dependent dispersion/mixing, unless effects of detailed heterogeneities below the transport modeling scale are properly integrated (Di Donato et al. 2003; John 2008; Li et al. 2011). In CTRW, τ and ξ are independent, stationary random

variables that follow a joint probability density function: $\psi(\xi, \tau) = \psi_s(\xi)\psi_t(\tau)$ (Srinivasan et al. 2010). A space-dependent memory function $\widetilde{M}(u; \mathbf{x})$ is formulated to model any unresolved heterogeneities below the modeling scale. To represent non-stationary trend, different transition-time probability distributions (parameterized by β, t_1, t_2) are assigned to various regions in the domain and be included deterministically in the drift and flux terms: $D_\psi(\mathbf{x})$ and $q_\psi(\mathbf{x})$ (Berkowitz et al. 2006). Alternative formulations of the memory function may incorporate the multi-rate mass transfer model (Fernàndez-Garcia et al. 2009).

Irrespective to the choice of simulation technique, transport modeling is often performed at a scale that is coarser than the finest resolution of heterogeneity. Different methods have been proposed for representing effects of heterogeneity/variability below the transport modeling scale. In this chapter, the phrase "fine scale" refers to a volume scale over which spatial heterogeneity at the Darcy scale is precisely described. For instance, the resolution of a fine-scale model may be comparable to that of the petrophysical log measurement (approximately 0.1 m × 0.1 m × 0.1 m). Performing numerical transport modeling at the fine-scale resolution would be impractical. Typical mesh for numerical simulation is often much coarser (e.g., 1-10 m), which is referred to as the "transport modeling scale" or "coarse scale" here.

Two main groups of techniques for scaling up dispersivity are: 1) stochastic perturbation or ensemble averaging and 2) volume averaging. In the ensemble averaging framework, an effective dispersivity is estimated from the

ensemble moments that describe the displacement of a solute plume (Gelhar and Axness 1983; Gelhar 1986; Neuman et al. 1987; Kitanidis 1988; Dagan 1989; Neuman and Zhang 1990; Rubin 2003). Expressions for effective dispersivity can be derived for different permeability covariance structures (Rubin et al. 1999). In the Lagrangian framework, the displacement moments can be evaluated from the displacement of a single particle over many realizations (Rubin et al. 1999; Wang and Kitanidis 1999) or the displacement of many particles over a single realization (Salamon et al. 2006a). The stochastic method is often limited to permeability distribution that is well defined. In the volume averaging framework, spatial averaging (spatial moments), instead of ensemble averaging (moments of the statistical distribution), is employed. An important requirement is that the length scale of heterogeneities must be much smaller than the averaging volume (i.e., a representative elementary volume (REV) for the heterogeneity length scale must be defined) (Leung and Srinivasan 2016). Therefore, periodic media is often used (Kitanidis 1992). In theory, if the restriction on the heterogeneity length scale is satisfied, both volume averaging and stochastic perturbation would yield the same results (Wang and Kitanidis 1999).

Therefore, the objective of this work is to devise a robust workflow, which is capable of handling a diverse range of heterogeneity distribution, for the scale-up of reservoir attributes (porosity and permeability) and dispersivities. It utilizes the concept of variance of mean (Leung and Srinivasan 2011). Instead of imposing that the averaging scale must be larger than the length scale of local heterogeneity, the idea is to transfer the uncertainty introduced during averaging

of reservoir attributes into the uncertainty in the effective parameters (Leung and Srinivasan 2012). This variance of mean can be computed directly from data or corresponding to a particular spatial correlation model; hence, there is no restriction on the type of heterogeneity distribution.

This workflow is an extension to the one presented in Vishal and Leung (2015), in which the effect of large-scale non-stationarity is completely neglected. Various aspects of the workflow have been modified: to scale up rock properties, each random variable is decomposed into the sum of a trend (available at the same resolution of the transport modeling scale) and a residual component. The workflow is revised to generate multiple realizations of the residual component at the transport modeling scale. Next, to scale up dispersivities, multiple geostatistical realizations of the same physical size as the transport modeling grid block is generated to describe the spatial heterogeneity (both trend plus residual) within the modeling block. Each realization is subjected to particle-tracking simulation. Effective longitudinal and transverse dispersivities are estimated by minimizing the difference in effluent history for each realization and that of an equivalent medium consisting of averaged homogeneous rock properties. Aggregating with the effective dispersivities for all realizations, probability distributions of effective dispersivities conditional to particular averaged rock properties are constructed. The rationale for adopting a Fickian RWPT model is that Fickian models can describe anomalous transport if detailed heterogeneities below the transport modeling scale is accounted for (Di Donato et al. 2003; John 2008; Li et al. 2011). John (2008) has explained that if all local heterogeneity

within a grid cell is modeled explicitly, Fickian transport is valid and a single value of effective dispersivity is computed based on that particular heterogeneity arrangement. Therefore, the idea is to represent uncertainties in small-scale heterogeneous structures, which contributes to non-Fickian behavior, with probability distributions of effective dispersivities.

An important contribution is that it offers a quantitative framework to scale up both rock and flow-related properties. The method is flexible in handling the diverse range of heterogeneity distribution, which may exhibit multi-scale characteristics. The amount of numerical dispersion is minimal, since the particle-tracking transport modeling step is free of numerical dispersion. This approach reinforces the notion that deterministic conditioning data does not exist in reservoir modeling.

In this chapter, first, background information and governing equations pertinent to particle-tracking transport modeling are summarized. Next, the scale-up methodology is explained. This is followed by a case study involving a synthetic reservoir model. Finally, impact on uncertainties in transport response due to heterogeneities at different levels is analyzed.

3.2 Flow and Transport Modeling in Porous Media

Transport of a solute component in a single-phase incompressible fluid flow can be represented by the ADE (advection-dispersion equation) (Bear 1979):

$$\frac{\partial C}{\partial t} + \nabla \cdot (C\boldsymbol{u}) - \nabla \cdot (\boldsymbol{D} \cdot \nabla C) = 0. \tag{3.1}$$

The above equation represents the conservation of mass at the Darcy scale. $C(\mathbf{x},t)$ is the solute concentration, which is defined as the mass per unit pore volume, with t and $\mathbf{x}$ denoting the temporal and spatial coordinates, respectively. The dispersion tensor, $\boldsymbol{D}$, is described by Bear (1979) and Binning and Celia (2002):

$$D_{ij} = \alpha_T |\boldsymbol{u}| \delta_{ij} + (\alpha_L - \alpha_T) \frac{u_i u_j}{|\boldsymbol{u}|} + D^d \varsigma_{ij}, \tag{3.2}$$

where α_L and α_T represent the longitudinal and transverse dispersivity, respectively; $\delta_{i,j}$ is the Kronecker symbol; D^d is the molecular diffusion coefficient; $\varsigma_{i,j}$ is the tortuosity tensor; $\boldsymbol{u}$ is the Darcy velocity, which is obtained from the momentum balance in Eq. (3.3):

$$\boldsymbol{u} = -\boldsymbol{K}\nabla h;\, \boldsymbol{K} = \frac{k\rho g}{\mu}, \tag{3.3}$$

where $\boldsymbol{k}$ is the permeability tensor, μ and ρ refer to the fluid viscosity and density, respectively, g is gravitational constant, h is the hydraulic head, and $\boldsymbol{K}$ is the hydraulic conductivity. The Darcy velocity is related to the average pore or interstitial velocity (V) via Eq. (3.4), where ϕ is the porosity:

$$V = \frac{\boldsymbol{u}}{\phi}. \tag{3.4}$$

In this work, an isotropic $\boldsymbol{K}$ is assumed (i.e., $\boldsymbol{K} = k$), which is further assumed to be empirically correlated with porosity (ϕ) according to Eq. (3.5) (Deutsch 2010):

$$\log_{10}(k) = \log_{10}(k_0) + a_1\phi + a_2\left(1 - e^{\frac{-3\phi}{\phi_c}}\right), \tag{3.5}$$

where k_o is the value for k when $\phi = 0$, and ϕ_c is a critical porosity above which the exponent function is almost flat; a_1 and a_2 are empirical constants.

In a particle-tracking framework, the total mass of a solute component is represented by with a large number of particles with mass Δm_i. At the new time step ($t+\Delta t$), the position of a particle is given by Eq. (3.6), which incorporates a drift term (i.e., advection) and a random Brownian motion term (i.e., diffusion/dispersion) (Tompson and Gelhar 1990; LaBolle et al. 1996; Hassan and Mohamed 2003):

$$\mathbf{x}_p(t + \Delta t) = \mathbf{x}_p(t) + A[\mathbf{x}_p(t)]\,\Delta t + B[\mathbf{x}_p(t)].\xi(t)\sqrt{\Delta t}$$
$$A = V + \nabla D, \; BB^T = 2D$$

(3.6)

where $\mathbf{x}_p$ is the position of particle at time t, Δt is the time step, and ξ is a random number with zero mean and unit variance. V refers to the velocity vector. According to Itô (1951), the particle density distribution $f(\mathbf{x}_p, t)$ obtained from Eq. (3.6) fulfills, in the limit of an infinitesimally step size and infinitely large number of particles, the Fokker-Planck equation, which is equivalent to Eq. (3.1) (Kinzelbach 1986):

$$\frac{\partial f}{\partial t} + \nabla \cdot (uf) = \nabla\nabla : (Df).$$

(3.7)

A RWPT implementation called RW3D-MRMT (Fernàndez-Garcia et al. 2005; Salamon et al. 2006a, 2006b; Salamon et al. 2007; Riva et al. 2008; Fernàndez-Garcia and Sanchez-Vila 2011) is applied for simulation of solute transport.

3.3 Method

A multi-scale workflow is presented to construct models of reservoir properties and effective dispersivities at the transport modeling (coarse) scale.

3.3.1 Scale-Up of Reservoir Properties

Scale-up is often performed because the volume support for data or measurement is smaller than the modeling scale. Averaging of heterogeneity below the transport modeling scale would lead to uncertainty, which is referred to as sub-scale variability. It is common to model reservoir attributes (such as porosity) as random variables, and the average over realizations/outcomes of a random variable would also be a random variable. In fact, the corresponding variance of mean is representative of the variability of the spatial average (i.e., sub-scale variability) at that particular volume scale V. This variance is large over very short length scales, but it starts decreasing as V increases, provided that the variable is stationary. This variance reaches a constant negative unit slope on a log-log plot of variance versus volume scale when $V \geq$ REV (Bear 1979). For $V >$ REV, sub-scale variability is considered negligible (Leung and Srinivasan 2011).

However, heterogeneity in petrophysical properties would often vary with length scales (Neuman 1994; Schulze-Makuch and Cherkauer 1998; Schulze-Makuch et al. 1999; Lake and Srinivasan 2004). Their multivariate statistics would tend to exhibit non-stationarity, characterized by ever-increasing variability with scale. As a result, its variance of mean would also increase with scale, and the determination of REV is impossible. The modeling of such variables is

facilitated by decomposing its variability into the sum of a non-stationary trend and fine-scale stationary residual. It is assumed that the trend component is defined at the transport modeling scale (i.e., no scale-up is necessary). Assuming that the residual is a scalar continuous random variable (Z), its spatial mean $\overline{Z}$ over a volume support V is defined as:

$$\overline{Z} = \left[\frac{1}{V_b} \int_{V_b} (Z)^{\omega} dV \right]^{1/\omega} \tag{3.8}$$

The variance of mean or $Var(\overline{Z})$ can be computed directly from the spatial averages of Z for different sizes of V according to Eq. (3.8). Alternatively, without any explicit assumption of the multivariate distribution, $Var(\overline{Z})$ can be obtained by applying a particular averaging window and computing the variance in the spatial mean. Different averaging schemes corresponding to different values of the exponent ω are possible. If Z is a Gaussian random variable with a variance σ^2, with a multivariate distribution described by a second-order stationary spatial correlation function ρ_{corr}, $Var(\overline{Z})$ can be computed by integrating ρ_{corr} over all possible lag distance η within V with Eq. (3.9), assuming linear averaging (i.e., $\omega = 1$) applies (Lake and Srinivasan 2004):

$$Var(\overline{Z}) = \frac{2\sigma^2}{V^2} \left(\int_V \int_\eta \rho_{corr}(\eta) d\eta d\xi \right) \tag{3.9}$$

When model length scale is smaller than the REV, additional variance due to sub-scale variability must be accounted for. Given that the volume support for the conditioning data is typically much less than that of the modeling scale, sub-scale variability in the conditioning value should be captured by sampling

multiple sets of conditioning data via bootstrapping (Leung and Srinivasan 2011). A plausible implementation is based on parametric bootstrapping of a likelihood function (whose variance is the variance of mean and the mean is the blockaverage of the actual measured values). For a Gaussian random variable, a Gaussian likelihood function is proposed. Finally, using a linearly-averaged semi-variogram $\bar{\gamma}$ for a Gaussian random variable (Journel and Hujbregts 1978), conditional simulation is performed on all sets of conditioning data (Leung and Srinivasan 2011). $\bar{\gamma}$, as defined in Eq. (3.10), can be estimated numerically by averaging the point-scale variogram values γ at various regularly-spaced points in two support volumes V and V'.

$$\bar{\gamma}(V,V') = \frac{1}{VV'} \int_V \int_{V'} \gamma(v,v') dv dv' \approx \frac{1}{nn'} \sum_{i=1}^{n} \sum_{j=1}^{n'} \gamma\left(\mathbf{h}_{ij}\right) \qquad (3.10)$$

In the presence of non-stationarity, the following decomposition is adopted:

$Z(\mathbf{x}) = \bar{Z}_T(\mathbf{x}) + Z_R(\mathbf{x})$, where $\bar{Z}_T(\mathbf{x})$ and $Z_R(\mathbf{x})$ refer to the trend and residual, respectively. The overbar denotes a quantity defined at the coarse scale. The procedure is summarized as follows:

1. Estimate $Z_R(\mathbf{x})$ and $\bar{Z}_T(\mathbf{x})$ at conditioning locations.

2. Estimate γ_R. Compute $Var(\bar{Z}_R)$ and $\bar{\gamma}_R$ based on Eqs. 3.9 and 3.10.

3. Draw multiple realizations of conditioning data of $Z_R(\mathbf{x})$ via bootstrapping. For example, a Gaussian likelihood function, whose mean is block average of the actual measured values and the variance is the variance of mean calculated in Step #2, can be adopted.

75

4. Construct realizations of $\bar{Z}_R(\mathbf{x})$ via sequential simulation for each conditioning data set from step #3: $\bar{\gamma}_R$ is obtained from Step #2; coarse-scale histogram is formulated with variance = $Var(\bar{Z}_R)$ and mean = fine-scale global mean of Z_R.

5. Construct realizations of $\bar{Z}_T(\mathbf{x})$.

6. Reconstruct realizations of $\bar{Z}(\mathbf{x}) = \bar{Z}_T(\mathbf{x}) + \bar{Z}_R(\mathbf{x})$ by combining the results from Steps #4 and 5.

7. Repeat Steps #4 to 6 for other conditioning data sets obtained in Step #3.

Porosity is modeled following the prescribed approach. Absolute permeability is assumed to be correlated with porosity by Eq. (3.5) across all scales. It should be emphasized that Steps #2-4 and #7 are similar to the original procedure in Vishal and Leung (2015).

3.3.2. Scale-Up of Transport Properties

Multiple geostatistical realizations of the same physical size as the transport modeling grid block are generated to describe the spatial heterogeneity below the modeling scale. Each realization is subjected to particle-tracking simulation. Effective longitudinal (α_L^*) and transverse (α_T^*) dispersivities are estimated simultaneously by minimizing the difference in effluent profile for each realization and that of an equivalent average medium. The difference, which is measured in terms of root mean square error, or *RMSE*, according to Eq. (3.11) (Nash and Sutcliffe 1970), is minimized using a non-linear regression scheme.

$$RMSE = \sqrt{\frac{1}{N-1} \sum_{i=1}^{N} \left[\left\langle C_{((\alpha_L, \alpha_T);(\bar{\phi}_R, \bar{\phi}_T))} \right\rangle_{(t_{i-1}-t_i)} - \left\langle C_{((\alpha_L^*, \alpha_T^*)|(\bar{\phi}_R, \bar{\phi}_T))} \right\rangle_{(t_{i-1}-t_i)} \right]^2} , (3.11)$$

where $\bar{\phi}_T$ and $\bar{\phi}_R$ refer to the trend and residual component at the coarse scale, respectively. In order to adopt the original procedure in Vishal and Leung (2015) for multi-scale heterogeneous formations, a few modifications are proposed. For each of the realizations of $\bar{\phi}$ from section 3.3.1, values of α_L^* and α_T^* are drawn from the probability distributions of $P\{\alpha_L^* | (\bar{\phi}_R, \bar{\phi}_T)\}$ and $P\{\alpha_T^* | (\bar{\phi}_R, \bar{\phi}_T)\}$. To establish these probability distributions, the histograms of $\bar{\phi}_R$ and $\bar{\phi}_T$ are divided to a number of bins n_{bR} and n_{bT}, respectively. For each of $n_{bR} \times n_{bT}$ bin combinations, a set of n_s sub-grid realizations of ϕ are constructed such that $\phi = \phi_R + \bar{\phi}_T$. Aggregating the results of α_L^* and α_T^* estimated from all n_s realizations would yield $P\{\alpha_L^* | (\bar{\phi}_R, \bar{\phi}_T)\}$ and $P\{\alpha_T^* | (\bar{\phi}_R, \bar{\phi}_T)\}$ for that particular bin combination. The revised work plan can be described as follow:

1. Assign n_{bR} bins and n_{bT} bins to the histograms of $\bar{\phi}_R$ and $\bar{\phi}_T$, respectively. A total of $n_{bR} \times n_{bT}$ bin combinations are possible.

2. For a particular bin combination, perform unconditional sequential simulation to sample n_s sub-grid realizations of ϕ_R. If ϕ_R follows Gaussian statistics, sub-grid realizations of $\phi_R \sim N(\bar{\phi}_{bR}, \sigma_R^2)$ can be constructed using the fine-scale variogram of γ_R. $N(\bar{\phi}_{bR}, \sigma_R^2)$ denotes a Gaussian model with mean $= \bar{\phi}_R$ of the corresponding bin (i.e., $\bar{\phi}_{bR}$) and variance $= \sigma_R^2$. ϕ are constructed as $\phi = \phi_R + \bar{\phi}_T$. Corresponding permeability value at each

location is computed according to Eq. (3.5). It is assumed that this relationship is scale invariant.

3. For each n_s sub-grid realization of ϕ obtained in Step #2, construct an equivalent homogeneous model.

4. Simulate velocity and solute transport by employing appropriate initial and boundary conditions for all n_s heterogeneous models and n_s homogeneous models constructed in Steps #2-3, respectively. Particle-based technique is used for transport modeling.

5. Estimate the effective dispersivities α_L^* and α_T^* by minimizing the *RMSE* in Eq. (3.11) for all n_s sub-grid realizations.

6. Steps #2-5 are repeated for all bin combinations to construct
   $$P\{\alpha_L^* \mid (\bar{\phi}_R, \bar{\phi}_T)\} \text{ and } P\{\alpha_T^* \mid (\bar{\phi}_R, \bar{\phi}_T)\}.$$

7. For each of the coarse-scale models from section 3.3.1, assign effective dispersivities at each location by sampling from $P\{\alpha_L^* \mid (\bar{\phi}_R, \bar{\phi}_T)\}$ and
   $$P\{\alpha_T^* \mid (\bar{\phi}_R, \bar{\phi}_T)\}.$$

The workflow for sections 3.3.1 and 3.3.2 are illustrated in Fig. 3.1. If the random variable does not follow Gaussian statistics, other sequential techniques for simulating continuous variables can be applied to generate the sub-grid and coarse-scale models. Instead of formulating γ_R and $\bar{\gamma}_R$, alternative multivariate statistics description can be adopted. Therefore, this proposed workflow is general, in the sense, that no explicit assumption of the multivariate distribution is required.

3.4 Case Study

A synthetic 2D domain with 1000×1000 blocks ($\Delta x = \Delta y = 2$ m) is considered. The "true" 1000×1000 model is assumed to be known, and there are a total of 18 wells, as shown in Fig. 3.2(A). It is further assumed that porosity values at a scale of 2 m are available from physical measurements at the well locations. The corresponding histogram and anisotropic variogram are shown in Fig. 3.3 and Fig. 3.4, respectively. Permeability (in md) is assumed to be correlated with porosity according to Eq. (3.5) ($k_0 = 0.01$, $\phi_c = 0.35$, $a_1 = 3.667$, and $a_2 = 4.151$). The "true" model of ϕ, as well as its respective trend and residual components, are shown in Fig. 3.5. Longitudinal dispersivity α_L is set to be 0.2 m, and the transverse dispersivity $\alpha_T = 0.1 \times \alpha_L$ (Perkins and Johnston 1963; Gelhar et al. 1992).

Performing transport simulation using many equi-probable realizations of porosity and permeability at the 2-m scale could be infeasible because of the high computational demands. An alternative is to construct a suite of coarse-scale 50×50 models with $\Delta x = \Delta y = 40$ m (Fig. 3.2B). The scale-up procedure described in section 3.3.1 is adopted to assign $\overline{\phi}$ and $\overline{k}$. Ten realizations of the trend component are generated with the conditioning data of $\overline{\phi}_T$ at the well locations. Regarding the residual component, $Var(\overline{\phi}_R)$ corresponding to a volume support of 40 m $\times$ 40 m is estimated to be approximately 0.599 according to Eq. (3.9). The coarse-scale histograms and variograms are presented in Fig. 3.6 and Fig. 3.7, respectively. Next, at each well location, ten sets of conditioning data of ϕ are sampled. Sequential Gaussian simulation or SGSIM (Deutsch and Journel 1998) is performed using the coarse-scale histograms and variograms to generate one

realization $\bar{\phi}_R$ corresponding to each of the 10 sets of conditioning data of ϕ_R. As a result, a total of 10 realizations of $\bar{\phi}_R$. In the end, combining the 10 realizations of $\bar{\phi}_T$ and 10 realizations of $\bar{\phi}_R$, a total of $10 \times 10 = 100$ realizations of $\bar{\phi}$ are obtained, and an example is shown in Fig. 3.8.

The procedure described in section 3.3.2 is subsequently adopted to scale up dispersivities. A detailed 20×20 sub-grid domain with $\Delta x = \Delta y = 2$ m is considered (Fig. 3.2C). As illustrated in Fig. 3.9, three bins ($n_{bR} = 3$) corresponding to $\bar{\phi}_R = 0.05, 0.075, 0.1$ and three bins ($n_{bT} = 3$) corresponding to $\bar{\phi}_T = 0.05, 0.15, 0.25$ are selected. For each of the bin combinations, 50 sub-grid realizations ($n_s = 50$) of ϕ are constructed by unconditional SGSIM (i.e., a total of $n_s \times n_{bR} \times n_{bT} = 450$ sub-grid realizations are generated). An example is illustrated in Fig. 3.9, where a randomly-selected realization corresponding to $\bar{\phi}_R = 0.1$ is combined with three different values of $\bar{\phi}_T$ to construct three sub-grid realizations of ϕ. Next, particle-tracking modeling is facilitated by placing three pairs of injector and producer along the edges of the sub-grid domain (Fig. 3.2C). Probability distributions of $\alpha_L{}^*$ and $\alpha_T{}^*$ for all possible combination of n_{bR} and n_{bT} are shown in Fig. 3.10. For each of the 100 coarse-scale models of porosity and permeability (e.g., Fig. 3.8), values of $\alpha_L{}^*$ and $\alpha_T{}^*$ are assigned to each location by sampling from the calibrated probability distributions. Each of the 100 models is subjected to particle-tracking simulation. At $t = 0$, 1×10^4 particles of equal mass are injected uniformly along the left edge of the domain. The ensuing

breakthrough concentration profiles between the coarse-scale models and the true fine-scale model are analyzed.

3.5 Results and Discussions

Among all the sub-grid realizations involved in this case study, four types of breakthrough characteristics are observed (Fig. 3.11). The corresponding reduction in *RMSE* during the estimation of effective dispersivities (α_L^* and α_T^*) is shown in Fig. 3.12. Approximately 100 iterations are needed before the error would diminish below a certain prescribed tolerance using the very fast simulated annealing scheme (Li et al. 2004). Multiple peaks are observed in several of these breakthrough profiles (e.g., type A and B) due to the significant variation in flow paths (and transit times) (Leibundgut et al. 2011). Since a single set of fine-scale dispersivity values has been assigned, it is unlikely to reproduce the multi-peaked feature. It has also been widely acknowledged that classical ADE, CTRW, or mobile-immobile fluid model (Toride et al. 1993; Field and Pinsky 2000; Cortis and Berkowitz 2005; Leij et al. 2012) may fail to capture similar multi-peaked feature, unless different mass transfer models (e.g., dispersivity) are assigned to regions with distinct flow behavior. Alternative models such as the multi-dispersion model (MDM) (Käss 1998), multi-flow multi-dispersion model (Leibundgut et al. 2011), weighted sum advection–dispersion equation (WSADE), or dual-advection dispersion equation (DADE) (Field and Leij 2012) can be considered to model the multi-peaked behavior.

The objective of this study is to quantify the uncertainty in solute transport as a result of both sub-scale variability and non-stationarity trend. The intent is to demonstrate that the coupling of both length scales of heterogeneity is important to modeling non-Fickian behavior at the transport modeling scale. Results of the cumulative mass flux ($\int \dot{m}dt/m_o$), where m_o and $\dot{m}$ refer to the total injected mass and outlet mass flow rate, respectively, and the instantaneous mass flux are presented in Fig. 3.13(A) and Fig. 3.14(A), respectively.

Firstly, in comparison to Vishal and Leung (2015), which ignored large-scale non-stationarity, the non-Fickian characteristics exhibited in the transport response here is dramatically more pronounced. Secondly, the true response (black in color) of the fine-scale model is completely captured by the responses of the coarse-scale models (red in color). Heavy-tailed effluent profile, multi-modal breakthrough, and early breakthrough are observed in both sets of responses, suggesting that non-Fickian characteristics can be captured when both large-scale non-stationarity and sub-scale variability are incorporated. The results support the conclusion that despite the difficulty in reproducing the multi-peaked breakthrough histories for some sub-grid realizations during the estimation of α_L^* and α_T^*, the complex non-Fickian behavior can still be captured in the coarse-scale models because the modeling workflow incorporates both the non-stationary trend and the probability distributions of $P\{\alpha_L^* \mid (\bar{\phi}_R, \bar{\phi}_T)\}$ and $P\{\alpha_T^* \mid (\bar{\phi}_R, \bar{\phi}_T)\}$, which effectively represent the sub-scale variability.

Three additional cases are considered next to understand the various aspects of this scale-up procedure. In the first case, scale-up is completely

ignored: fine-scale values (ϕ, k, α_L, and α_T) are assigned in the coarse-scale models. The results are shown in Fig. 3.13(B) and Fig. 3.14(B). There appears to be a systematic delay in particle arrival time, as compared to the true model, during both the early and late times.

In the second case, only scale-up of rock properties (i.e., porosity and permeability) is performed, while fine-scale dispersivity values are assigned in the coarse-scale models. The results, as shown in Fig. 3.13(C) and Fig. 3.14(C), suggest that the uncertainty encompassed by the coarse-scale models has captured the fine-scale response; however, as compared to Fig. 3.13(A), it is clear that there is a systematic delay in particle arrival time.

The last case is the same as the original fully scaled-up case, except that a single set of α_L^* and α_T^* value is assigned uniformly across the entire domain. Larger uncertainties are demonstrated by the coarse-scale models in Fig. 3.13(D) and Fig. 3.14(D), in comparison to Fig. 3.13(A) and Fig. 3.14(A), despite that both sets of coarse-scale models have sufficiently captured the fine-scale response. It appears that by assigning the same α_L^* and α_T^* values everywhere and not randomizing the sub-scale variability spatially would exaggerate the uncertainties in particle movement in the coarse-scale models and delay the particle arrival time. In the end, it is concluded from Fig. 3.13 that the fully scaled-up case (A) offers the most reasonable representation of uncertainty around the true case in both early and late times. It can be also observed that the fully scale-up modes show greater uncertainties at the late time compare to other scenarios.

Next, the relative influence of sub-scale variability and non-stationary trend on the overall uncertainty in transport response is investigated. To this end, a single trend model is considered, but its relative contribution is varied. In particular, three scenarios with different combination of trend and residual components are tested: (1) 0% residual and 100% trend; (2) 25% residual and 75% trend and (3) 75% residual and 25% trend. The results are compared in Fig. 3.15. As expected, in the absence of any residual component (i.e., 100% trend), the coarse-scale model should reproduce the true fine-scale model exactly, since (1) no additional uncertainty is introduced due to scale-up and (2) the adopted particle-tracking technique is free of numerical dispersion. However, as the residual component becomes more dominant, the associated sub-scale variability would also increase, which, in turn, amplifies the uncertainty in the ensuing coarse-scale transport response (left column). An important message is that since the decision of stationarity is often subjective in most practical subsurface modeling applications (even after all conditioning data is honored), this decision has significant ramification in how sub-scale variability is subsequently represented at the transport modeling scale and how it might impact the fidelity of the ensuing coarse-scale models.

The computational time involved is compared in Table 3.1. A Linux-based computing cluster, which is available on the WestGrid, is used (Vishal and Leung 2015). As expected, computational requirement for transport modeling generally overwhelms that for the velocity computations. In practice, scarce data

compounded with varying volume support renders transport modeling involving fine-scale realizations to be generally impractical.

3.6 Conclusion

1. A novel multi-scale workflow based on the volume variance concept is proposed to facilitate scale-up of both reservoir attributes and effective dispersivities in a systematic manner that incorporates both sub-scale variability and large-scale non-stationary trend. The main idea is to construct conditional probability distributions of effective dispersivities at the transport modeling scale that would capture the sub-scale variability.

2. Although a covariance-based Gaussian model was adopted in the case study, the method does not require any explicit assumption regarding the multivariate distribution of the heterogeneity. The variance of mean calculation and the bootstrapping step can be carried out by applying a particular averaging window and computing the statistics pertinent to the spatial mean. Any sequential technique for simulating continuous variables can be adopted subsequently to generate the sub-grid and coarse-scale models.

3. The results confirm that multi-scale heterogeneities contribute to anomalous transport. Non-Fickian features, such as heavy-tailed multi-peaked effluent history and early breakthrough, are observed. The rationale for adopting a Fickian RWPT transport model is that Fickian models can describe anomalous transport if uncertainty in multi-scale heterogeneities is properly integrated. This is accomplished by calibrating and sampling from a distribution of

effective dispersivity based on the Fickian model over numerous sub-grid realizations of heterogeneity.

4. In comparison to our previous study that neglected large-scale non-stationarity, the non-Fickian characteristics modeled in this work is dramatically more pronounced.

5. The decision of stationarity has significant impact on how sub-scale variability is subsequently represented at the transport modeling scale. In the absence of sub-scale variability, coarse-scale models that are generated with the proposed algorithm are identical to the fine-scale model re-gridded on a coarse mesh. As the contribution of the residual component becomes more dominant, the associated sub-scale variability would also increase, which, in turn, amplifies the uncertainty in the ensuing coarse-scale transport response.

6. It is recommended that other transport models can be employed to simulate the multi-modal effluent profiles of the sub-grid models.

References

Aronofsky, J. S., & Heller, J. P. (1957). A diffusion model to explain mixing of flowing miscible fluids in porous media. *Trans AIME, 210(12)*, (pp. 345-349).

Bear, J. (1979). *Hydraulics of groundwater.* New York: McGraw-Hill.

Becker, M. W., & Shapiro, A. M. (2003). Interpreting tracer breakthrough tailing from different forced-gradient tracer experiment configurations in fractured bedrock. *Water Resour Res, 39(1)*, 1024.

Berkowitz, B., Cortis, A., Dentz, M., & Scher, H. (2006). Modeling non-Fickian transport in geological formations as a continuous time random walk. *Reviews of Geophysics, 44(2)*.

Berkowitz, B., Scher, H., & Silliman, S. E. (2000). Anomalous transport in laboratory-scale, heterogeneous porous media. *Water Resour Res, 36(1)*, (pp. 149-158).

Bijeljic, B., Raeini, A., Mostaghimi, P., & Blunt, M. J. (2013). Predictions of non-Fickian solute transport in different classes of porous media using direct simulation on pore-scale images. *Physical Review E, 87(1)*, 013011.

Binning, P., & Celia, M. A. (2002). A forward particle tracking Eulerian–Lagrangian localized adjoint method for solution of the contaminant transport equation in three dimensions. *Adv Water Resour, 25(2)*, (pp. 147-157).

Cortis, A., & Berkowitz, B. (2005). Computing "anomalous" contaminant transport in porous media: The CTRW MATLAB toolbox. *Ground Water, 43 (6)*, 947-950.

Dagan, G. (1989). *Flow and transport in porous formations.* New-York: Springer-Verlag.

Dentz, M., Cortis, A., Scher, H., & Berkowitz, B. (2004). Time behavior of solute transport in heterogeneous media: transition from anomalous to normal transport. *Advances in Water Resources, 27(2)*, (pp. 155-173).

Deutsch, C. V. (2010). Estimation of vertical permeability in the McMurray Formation. *Journal of Canadian Petroleum Technology, 49 (12)*, 10-18.

Deutsch, C. V., & Journel, A. G. (1998). *Geostatistical software library and users guide.* New York: Oxford university press.

Di Donato, G., Obi, E. O., & Blunt, M. J. (2003). nomalous transport in heterogeneous media demonstrated by streamline-based simulation. *Geophys. Res. Lett., 30(12)*.

Dullien, F. A. (2012). *Porous media: fluid transport and pore structure.* New York : Academic press.

Fanchi, J. R. (1983). Multidimensional numerical dispersion. *SPE J, 23(1)*, (pp. 143-151).

Fernàndez-Garcia, D., & Sanchez-Vila, X. (2011). Optimal reconstruction of concentrations, gradients and reaction rates from particle distributions. *J Contam Hydrol, (120-121)*, (pp. 99-114).

Fernàndez-Garcia, D., Illangasekare, T. H., & Rajaram, H. (2005). Differences in the scale-dependence of dispersivity estimated from temporal and spatial moments in chemically and physically heterogeneous porous media. *Adv Water Resour, 28(7)*, (pp. 745-759).

Fernàndez-Garcia, D., Llerar-Meza, G., & Gómez-Hernández, J. J. (2009). Upscaling transport with mass transfer models: Mean behavior and propagation of uncertainty. *Water Resour Res, 45(10)*.

Field, M. S., & Leij, F. J. (2012). Solute transport in solution conduits exhibiting multi-peaked breakthrough curves. *Journal of hydrology, 440*, 26-35.

Field, M. S., & Pinsky, P. F. (2000). A two-region nonequilibrium model for solute transport in solution conduits in karstic aquifers. *Journal of Contaminant Hydrology, 44 (3)*, 329-351.

Fleurant, C., & Van Der Lee, J. (2001). A stochastic model of transport in three-dimensional porous media. *Math Geol, 33(4)*, (pp. 449-474).

Gelhar, L. W. (1986). Stochastic subsurface hydrology from theory to applications. *Water Resources Research, 22(9s)*, 135S–145S.

Gelhar, L. W., & Axness, C. L. (1983). Three-dimensional stochastic analysis of macrodispersion in aquifers. *Water Resour.Res, 19 (1)*, 161-180.

Gelhar, L. W., Welty, C., & Rehfeldt, K. R. (1992). A critical review of data on field-scale dispersion in aquifers. *Water Resour Res, 28(7)*, (pp. 1955-1974).

Gouze, P., Le Borgne, T., Leprovost, R., Lods, G., Poidras, T., & Pezard, P. (2008). Non-Fickian dispersion in porous media: 1. multiscale

measurements using single-well injection withdrawal tracer tests. *Water Resour Res, 44(6)*.

Gylling, B., Moreno, L., & Neretnieks, I. (1999). The channel network model—A tool for transport simulations in fractured media. *Ground Water, 37(3)*, (pp. 367-375).

Hassan, A. E., & Mohamed, M. M. (2003). On using particle tracking methods to simulate transport in single-continuum and dual continua porous media. *J Hydrol, 275(3)*, (pp. 242-260).

Itô, K. (1951). *On stochastic differential equations* (Vol. 4). Rhode Island, Rhode Island: Mem. Am. Math Soc.

Jha, R. K., Bryant, S., & Lake, L. W. (2011). Effect of diffusion on dispersion. *SPE J, 16(1)*, (pp. 65-77).

John, A. K. (2008). *Dispersion in Large Scale Permeable Media (Dissertation).* University of Texas at Austin.

John, A. K., Lake, L. W., Bryant, S., & Jennings, J. W. (2010). Investigation of mixing in field-scale miscible displacements using particle-tracking simulations of tracer floods with flow reversal. *SPE J, 15(3)*, (pp. 598-609).

Journel, A. G., & Huijbregts, C. J. (1978). *Mining geostatistics.* London: Academic press.

Käss, W. (1998). *Tracing Technique in Geohydrology.* Rotterdam, The Netherlands: A.A. Balkema.

Kinzelbach, W. (1986). *Groundwater modelling: an introduction with sample programs in BASIC* (Vol. 25). New York: Elsevier.

Kitanidis, P. K. (1988). Prediction by the method of moments of transport in a heterogeneous formation. *Journal of Hydrology, 102(1)*, 453-473.

Kitanidis, P. K. (1992). Analysis of macrodispersion through volume-averaging: Moment equations. *Stochastic Hydrology and Hydraulics, 6(1)*, 5-25.

Kreft, A., & Zuber, A. (1978). On the physical meaning of the dispersion equation and its solutions for different initial and boundary conditions. *Chemical Engineering Science*(33(11)), 1471-1480.

LaBolle, E. M., Fogg, G. E., & Tompson, A. F. (1996). Random-walk simulation of transport in heterogeneous porous media: Local mass-conservation problem and implementation methods. *Water Resour Res, 32(3)*, (pp. 583-593).

Lake, L. W., & Srinivasan, S. (2004). Statistical scale-up of reservoir properties: Concepts and applications. *J Pet Sci Eng, 44(1)*, (pp. 27-39).

Lantz, R. B. (1971). Quantitative evaluation of numerical diffusion (truncation error). *Society of Petroleum Engineers Journal, 11(03)*, (pp. 315-320).

Le Borgne, T., & Gouze, P. (2008). Non-Fickian dispersion in porous media: 2. Model validation from measurements at different scales. *Water Resour Res, 44(6)*.

Leibundgut, C., Maloszewski, P., & Külls, C. (2011). *Tracers in hydrology.* Chichester, U. K: Wiley-Blackwell.

Leij, F. J., Toride, N., Field, M. S., & Sciortino, A. (2012). Solute transport in dual-permeability porous media. *Water Resources Research, 48(4)*.

Leung, J. Y., & Srinivasan, S. (2011). Analysis of uncertainty introduced by scaleup of reservoir attributes and flow response in heterogeneous reservoirs. *SPE J, 16(3)*, (pp. 713-724).

Leung, J. Y., & Srinivasan, S. (2012). Scale-up of mass transfer and recovery performance in heterogeneous reservoirs. *J Pet Sci Eng, (86-87)*, (pp. 71-86).

Leung, J. Y., & Srinivasan, S. (2016). Effects of reservoir heterogeneity on scaling of effective mass transfer coefficient for solute transport. *J Contam Hydrol, 192*, (pp.181-193).

Levy, M., & Berkowitz, B. (2003). Measurement and analysis of non-fickian dispersion in heterogeneous porous media. *J Contam Hydrol, 64(3)*, (pp. 203-226).

Li, L., Zhou, H., & Gómez-Hernández, J. J. (2011). A comparative study of three-dimensional hydraulic conductivity upscaling at the macro-dispersion experiment (MADE) site, Columbus Air Force Base, Mississippi (USA). *Journal of Hydrology, 404(3)*, (pp. 278-293).

Li, X., Koike, T., & Pathmathevan, M. (2004). A very fast simulated re-annealing (VFSA) approach for land data assimilation. *Comput Geosci, 30(3)*, (pp. 239-248).

Mahadevan, J., Lake, L. W., & Johns, R. T. (2003). Estimation of true dispersivity in field-scale permeable media. *SPE J, 8(3)*, (pp. 272-279).

Nash, J., & Sutcliffe, J. V. (1970). River flow forecasting through conceptual models part I—A discussion of principles. *Journal of hydrology, 10(3)*, (pp. 282-290).

Neuman, S. P. (1994). Generalized scaling of permeabilities: Validation and effect of support scale. *Geophysical Research Letters, 21(5)*, (pp. 349-352).

Neuman, S. P., & Zhang, Y. K. (1990). A quasi-linear theory of non-Fickian and Fickian subsurface dispersion: 1. Theoretical analysis with application to isotropic media. *Water Resources Research, 26(5)*, 887-902.

Neuman, S. P., Winter, C. L., & Newman, C. M. (1987). Stochastic theory of field-scale Fickian dispersion in anisotropic porous media. *Water Resources Research, 23(3)*, 453-466.

Parker, J. C. (1984). Analysis of solute transport in column tracer studies. *Soil Science Society of America Journal*(48(4)), 719-724.

Parker, J. C., & Genuchten, M. T. (1984). Flux-averaged and volume-averaged concentrations in continuum approaches to solute transport. *Water Resources Research*(20(7)), 866-872.

Pedretti, D., Fernàndez-Garcia, D., Sanchez-Vila, X., Bolster, D., & Benson, D. A. (2014). Apparent directional mass-transfer capacity coefficients in three-dimensional anisotropic heterogeneous aquifers under radial convergent transport. *Water Resour Res, 50(2)*, (pp. 1205-1224).

Perkins, T. K., & Johnston, O. C. (1963). A review of diffusion and dispersion in porous media. *SPE J, 3(01)*, (pp. 70-84).

Riva, M., Guadagnini, A., Fernandez-Garcia, D., Sanchez-Vila, X., & Ptak, T. (2008). Relative importance of geostatistical and transport models in describing heavily tailed breakthrough curves at the Lauswiesen site. *J Contam Hydrol, 101(1)*, (pp. 1-13).

Rubin, Y. (2003). *Applied stochastic hydrogeology.* Oxford University Press, Oxford: UK.

Rubin, Y., Sun, A., Maxwell, R., & Bellin, A. (1999). The concept of block-effective macrodispersivity and a unified approach for grid-scale-and plume-scale-dependent transport. *Journal of Fluid Mechanics, 395*, 161-180.

Salamon, P., Fernàndez-Garcia, D., & Gómez-Hernández, J. J. (2006a). A review and numerical assessment of the random walk particle tracking method. *Journal of contaminant hydrology, 87(3)*, (pp. 277-305).

Salamon, P., Fernàndez-Garcia, D., & Gómez-Hernández, J. J. (2006b). Modeling mass transfer processes using random walk particle tracking. *Water Resour Res, 42(11)*.

Salamon, P., Fernandez-Garcia, D., & Gómez-Hernández, J. J. (2007). Modeling tracer transport at the MADE site: the importance of heterogeneity. *Water resources research, 43(8)*.

Scheidegger, A. E. (1959). An evaluation of the accuracy of the diffusivity equation for describing miscible displacement in porous media. *Proc. Theory Fluid Flow Porous Media Conf*, (pp. 101-116).

Schulze-Makuch, D., & Cherkauer, D. S. (1998). Variations in hydraulic conductivity with scale of measurement during aquifer tests in heterogeneous, porous carbonate rocks. *Hydrogeology Journal, 6(2)*, (pp. 204-215).

Schulze-Makuch, D., Carlson, D. A., Cherkauer, D. S., & Malik, P. (1999). Scale dependency of hydraulic conductivity in heterogeneous media. *Ground Water, 37(6)*, (pp. 904-919).

Srinivasan, G., Tartakovsky, D. M., Dentz, M., Viswanathan, H., Berkowitz, B., & Robinson, B. A. (2010). Random walk particle tracking simulations of non-Fickian transport in heterogeneous media. *Journal of Computational Physics, 229(11)*, (pp. 4304-4314).

Tompson, A. F., & Gelhar, L. W. (1990). Numerical simulation of solute transport in three-dimensional, randomly heterogeneous porous media. *Water Resour Res, 26(10)*, (pp. 2541-2562).

Toride, N., Leij, F. J., & Genuchten, M. T. (1993). A comprehensive set of analytical solutions for nonequilibrium solute transport with first-order decay and zero-order production. *Water Resources Research, 29 (7)*, 2167-2182.

Vishal, V., & Leung, J. Y. (2015). Modeling impacts of subscale heterogeneities on dispersive solute transport in subsurface systems. *Journal of contaminant hydrology, 182*, (pp. 63-77).

Wang, J., & Kitanidis, P. K. (1999). Analysis of macrodispersion through volume averaging: comparison with stochastic theory. *Environmental Research and Risk Assessment, 13(1-2)*, 66-84.
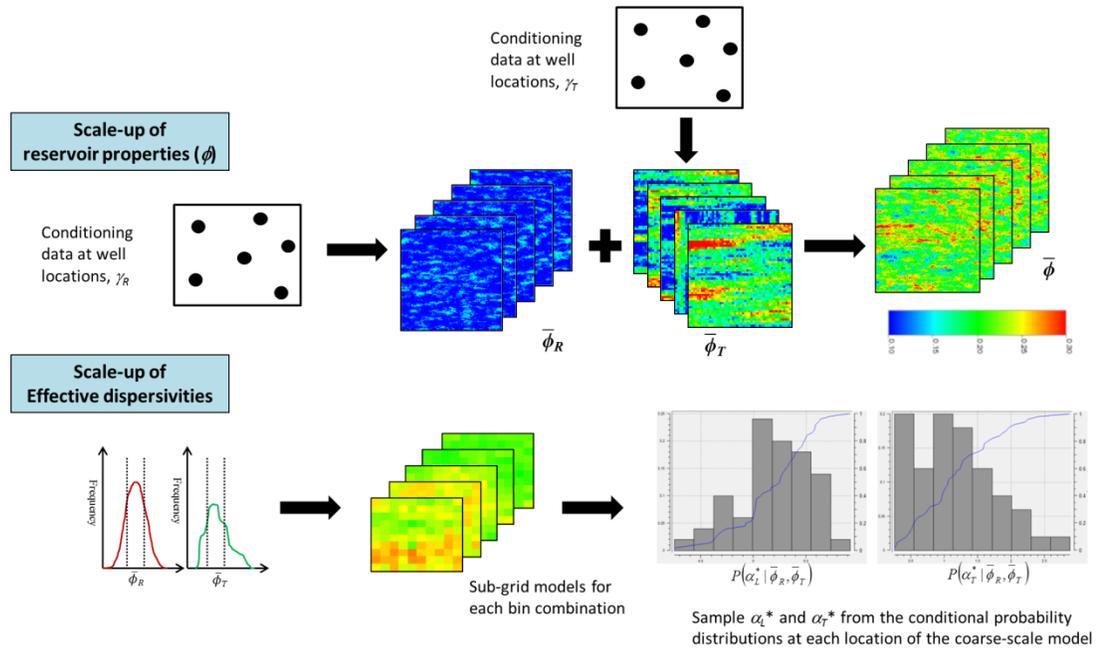
Figure 3.1: Workflow to scale up reservoir properties and transport properties.
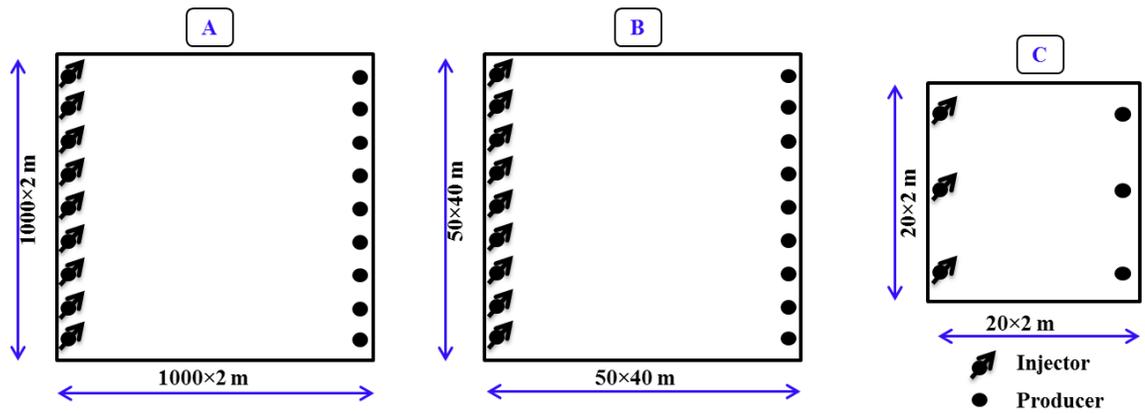
Figure 3.2: Boundary conditions and model set-up for (A) true fine-scale, (B) coarse-scale and (C) sub-grid models used in the case study.
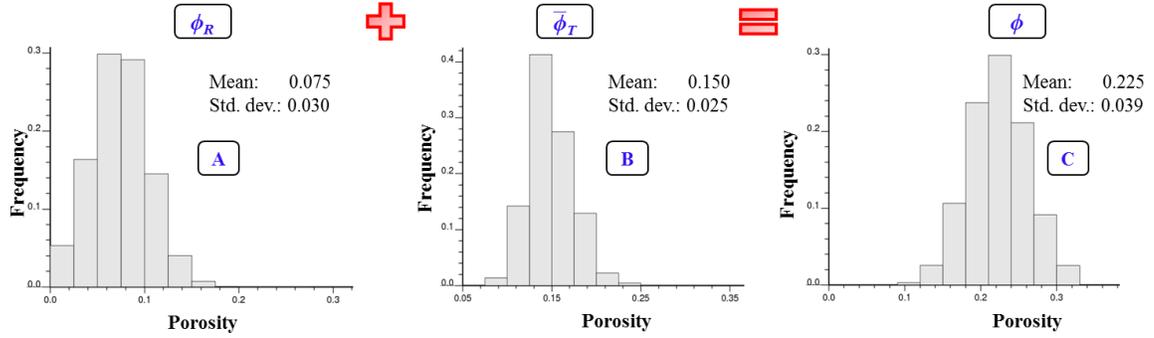
Figure 3.3: Histogram of porosity (ϕ), which is decomposed into a sum of residual component (ϕ_R in A) and trend component ($\bar{\phi}_T$ in B), at the fine scale.
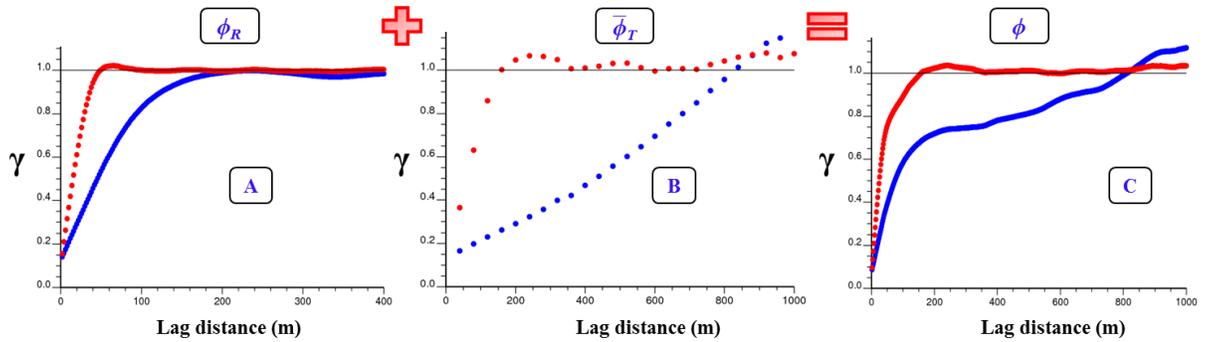
Figure 3.4: Anisotropic variogram of porosity (ϕ), which is decomposed into a sum of residual component (ϕ_R in A) and trend component ($\bar{\phi}_T$ in B), at the fine scale.
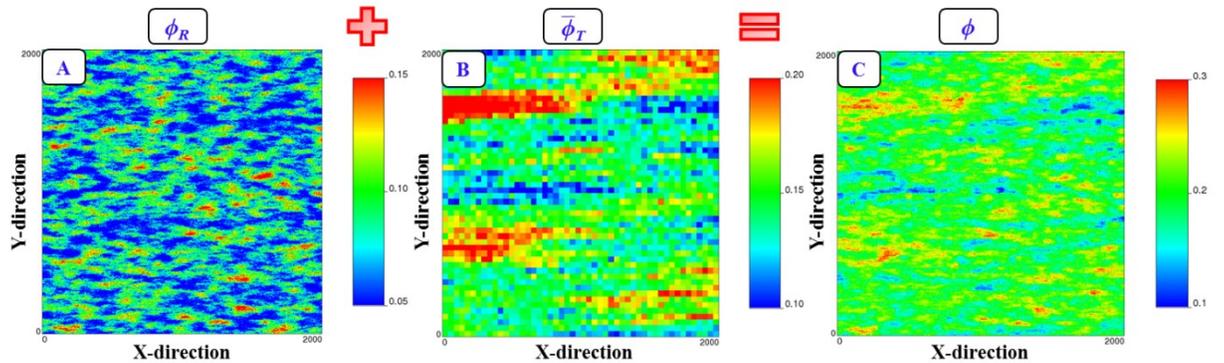
Figure 3.5: Distribution of porosity (ϕ), which is decomposed into a sum of residual component (ϕ_R in A) and trend component ($\bar{\phi}_T$ in B), for the true fine-scale model.

98
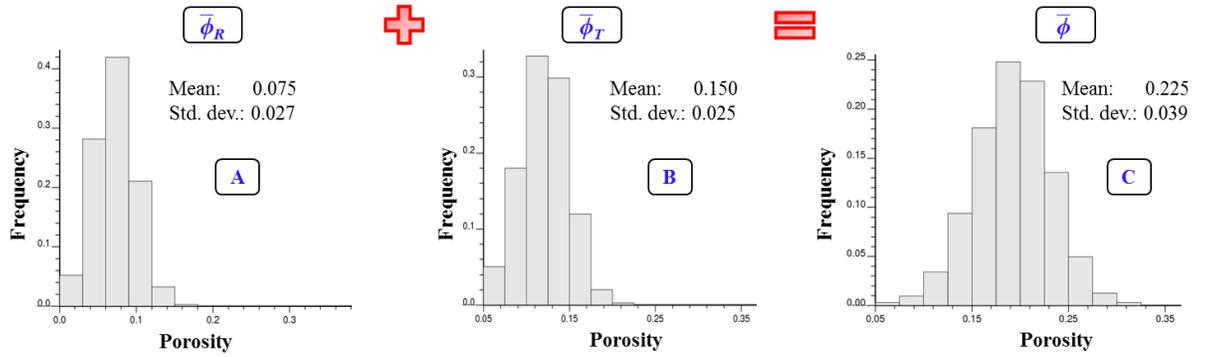
Figure 3.6: Histogram of porosity ($\bar{\phi}$), which is decomposed into a sum of residual component ($\bar{\phi}_R$ in A) and trend component ($\bar{\phi}_T$ in B), at the coarse scale or transport modeling scale.
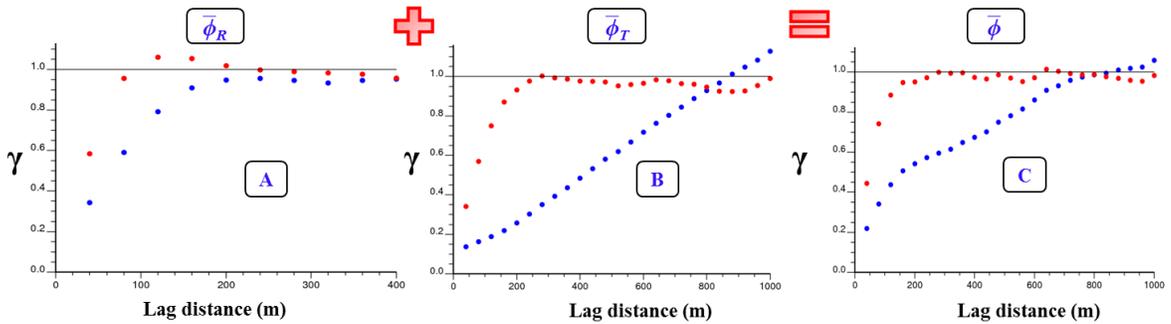
Figure 3.7: Variogram of porosity ($\bar{\phi}$), which is decomposed into a sum of residual component ($\bar{\phi}_R$ in A) and trend component ($\bar{\phi}_T$ in B), at the coarse scale or transport modeling scale.
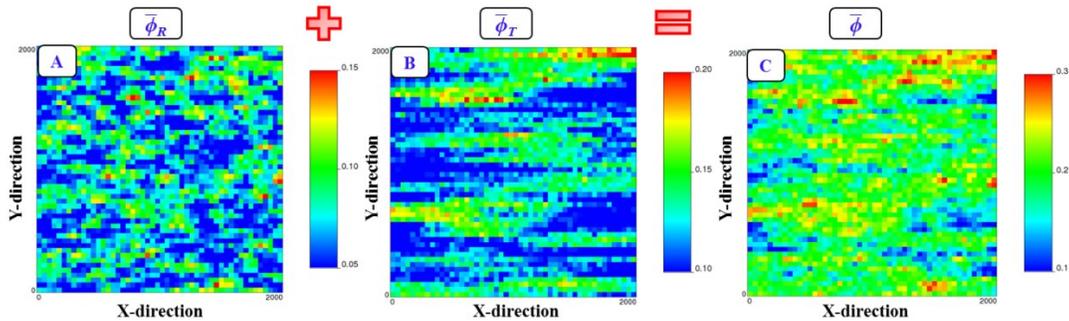
Figure 3.8: Distribution of porosity ($\bar{\phi}$), which is decomposed into a sum of residual component ($\bar{\phi}_R$ in A and trend component ($\bar{\phi}_T$ in B), for one realization at the coarse scale or transport modeling scale.
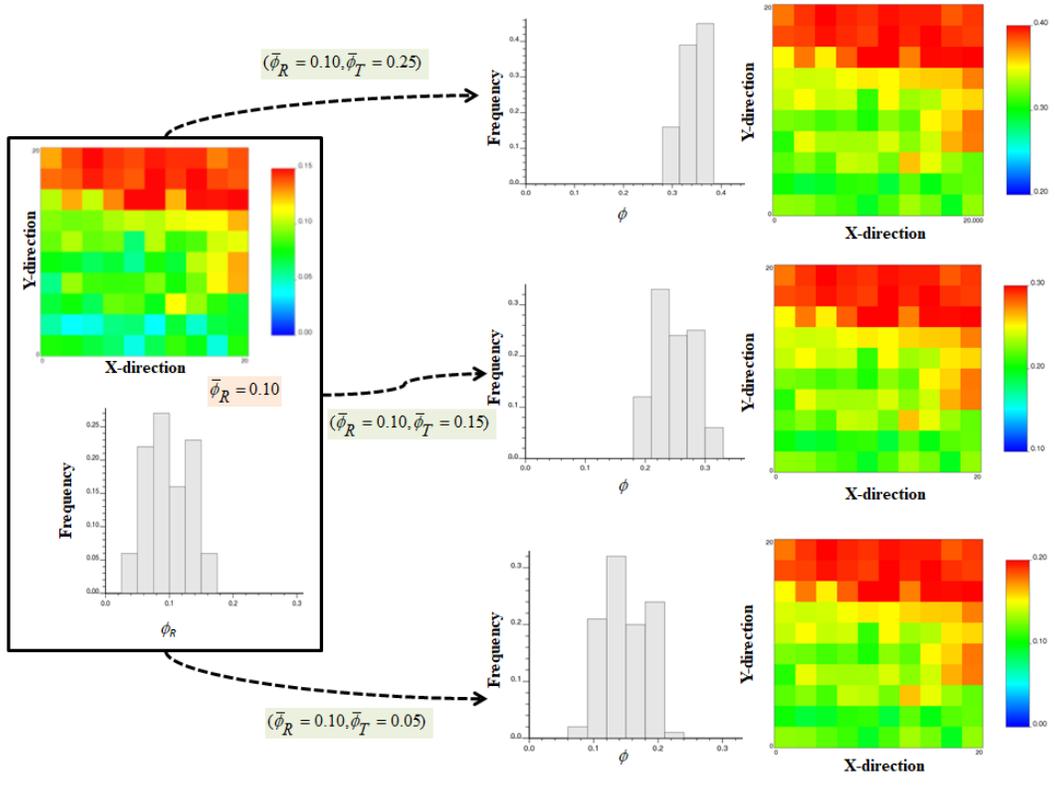
Figure 3.9: Left: a randomly-selected realization of ϕ_R corresponding to $\bar{\phi}_R = 0.1$ (top) and the corresponding histogram (bottom). Right: this realization is subsequently combined with three different values of $\bar{\phi}_T$ to generate three sub-grid realizations of ϕ such that $\phi = \phi_R + \bar{\phi}_T$. Histograms corresponding to each model of ϕ are also shown.
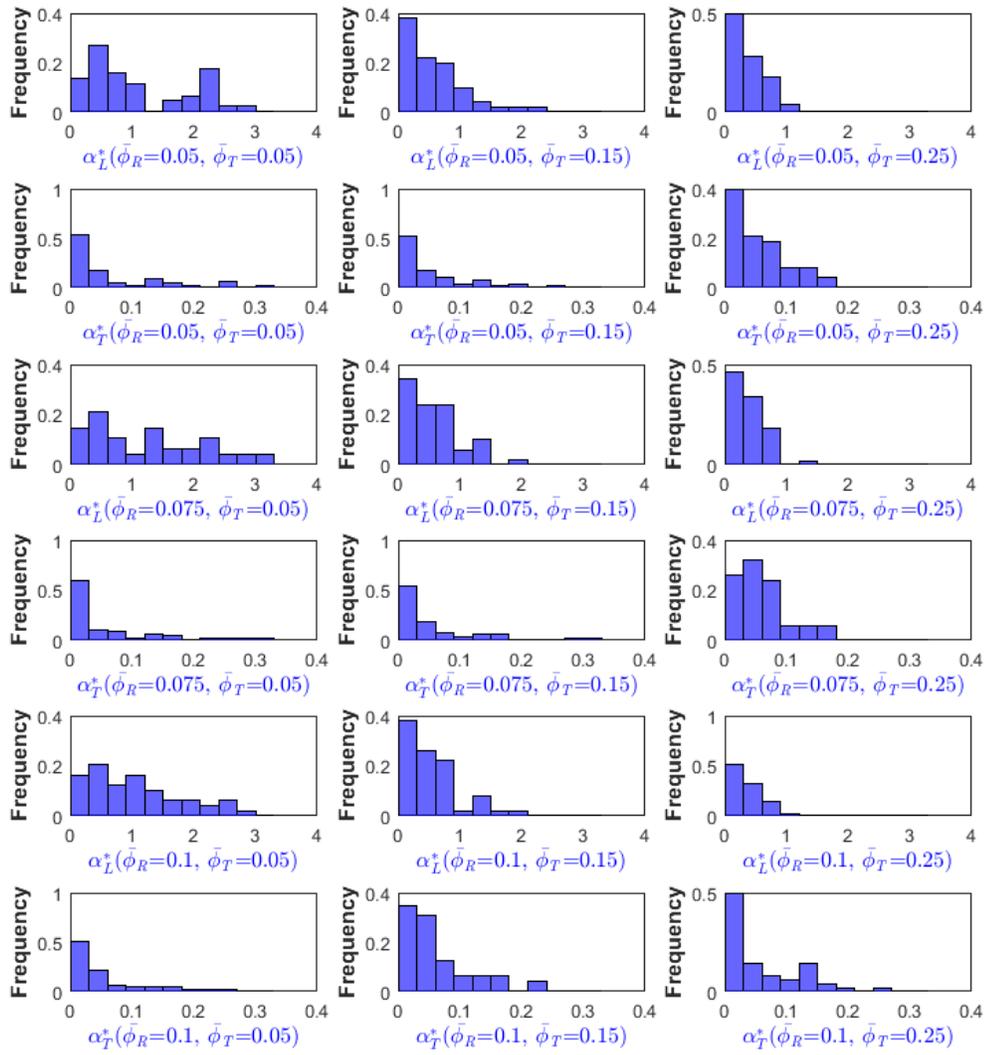
Figure 3.10: Probability distributions of effective dispersivities for different bin combinations of $\bar{\phi}_R$ (0.05, 0.075, and 0.1) and $\bar{\phi}_T$ (0.05, 0.15, and 0.25).
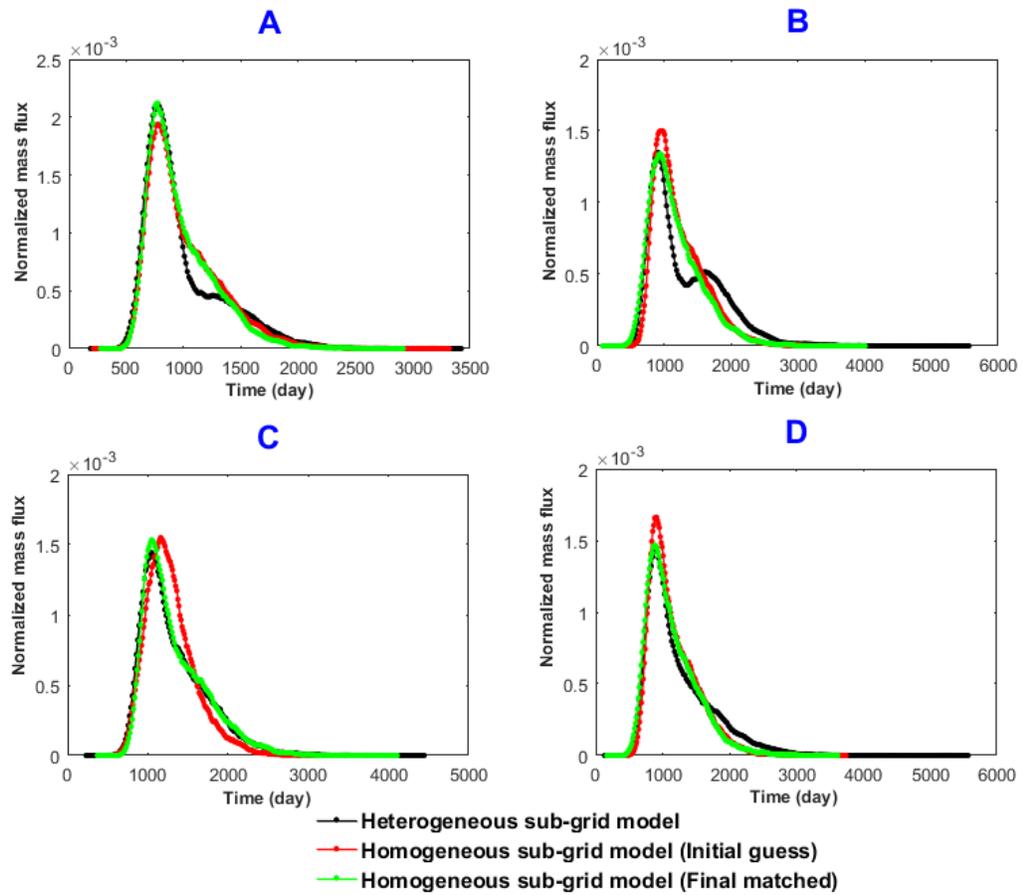
Figure 3.11: Comparison of breakthrough effluent histories between the heterogeneous and equivalent homogeneous sub-grid models. Four possible scenarios are shown.
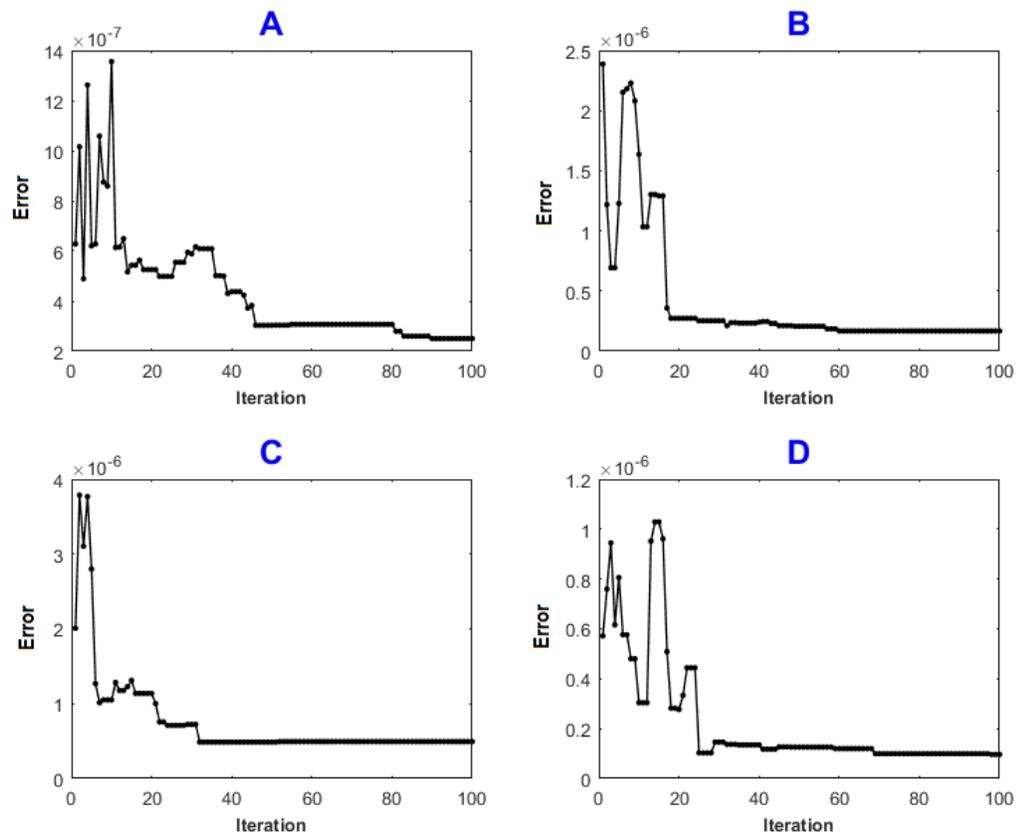
Figure 3.12: Reduction in *RMSE* corresponding to the four breakthrough effluent histories in Fig. 3.11.
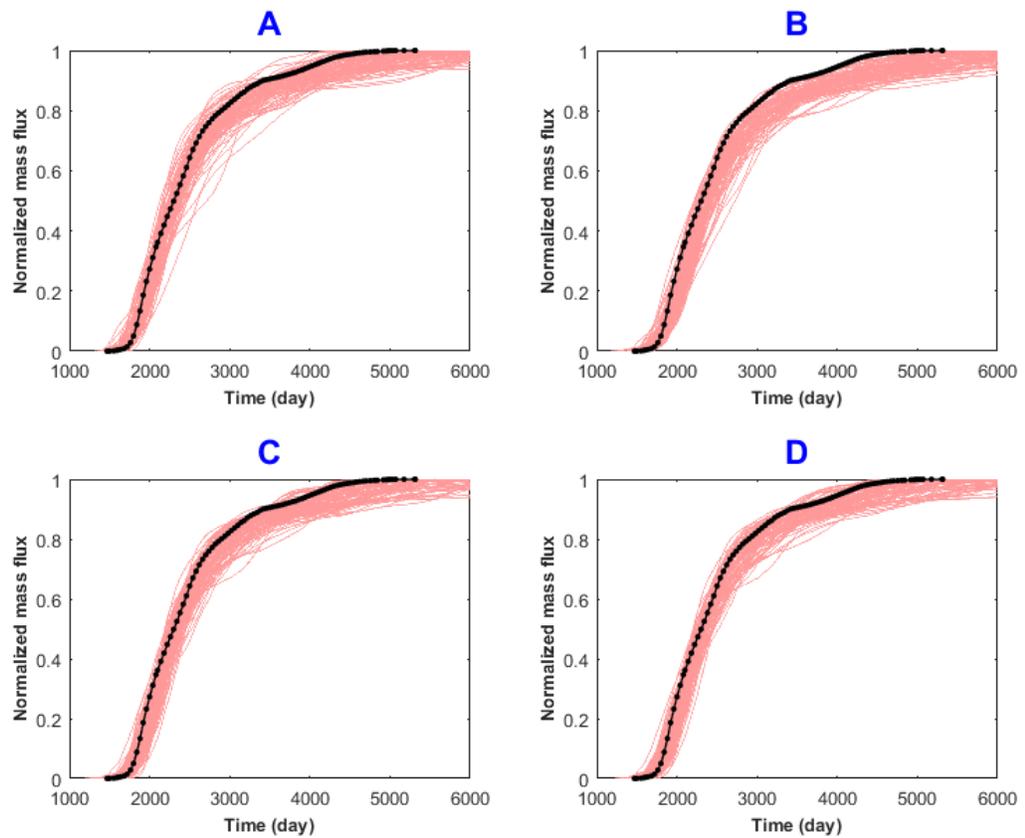
Figure 3.13: Normalized cumulative flux profiles for: (A) fully scale-up models, (B) models where no scale-up is performed, (C) models where reservoir attributes are scaled up, but scale-up of dispersivities is omitted, and (D) fully scaled-up models but with constant α_L^* and α_T^*. The black curve corresponds to the true fine-scale model.
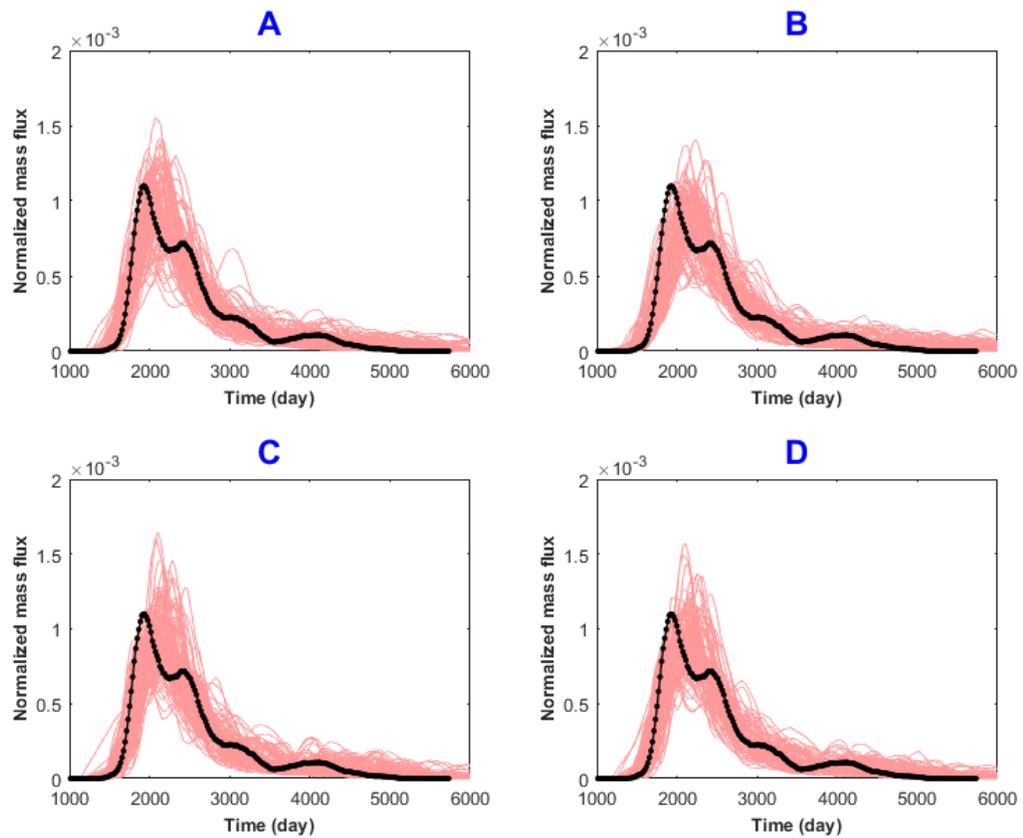
Figure 3.14: Normalized instantaneous flux profiles for: (A) fully scale-up models, (B) models where no scale-up is performed, (C) models where reservoir attributes are scaled up, but scale-up of dispersivities is omitted, and (D) fully scaled-up models but with constant α_L^* and α_T^*. The black curve corresponds to the true fine-scale model.
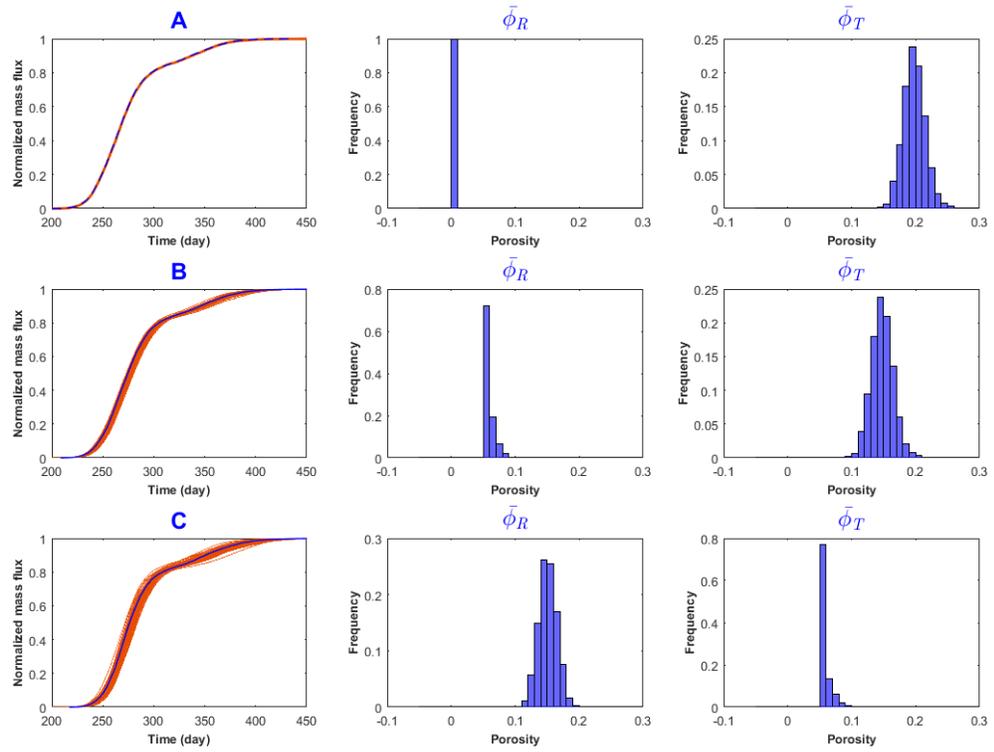
Figure 3.15: Normalized cumulative mass flux profiles (left) and histograms of $\bar{\phi}_R$ and $\bar{\phi}_T$ (middle and right) for: (A) 0% residual and 100% trend, (B) 25% residual and 75% trend, (C) 75% residual and 25% trend. The blue curve corresponds to the true fine-scale model.

Table 3.1: Computational time demand

		Number of runs	Computational time (Velocity + Transport) Calculations	Remarks
1)	Fine-scale model (1000×1000 with 2×2m grid size)	1	(540 sec + 1084 sec) = 1624 sec	
2)	Sub-grid model (20×20 with 2×2m grid size)	(50 heterogeneous models + 50 homogeneous models) x 9 $\bar{\phi}$ levels	(350 sec + 560 sec) x 9 = 8190 sec	Calculation of $P(\alpha_L{*}|\bar{\phi})$ and $P(\alpha_T{*}|\bar{\phi})$ with 100 iterations using parallel computing scheme
3)	Coarse-scale model (50×50 with 40×40m grid size)	100	(50 sec + 1057 sec) x 100 = 110700 sec	Fully scaled-up model

Chapter 4: Statistical Scale-Up of 3D Particle-Tracking Simulation for Non-Fickian Dispersive Solute Transport Modeling[3]

4.1 Introduction

Prediction of flow and mass transport in practical subsurface applications is often uncertain due to the lack of conditioning data and heterogeneity spanning over multiple scales. This uncertainty poses a number of challenges for numerical simulation. First, simulation should be conducted using numerous realizations of reservoir properties. Next, even if detailed description of the heterogeneity is available, conducting flow simulations on these types of fine-scale models requires much computational effort. A viable option is to utilize low-resolution coarsened models. As a result, both reservoir and flow/transport attributes must be scaled up properly. In addition, the loss of information due to this coarsening procedure must be quantified.

A number of transport modeling methods are available. One option to model solute transport in single-phase miscible system, including convection and spreading (diffusion and dispersion), is the Fickian advection-dispersion/diffusion equation (ADE). Pore-level mixing, as described in Dentz et al. (2011), is not considered here. Conventional discretization techniques (e.g., finite difference) may suffer various computational restrictions including artificial dispersion and

inaccurate predictions at high Péclet number (Pulloor Kuttanikkad 2009). A widely-adopted alternative is the random walk particle tracking (RWPT) approach, which is generally free from most discretization effects (Benson et al. 2017).

RWPT predictions resemble those obtained by the ADE, whose derivation involves several assumptions that lead to a classical Gaussian/Fickian transport behavior (Berkowitz et al. 2006): (1) it assumes the existence of a representative elementary volume (REV), that is, the medium is homogeneous or, at least, is described by local, averaged properties; (2) the spatial and temporal variation of the velocity field is constant inside the REV; (3) Darcy's law applies; (4) solute transport can be split into advection part and hydrodynamic dispersion part; and (5) dispersion follows the Fick's law. These assumptions essentially ignore any heterogeneity with a length scale that is smaller than the support volume on which the ADE parameters are defined. Many previous studies have examined the application and potential limitations of the ADE. For example, the resident concentration, C_r (X, t), form of the ADE gives incorrect volume-averaged concentration, if Dirichlet boundary condition is combined for pulse injection. However, flux-weighted concentration, C_f (X, t), form of the ADE gives correct flux-averaged concentration for Dirichlet boundary condition (Kreft and Zuber 1978; Parker 1984; Parker and Genuchten 1984).

However, anomalous (or non-Fickian) behavior, which is characterized by long-tailed effluent history and early breakthrough, is often observed in heterogeneous media, rendering the presence of dispersion to be scale dependent

(Gelhar et al. 1992). This dependency on scale is widely concluded to be the outcome of preferential flow paths due to multi-scale heterogeneity; examples include trapping of solute particles in microscopic stagnant pores or diffusion-dominated regions (Neretnieks et al. 1982) and dramatic difference in permeability in fractured formations (Berkowitz and Scher 1997; Geiger et al. 2010). Moreover, boundary conditions such as convergent radial flow around sources may also introduce anomalous behavior (Pedretti et al. 2014).

The main challenge with using the classical deterministic ADE to capture anomalous behavior is that unresolved heterogeneities is not properly captured (Jha et al. 2011). It does not account for any additional spreading that has taken place due to unresolved heterogeneity below the volume scale of the ADE model. It is true that the ADE should reflect anomalous behavior correctly if heterogeneities are characterized explicitly at all scales (Li et al. 2011). In order to incorporate the uncertainty in heterogeneity distribution and its effect on solute transport, the classical ADE can be generalized to derive non-local formulations in space and/or time following a stochastic framework; examples include the fractional ADE (fADE), multiple-rate mass transfer (MRMT), and the continuous-time random walk (CTRW) approach (Berkowitz and Scher 1995; Haggerty and Gorelick 1995; Metzler and Klafter 2000), which are based on the generalized master equation (Kenkre et al. 1973), or the particle-tracking method that is based on the generalized Langevin equation (Srinivasan et al. 2010). For this particular study, the latter approach is implemented. It is essentially a hybrid particle-based CTRW formulation, where the transit time step, instead of being

deterministic of fixed duration (as in RWPT), is sampled from a probability density distribution. No specific assumption (e.g., stationarity) regarding the distributions of the transition length and time is needed (Srinivasan et al. 2010). This formulation, as compared to CTRW, offers a convenient alternative to incorporate force fields and other boundary conditions (Metzler and Klafter 2000).

Beyond the choice of transport modeling method, the next step for performing coarse-scale simulations is to scale up the relevant transport properties. The above discussion assumes that transport modeling is performed at the finest resolution of heterogeneity (any unresolved heterogeneities below this scale will be incorporated in the formulation of the probabilistic transition time). However, transport modeling is often performed at a scale that is coarser than the finest resolution of heterogeneity. Two modeling scales are referred to in this chapter:

- "Fine scale" denotes a scale over which detailed model of heterogeneity is defined (typically on the order of centimeter, over which core and log measurements are available).

- "Coarse scale" denotes the transport modeling scale, over which numerical flow and transport simulation is performed (typically on the order of meter).

A number of techniques have been described in the literature for computing the effective coarse-scale dispersivity, and these techniques can be generally classified into two groups: (1) ensemble averaging or stochastic perturbation (based on ensemble moments) and (2) volume averaging (based on spatial

moments). In the ensemble averaging framework, an effective dispersivity is estimated from statistical moments (Gelhar 1986; Kitanidis 1988; Dagan 1989; Neuman and Zhang 1990; Rubin 2003). This method is useful provided that permeability distribution (e.g., covariance structure) can be well defined (Rubin et al. 1999). In the volume averaging framework, spatial moments, instead of ensemble moments, are employed. An important requirement is that a representative elementary volume (REV) for the heterogeneity length scale must be defined (Leung and Srinivasan 2016). Therefore, periodic media is often used (Kitanidis 1992). In theory, if the restriction on the heterogeneity length scale and the assumption of ergodicity are satisfied, both techniques are essentially equivalent (Wang and Kitanids 1999).

In this work, a statistical workflow is devised to facilitate the representation of uncertainty as a result of scale-up in coarse-scale models. The general workflow is an extension to the one presented in Vishal and Leung (2015; 2017); however, this work offers two important improvements. First, to account for any heterogeneity below the fine scale, a hybrid particle-based CTRW formulation is implemented such that the transition time is drawn randomly from a distribution. Certain elements of the proposed method are similar to many existing hierarchical CTRW formulations for modeling multi-scale heterogeneities. However, the main difference is that it does not impose any specific length scale requirement regarding the sub-grid heterogeneity. For instance, it is assumed in Cortis et al. (2004) that, other than the unresolved heterogeneity below the fine scale, any additional heterogeneity is exhibited at a

scale much larger than the transport modeling scale. A rigorous hierarchical procedure was also presented in Rhodes et al. (2008) to scale up the transition time distribution sequentially over multiple scales; a deterministic distribution is achieved after every upscaling step, which is valid where there is a distinct separation of heterogeneity length scales. The method proposed here aims to capture the effects of heterogeneity at the intermediate scale, which is often comparable to the transport modeling scale. In particular, it couples the scale-up workflows for both reservoir and transport parameters.

Though some preliminary results have been included in Vishal and Leung (2017), the modeling procedure has not been fully validated and was limited to 2D. In this work, a comprehensive comparison with the analytical solution and CTRW is presented. In addition, the effect of gravity in a 3D model is examined. The method may handle a diverse range of heterogeneity distribution, in that it does not invoke any explicit assumption regarding the multivariate distribution of the heterogeneity; it utilizes the theory of volume variance (Lake and Srinivasan 2004), which can be computed directly from data or a given variogram (γ) model. Without imposing that the averaging scale must be larger than the length scale of local heterogeneity, the idea is to quantify and transfer the uncertainty in scale-up into the variability exhibited by the coarse-scale models (Leung and Srinivasan 2011, 2012). The main contribution is that it offers a hierarchical approach, such that heterogeneity at multiple scales is properly represented to the transport modeling scale. The significance of capturing directly the uncertainty in effective transport properties is examined.

The organization of this chapter is as follows: mathematical detail of the particle-based CTRW formulation is outlined. Next, the proposed scale-up method and a synthetic case study are described. They are followed by discussions and conclusions.

4.2 Particle-Based CTRW Formulation

The Fickian-based ADE is described by Eq. (4.1) (Bear 1979):

$$\frac{\partial c(\boldsymbol{X},t)}{\partial t} = \nabla \cdot (\boldsymbol{D}\nabla c(\boldsymbol{X},t)) - \nabla \cdot (\boldsymbol{V}c(\boldsymbol{X},t)). \tag{4.1}$$

$c(\boldsymbol{X}, t)$ denotes the solute concentration as a function of spatial coordinates ($\boldsymbol{X}$) and time (t). $\boldsymbol{V}$ is the superficial velocity, and $\boldsymbol{D}$ denotes the dispersion tensor. The velocity field is calculated according to the continuity equation, Eq. (4.2), for a steady-state incompressible system and the Darcy law, which is shown in Eq. (4.3):

$$\nabla \cdot \boldsymbol{V} = 0. \tag{4.2}$$

$$\boldsymbol{V} = -\frac{\boldsymbol{k}}{\mu}(\nabla p - \rho \boldsymbol{g}). \tag{4.3}$$

$\boldsymbol{k}$, μ, and p denote the permeability, viscosity, and pressure, respectively. To solve this set of equations in the particle-tracking framework, representative walkers (particles) of identical mass are injected; over a specified time step (Δt), the displacement of each particle is computed by the sum of a drift term (advection) and a dispersion/diffusion term (according to Eq. 4.4) (Delay et al. 2005):

$$X_p(t + \Delta t) = X_p(t) + A[X_p(t)]\Delta t + B[X_p(t)]\xi(t)\sqrt{\Delta t}.$$

$$A = V + \nabla D,\ BB^T = 2D.$$

(4.4)

$X_p(t)$ is the particle position at time t; ξ is an independent random normal deviate with a zero mean and a variance of one. The key difference between RWPT and CTRW lies in the distribution of Δt. In this work, a hybrid formulation was proposed by Srinivasan et al. (2010) based on the Langevin equation, in which Δt is assumed to be random (stochastic):

$$X_p(\tau + \Delta \tau) = X_p(\tau) + A[X_p(\tau)]\Delta \tau + B[X_p(\tau)]\xi(\tau)\sqrt{\Delta \tau}.$$

$$t(\tau + \Delta \tau) = t(\tau) + \eta(\tau, \Delta \tau).$$

(4.5)

Transition length, ξ, and transition time, η, are sampled from their joint probability density function (pdf). In the above framework, time steps are sampled from transition time pdf and implicitly incorporated. The general modeling framework is adopted from a popular and well established random-walk particle-tracking algorithm called RW3D-MRMT (Fernàndez-Garcia et al. 2005; Salamon et al. 2006a, 2006b; Fernàndez-Garcia and Sanchez-Vila 2011; Salamon et al. 2007; Riva et al. 2008). Given that RW3D-MRMT is not compatible with probabilistic time steps, to sample random time steps, TPL distribution, which requires three parameters β, t_1, and t_2 to define, is included in the modified version of the RW3D-MRMT code in this work. Since β, t_1, and t_2 command the transport migration and are expected to vary spatially, they are treated in the same fashion as in the case for dispersivity, which is a location- or cell-dependent variable. With the use of random time steps, this hybrid formulation is identical to the general CTRW formulation. The main Fokker-Planck with memory equation

(FPME) is presented below, whose equivalency with the classical Generalized Master has been established by Berkowitz et al. (2002). The transition position (X) and transition (or waiting) times (t) are coupled by a joint pdf, $\psi(X, t)$:

$$s\widetilde{c}(X,s) - c_o(X) = -\widetilde{M}(s)\big(V \cdot \nabla\widetilde{c}(X,s) - \nabla \cdot (D\nabla\widetilde{c}(X,s)\big), \qquad (4.6)$$

The tilde "~"denotes the Laplace space, and $c_o(X)$ refers to the initial condition. D and V are the dispersion tensor and the transport velocity, respectively. They are defined by the second and first moments of the transition length, $p(X)$, which is often assumed to be Gaussian:

$$v_i = \frac{1}{t_1}\int_{\mathfrak{R}} p(X)X_i dX = \frac{1}{t_1}\sum_X X_i p(X).$$
$$D_{ij} = \frac{1}{2t_1}\int_{\mathfrak{R}} p(X)X_i X_j dX = \frac{1}{2t_1}\sum_X X_i X_j p(X). \qquad (4.7)$$

v_i is the component of V along direction i. t_1 is the lower cut-off time. $\widetilde{M}(s)$ is the memory function, which is the key for representing any unresolved heterogeneity below the model resolution:

$$\widetilde{M}(s) = \frac{st_1\widetilde{\varphi}(s)}{1-\widetilde{\varphi}(s)}. \qquad (4.8)$$

Eq. (4.6) is obtained by decoupling the joint probability density function $\psi(X, t)$ with the Laplace transform:

$$\widetilde{\psi}(X,s) = p(X)\widetilde{\varphi}(s). \qquad (4.9)$$

$\widetilde{\varphi}(s)$ is the Laplace transform of the pdf of the transition time, $\varphi(t)$. The formulation of $\varphi(t)$ represents the heart of the CTRW method, as it is used to calculate the memory equation and characterizes the nature of the solute transport.

Possible choices for $\varphi(t)$ may include the truncated power law (TPL) model (Eq. 4.10), and the modified exponential model (Eq. 4.11) (Cortis et al. 2004).

$$\varphi(t) = \frac{(1 + t/t_1)^{-1-\beta}}{t_1 r^\beta \Gamma(-\beta, r)} e^{\left(-\frac{t_1 + t}{t_2}\right)}, r = \frac{t_1}{t_2}, t_1 < t_2, 0 \le \beta \le 2. \qquad (4.10)$$

$$\varphi(t) = \frac{1}{t_1} e^{\left(-\frac{t}{t_1}\right)}. \qquad (4.11)$$

The exponent β controls the migration of the transport particles; t_2 is the upper cut-off time, and Γ is the incomplete Gamma function (Dentz et al. 2004; Cortis et al. 2004). The TPL model, which is parameterized by β, t_1, and t_2, is quite versatile for characterizing a wide range of transport behavior. For example, the TPL converges to the asymptotic model for large value of t_2. On the other hand, β controls the transition between non-Fickian to Fickian behavior, and, as a result, it varies as a function of heterogeneity. Three regimes of transport can be characterized based on β values. When $\beta > 2$, the TPL-CTRW model is reduced to the ADE. It yields the classical Fickian behavior, which can also be achieved with the exponential model, where the center of mass travels at the mean fluid velocity (Margolin et al. 2003; Gao et al. 2009). For $1 < \beta < 2$, the center of mass travels with a constant velocity, but the breakthrough profiles are asymmetric with heavy tails at late times; as β increases, the breakthrough profiles become less dispersed. For $0 < \beta < 1$, the breakthrough profiles display the most anomalous characteristics. It should be noted that non-Fickian behavior is observed for $t_1 \le t \le t_2$ and $0 < \beta < 2$, but the transport behavior becomes Fickian again for $t \ge t_2$.

This hybrid particle-based CTRW model is validated against the general CTRW method. For a 1D porous medium with homogeneous properties and the following conditions (Kreft and Zuber 1978):

Boundary conditions: $c(X_1 = 0, t) = c_o$ and $c(X_1 = L, t) = 0.$ (4.12)

Initial conditions: $c(X_1, t = 0) = 0.$ (4.13)

The analytical solution for the flux-average concentration (c_f) in the Laplace form is:

$$\tilde{c}_f(X_1, s) = c_o \exp\left[-\frac{vX_1}{2D_L}\left\{\sqrt{1 + 4\frac{sD_L}{\tilde{M}(s)v^2}} - 1\right\}\right].$$ (4.14)

$D_L = \alpha_L v$ is the longitudinal dispersion coefficient, where α_L denotes the longitudinal dispersivity. Solutions of the particle-tracking model are verified against Eq. (4.14), as implemented in the CTRW MATLAB toolbox (Cortis and Berkowitz 2005; Cortis et al. 2010). A total of 10^4 particles with fluid velocity (v) = 0.0342 km/yr; α_L = 0.5 km; α_T = 0 km (since, it is 1D model); $t_1 = 2.84 \times 10^{-2}$ yr, $t_2 = 4.44 \times 10^4$ yr; β = 1.35 are used. The ensuing break-through profiles corresponding to the Fickian model using Eq. (4.11) and the non-Fickian model using Eq. (4.10) are compared in Fig. 4.1. To test the particle-tracking formulation with the TPL model in higher dimensions, numerous layering configurations are examined in Fig. 4.2.

Next, sensitivity of the TPL parameters (β, t_1, and t_2) on the anomalous behavior is examined. Fig. 4.3 presents the temporal flux-weighted mass profiles and the corresponding cumulative profiles for several values of β. As expected, as β decreases, the temporal mass profiles exhibit longer tail and later breakthrough.

To compare with the analytical solution of ADE, the spatial volume-averaged mass profiles for several values of β are compared with the exponential model and the ADE method in Fig. 4.4. The results confirm that the exponential and ADE models are analogous. In addition, the concentration at the inlet, $X_I = L = 0$, increases with decreasing β, corresponding to larger residence times in a boundary cell. The consequence of larger residence time is that a particle is transported at a slower rate and taking longer to reach the outlet; as a result, more tailing characteristic can be observed as β decreases.

4.3 Construction of Coarse-Scale Models

Mathematical formulation of a multi-scale workflow for constructing models of reservoir properties and effective dispersivities and truncated power law parameters β^*, t_1^*, and t_2^* at the transport modeling (coarse) scale for particle-tracking simulation is presented next.

4.3.1 Coarse-Scale Reservoir Properties

Sub-scale variability refers to the uncertainty introduced due to the averaging of heterogeneous properties at the modeling scale. Reservoir attributes, such as porosity and permeability, are typically modeled as random variables; therefore, their spatial averages are also random variables. In this chapter, only distributions with first and second moments are considered. The variance of mean for a certain attribute represents the variability of its spatial average at that particular spatial volume V. This variance would decrease with increasing V, if the multivariate

distribution of this attribute is stationary. In fact, the log-log plot of this variance as a function of V would reach a constant negative unit slope, where $V \geq \text{REV}$, indicating that sub-scale variability is no longer important (Bear 1979). For a scalar continuous random variable (Z), the corresponding spatial mean $\overline{Z}$ over a volume support V is defined as:

$$\overline{Z} = \left[\frac{1}{V} \int_V (Z)^\omega dV \right]^{1/\omega} \tag{4.15}$$

There is no need to invoke any explicit assumption of the multivariate distribution of Z; the spatial averages of Z for different sizes of V can be calculated according to Eq. (4.15) using an averaging window of different sizes, and the variance in the spatial mean is readily computed. In fact, different choice of ω would result in different averaging schemes; for example, $\omega = 1$ corresponds to an arithmetic average, whereas $\omega = -1$ for harmonic average. In the special case of Z following a Gaussian distribution with a variance σ^2 and a second-order stationary spatial correlation function ρ_{corr}, one can integrate ρ_{corr} over all lag distances (η) within V according to Eq. (4.16) (Lake and Srinivasan 2004), which assumes that linear averaging (i.e., $\omega = 1$) applies.

$$Var(\overline{Z}) = \frac{2\sigma^2}{V^2} \left(\int_V \int_\eta \rho_{corr}(\eta) d\eta d\xi \right). \tag{4.16}$$

ξ is the position vector that is to be integrated over the entire averaging volume of V. In most cases, the volume support for the conditioning data is less than that of the modeling scale, bootstrapping is used to sample multiple sets of conditioning data, in order to represent the sub-scale variability (Leung and Srinivasan 2011).

For instance, a parametric bootstrapping scheme can be formulated to sample from a distribution, whose mean is the average of measured data values over the coarse-scale volume and the variance being the variance of mean. If Gaussian statistics is applicable, a Gaussian distribution can be assumed. In such cases, conditional simulation can be performed using a linearly-averaged $\bar{\gamma}$ according to Eq. (4.17) (Journel and Hujbregts 1978). V and V' refer to the two support volumes, and Eq. (4.17) can be approximated numerically from the point-scale values of γ at various regularly-spaced intervals, where $\mathbf{h}_{ij}$ is the lag distance between locations i and j.

$$\bar{\gamma}(V,V') = \frac{1}{VV'} \int_V \int_{V''} \gamma(v,v')dvdv' \approx \frac{1}{nn'}\sum_{i=1}^{n}\sum_{j=1}^{n'}\gamma\left(\mathbf{h}_{ij}\right) \tag{4.17}$$

A statistical scale-up procedure from Leung and Srinivasan (2011) is adopted to construct realizations of $Z(\mathbf{x})$ at the model scale.

1. Estimate γ. Compute $Var(\bar{Z})$ and $\bar{\gamma}$ based on Eqs. (16) and (17).

2. Apply parametric bootstrapping to sample multiple conditioning data sets of $\bar{Z}(\mathbf{x})$ at the coarse scale. For instance, a Gaussian function can be used, where the mean is the average of measured data values over the coarse-scale block, while the variance is equal to the variance of mean.

3. For each of the conditioning data sets, perform conditional simulation and construct realizations of $\bar{Z}(\mathbf{x})$ at the modeling scale using $\bar{\gamma}$ and the coarse-scale histogram, whose mean is the same as the global mean of $Z(\mathbf{x})$, but the variance is equal to $Var(\bar{Z})$.

If the random variable does not follow Gaussian statistics, other sequential techniques for simulating continuous variables can be applied to generate the coarse-scale models. Instead of the variogram formulation, alternative multivariate statistics description can be adopted. In this chapter, absolute permeability (k) is assumed to be precisely correlated to porosity: $k = a \times \phi^b$, (a and b are calibrated constants). Therefore, linearly averaging is also applicable with the following transform: $(k/a)^{1/b}$; the implication is that the correlation is scale invariant. In principle, a flow-based procedure, as described in the next section, can also be employed to scale up permeability.

4.3.2 Coarse-Scale Parameterization of Transition Time Distribution

The idea is to represent sub-scale variability in effective transport parameters with probability distributions. A modification is introduced to the workflow originally presented in Vishal and Leung (2015). The main limitation of the previous work is that an ADE-based RWPT transport model in 2D was used, such that the workflow was suitable for scaling up effective dispersivities only. Therefore, the objective here is to extend the procedure to construct parameters of the coarse-scale transition time distributions (i.e., β^*, t_1^*, t_2^*) in 3D. The steps are described as follow:

1. Divide the histogram of $\overline{\phi}$ into n_b bins.

2. For each bin, generate n_s unconditional sub-grid realizations of $\overline{\phi}$. If ϕ follows Gaussian statistics, variogram γ, together with a histogram consisting of mean = $\overline{\phi}_b$ and variance = σ^2 can be used.

3. For each of the n_s sub-grid models, create an averaged homogeneous model.

4. Simulate flow and transport for all models from the last two steps.

5. Estimate β^*, t_1^* and t_2^* by minimizing the mismatch in effluent history between the sub-grid models in step #2 and the equivalent averaged models in step #3.

6. Collect the results for all bins to construct $P\{\beta^* | \bar{\phi}_i\}, P\{t_1^* | \bar{\phi}_i\}$, and $P\{t_2^* | \bar{\phi}_i\}$ for $i = 1,...,n_b$.

7. Values of β^*, t_1^* and t_2^* are assigned to each coarse-scale model constructed in section 4.3.1. At each location, sample β^*, t_1^* and t_2^* from $P\{\beta^* | \bar{\phi}\}, P\{t_1^* | \bar{\phi}\}$, and $P\{t_2^* | \bar{\phi}\}$, respectively.

The workflow for sections 4.3.1 and 4.3.2 are illustrated in Fig. 4.5. Once again, if the random variable does not follow Gaussian statistics, alternative multivariate statistics description can be adopted to construct the sub-grid realizations.

4.4 Case Study

A synthetic three-dimensional model of size 500 m × 500 m × 15 m ($\Delta x = \Delta y = \Delta z = 1$ m) is considered. In this example, it is assumed that the "true" 500 m × 500 m × 15 m model is known. Two wells, which are perforated in layers 6 (numbering starts from the top) through 10, are place at the opposite corners diagonally. It is assumed that fine-scale porosity (ϕ) values at a resolution of 1 m are extracted from physical measurements at the well locations, and $\phi \sim N(0.25,$

0.07). The corresponding histogram and anisotropic (spherical) variograms are shown in Fig. 4.6(A) and Fig. 4.7(A), respectively. The true model of ϕ at the fine scale is also shown in Fig. 4.8(A). ϕ ranges from 0.05 to 0.35 (with a global mean of 0.25). As mentioned in section 4.3.1, k (md) is modeled as $25{,}000 \times \phi^2$ (it ranges between 81 mD and 3060 mD, with a mean of 1570 mD). In addition, longitudinal dispersivity α_L is set to be 1.0 m, with horizontal transverse dispersivity $\alpha_T = 0.1 \times \alpha_L$ and vertical transverse dispersivity $\alpha_V = 0.01 \times \alpha_L$ (Perkins and Johnston 1963; Gelhar et al. 1992). To define the anomalous transport, the TPL model is used: β, t_1, and t_2 are set to be 4 yr, 10^4 yr, and 1.25, respectively.

Considering that a model of $500 \times 500 \times 15$ would be too computationally inefficient, a set of $50 \times 50 \times 3$ models ($\Delta x = \Delta y = 10$ m and $\Delta z = 5$ m) will be constructed. The workflow described in section 4.3.1 is adopted to scale up porosity and permeability. A normalized variance of mean of 0.66 is obtained based on Eq. (4.15), and $\bar{\gamma}$ are calculated based on Eq. (4.16). The corresponding coarse-scale histograms and variograms are presented in Fig. 4.6(B) and Fig. 4.7(B), respectively. Next, 10 sets of conditioning data of ϕ are sampled according to step #2 in section 4.3.1. Conditional sequential Gaussian simulation (Deutsch and Journel 1998) is implemented to generate 10 realizations of $\bar{\phi}$ for each conditioning data set, as described in step #3 in section 4.3.1. In the end, a total of $10 \times 10 = 100$ realizations of $\bar{\phi}$ are available. As an example, a randomly-selected realization is shown in Fig. 4.8(B). Comparing Fig. 4.8(B) with Fig.

4.8(A), the coarse-scale realization is much smoother, since $Var(\bar{\phi}) < Var(\phi)$ and the ranges in the $\bar{\gamma}$ model are larger than those in γ.

The workflow described in section 4.3.2 is implemented to scale-up t_1, t_2, and β. The histogram in Fig. 4.6(B) is divided into three bins, corresponding to $\bar{\phi}$ = 0.15, 0.25, and 0.35. Fifty sub-grid (10 × 10 × 5 with $\Delta x = \Delta y = \Delta z = 1$ m) realizations are constructed for each bin. A sample realization corresponding to $\bar{\phi}$ = 0.25 is shown in Fig. 4.8(C); its histogram is also shown in Fig. 4.6(C). As expected, the statistics of this sub-grid model should be identical to those of the fine-scale model. Next, each sub-grid realization is subjected to particle-tracking modeling: an injector and a producer are placed diagonally across the domain. Effective parameters of β^*, t_1^* and t_2^* are estimated by minimizing the differences in the breakthrough concentration profiles, as shown in Fig. 4.9, using a very fast simulated annealing (VFSA) scheme (Li et al. 2004). Fig. 4.10 confirms that it is impossible to match the effluent history of the heterogeneous model with an equivalent sub-grid homogeneous model, if a Fickian RWPT transport model is used (i.e., using a constant transition time and tuning only effective dispersivities α^*). This conclusion corroborates with those in Ferreira and Pinto (2014 and 2015), who also reported that the classical ADE model does not capture the long tail of the breakthrough profile at late times. Finally, probability distributions of β^*, t_1^*, and t_2^* are established. An example corresponding to bin-mean $\bar{\phi}$ = 0.25 is shown in Fig. 4.11 (3rd row). Three additional cases are also considered: (1) only scale-up of β is considered, (2) only scale-up of β and t_1 are considered, and (3) scale-up of α_L, α_T and α_V are considered for Fickian model (constant transition

time). The objective is to assess the sensitivity of coarse-scale model predictions to the scale-up of different parameters. Therefore, the corresponding probability distributions are also shown in Fig. 4.11.

4.5 Results and Discussions

The workflow presented in the previous sections has facilitated the model construction for all four coarse-scale parameters: α^* β^*, t_1^* and t_2^*. However, theses parameters are conventionally estimated from effluent histories indirectly; this inverse problem is inherently ill-posed, and the sensitivity of these parameters is not clearly defined, allowing all four parameters and the type of model (ADE vs. CTRW) to be arbitrarily adjusted to achieve a match with any given effluent profile (e.g., Cortis et al. 2010). Therefore, four separate sets of coarse-scale models are constructed to examine the effectiveness of the proposed method in the scale-up of different variables. To facilitate the comparison among different cases, effluent histories for all four scenarios are compared in Fig. 4.12 and Fig. 4.13.

In Case A, the coarse-scale reservoir properties are computed according to section 4.3.1, while the scale-up procedure in section 4.3.2 is applied to compute effective dispersivities (α_L^*, α_T^* and α_V^*). This case mimics a Fickian RWPT model, since a constant transition time for transport evolution is assumed. This transport model does not account for the unresolved heterogeneity which is occurred below the fine scale. The results of this scenario are shown in Fig. 4.12(A) and Fig. 4.13(A). Case A serves to illustrate the impact of β, t_1, and t_2 on

transport. The true response in the subplot for this case corresponds to the fine-scale solution with α_L, α_T and α_V.

Next, coarse-scale reservoir and transport properties are computed according to the methods in sections 4.3.1 and 4.3.2. Three scenarios (Cases B-D) are set up to assess the sensitivity of coarse-scale model predictions to the scale-up of different parameters, and the results are compared in Fig. 4.12 and Fig. 4.13. In Case B, only coarse-scale values of β are computed, while fine-scale α_L, α_T, α_V, t_1, and t_2 values are employed. The results are shown in Fig. 4.12(B) and Fig. 4.13(B). Case C is similar to the Case B, but both coarse-scale β^* and $t_1{}^*$ are considered (fine-scale α_L, α_T, α_V, and t_2 values are used). Finally, in Case D, coarse-scale values for all three parameters β^*, $t_1{}^*$, and $t_2{}^*$ (with fine-scale α_L, α_T, α_V) are used. It is encouraging to observe that the true response of the fine-scale model is completely bracketed by the responses of the coarse-scale models. Common non-Fickian signatures, including early peak and heavy-tailed concentration profile, are highly noticeable in both sets of responses, due to both sub-grid variability and unresolved heterogeneity below the fine scale. As expected, there is no well-defined relationship between β, t_1 and t_2. However, it appears that β is sensitive to sub-grid heterogeneity, and its variability increases with scale (β^* ranges between 1.1747 and 1.2830, as compared to $\beta = 1.25$). The other two parameters, $t_1{}^*$ and $t_2{}^*$, appear to increase with β^*. To compare the difference in spatial particle distribution, the corresponding profiles for all 4 cases at 250, 500, and 750 days are compared in Fig. 4.14. Far more spread is observed in the transport evolution when a non-Fickian model is employed: for instance,

unlike the non-Fickian model, distinct clusters of particle distribution are observed at various time levels if Fickian transport is assumed.

The computational time for this example is documented in Table 4.1. A Linux-based high-performance computing facility managed by WestGrid is employed. It consists of 240 nodes with Xeon X5675 processors [12 cores (2 x 6) and 24 GB of memory] and 160 nodes with Xeon L5420 processors [8 cores (2 x 4) and 16 GB of memory]. As expected, computational requirement for transport modeling generally far exceeds that for the velocity computations. In practice, scarce data compounded with varying volume support renders transport modeling using numerous fine-scale realizations rather impossible. Therefore, the presented approach offers a comprehensive framework for performing coarse-scale particle-tracking simulations that reflect heterogeneities at multiple scales.

4.6 Conclusion

1. A new multi-scale particle-tracking model is formulated. A hybrid particle-tracking model, which utilizes a stochastic transition time function, similar to that of CTRW formulation, is formulated. It accounts for unresolved sub-grid heterogeneities smaller than the fine-scale level. A statistical procedure has been presented to estimate conditional probability distributions of effective reservoir variables, dispersivity and parameterization of transition time distribution at any coarse scale. The method enables sub-scale variability to be properly represented in the coarse-scale models.

2. The method does not assume a distinct separation of heterogeneity length scales. It can be used when the transport modeling scale is comparable to the length scale of heterogeneity at the sub-grid level. A coupled scale-up workflow for modeling reservoir and transport parameters is presented.

3. A special example involving the covariance-based Gaussian model was adopted in the case study. Responses from the coarse-scale models are bracketing the fine-scale results. Many of the anomalous characteristics associated with multi-scale heterogeneities, including early breakthrough, spread-out plume and heavy-tailed effluent profile, are captured. This study has not revealed a clear relationship between β^*, t_1^* and t_2^*; it is clear, however, that β is a function of sub-grid heterogeneity and its variability increases with scale. The other parameters, t_1^* and t_2^*, also seem to increase with β^*.

4. It is widely accepted that non-Fickian behavior originates from multi-scale heterogeneous rock properties. The results confirm that accounting for both unresolved heterogeneities below the fine scale and the sub-scale variability due to averaging or scale up is necessary for modeling non-Fickian characteristics.

References

Bear, J. (1979). *Hydraulics of groundwater.* New York: McGraw-Hill.

Benson, D. A., Aquino, T., Bolster, D., Engdahl, N., Henri, C. V., & Fernàndez-Garcia, D. (2017). A comparison of Eulerian and Lagrangian transport and non-linear reaction algorithms. *Advances in Water Resources, 99*, 15-37.

Berkowitz, B., & Scher, H. (1995). On characterization of anomalous dispersion in porous and fractured media. *Water Resour. Res., 31(6)*, 1461–1466.

Berkowitz, B., & Scher, H. (1997). Anomalous transport in random fracture networks. *Physical review letters, 79*, 4038–4041.

Berkowitz, B., Cortis, A., Dentz, M., & Scher, H. (2006). Modeling non-Fickian transport in geological formations as a continuous time random walk. *Reviews of Geophysics, 44(2)*.

Berkowitz, B., Klafter, J., Metzler, R., & Scher, H. (2002). Physical pictures of transport in heterogeneous media: Advection-dispersion, random-walk, and fractional derivative formulations. *Water Resources Research, 38(10)*.

Cortis, A., & Berkowitz, B. (2005). Computing "anomalous" contaminant transport in porous media: the CTRW MATLAB toolbox. *Ground Water, 43(6)*, (pp. 947-950).

Cortis, A., Emmanuel, S., Rubin, S., Willbrand, K., & Berkowitz, B. (2010). *The CTRW Matlab toolbox v3.1: a practical user's guide*. Retrieved from http://www.weizmann.ac.il/ESER/People/Brian/CTRW.

Cortis, A., Gallo, C., Scher, H., & Berkowitz, B. (2004). Numerical simulation of non-Fickian transport in geological formations with multiple-scale heterogeneities. *Water Resour Res, 40(4)*.

Dagan, G. (1989). *Flow and transport in porous formations.* New-York: Springer-Verlag.

Delay, F., Ackerer, P., & Danquigny, C. (2005). Simulating solute transport in porous or fractured formations using random walk particle tracking. *Vadose Zone Journal, 4(2)*, (pp. 360-379).

Dentz, M., Cortis, A., Scher, H., & Berkowitz, B. (2004). Time behavior of solute transport in heterogeneous media: transition from anomalous to normal transport. *Advances in Water Resources, 27(2)*, (pp. 155-173).

Deutsch, C. V., & Journel, A. G. (1998). *Geostatistical software library and users guide.* New York: Oxford university press.

Fernàndez-Garcia, D., & Sanchez-Vila, X. (2011). Optimal reconstruction of concentrations, gradients and reaction rates from particle distributions. *J Contam Hydrol, (120-121)*, (pp. 99-114).

Fernàndez-Garcia, D., Illangasekare, T. H., & Rajaram, H. (2005). Differences in the scale-dependence of dispersivity estimated from temporal and spatial moments in chemically and physically heterogeneous porous media. *Adv Water Resour, 28(7)*, (pp. 745-759).

Ferreira, J. A., & Pinto, L. (2014). Non-Fickian tracer transport in porous media. *Proceedings of the 14th International Conference on Computational and*

Mathematical Methods in Science and Engineering (pp. 543-554). Rota (Cádiz), Spain: CMMSE.

Ferreira, J. A., & Pinto, L. (2015). An integro-differential model for non-Fickian tracer transport in porous media: validation and numerical simulation. *Mathematical Methods in the Applied Sciences*.

Gao, G., Zhan, H., Feng, S., Huang, G., & Mao, X. (2009). Comparison of alternative models for simulating anomalous solute transport in a large heterogeneous soil column. *Journal of hydrology, 377(3)*, (pp. 391-404).

Geiger, S., Cortis, A., & Birkholzer, J. T. (2010). Upscaling solute transport in naturally fractured porous media with the continuous time random walk method. *Water Resources Research, 46(12)*.

Gelhar, L. W. (1986). Stochastic subsurface hydrology from theory to applications. *Water Resources Research, 22(9s)*, 135S–145S.

Gelhar, L. W., Welty, C., & Rehfeldt, K. R. (1992). A critical review of data on field-scale dispersion in aquifers. *Water Resour Res, 28(7)*, (pp. 1955-1974).

Haggerty, R., & Gorelick, S. M. (1995). Multiple-rate mass transfer for modeling diffusion and surface reactions in media with pore-scale heterogeneity. *Water Resources Research, 31(10)*, 2383-2400.

Jha, R. K., Bryant, S., & Lake, L. W. (2011). Effect of diffusion on dispersion. *SPE J, 16(1)*, (pp. 65-77).

Journel, A. G., & Huijbregts, C. J. (1978). *Mining geostatistics.* London: Academic press.

Kenkre, V. M., Montroll, E. W., & Shlesinger, M. F. (1973). Generalized master equations for continuous-time random walks. *ournal of Statistical Physics, 9(1)*, 45-50.

Kitanidis, P. K. (1988). Prediction by the method of moments of transport in a heterogeneous formation. *Journal of Hydrology, 102(1)*, 453-473.

Kitanidis, P. K. (1992). Analysis of macrodispersion through volume-averaging: Moment equations. *Stochastic Hydrology and Hydraulics, 6(1)*, 5-25.

Kreft, A., & Zuber, A. (1978). On the physical meaning of the dispersion equation and its solutions for different initial and boundary conditions. *Chemical Engineering Science, 33(11)*, (pp. 1471-1480).

Lake, L. W., & Srinivasan, S. (2004). Statistical scale-up of reservoir properties: Concepts and applications. *J Pet Sci Eng, 44(1)*, (pp. 27-39).

Leung, J. Y., & Srinivasan, S. (2011). Analysis of uncertainty introduced by scaleup of reservoir attributes and flow response in heterogeneous reservoirs. *SPE J, 16(3)*, (pp. 713-724).

Leung, J. Y., & Srinivasan, S. (2012). Scale-up of mass transfer and recovery performance in heterogeneous reservoirs. *J Pet Sci Eng, (86-87)*, (pp. 71-86).

Leung, J. Y., & Srinivasan, S. (2016). Effects of reservoir heterogeneity on scaling of effective mass transfer coefficient for solute transport. *J Contam Hydrol, 192*, (pp.181-193).

Li, L., Zhou, H., & Gómez-Hernández, J. J. (2011). A comparative study of three-dimensional hydraulic conductivity upscaling at the macro-dispersion

experiment (MADE) site, Columbus Air Force Base, Mississippi (USA). *J Hydrol, 404(3)*, (pp. 278-293).

Li, X., Koike, T., & Pathmathevan, M. (2004). A very fast simulated re-annealing (VFSA) approach for land data assimilation. *Comput Geosci, 30(3)*, (pp. 239-248).

Margolin, G., Dentz, M., & Berkowitz, B. (2003). Continuous time random walk and multirate mass transfer modeling of sorption. *Chemical physics, 295(1)*, (pp. 71-80).

Metzler, R., & Klafter, J. (2000). The random walk's guide to anomalous diffusion: a fractional dynamics approach. *Physics Reports, 339*, 1–77.

Neretnieks, I., Eriksen, T., & Tähtinen, P. (1982). Tracer movement in a single fissure in granitic rock: Some experimental results and their interpretation. *Water resources research, 18(4)*, 849-858.

Neuman, S. P., & Zhang, Y. K. (1990). A quasi-linear theory of non-Fickian and Fickian subsurface dispersion: 1. Theoretical analysis with application to isotropic media. *Water Resources Research, 26(5)*, 887-902.

Parker, J. C. (1984). Analysis of solute transport in column tracer studies. *Soil Science Society of America Journal*(48(4)), 719-724.

Parker, J. C., & Genuchten, M. T. (1984). Flux-averaged and volume-averaged concentrations in continuum approaches to solute transport. *Water Resources Research*(20(7)), 866-872.

Pedretti, D., Fernàndez-Garcia, D., Sanchez-Vila, X., Bolster, D., & Benson, D. A. (2014). Apparent directional mass-transfer capacity coefficients in

three-dimensional anisotropic heterogeneous aquifers under radial convergent transport. *Water Resour Res, 50(2)*, (pp. 1205-1224).

Perkins, T. K., & Johnston, O. C. (1963). A review of diffusion and dispersion in porous media. *SPE J, 3(01)*, (pp. 70-84).

Pulloor Kuttanikkad, S. (2009). *Pore-scale Direct Numerical Simulation of Flow and Transport in Porous Media (Dissertation).* Heidelberg University, Germany.

Riva, M., Guadagnini, A., Fernandez-Garcia, D., Sanchez-Vila, X., & Ptak, T. (2008). Relative importance of geostatistical and transport models in describing heavily tailed breakthrough curves at the Lauswiesen site. *J Contam Hydrol, 101(1)*, (pp. 1-13).

Rubin, Y. (2003). *Applied stochastic hydrogeology.* Oxford University Press, Oxford: UK.

Rubin, Y., Sun, A., Maxwell, R., & Bellin, A. (1999). The concept of block-effective macrodispersivity and a unified approach for grid-scale-and plume-scale-dependent transport. *Journal of Fluid Mechanics, 395*, 161-180.

Salamon, P., Fernàndez-Garcia, D., & Gómez-Hernández, J. J. (2006a). A review and numerical assessment of the random walk particle tracking method. *Journal of contaminant hydrology, 87(3)*, (pp. 277-305).

Salamon, P., Fernàndez-Garcia, D., & Gómez-Hernández, J. J. (2006b). Modeling mass transfer processes using random walk particle tracking. *Water Resour Res, 42(11)*.

Salamon, P., Fernandez-Garcia, D., & Gómez-Hernández, J. J. (2007). Modeling tracer transport at the MADE site: the importance of heterogeneity. *Water resources research, 43(8)*.

Srinivasan, G., Tartakovsky, D. M., Dentz, M., Viswanathan, H., Berkowitz, B., & Robinson, B. A. (2010). Random walk particle tracking simulations of non-Fickian transport in heterogeneous media. *Journal of Computational Physics, 229(11)*, (pp. 4304-4314).

Vishal, V., & Leung, J. Y. (2015). Modeling impacts of subscale heterogeneities on dispersive solute transport in subsurface systems. *Journal of contaminant hydrology, 182*, (pp. 63-77).

Vishal, V., & Leung, J. Y. (2017). Statistical scale-up of dispersive transport in heterogeneous reservoir. In *In Geostatistics Valencia 2016* (pp. 733-743). Springer International Publishing.

Wang, J., & Kitanidis, P. K. (1999). Analysis of macrodispersion through volume averaging: comparison with stochastic theory. *Environmental Research and Risk Assessment, 13(1-2)*, 66-84.
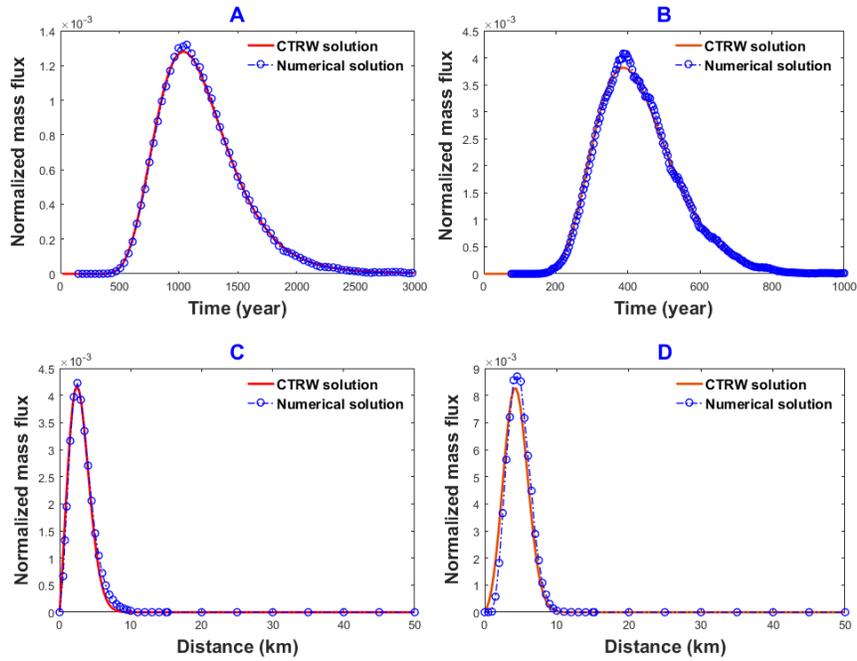
Figure 4.1: Comparison of particle-tracking approach (blue) with the CTRW method (red): Top – temporal flux-weighted mass profile at $X_1 = L = 15.2$ km: (A) non-Fickian model based on Eq. (4.10) and (B) Fickian model based on Eq. (4.11); bottom: spatial flux-weighted mass profile at $t = 100$ yr: (C) non-Fickian model based on Eq. (4.10) and (D) Fickian model Eq. (4.11).
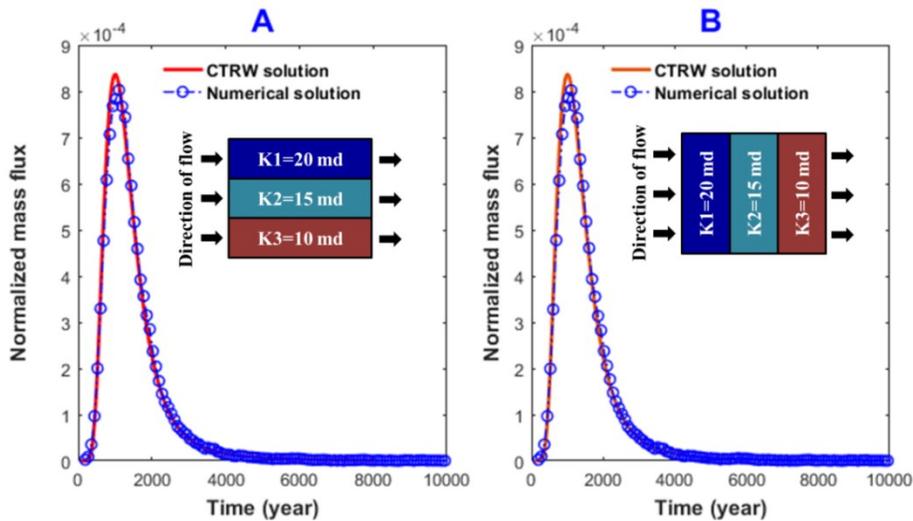
Figure 4.2: Temporal flux-weighted mass profile at $X_1 = L = 16.0$ km when stratified porous media is: (A) parallel and (B) perpendicular to the layered porous medium.
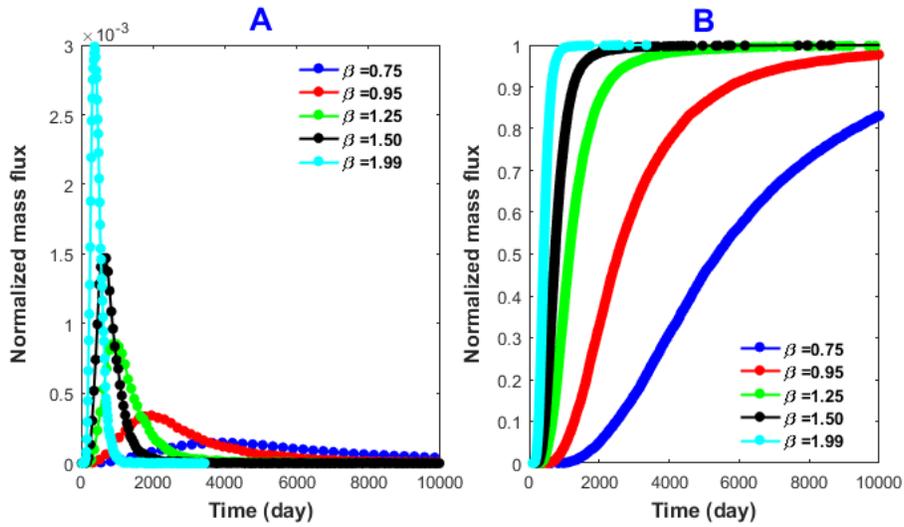
Figure 4.3: (A) Temporal flux-weighted mass profile and (B) temporal flux-weighted cumulative mass profile at $X_1 = L = 15.2$ km for several values of β.
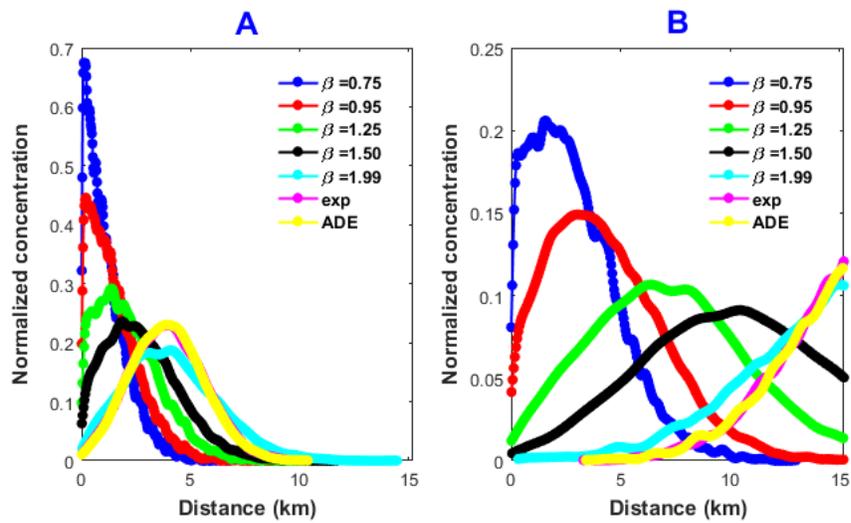
Figure 4.4: Spatial volume-averaged mass profile at (A) $t = 100$ yr and (B) $t = 500$ yr.
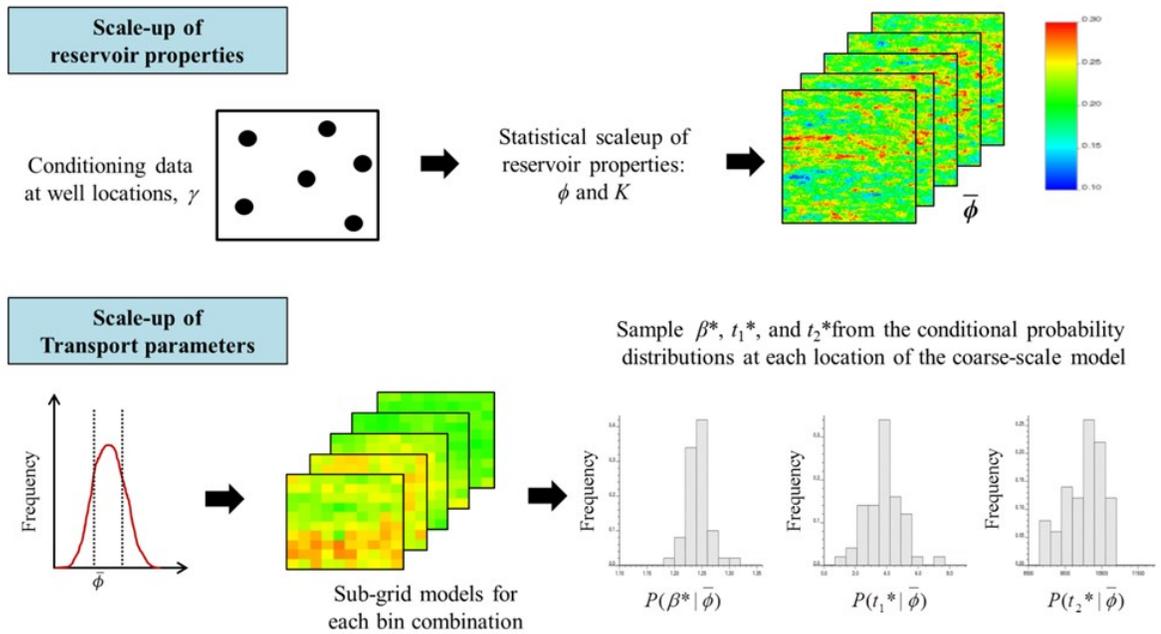
Figure 4.5: Workflow to scale up reservoir properties and transport properties.
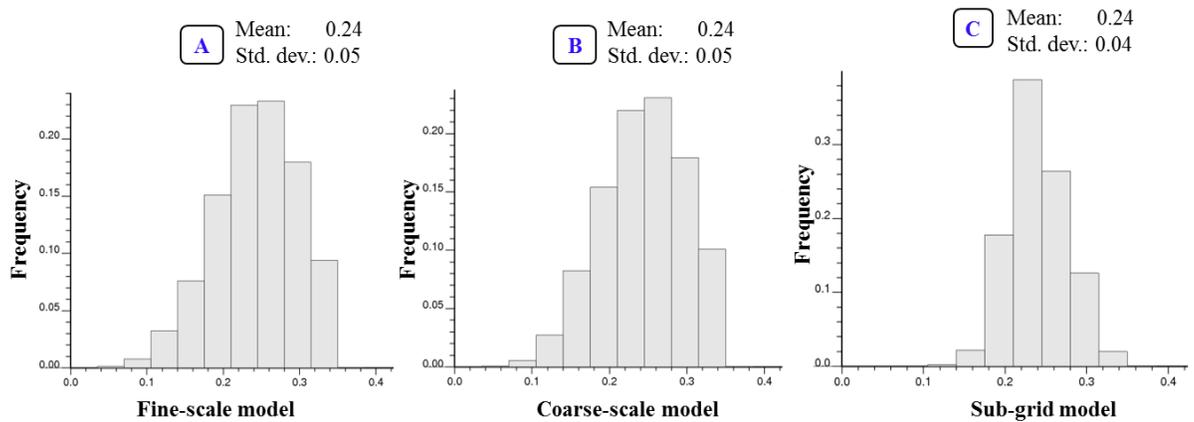
Figure 4.6: Histogram of porosity: (A) fine-scale model, (B) coarse-scale model, and (C) sub-grid model.
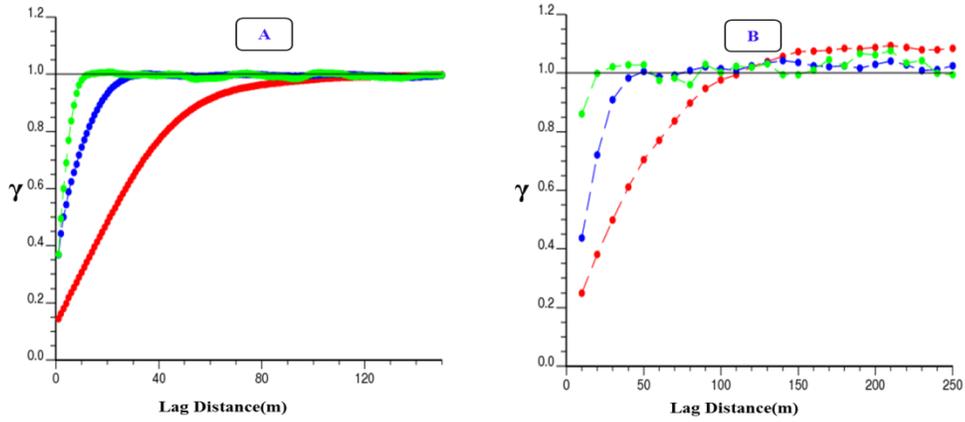
Figure 4.7: Variograms of (A) fine-scale model and (B) coarser-scale model. Red: horizontal maximum; blue: horizontal minimum; green: vertical direction.
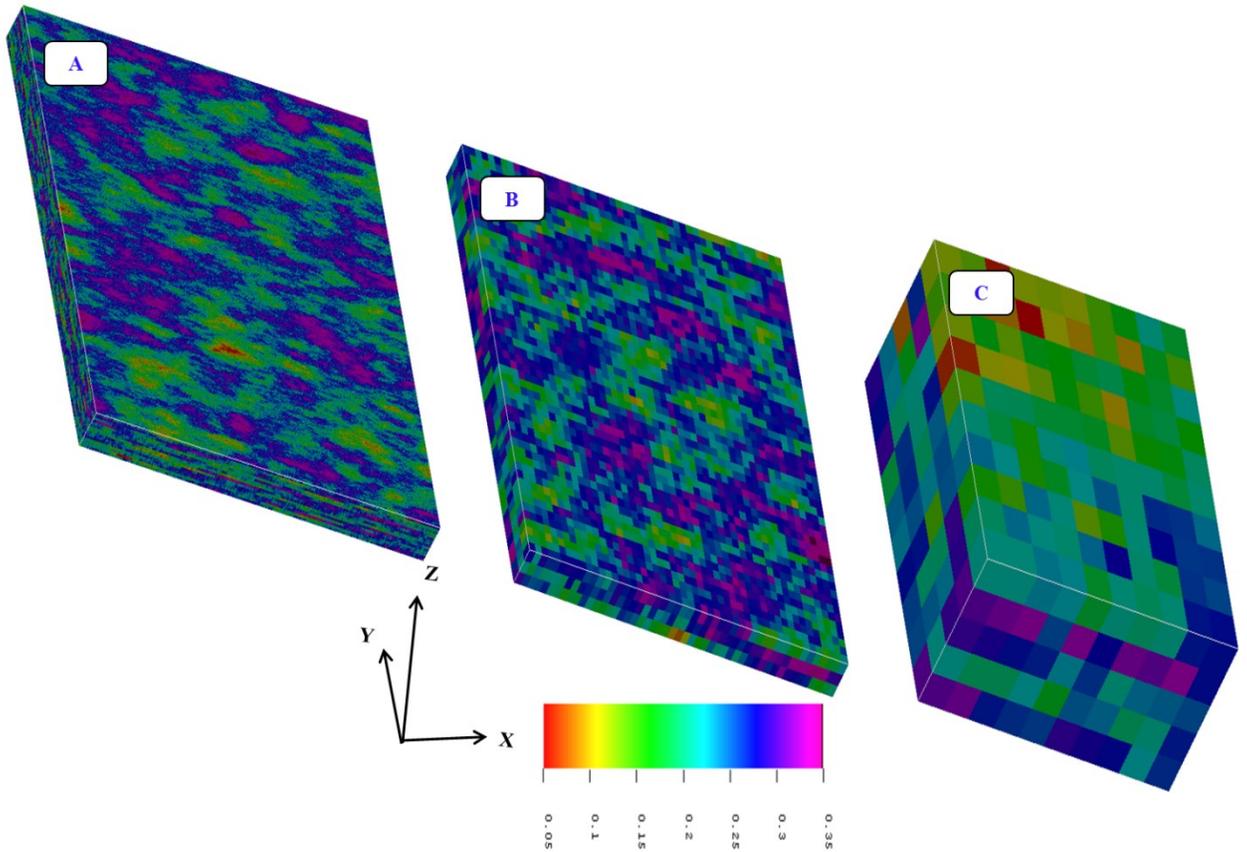
Figure 4.8: Distribution of porosity: (A) fine-scale model, (B) coarse-scale model, and (C) sub-grid model.
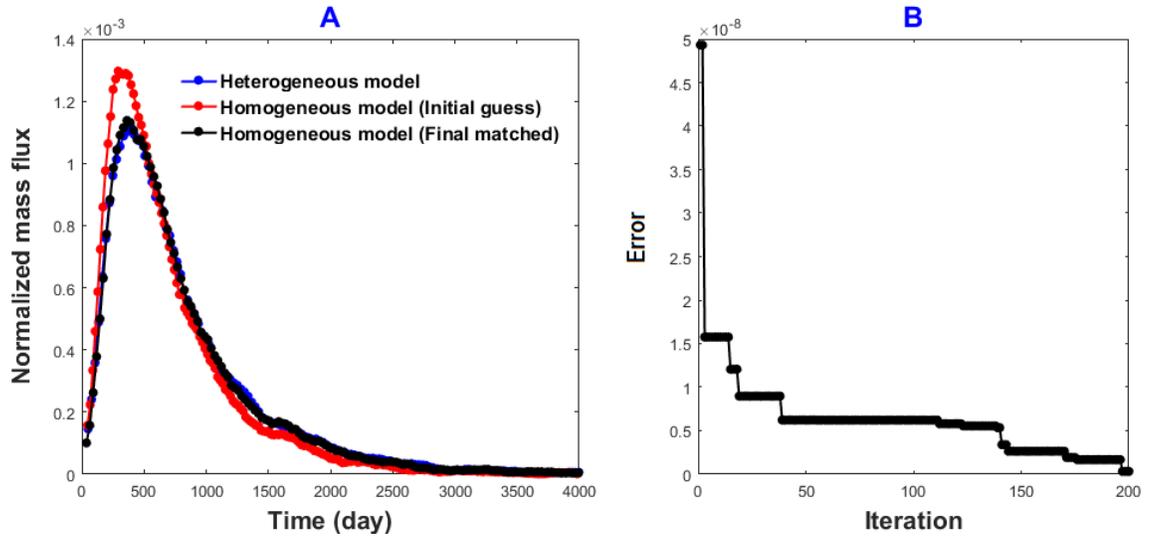
Figure 4.9: (A) Comparison of breakthrough effluent histories between the heterogeneous and the equivalent homogeneous sub-grid models (B) Reduction in error over iterations.
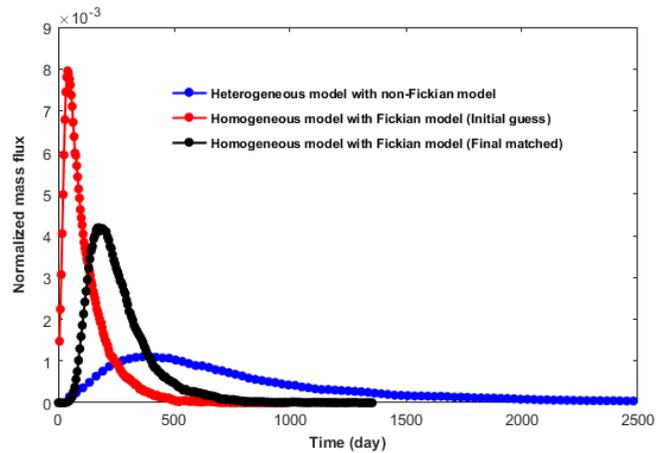
Figure 4.10: Breakthrough effluent history of the original heterogeneous model cannot be matched with an equivalent homogeneous sub-grid model, if a Fickian RWPT is used instead.
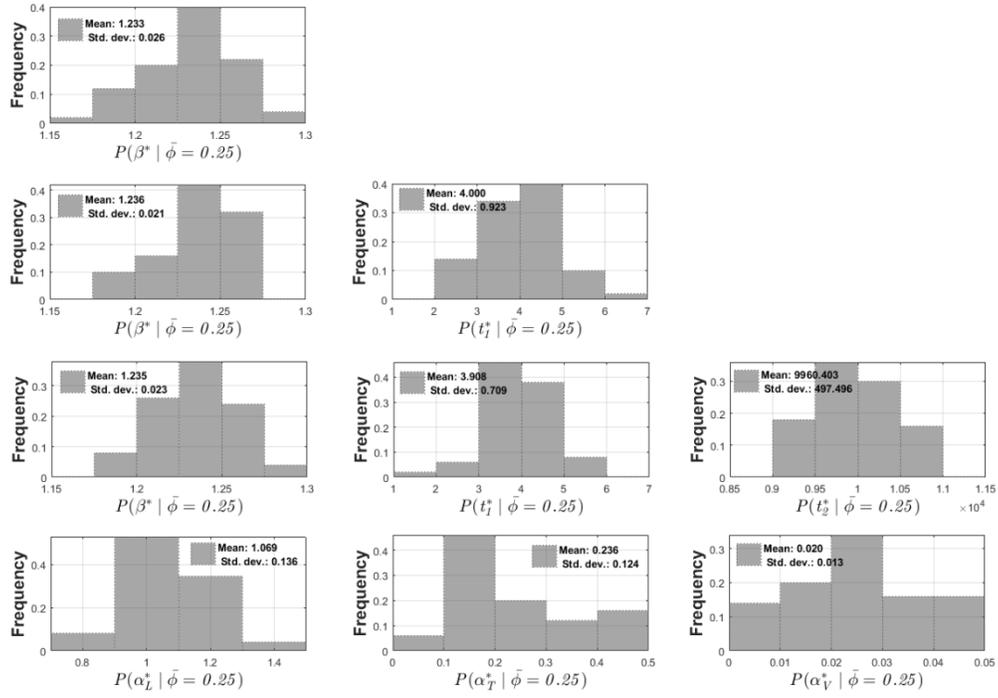
Figure 4.11: Distribution of effective values of β^* (top), β^* and t_1^* (2nd row), β^*, t_1^*, and t_2^* (3rd row) for non-Fickian model, and α_L^*, α_T^*, and α_V^* (bottom) for Fickian model, considering a selected bin-mean of $\bar{\phi} = 0.25$.
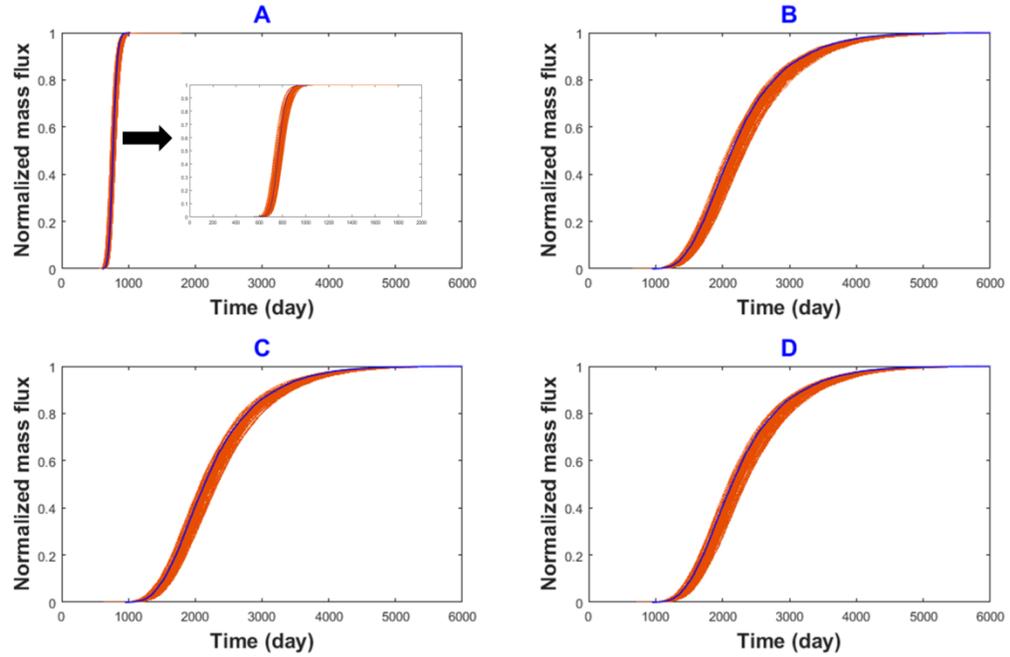
Figure 4.12: Normalized effluent profiles of cumulative mass flux for the four sets of coarse-scale models with different effective transport parameters: (A) Fickian model with α_L^*, α_T^*, and α_V^*, (B) non-Fickian model with β^*, (C) non-Fickian model with β^* and t_1^*, (D) non-Fickian model with β^*, t_1^*, and t_2^*. The blue curve corresponds to the true fine-scale model.
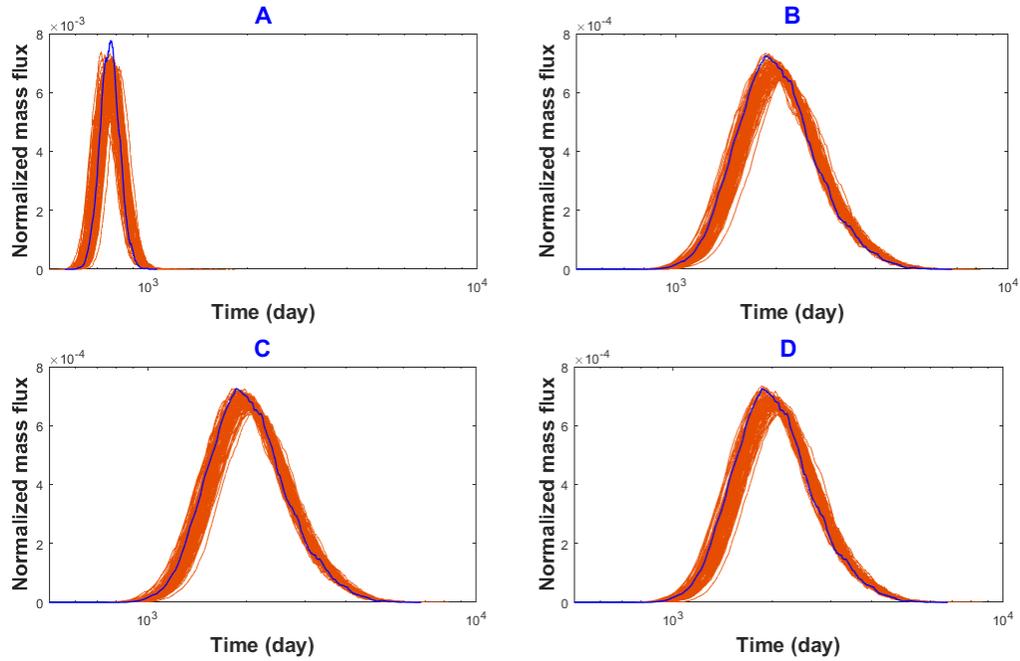
Figure 4.13: Normalized effluent profiles of instantaneous mass flux for the four sets of coarse-scale models with different effective transport parameters: (A) Fickian model with α_L^*, α_T^*, and α_V^*, (B) non-Fickian model with β^*, (C) non-Fickian model with β^* and t_1^*, (D) non-Fickian model with β^*, t_1^*, and t_2^*. The blue curve corresponds to the true fine-scale model.
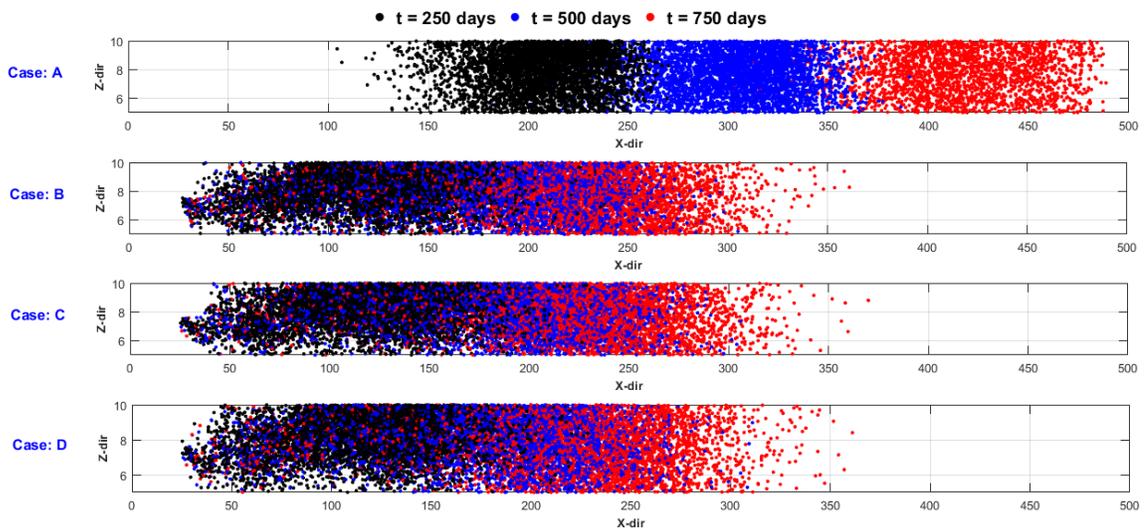
Figure 4.14: Particle distribution for coarse-scale models at 250, 500, and 750 days.

Table 4.1: Computational time

		Number of simulations run	Simulation time for Jasper cluster		Comments
			(Velocity + Transport) Calculations		
1)	Fine-scale or true model (500×500×15 with 1×1×1m grid size)	1	(2025 sec + 250 sec) = 2275 sec		
2)	Sub-grid model (10×10×5 with 1×1×1m grid size)	(50 heterogeneous models + 50 homogeneous models) x 3 $\bar{\phi}$ levels	(370 sec + 520 sec) x 3 = 2670 sec		Calculation of P(β*| $\bar{\phi}$) with100 iterations in VFSA using parallel computing scheme
3)	Coarse-scale model (50×50×3 with 10×10×5m grid size)	100	(1250 sec + 280 sec) x 100 = 153000 sec		Fully scaled-up model

Chapter 5: A Multi-Scale Particle-Tracking

Framework for Dispersive Solute

Transport Modeling[4]

5.1 Introduction

It has been widely reported that dispersivity increases with travel distance (Gelhar et al. 1992; Fleurant and Van Der Lee 2001) and time (Binning and Celia 2002). This scale-dependent characteristic has contributed to non-Fickian, anomalous, or non-Gaussian (Berkowitz et al. 2000; John 2008) transport behavior, including an early breakthrough, a slow moving concentration peak, and a heavy-tailed effluent profile in the late times. Though near-well radial flow may introduce non-Fickian behavior (Pedretti et al. 2014), most non-Fickian features stem from multi-scale heterogeneities (Berkowitz et al. 2006; Le Borgne and Gouze 2008; Bijeljic et al. 2013): large-scale trends (Gylling et al. 1999; Becker and Shapiro 2003) and small-scale variability (Dentz et al. 2004).

Representing non-Fickian behavior, however, in solute transport modeling is not trivial. Many grid-based discretization schemes entail significant numerical dispersion (Lantz 1971; Fanchi 1983; Haajizadeh et al. 1999, Binning and Celia 2002). Though numerical dispersion can be alleviated by incorporating higher-order approximations, it cannot be eliminated completely when modeling physical dispersion. Boso et al. (2013) compared five popular schemes, including both

---

grid-based and grid-free Lagrangian particle-tracking methods, and reaffirmed that the grid-based schemes would overestimate mixing because of spurious numerical dispersion, while particle-tracking schemes are free of numerical dispersion. Two types of particle-tracking formulations are available (Lichtner et al. 2002; Fernàndez-Garcia and Sanchez-Vila 2011; Benson et al. 2017). In random-walk particle tracking (RWPT), a deterministic transit time step ($\tau = \Delta t$) is considered, whereas the transition vector, ξ, is a normally-distributed random variable with zero mean and unit variance (Salamon et al. 2006a; Srinivasan et al. 2010; Pedretti and Fernàndez-Garcia 2013). RWPT predictions resemble those obtained by the Fickian advection-dispersion equation (ADE), since it involves equilibrium at the local scale; this assumption ignores any heterogeneity with a length scale that is smaller than the support volume on which the ADE parameters are defined. Many previous studies have examined the application and potential limitations of the ADE in both Fickian and non-Fickian transport modeling (Aronofsky and Heller 1957; Scheidegger 1959; Levy and Berkowitz 2003; Berkowitz et al. 2006; Neuman and Tartakovsky 2009; Jha et al. 2011). Alternative non-local formulations, including multi-rate mass transfer models (MRMT) (Haggerty and Gorelick 1995), memory functions (Carrera et al. 1998), fractional advection-dispersion equations (fADE) (Benson et al. 2000), and continuous time random walk (CTRW) (Berkowitz et al. 2006), were introduced. In CTRW, τ and ξ are random variables characterized by a joint probability density function, $\psi(\xi, \tau)$; no specific assumption (e.g., stationarity) regarding the distributions of ξ and τ is needed (Srinivasan et al. 2010). Non-stationary trend

can be represented in the drift and flux terms, $D_\psi(\mathbf{x})$ and $q_\psi(\mathbf{x})$, by assigning different distribution of τ to distinct regions in the domain (Cortis et al. 2004; Berkowitz et al. 2006). Unresolved heterogeneities (below the modeling scale) that may contribute to the non-Fickian behavior are modeled using a space-dependent memory function, $M(u;\mathbf{x})$ (Fernàndez-Garcia et al. 2009). A hybrid particle-based CTRW formulation, which is capable of handling non-Fickian behavior of transport in porous media, was developed by Srinivasan et al. (2010). It is based on the generalized Langevin equations (Fogedby 1994; Kleinhans and Friedrich 2007), where τ for each step, instead of being deterministic of fixed duration, is sampled from a probability density distribution. This method, as compared to CTRW, offers a convenient alternative to incorporate force fields and other boundary conditions (Metzler and Klafter 2000). A version of this hybrid particle-based CTRW formulation is adopted in this study.

The above discussion assumes that transport modeling is performed at the finest resolution of heterogeneity (any unresolved heterogeneities below this scale will be incorporated in the formulation of τ). However, transport modeling is often performed at a scale that is coarser than the finest resolution of heterogeneity. Therefore, scale-up of the probability distribution of τ should be considered. Two modeling scales, as illustrated in Fig. 5.1, are referred to in this chapter:

- "Fine scale" refers to a length scale over which the detailed description about heterogeneity is prescribed (typically on the order of centimeter, over which

core and log measurements are available); structures that are smaller than this scale can be captured through the probabilistic distribution of τ;

- "Coarse scale" refers to the transport modeling scale, over which numerical flow and transport simulation is performed (typically on the order of meter). To construct a model at the coarse scale, it is important to account for heterogeneity corresponding to a number of length scales: (1) non-stationarity (trend), which is assumed to be defined at the same resolution of the transport modeling scale and (2) sub-scale variability that captures the smoothing of fine-scale heterogeneity and the associated uncertainties.

Different approaches are available for computing effective transport parameters at the coarse scale, particularly in the subject of dispersion modeling. In the ensemble averaging framework, an effective dispersivity is estimated from the ensemble moments (moments of the statistical distribution) describing the displacement of a solute plume (Gelhar and Axness 1983; Dagan 1982, 1984, 1987, 1989; Gelhar 1986; Neuman et al. 1987; Kitanidis 1988; Neuman and Zhang 1990; Rubin 2003; Berentsen et al. 2007). This method is useful provided that permeability distribution (e.g., covariance structure) can be well defined. In the volume averaging framework, spatial moments, instead of ensemble moments, are employed (Efendiev et al. 2000). It is assumed that the length scale of heterogeneity is much smaller than the averaging volume (Leung and Srinivasan 2016). In theory, if the restriction on the heterogeneity length scale is satisfied, both volume averaging and stochastic perturbation would yield the same results (Kitanidis 1992; Wang and Kitanids 1999).

This work describes a new unified particle-tracking workflow that incorporates scale-up of effective dispersion and reservoir attributes (porosity and permeability) in a consistent manner. Solute transport is simulated following the particle-based CTRW formulation (Srinivasan et al. 2010), with the transition time (τ) distribution being parameterized in accordance to the truncated power-law (t_1, t_2 and β): t_1 = the median waiting time; t_2 = the cut-off time after which Fickian transport is observed; β = exponent controlling the extent of anomalous behavior. Instead of computing effective dispersivities, this work examines the scale-up of t_1, t_2 and β. The method is flexible that it does not invoke any explicit assumption regarding the multivariate distribution of the heterogeneity; it utilizes the theory of volume variance (Lake and Srinivasan 2004). Without imposing that the averaging scale must be larger than the length scale of local heterogeneity, the idea is to quantify and transfer the uncertainty in scale-up into the variability exhibited by the coarse-scale models (Leung and Srinivasan 2011, 2012). The volume variance can be computed directly from data or corresponding to a particular spatial correlation model.

The general workflow is based on that presented in Vishal and Leung (2015). However, this work offers two important improvements. First, non-stationary trend (available on the same resolution of the transport modeling scale) is considered. Second, heterogeneity below the fine scale is captured with the use of probabilistic distribution of the transition time (τ). To scale up rock properties, each random variable is modeled as the sum of a trend and a residual. Multiple realizations of the residual at the transport modeling scale are sampled. Next, to

scale up t_1, t_2, and β, a set of models depicting detailed the heterogeneities at the fine scale and of the same physical size as the transport modeling grid block is subjected to particle-based CTRW simulation. Effective t_1, t_2, and β (t_1^*, t_2^*, and β^*) are estimated by matching the corresponding effluent history for each model with an equivalent medium consisting of averaged homogeneous rock properties. Conditional probability distributions of t_1^*, t_2^*, and β^* are constructed. The significance of capturing directly the uncertainty in effective transport properties is investigated. The main contribution of this work is that it offers a hierarchical approach, such that heterogeneity at multiple scales are properly represented during the scale-up of t_1, t_2, β and other reservoir attributes to the transport modeling scale.

This chapter is organized as follows. In section 5.2, the governing equations for flow and transport, including the relevant particle-tracking methods, are described. In section 5.3, the proposed method is presented. A synthetic case study is discussed in sections 5.4 and 5.5. Conclusions are summarized in section 5.6.

5.2 Governing Equations of Flow and Transport in Porous Media

Transport of a solute in single phase at the Darcy scale can be described by the Fickian-based advection-dispersion equation (ADE) (Bear 1979):

$$\frac{\partial C}{\partial t} + \nabla \cdot (C\boldsymbol{u}) - \nabla \cdot (\boldsymbol{D} \cdot \nabla C) = 0, \tag{5.1}$$

where $C(\mathbf{x},t)$ is the volumetric concentration of the solute, which is a function of position ($\mathbf{x}$) and time (t). $\mathbf{D}$ is the local-scale dispersion coefficient tensor (Binning and Celia 2002):

$$\mathbf{D}_{ij} = \underbrace{D^d \varsigma_{ij}}_{\text{molecular diffusion}} \underbrace{+ \alpha_T |\mathbf{u}| \delta_{ij} + (\alpha_L - \alpha_T) \frac{u_i u_j}{|\mathbf{u}|}}_{\text{mechanical dispersion}}, \tag{5.2}$$

where α_T and α_L represent the transverse and longitudinal dispersivities, respectively; D^d is the effective molecular diffusion coefficient; $\varsigma_{i,j}$ is the tortuosity tensor; $\mathbf{u}$ is the superficial velocity (Eq. 5.3), which is constant for the steady-state flow of an incompressible fluid. Its component along the ith direction is denoted by u_i. It is related to the interstitial velocity according to Eq. (5.4).

$$\mathbf{u} = -\mathbf{K}\nabla h; \mathbf{K} = \frac{k \rho g}{\mu}; \tag{5.3}$$

$$V = \frac{q}{\phi S} = \frac{\mathbf{u}}{\phi}, \tag{5.4}$$

where V and q refer to the interstitial velocity and volumetric flow rate, respectively. S is the cross-section area, k is the permeability tensor, μ is the fluid viscosity, h is the hydraulic head, $\mathbf{K}$ is the hydraulic conductivity tensor, ϕ is the porosity, ρ is the fluid density, and g is gravitational constant.

To implement these governing equations in a conservative Lagrangian particle-tracking framework, the total mass of the injected solute component (m_o) is divided into a large number (N_p) of independent small particles with $m = m_o / N_p$. Each particle is advanced by successive jumps, with each jump composed of a drift component representing advection and a Brownian component representing

dispersion. For the RWPT method, the location of a particle at the new time level $(t+\Delta t)$ is computed following the Fokker-Plank approach (Kinzelbach and Uffink 1991) that demonstrates the equivalence between Eq. (5.1) and the following stochastic differential equations (Tompson and Gelhar 1990; LaBolle et al. 1996; Hassan and Mohamed 2003):

$$\mathbf{x}_p(t+\Delta t) = \mathbf{x}_p(t) + \underbrace{A[\mathbf{x}_p(t)]\Delta t}_{\text{advective (determini stic)}} + \underbrace{B[\mathbf{x}_p(t)].\boldsymbol{\xi}(t)\sqrt{\Delta t}}_{\text{dispersive (stochasti c)}};$$

$$A = V + \nabla D, \ BB^T = 2D,$$

$$\tag{5.5}$$

where $\mathbf{x}_p$ is the coordinate vector of the particle at time t, and the transition length (ξ) is a vector of normally distributed independent random numbers with zero mean and unit variance. B is the velocity-dependent dispersion displacement matrix, and A is the drift vector incorporating effects of the flow field and the divergence of D (Lichtner et al. 2002). The time step Δt is deterministically known and constant for all particles. Srinivasan et al. (2010) proposed a hybrid particle-based CTRW formulation, in which the RWPT framework is modified with the transition time being stochastic and varying among particles:

$$\mathbf{x}_p(s+\Delta s) = \mathbf{x}_p(s) + A[\mathbf{x}_p(s)]\Delta s + B[\mathbf{x}_p(s)]\cdot\boldsymbol{\xi}(s)\sqrt{\Delta s}.$$
$$t(s+\Delta s) = t(s) + \tau(s,\Delta s).$$

$$\tag{5.6}$$

The ξ and τ are spatial and temporal random series which are distributed according to the joint transition displacement and time distribution $\psi(\xi, \tau)$. It is often assumed that $\psi(\xi, \tau)$ is mutually uncorrelated in space and time, such that $\psi(\xi, \tau) = \psi_s(\xi)\psi_t(\tau)$. The space function $\psi_s(\xi)$ is assumed to be Gaussian, whereas

time function $\psi_t(\tau)$ can be characterized by the truncated power law (TPL) distribution:

$$\psi_t(\tau) = \frac{(1+\tau/t_1)^{-1-\beta}}{t_1 r^\beta \Gamma(-\beta, r)} e^{\left(-\frac{t_1+\tau}{t_2}\right)}, r = \frac{t_1}{t_2}, t_1 < t_2, 0 \le \beta \le 2. \qquad (5.7)$$

Γ is the incomplete Gamma function. Eq. (5.7) is parameterized using the variables β, t_1 and t_2, which depend on the underlying heterogeneity. In this work, a RWPT formulation called RW3D-MRMT (Fernàndez-Garciaet al. 2005; Salamon et al. 2006a, 2006b; Fernàndez-Garciaand Sanchez-Vila 2011; Salamon et al. 2007; Riva et al. 2008) is modified according to Eq. (5.6) to incorporate the stochastic time step. The modified formulation has validated against 1-D and 2-D analytical solution and other CTRW algorithms (Vishal and Leung 2017).

5.3 A Multi-Scale Particle-Tracking Approach

Mathematical formulation of a multi-scale workflow for constructing models of reservoir properties and effective truncated power law parameters β^*, t_1^*, and t_2^* at the transport modeling (coarse) scale for particle-tracking simulation is presented next.

5.3.1 Modeling of Reservoir Properties

Averaging of heterogeneity below the modeling resolution would introduce uncertainty in the ensuing models. This uncertainty is referred to as sub-scale variability. Given that reservoir attributes, including porosity and permeability, are modeled as random variables, their spatial averages are also random variables.

The variance of mean of the attribute is a measure of the variability of the spatial average at that particular spatial volume V. Assuming stationarity, this variance would decrease with increasing V. In fact, this variance would reach a constant negative unit slope on a log-log plot against V, when the volume support is greater than or equal to the representative elementary volume (REV), a scale beyond which the sub-scale variability becomes negligible (Bear 1979). However, multivariate statistics of petrophysical properties would often exhibit non-stationarity and scale dependency (Neuman 1994; Schulze-Makuch and Cherkauer 1998; Schulze-Makuch et al. 1999). For such cases, a stabilized negative unit slop representative of the REV cannot be easily observed.

The modeling of such variables is facilitated by decomposing its variability into the sum of a non-stationary trend and a stationary residual. The trend component is assumed to be available at the transport modeling scale (this assumption is justified given that non-stationarity is generally inferred over a scale much larger than that for the transport model). Assuming that the residual is a scalar continuous random variable (Z), the corresponding spatial mean $\overline{Z}$ over a volume support V is defined as:

$$\overline{Z} = \left[\frac{1}{V} \int_V (Z)^\omega dV \right]^{1/\omega} \tag{5.8}$$

The variance of mean or $Var(\overline{Z})$ can be computed directly from the spatial averages of Z for different sizes of V according to Eq. (5.9), without invoking any explicit assumption of the multivariate distribution of Z; an averaging window can be assigned and the variance in the spatial mean is

computed. In fact, different averaging schemes can be employed depending on the choice of ω. If Z is a Gaussian random variable with a variance σ^2, with a multivariate distribution described by a second-order stationary spatial correlation function ρ_{corr}, $Var(\overline{Z})$ can also be computed by integrating ρ_{corr} over all possible lag distance η within V with Eq. (5.9) (Lake and Srinivasan 2004):

$$Var(\overline{Z}) = \frac{2\sigma^2}{V^2}\left(\int_V \int_\eta \rho_{corr}(\eta)d\eta d\xi\right). \tag{5.9}$$

Eq. (5.9) assumes that linear averaging (i.e., $\omega = 1$) applies. When the volume support for the conditioning data is less than that of the modeling scale, sub-scale variability can be represented by sampling multiple sets of conditioning data via bootstrapping (Leung and Srinivasan 2011). Parametric bootstrapping of a likelihood function (whose mean is the block-average of the actual measured values and the variance is the variance of mean) can be adopted. For a Gaussian random variable, a Gaussian likelihood function can be assumed; in addition, an average semi-variogram $\overline{\gamma}$ (Journel and Hujbregts 1978) can be computed, facilitating conditional simulation to be performed on all sets of conditioning data (Leung and Srinivasan 2011). $\overline{\gamma}$ corresponding to two support volumes V and V' is defined according to Eq. (5.10); it can be approximated numerically by averaging the point-scale values of γ at various regularly-spaced points.

$$\overline{\gamma}(V,V') = \frac{1}{VV'}\int_V \int_{V''}\gamma(v,v')dvdv' \approx \frac{1}{nn'}\sum_{i=1}^{n}\sum_{j=1}^{n'}\gamma(\mathbf{h}_{ij}) \tag{5.10}$$

A procedure, which is an extension to that presented in Leung and Srinivasan (2011), is adopted to construct realizations of $Z(\mathbf{x})$ at the model scale.

It is assumed that $Z(\mathbf{x}) = \overline{Z}_T(\mathbf{x}) + Z_R(\mathbf{x})$, where $\overline{Z}_T(\mathbf{x})$ and $Z_R(\mathbf{x})$ refer to the trend and the residual, respectively:

1. Compute $Z_R(\mathbf{x})$ at conditioning locations: $Z_R(\mathbf{x}) = Z(\mathbf{x}) - \overline{Z}_T(\mathbf{x})$.

2. Estimate γ_R. Compute $Var(\overline{Z}_R)$ and $\overline{\gamma}_R$ based on Eqs. 9 and 10.

3. Draw multiple sets of coarse-scale conditioning data values of $\overline{Z}_R$ via bootstrapping. For instance, a Gaussian likelihood function, whose mean and the variance are block-average of the actual measured values and the variance of mean calculated in Step #2 can be adopted.

4. Perform conditional simulation and construct realizations of $\overline{Z}_R(\mathbf{x})$ at the modeling scale using the $\overline{\gamma}_R$ from Step #2 and coarse-scale histogram [mean = fine-scale global mean of $Z_R(\mathbf{x})$; variance = $Var(\overline{Z}_R)$] for one set of the conditioning data from step #3.

5. Reconstruct realizations of $\overline{Z}(\mathbf{x}) = \overline{Z}_T(\mathbf{x}) + \overline{Z}_R(\mathbf{x})$.

6. Repeat steps #4 and 5 for other conditioning data sets obtained in Step #3. It is assumed that permeability is correlated with porosity as $k = a \times \phi^b$, where a and b are empirical constants. It is also assumed that this relationship is scale invariant.

5.3.2 Modeling of Effective Transition Time Distribution

Vishal and Leung (2015) proposed a work flow to represents sub-scale variability in transport parameter (e.g., effective dispersivity) with probability distributions. However, their work did not incorporate any non-stationary trend; furthermore, an

ADE-based RWPT transport modeling tool was used, ignoring any unresolved heterogeneities below the fine scale. Hence, to account for multi-scale heterogeneity, a more general workflow is proposed here. First, multiple high-resolution (sub-grid) realizations depicting the detailed fine-scale heterogeneity arrangement and of the same physical size of the transport modeling grid cell are constructed. Each realization is subjected to particle-tracking simulation. Next, an averaged homogeneous model with uniform properties is constructed. Truncated power law parameters (β^*, $t_1{}^*$ and $t_2{}^*$) of the homogeneous model are adjusted by minimizing the difference in effluent concentration profiles between the homogeneous model and the high-resolution model, which is defined in terms of the root mean square error or RMSE in Eq. (5.11) (Nash and Sutcliffe 1970), with a nonlinear regression scheme.

$$RMSE = \sqrt{\frac{1}{N-1}\sum_{i=1}^{N}\left[\left\langle C_{(\beta,t_1,t_2)}\right\rangle_{(t_{i-1}-t_i)} - \left\langle C_{(\beta^*,t_1^*,t_2^*)}\right\rangle_{(t_{i-1}-t_i)}\right]^2}, \qquad (5.11)$$

where $\left\langle C\right\rangle_{(t_{i-1}-t_i)}$ is the average concentration over the time interval between t_{i-1} and t_i. N is the number of time steps. The adjusted values are considered as effective values corresponding to that particular sub-grid realization. The steps can be outlined as follow:

1. Assign n_{bR} bins and n_{bT} bins to the histograms of $\bar{\phi}_R$ and $\bar{\phi}_T$, respectively. A total of $n_{bR} \times n_{bT}$ bin combinations are possible.

2. For a given bin combination, perform unconditional simulation to generate n_s sub-grid realizations of ϕ_R. If ϕ_R is assumed to be Gaussian, variogram

γ_R, together with a histogram consisting of mean = $\bar{\phi}_{bR}$ and variance = σ_R^2 can be used. Finally, ϕ is re-constructed as the sum of ϕ_R and $\bar{\phi}_T$.

3. Construct an equivalent homogeneous model corresponding to each model from Step #2.

4. Simulate velocity and solute transport using all n_s set of heterogeneous and homogeneous models constructed in Steps #2-3. Particle-based technique (Eqs. 6-7) is used for transport modeling. Estimate β^*, t_1^* and t_2^* for all n_s sub-grid realizations.

5. Repeat Steps #2-4 to construct $P\{\beta^* \mid (\bar{\phi}_R, \bar{\phi}_T)\}$ $P\{t_1^* \mid (\bar{\phi}_R, \bar{\phi}_T)\}$ and $P\{t_2^* \mid (\bar{\phi}_R, \bar{\phi}_T)\}$.

6. For each coarse-scale model constructed in section 5.3.1, at each location, sample β^*, t_1^* and t_2^* from $P\{\beta^* \mid (\bar{\phi}_R, \bar{\phi}_T)\}$, $P\{t_1^* \mid (\bar{\phi}_R, \bar{\phi}_T)\}$ and $P\{t_2^* \mid (\bar{\phi}_R, \bar{\phi}_T)\}$.

The workflow for sections 5.3.1 and 5.3.2 are illustrated in Fig. 5.2. For non-Gaussian continuous variables, other multivariate statistics description can be adopted to generate the sub-grid realizations (Steps #2-3) and the coarse-scale models (section 5.3.1), instead of computing γ_R and $\bar{\gamma}_R$. Therefore, the overall workflow is rather flexible and is not restricted to particular forms of the multivariate distribution.

159

5.4 Case Study

The proposed approach is illustrated with a synthetic case study involving a 2000 m × 2000 m domain along the 2-D x-y plan. It is assumed that the "true" fine-scale (1000 × 1000) model of porosity and permeability at a resolution of $\Delta x = \Delta y = 2$ m is known. However, it is often impractical to perform transport modeling with the fine-scale model; instead, a suite of coarsened 100 × 100 models with $\Delta x = \Delta y = 20$ m (Fig. 5.3B) are used. The proposed method is applied to generate these coarse-scale models, and the results are compared to those obtained with the fine-scale model. It is supposed that a total of 18 wells are placed along the opposite sides of the domain (Fig. 5.3A). Porosity values at a resolution of 2 m are extracted from petrophysical log/core analysis, and they are considered as conditioning data. As mentioned in section 5.3.1, a scale-invariant relationship between permeability (in mD) and porosity is adopted: ($k = 25000\phi^2$). The histogram and variogram corresponding to ϕ, ϕ_R and $\bar{\phi}_T$ are presented in Fig. 5.4 and Fig. 5.5, respectively. The "true" model of ϕ, as well as its respective trend and residual components, are shown in Fig. 5.6. Fine-scale transport parameters are assumed to be known (e.g., from laboratory measurements): longitudinal dispersivity or $\alpha_L = 2.0$ m, while transverse dispersivity or $\alpha_T = 0.1 \times \alpha_L$ (Perkins and Johnston 1963; Gelhar et al. 1992). Parameters of the TPL model, t_1, t_2 and β are set to be 4 years, 10^4 years and 1.25, respectively.

The procedure described in section 5.3.1 is adopted to model coarse-scale porosity and permeability distributions. $Var(\bar{Z}_R)$ corresponding to a volume support of 20 m × 20 m is approximately 0.9 according to Eq. (5.9). The coarse-

scale histograms and variograms ($\overline{\gamma}_R$ calculated from γ_R with Eq. 5.10) are presented in Fig. 5.7and Fig. 5.8, respectively. Conditional sequential Gaussian simulations (SGSIM), as implemented in *GSLIB* (Deutsch and Journel 1998), are performed to generate 10 realizations of $\overline{\phi}_R$ and $\overline{\phi} = \overline{\phi}_R + \overline{\phi}_T$ for each of the 10 conditioning data sets. As a result, a total of $10 \times 10 = 100$ realizations of scaled-up distribution of $\overline{\phi}$ are obtained. A randomly-selected realization is shown in Fig. 5.9.

The scale-up procedure presented in section 5.3.2 is implemented to compute β^*, t_1^* and t_2^*. Three bins for the residual component (i.e., $n_{bR} = 3$) corresponding to $\overline{\phi}_R = 0.05, 0.075, 0.1$ and three bins for the trend component (i.e., $n_{bT} = 3$) corresponding to $\overline{\phi}_T = 0.05, 0.15, 0.25$ are selected. For each of the bin combinations, 50 unconditional sub-grid realizations ($n_s = 50$) of ϕ are constructed. The domain of a 10×10 sub-grid realization ($\Delta x = \Delta y = 2$ m) is illustrated in Fig. 5.3(C). Fig. 5.10 illustrates how a randomly-selected realization corresponding to $\overline{\phi}_R = 0.1$ is combined with three different values of $\overline{\phi}_T$ to construct three sub-grid realizations of ϕ. This procedure would yield a total of $n_s \times n_{bR} \times n_{bT} = 450$ sub-grid realizations, and corresponding to each realization, an equivalent average model with homogeneous properties is generated. Next, particle-tracking modeling is facilitated by placing three pairs of injector and producer along the opposite sides of the domain (Fig. 5.3C). Fig. 5.11(A) shows a comparison of breakthrough effluent histories between the heterogeneous and the equivalent homogeneous sub-grid models. As shown in Fig. 5.11(B), the *RMSE* is reduced below a certain pre-defined tolerance in fewer than 100 iterations using

an implementation of the very fast simulated annealing (VFSA) scheme (Li et al. 2004). $P\{\beta^* \mid (\bar{\phi}_R, \bar{\phi}_T)\}$ $P\{t_1^* \mid (\bar{\phi}_R, \bar{\phi}_T)\}$ and $P\{t_2^* \mid (\bar{\phi}_R, \bar{\phi}_T)\}$ for $\bar{\phi}_R = 0.1$ and $\bar{\phi}_T = 0.15$ are shown in Fig. 5.12.

Two additional cases are tested: (1) only scale-up of β is considered and (2) only scale-up of β and t_1 are considered. The objective is to assess the sensitivity of coarse-scale model predictions to the scale-up of different parameters. Therefore, the corresponding probability distributions are also shown in Fig. 5.12.

5.5 Results and Discussions

The workflow presented thus far facilitates all 3 parameters, β^*, t_1^* and t_2^*, to be estimated at the coarse scale. However, β, t_1 and t_2 are typically estimated from effluent histories indirectly; this inverse problem in inherently ill-posed, but the sensitivity of these parameters is not clearly defined. All three parameters and the type of model (ADE vs. CTRW) can be arbitrarily adjusted to match a given effluent profile, such as the 1D toolbox developed by Cortis et al. (2010).

Four sets of coarse-scale models are constructed to examine the scale-up procedure, as well as the impact of heterogeneity at different scales. To facilitate the comparison among different cases, effluent histories corresponding to these four sets of coarse-scale models are shown in Fig. 5.13 and Fig. 5.14.

In Case A, the scale-up procedure in section 5.3.2 is applied to compute effective dispersivities (α_L^* and α_T^*), instead of t_1^*, t_2^* and β^*. The results of Case A are shown in Fig. 5.13(A) and Fig. 5.14(A). The results reaffirm that if fine-

scale values of t_1, t_2 and β are assigned (without scale-up), the coarse-scale response would likely be overly smoothened (becoming more Gaussian or Fickian) by scaling up of α_L and α_T instead. This is evidenced by an increased variability among the cumulative mass flux profiles for Case A, as compared to other Cases (B-D), in Fig. 5.13. There are also more profiles in Fig. 5.14(A) that are exhibiting earlier peak arrival when compared with the true case.

Next, three scenarios (Cases B-D) are set up to assess the sensitivity of coarse-scale model predictions to the scale-up of different parameters. In Case B, only coarse-scale values of β are computed, while fine-scale α_L, α_T, t_1 and t_2 values are employed. The results are shown in Fig. 5.13(B) and Fig. 5.14(B). Case C is the same as Case B, except for that the coarse-scale values for both β and t_1 are considered (fine-scale α_L, α_T and t_2 values are used). The results are shown in Fig. 5.13(C). In Case D, coarse-scale values of all three parameters, β, t_1, and t_2, are considered (fine-scale α_L and α_T values are used). The results are shown in Fig. 5.13(D). It is observed that the true response (blue in color) of true fine-scale model is completely captured by the responses of the coarse-scale models (orange in color) from all three cases. As expected, there is no well-defined relationship between β, t_1 and t_2. However, it is clear that β is a function of sub-grid heterogeneity, and its variability increases with scale (β^* ranges between 1.18 and 1.32, as compared to $\beta = 1.25$). The other two parameters, t_1^* and t_2^*, appear to increase with β^*.

With the implementation of the particle-based CTRW transport model, non-Fickian characteristics, such as early breakthrough and heavy-tailed effluent

history profile is easily observed. The particle distribution and resident concentration (volume-averaged concentration) at 1500 days are also presented in Fig. 5.15. It is clear that transport evolution with a non-Fickian model has resulted in a much wider spread. This non-Fickian feature results from the coupling of non-stationary trend, unresolved heterogeneity below the fine scale, as well the sub-scale variability introduced during scale-up to the transport modeling scale.

The computational requirement is examined in Table 5.1. A high-performance Linux-based computing environment is employed for the velocity and transport calculations. It consists of 240 nodes with Xeon X5675 processors [12 cores (2 x 6) and 24 GB of memory] and 160 nodes with Xeon L5420 processors 8 cores (2 x 4) and 16 GB of memory]. The X5675 nodes are connected at 40 Gbit/s, with a 1:1 blocking factor, while the L5420 nodes are connected at 20 Gbit/s, with a 2:1 blocking factor. Similar to the observations in Vishal and Leung (2015), significant savings in computational requirement can be realized with the coarse-scale models Therefore, the ability to construct coarse-scale models that capture the impacts of multi-scale heterogeneities in transport response is crucial.

5.6 Conclusions

1. A new unified multi-scale particle-tracking framework was developed. The methodology was formulated to facilitate the scale-up of truncated power law parameters (waiting time, cut-off time, and exponent) and reservoir attributes (porosity and permeability) for dispersive solute transport in single-phase flow. Heterogeneity spanning over multiple scales, including non-stationary

trend, unresolved heterogeneity below the fine scale, as well the sub-scale variability introduced during scale-up is incorporated.

2. First, to capture unresolved heterogeneity below the fine scale, a particle-based non-Fickian transport model, which utilizes a stochastic transition time function, is adopted. Next, to incorporate non-stationary trend, which is defined at the same resolution of the transport modeling scale, is employed. Finally, to calibrate the sub-scale variability introduced due to the change in volume support between the transport modeling scale and the fine scale, a numerical procedure is presented to establish the probability distributions of effective (coarse-scale) transition time distributions conditional to the averaged reservoir properties at the transport modeling scale.

3. It is not necessary to assume any specific multivariate distribution of the heterogeneity. The variance of mean and the bootstrapping can be implemented using a certain averaging window and computing the statistics pertinent to the spatial mean. Any sequential simulation technique for continuous variables can be adopted to generate the sub-grid and coarse-scale models of reservoir attributes.

4. A special example involving the covariance-based Gaussian model was adopted in the case study. Predictions from the coarse-scale models are capable of capturing the "true" fine-scale response. Many of the anomalous characteristics associated with multi-scale heterogeneities, including early breakthrough, spread-out plume and heavy-tailed effluent profile, are captured.

References

Aronofsky, J. S., & Heller, J. P. (1957). A diffusion model to explain mixing of flowing miscible fluids in porous media. *Trans AIME, 210(12)*, (pp. 345-349).

Bear, J. (1979). *Hydraulics of groundwater.* New York: McGraw-Hill.

Becker, M. W., & Shapiro, A. M. (2003). Interpreting tracer breakthrough tailing from different forced-gradient tracer experiment configurations in fractured bedrock. *Water Resour Res, 39(1)*, 1024.

Benson, D. A., Aquino, T., Bolster, D., Engdahl, N., Henri, C. V., & Fernàndez-Garcia, D. (2017). A comparison of Eulerian and Lagrangian transport and non-linear reaction algorithms. *Advances in Water Resources, 99*, 15-37.

Benson, D. A., Wheatcraft, S. W., & Meerschaert, M. M. (2000). Application of a fractional advection-dispersion equation. *Water Resources Research, 36(6)*, 1403-1412.

Berentsen, C. W., Van Kruijsdijk, C. P., & Verlaan, M. L. (2007). Upscaling, relaxation and reversibility of dispersive flow in stratified porous media. *Transport Porous Med, 68(2)*, (pp. 187-218).

Berkowitz, B., Cortis, A., Dentz, M., & Scher, H. (2006). Modeling non-Fickian transport in geological formations as a continuous time random walk. *Reviews of Geophysics, 44(2)*.

Berkowitz, B., Scher, H., & Silliman, S. E. (2000). Anomalous transport in laboratory-scale, heterogeneous porous media. *Water Resour Res, 36(1)*, (pp. 149-158).

Bijeljic, B., Raeini, A., Mostaghimi, P., & Blunt, M. J. (2013). Predictions of non-Fickian solute transport in different classes of porous media using direct simulation on pore-scale images. *Physical Review E, 87(1)*, 013011.

Binning, P., & Celia, M. A. (2002). A forward particle tracking Eulerian–Lagrangian localized adjoint method for solution of the contaminant transport equation in three dimensions. *Adv Water Resour, 25(2)*, (pp. 147-157).

Boso, F., Bellin, A., & Dumbser, M. (2013). Numerical simulations of solute transport in highly heterogeneous formations: A comparison of alternative numerical schemes. *Advances in Water Resources, 52*, 178-189.

Carrera, J., Sánchez-Vila, X., Benet, I., Medina, A., Galarza, G., & Guimerà, J. (1998). On matrix diffusion: formulations, solution methods and qualitative effects. *Hydrogeology Journal, 6(1)*, 178-190.

Cortis, A., Emmanuel, S., Rubin, S., Willbrand, K., & Berkowitz, B. (2010). *The CTRW Matlab toolbox v3.1: a practical user's guide*. Retrieved from http://www.weizmann.ac.il/ESER/People/Brian/CTRW.

Cortis, A., Gallo, C., Scher, H., & Berkowitz, B. (2004). Numerical simulation of non-Fickian transport in geological formations with multiple-scale heterogeneities. *Water Resour Res, 40(4)*.

Dagan, G. (1982). Stochastic modeling of groundwater flow by unconditional and conditional probabilities: 1. Conditional simulation and the direct problem. *Water Resources Research, 18(4)*, 813-833.

Dagan, G. (1984). Solute transport in heterogeneous porous formations. *Journal of fluid mechanics, 145*, 151-177.

Dagan, G. (1987). Theory of solute transport by groundwater. *Annual review of fluid mechanics, 19 (1)*, 183-213.

Dagan, G. (1989). *Flow and transport in porous formations.* New-York: Springer-Verlag.

Dentz, M., Cortis, A., Scher, H., & Berkowitz, B. (2004). Time behavior of solute transport in heterogeneous media: transition from anomalous to normal transport. *Advances in Water Resources, 27(2)*, (pp. 155-173).

Deutsch, C. V., & Journel, A. G. (1998). *Geostatistical software library and users guide.* New York: Oxford university press.

Efendiev, Y., Durlofsky, L. J., & Lee, S. H. (2000). Modeling of subgrid effects in coarse-scale simulations of transport in heterogeneous porous media. *Water Resour Res, 36(8)*, (pp. 2031-2041).

Fanchi, J. R. (1983). Multidimensional numerical dispersion. *SPE J, 23(1)*, (pp. 143-151).

Fernàndez-Garcia, D., & Sanchez-Vila, X. (2011). Optimal reconstruction of concentrations, gradients and reaction rates from particle distributions. *J Contam Hydrol, (120-121)*, (pp. 99-114).

Fernàndez-Garcia, D., Illangasekare, T. H., & Rajaram, H. (2005). Differences in the scale-dependence of dispersivity estimated from temporal and spatial moments in chemically and physically heterogeneous porous media. *Adv Water Resour, 28(7)*, (pp. 745-759).

Fernàndez-Garcia, D., Llerar-Meza, G., & Gómez-Hernández, J. J. (2009). Upscaling transport with mass transfer models: Mean behavior and propagation of uncertainty. *Water Resour Res, 45(10)*.

Fleurant, C., & Van Der Lee, J. (2001). A stochastic model of transport in three-dimensional porous media. *Math Geol, 33(4)*, (pp. 449-474).

Fogedby, H. C. (1994). Langevin equations for continuous time Lévy flights. *Physical Review E, 50, 1657*.

Gelhar, L. W. (1986). Stochastic subsurface hydrology from theory to applications. *Water Resources Research, 22(9s)*, 135S–145S.

Gelhar, L. W., & Axness, C. L. (1983). Three-dimensional stochastic analysis of macrodispersion in aquifers. *Water Resour.Res, 19 (1)*, 161-180.

Gelhar, L. W., Welty, C., & Rehfeldt, K. R. (1992). A critical review of data on field-scale dispersion in aquifers. *Water Resour Res, 28(7)*, (pp. 1955-1974).

Gylling, B., Moreno, L., & Neretnieks, I. (1999). The channel network model—A tool for transport simulations in fractured media. *Ground Water, 37(3)*, (pp. 367-375).

Haajizadeh, M., Fayers, F. J., Cockin, A. P., Roffey, M., & Bond, D. J. (1999). On the importance of dispersion and heterogeneity in the compositional simulation of miscible gas processes. *In SPE Asia Pacific Improved Oil Recovery Conference.* Kuala Lumpur, Malaysia: Society of Petroleum Engineers.

Haggerty, R., & Gorelick, S. M. (1995). Multiple-rate mass transfer for modeling diffusion and surface reactions in media with pore-scale heterogeneity. *Water Resources Research, 31(10)*, 2383-2400.

Hassan, A. E., & Mohamed, M. M. (2003). On using particle tracking methods to simulate transport in single-continuum and dual continua porous media. *J Hydrol, 275(3)*, (pp. 242-260).

Jha, R. K., Bryant, S., & Lake, L. W. (2011). Effect of diffusion on dispersion. *SPE J, 16(1)*, (pp. 65-77).

John, A. K. (2008). *Dispersion in Large Scale Permeable Media (Dissertation).* University of Texas at Austin.

Journel, A. G., & Huijbregts, C. J. (1978). *Mining geostatistics.* London: Academic press.

Kinzelbach, W., & Uffink, G. (1991). The random walk method and extensions in groundwater modelling. In J. Bear, & M. Y. Corapcioglu, *Transport Processes in Porous Media* (pp. 761-787). The Netherlands: Kluwer Academic Publishers.

Kitanidis, P. K. (1988). Prediction by the method of moments of transport in a heterogeneous formation. *Journal of Hydrology, 102(1)*, 453-473.

Kitanidis, P. K. (1992). Analysis of macrodispersion through volume-averaging: Moment equations. *Stochastic Hydrology and Hydraulics, 6(1)*, 5-25.

Kleinhans, D., & Friedrich, R. (2007). Continuous-time random walks: Simulation of continuous trajectories. *Physical Review E, 76, 061102/1–6.*

LaBolle, E. M., Fogg, G. E., & Tompson, A. F. (1996). Random-walk simulation of transport in heterogeneous porous media: Local mass-conservation problem and implementation methods. *Water Resour Res, 32(3)*, (pp. 583-593).

Lake, L. W., & Srinivasan, S. (2004). Statistical scale-up of reservoir properties: Concepts and applications. *J Pet Sci Eng, 44(1)*, (pp. 27-39).

Lantz, R. B. (1971). Quantitative evaluation of numerical diffusion (truncation error). *Society of Petroleum Engineers Journal, 11(03)*, (pp. 315-320).

Le Borgne, T., & Gouze, P. (2008). Non-Fickian dispersion in porous media: 2. Model validation from measurements at different scales. *Water Resour Res, 44(6)*.

Leung, J. Y., & Srinivasan, S. (2011). Analysis of uncertainty introduced by scaleup of reservoir attributes and flow response in heterogeneous reservoirs. *SPE J, 16(3)*, (pp. 713-724).

Leung, J. Y., & Srinivasan, S. (2012). Scale-up of mass transfer and recovery performance in heterogeneous reservoirs. *J Pet Sci Eng, (86-87)*, (pp. 71-86).

Leung, J. Y., & Srinivasan, S. (2016). Effects of reservoir heterogeneity on scaling of effective mass transfer coefficient for solute transport. *J Contam Hydrol, 192*, (pp.181-193).

Levy, M., & Berkowitz, B. (2003). Measurement and analysis of non-fickian dispersion in heterogeneous porous media. *J Contam Hydrol, 64(3)*, (pp. 203-226).

Li, X., Koike, T., & Pathmathevan, M. (2004). A very fast simulated re-annealing (VFSA) approach for land data assimilation. *Comput Geosci, 30(3)*, (pp. 239-248).

Lichtner, P. C., Kelkar, S., & Robinson, B. (2002). New form of dispersion tensor for axisymmetric porous media with implementation in particle tracking. *Water Resources Research, 38(8)*.

Metzler, R., & Klafter, J. (2000). The random walk's guide to anomalous diffusion: a fractional dynamics approach. *Physics Reports, 339*, 1–77.

Nash, J., & Sutcliffe, J. V. (1970). River flow forecasting through conceptual models part I—A discussion of principles. *Journal of hydrology, 10(3)*, (pp. 282-290).

Neuman, S. P. (1994). Generalized scaling of permeabilities: Validation and effect of support scale. *Geophysical Research Letters, 21(5)*, (pp. 349-352).

Neuman, S. P., & Tartakovsky, D. M. (2009). Perspective on theories of non-Fickian transport in heterogeneous media. *Advances in Water Resources, 32(5)*, 670-680.

Neuman, S. P., & Zhang, Y. K. (1990). A quasi-linear theory of non-Fickian and Fickian subsurface dispersion: 1. Theoretical analysis with application to isotropic media. *Water Resources Research, 26(5)*, 887-902.

Neuman, S. P., Winter, C. L., & Newman, C. M. (1987). Stochastic theory of field-scale Fickian dispersion in anisotropic porous media. *Water Resources Research, 23(3)*, 453-466.

Pedretti, D., & Fernàndez-Garcia, D. (2013). An automatic locally-adaptive method to estimate heavily-tailed breakthrough curves from particle distributions. *Advances in Water Resources, 59*, 52-65.

Pedretti, D., Fernàndez-Garcia, D., Sanchez-Vila, X., Bolster, D., & Benson, D. A. (2014). Apparent directional mass-transfer capacity coefficients in three-dimensional anisotropic heterogeneous aquifers under radial convergent transport. *Water Resour Res, 50(2)*, (pp. 1205-1224).

Perkins, T. K., & Johnston, O. C. (1963). A review of diffusion and dispersion in porous media. *SPE J, 3(01)*, (pp. 70-84).

Riva, M., Guadagnini, A., Fernandez-Garcia, D., Sanchez-Vila, X., & Ptak, T. (2008). Relative importance of geostatistical and transport models in describing heavily tailed breakthrough curves at the Lauswiesen site. *J Contam Hydrol, 101(1)*, (pp. 1-13).

Rubin, Y. (2003). *Applied stochastic hydrogeology.* Oxford University Press, Oxford: UK.

Salamon, P., Fernàndez-Garcia, D., & Gómez-Hernández, J. J. (2006a). A review and numerical assessment of the random walk particle tracking method. *Journal of contaminant hydrology, 87(3)*, (pp. 277-305).

Salamon, P., Fernàndez-Garcia, D., & Gómez-Hernández, J. J. (2006b). Modeling mass transfer processes using random walk particle tracking. *Water Resour Res, 42(11)*.

Salamon, P., Fernandez-Garcia, D., & Gómez-Hernández, J. J. (2007). Modeling tracer transport at the MADE site: the importance of heterogeneity. *Water resources research, 43(8)*.

Scheidegger, A. E. (1959). An evaluation of the accuracy of the diffusivity equation for describing miscible displacement in porous media. *Proc. Theory Fluid Flow Porous Media Conf*, (pp. 101-116).

Schulze-Makuch, D., & Cherkauer, D. S. (1998). Variations in hydraulic conductivity with scale of measurement during aquifer tests in heterogeneous, porous carbonate rocks. *Hydrogeology Journal, 6(2)*, (pp. 204-215).

Schulze-Makuch, D., Carlson, D. A., Cherkauer, D. S., & Malik, P. (1999). Scale dependency of hydraulic conductivity in heterogeneous media. *Ground Water, 37(6)*, (pp. 904-919).

Srinivasan, G., Tartakovsky, D. M., Dentz, M., Viswanathan, H., Berkowitz, B., & Robinson, B. A. (2010). Random walk particle tracking simulations of non-Fickian transport in heterogeneous media. *Journal of Computational Physics, 229(11)*, (pp. 4304-4314).

Tompson, A. F., & Gelhar, L. W. (1990). Numerical simulation of solute transport in three-dimensional, randomly heterogeneous porous media. *Water Resour Res, 26(10)*, (pp. 2541-2562).

Vishal, V., & Leung, J. Y. (2017). Statistical Scale-Up of Dispersive Transport in Heterogeneous Reservoir. *In Geostatistics Valencia 2016*, (pp. 733-743). Springer International Publishing.

Vishal, V., & Leung, J. Y. (2015). Modeling impacts of subscale heterogeneities on dispersive solute transport in subsurface systems. *Journal of contaminant hydrology, 182*, (pp. 63-77).

Wang, J., & Kitanidis, P. K. (1999). Analysis of macrodispersion through volume averaging: comparison with stochastic theory. *Environmental Research and Risk Assessment, 13(1-2)*, 66-84.
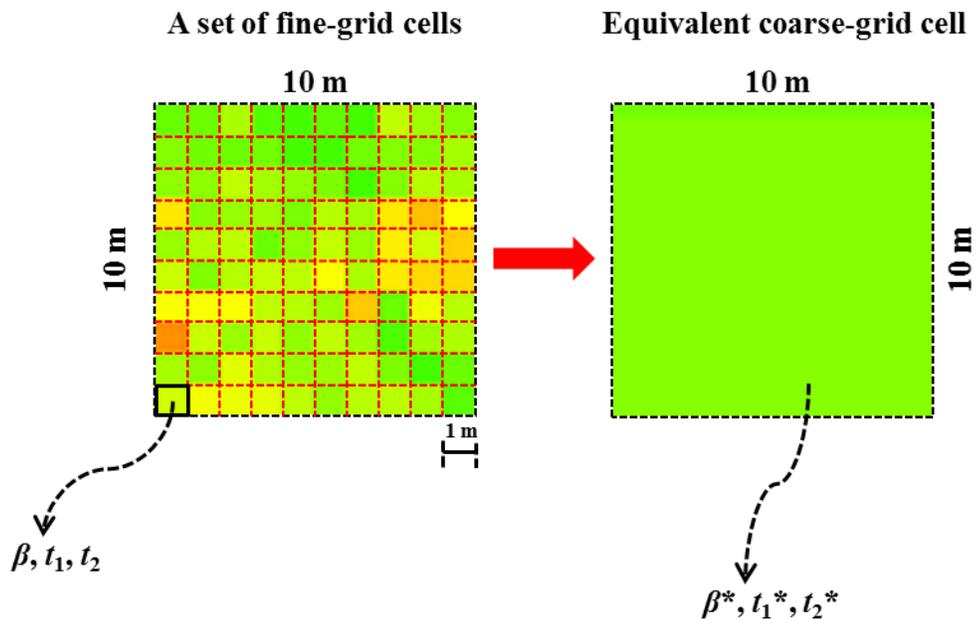
Figure 5.1: Schematic illustrating the difference between fine scale and coarse scale.
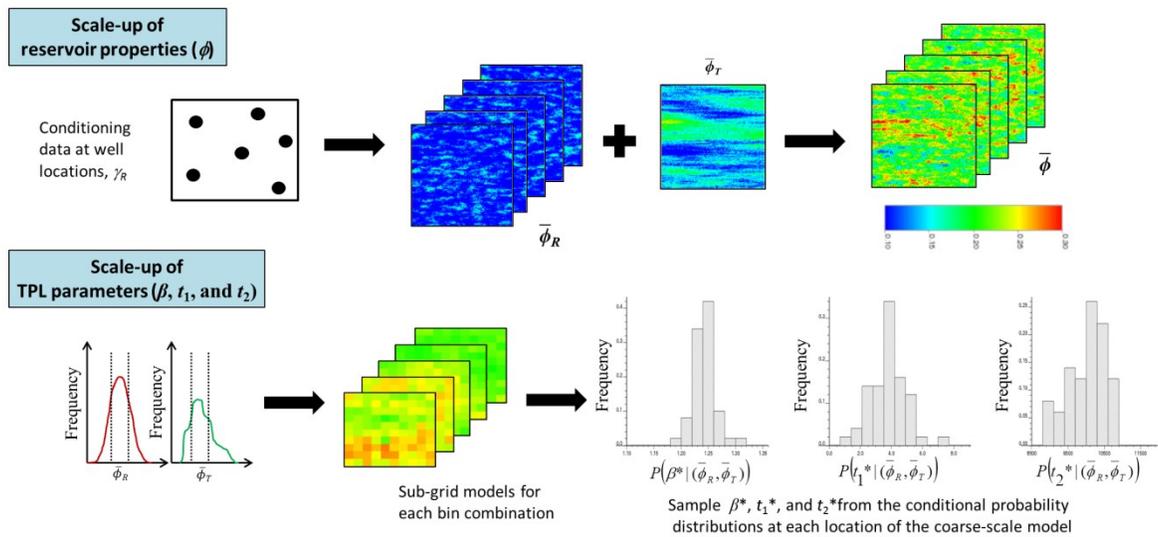
Figure 5.2: Workflow to scale up reservoir properties and transport properties.
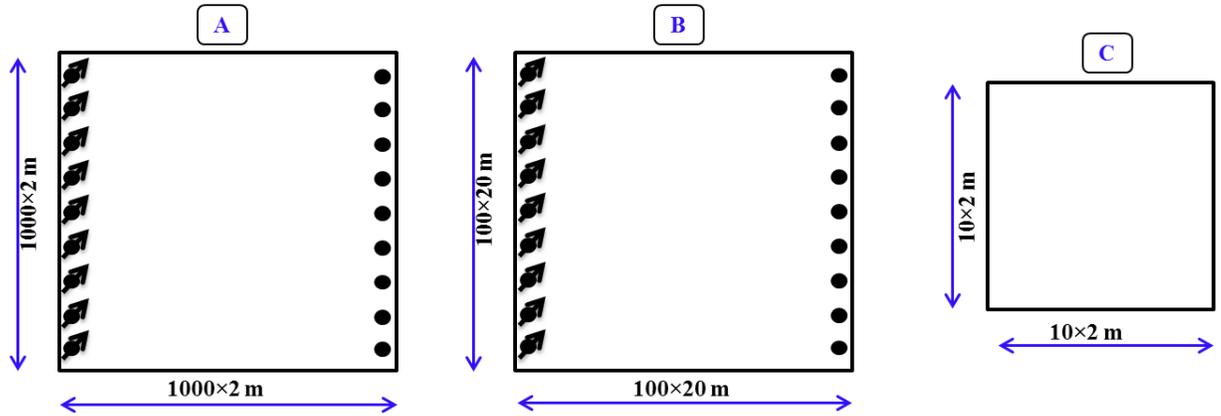
Figure 5.3: Boundary conditions and configuration for the (A) fine-scale model, (B) coarse-scale model and (C) sub-grid model used in the case study.
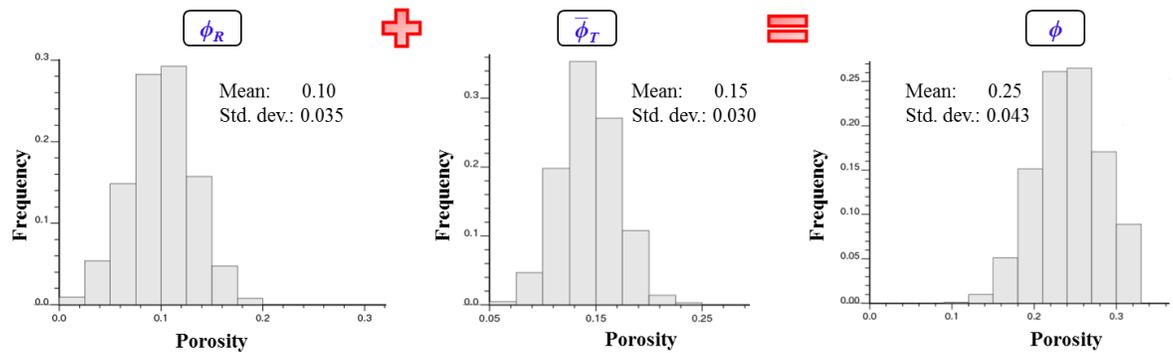
Figure 5.4: Histogram of fine-scale porosity (ϕ), which is decomposed into a sum of residual component (left) and trend component (middle).

Figure 5.5: Variogram of fine-scale porosity (ϕ) (right); variogram of the trend component (middle); variogram of the residual component (left).

Figure 5.6: Distribution of porosity (ϕ), which is decomposed into a sum of residual component (left) and trend component (middle), for the true fine-scale model.
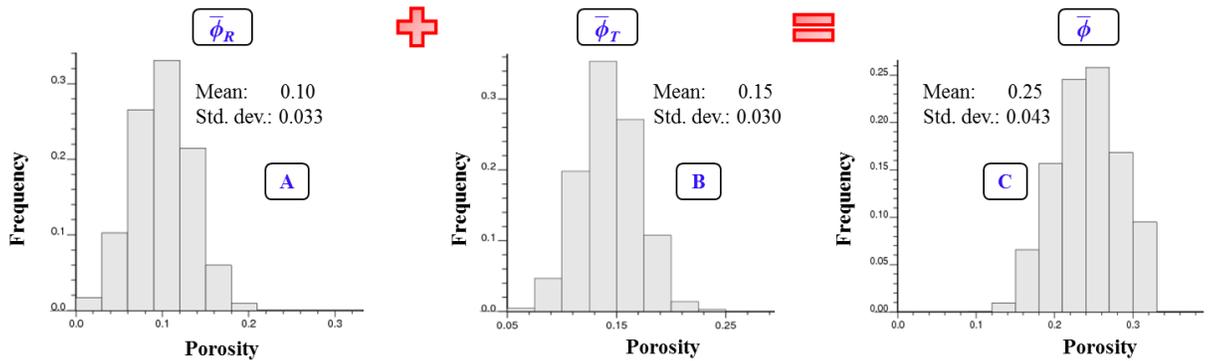
Figure 5.7: Histogram of coarse-scale porosity ($\bar{\phi}$), which is decomposed into a sum of residual component (left) and trend component (middle).
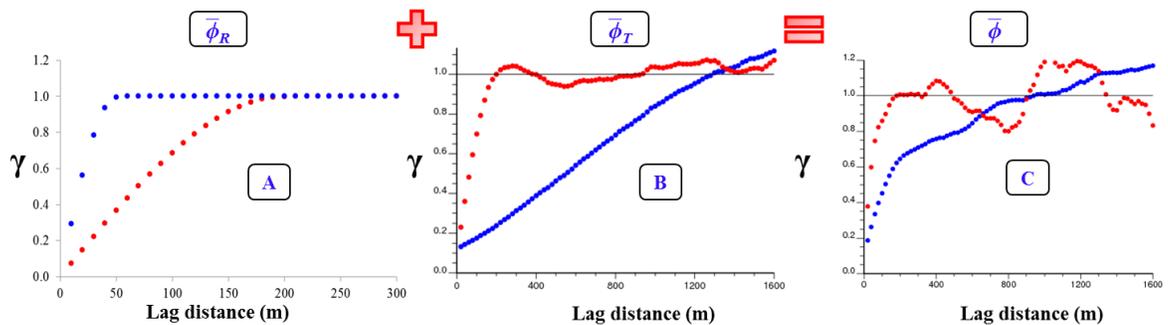
Figure 5.8: Variogram of coarse-scale porosity ($\bar{\phi}$) (right); variogram of the trend component (middle); variogram of the residual component (left).

178
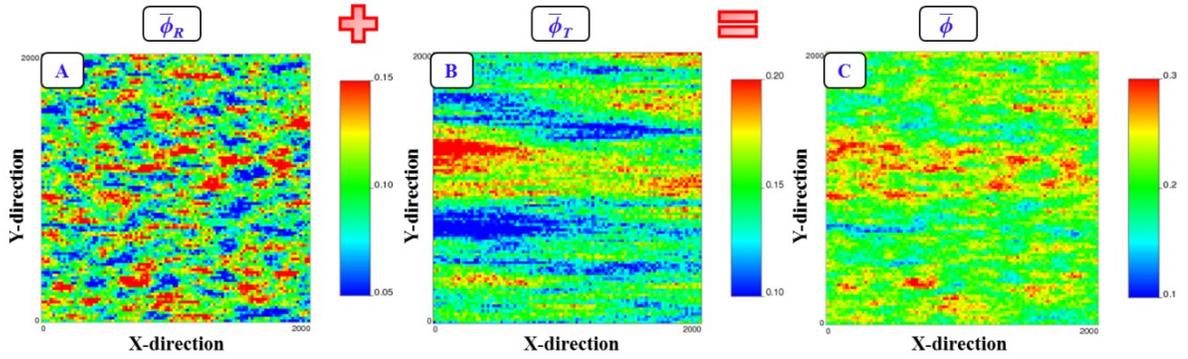
Figure 5.9: Distribution of porosity ($\bar{\phi}$), which is decomposed into a sum of residual component (left) and trend component (middle), for one realization of the coarse-scale model.
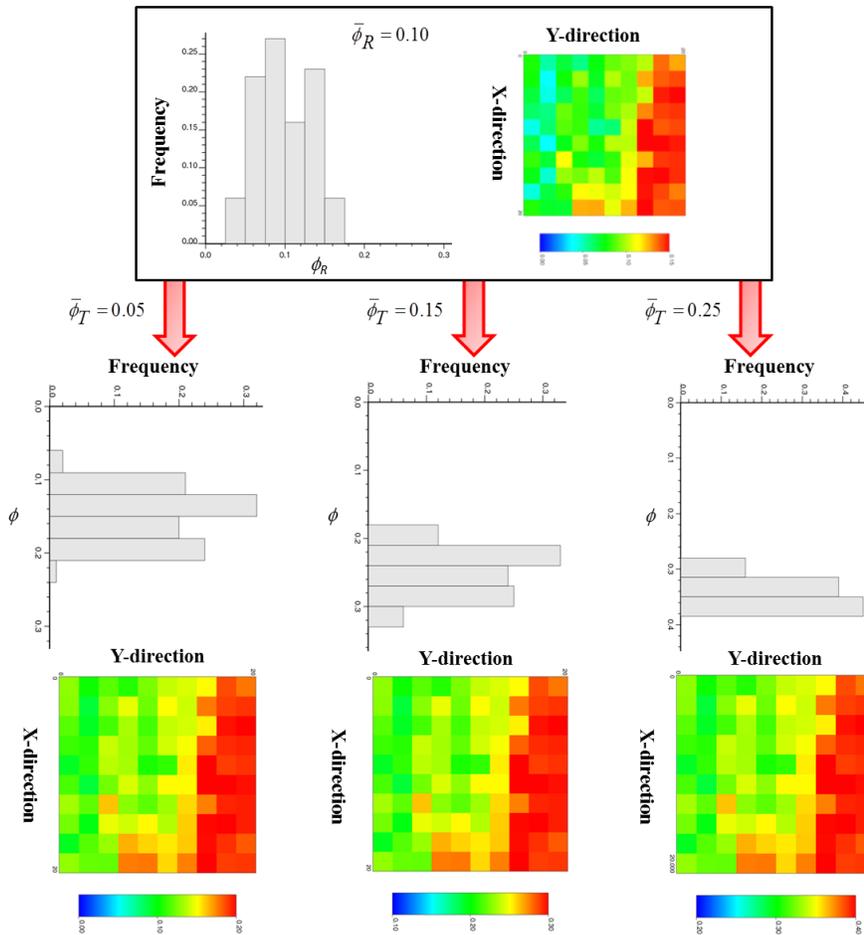
Figure 5.10: Histogram and a randomly-selected realization of ϕ_R corresponding to $\bar{\phi}_R = 0.1$ (top). It is subsequently combined with three different values of $\bar{\phi}_T$ to generate three realizations of ϕ such that $\phi = \phi_R + \bar{\phi}_T$ (bottom). The corresponding histogram is shown on top of each realization of ϕ.
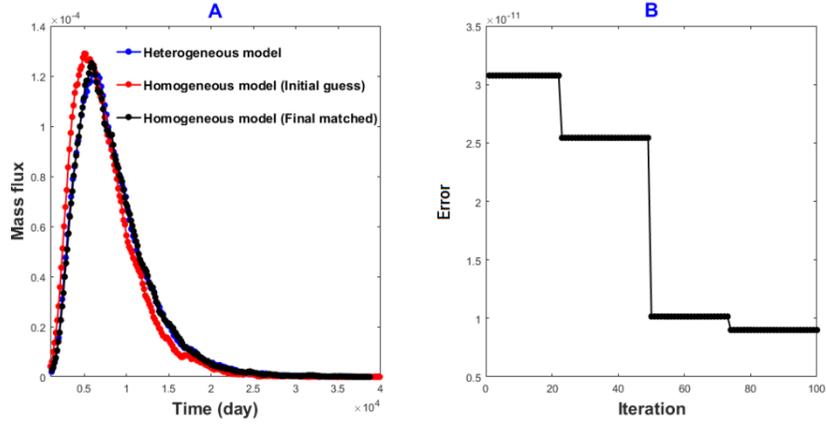
Figure 5.11: (A) Comparison of breakthrough effluent histories between the heterogeneous and equivalent homogeneous sub-grid models. (B) Reduction in *RMSE* over iterations.
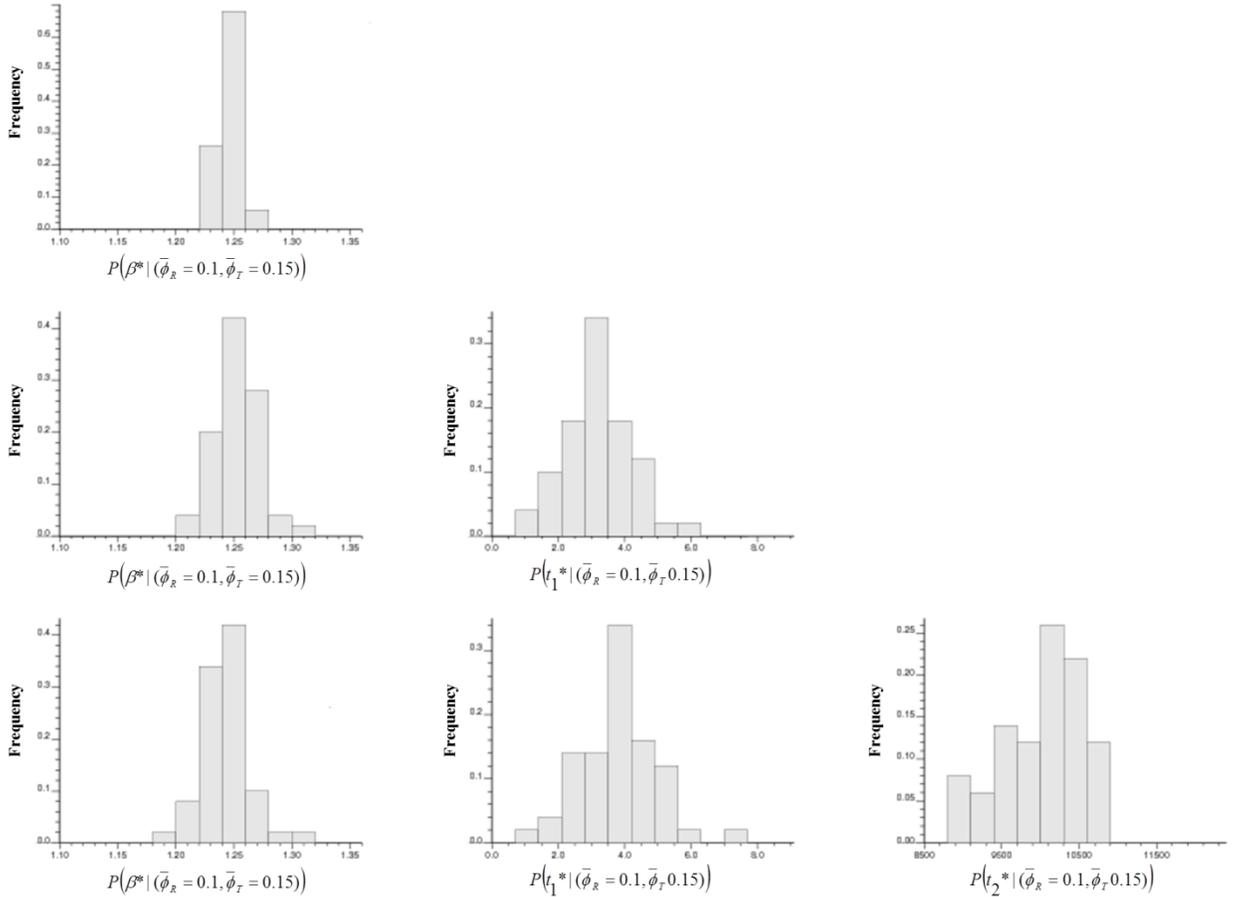
Figure 5.12: Distribution of effective values of β^* (top), β^* and t_1^* (middle), β^*, t_1^*, and t_2^* (bottom) for a selected bin combination of $\bar{\phi}_R = 0.1$ and $\bar{\phi}_T = 0.15$.
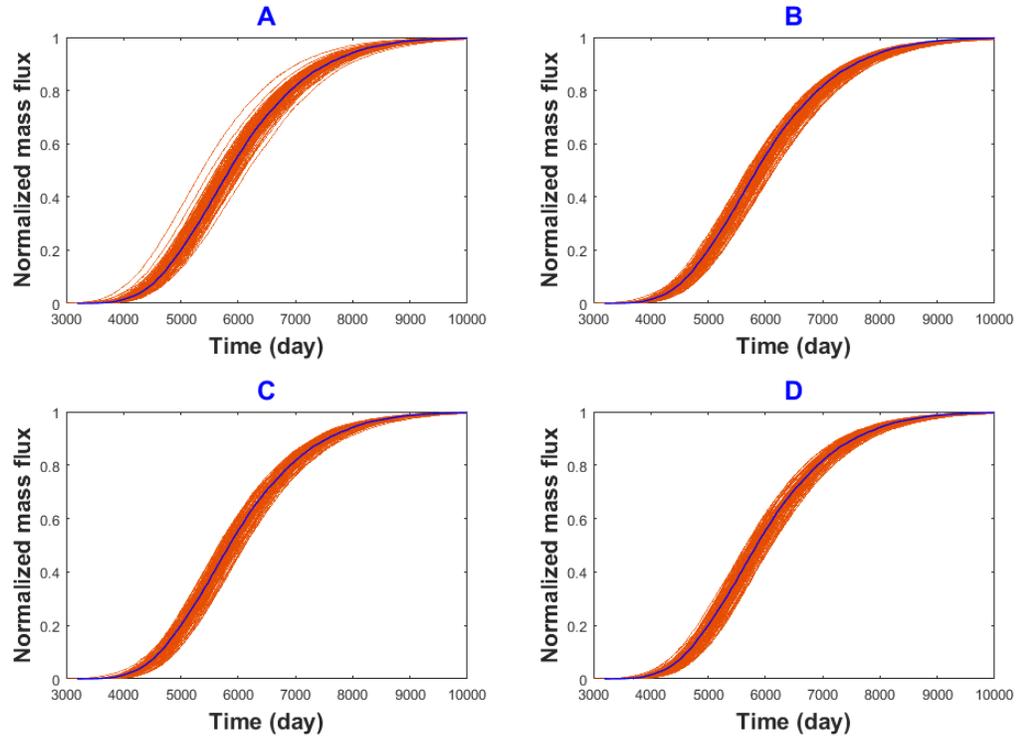
Figure 5.13: Normalized effluent profiles of cumulative mass flux for the four sets of coarse-scale models with different effective transport parameters: (A) α_L^* and α_T^*, (B) β^*, (C) β^* and t_1^*, and (D) β^*, t_1^* and t_2^*. The blue curve corresponds to the true fine-scale model.
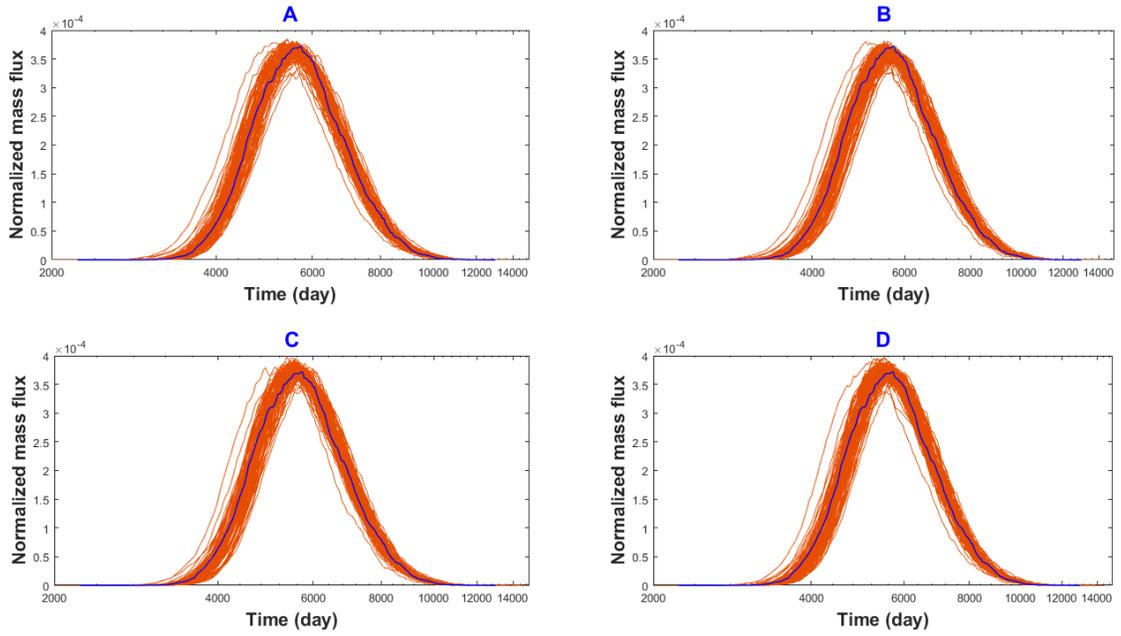
Figure 5.14: Normalized effluent profiles of instantaneous mass flux for the four sets of coarse-scale models with different effective transport parameters: (A) α_L^* and α_T^*, (B) β^*, (C) β^* and t_1^*, and (D) β^*, t_1^* and t_2^*. The blue curve corresponds to the true fine-scale model.
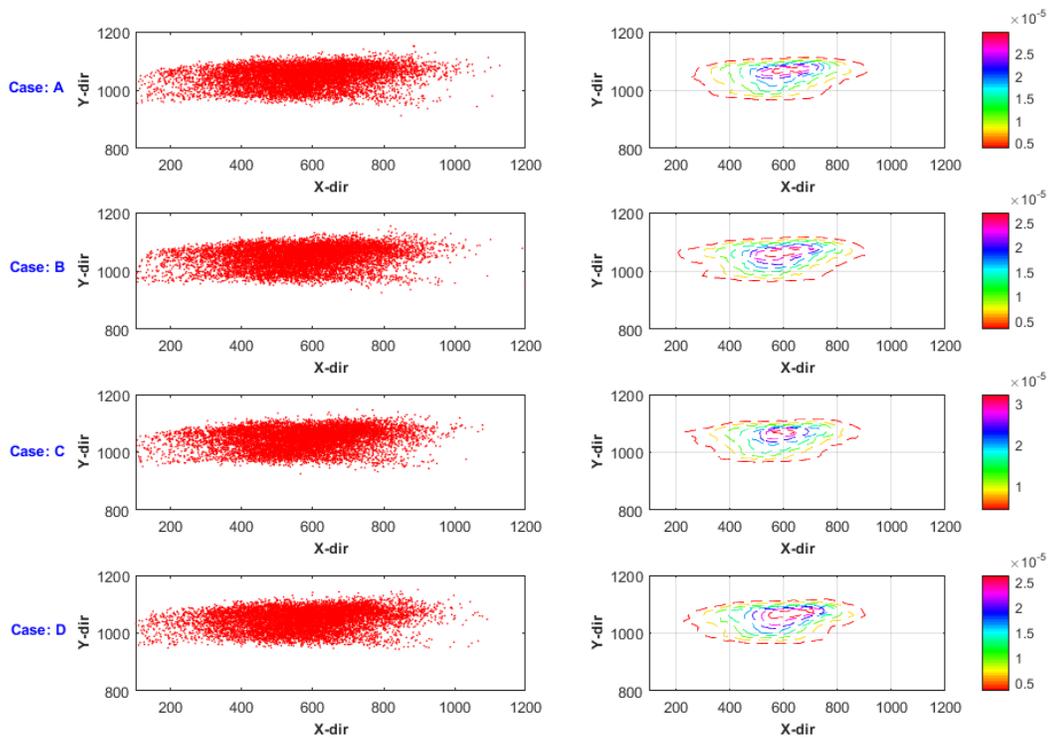
Figure 5.15: Particle distribution (left) and the corresponding resident concentration profile (right) at 1500 days.

Table 5.1: Compilation of computational time

		Number of runs	Computational time using Jasper cluster (Velocity + Transport) Calculations	Remarks
1)	Fine-scale model (1000×1000 with 2×2m grid size)	1	(540 sec + 1200 sec) = 1740 sec	
2)	Sub-grid model (10×10 with 2×2m grid size)	(50 heterogeneous models + 50 homogeneous models) x 9 $\bar{\phi}$ levels	(345 sec + 570 sec) x 9 = 8235 sec	Calculation of P(α_L*|$\bar{\phi}$) and P(α_T*|$\bar{\phi}$) with100 iterations in VFSA using parallel computing scheme
3)	Coarse-scale model (100×100 with 20×20m grid size)	100	(45 sec + 1065 sec) x 100 = 111000 sec	Fully scaled-up model

183

Chapter 6: A Novel Framework for Integration of Random-Walk Particle-Tracking Simulation in Subsurface Multi-Phase Immiscible Flow Modeling[5]

6.1 Introduction

The problem of single- or multi- phase flow in porous media is of great interest in hydrogeological or petroleum engineering because of a variety of applications, such as subsurface remediation of organic contaminants, carbon dioxide sequestration in geological formations, and oil or gas recovery from hydrocarbon reservoirs.

The governing equations pertinent to mass, momentum and energy balances are generally described by a set of partial differential equations (PDEs). Since analytical solution methods often invoke many stringent assumptions (e.g., homogeneous properties and simple initial/boundary conditions), numerical methods could provide reliable approximate solution to the complex governing PDEs. Numerical methods to solve the PDEs can be categorized into Eulerian, Lagrangian and mixed Eulerian-Lagrangian (Zheng and Bennett 2002). Eulerian approach models fluid (e.g. tracer, pollutant) motion by focusing on specific locations in the space through which the fluid flows as time passes, while Lagrangian approach follows an individual particle as it moves through space and time. In other words, Eulerian method considers fluid in a collective sense, while Lagrangian method assumes fluid as a bunch of particles. Common Eulerian-

based approaches are finite-difference (FD), finite-element (FE), and finite volume (FV). In the FD method, derivative functions are approximated by the Taylor series State variable, namely saturation and composition, are taken to be constant within a computational grid cell, whereas pressure is calculated at a fixed location (i.e., grid-cell center) or as an average cell pressure. Despite its ease of implementation in 3D, the FD technique has some significant disadvantages, including numerical dispersion (artificial dispersion), grid orientation effects, inaccuracy in flux calculations in heterogeneous media with capillary pressure contrast, and incompatibility with unstructured grids (Firoozabadi and Hoteit 2007). In the FV approach, the governing equations are integrated over a particular control volume (i.e., grid cell), which is more suited for unstructured grids. It still suffers from numerical dispersion, grid orientation effects and, to a lesser extent, flux calculation for complex problems such as fractured reservoirs. In the FE approach, the unknown variables, such as saturation or concentration, are approximated by using known test functions, which can be linear or higher-order polynomial expansions in terms of unknown variables at appropriate geometric locations (nodes) for certain grid elements; the spatial interpolation of variables within a given cell or element helps to alleviate numerical dispersion to some extent. FD/FV solution methods are implemented in common subsurface flow simulators, due to its flexibility for integrating well models and coupling with complex phase behavior calculations. Higher-order schemes are often needed to suppress numerical dispersion. However, in most cases, numerical dispersion

still overwhelms physical dispersion (spreading of saturation/concentration front due to heterogeneities and velocity variations).

Lagrangian method, which is commonly referred to as particle tracking, offers viable grid-free solution alternative to the Eulerian framework. Its primary advantage is the absence of numerical dispersion. It can model shocks corresponding to a hyperbolic PDE with no limits on the mesh size (Delay et al. 2005; Salamon et al. 2006a).In particle-tracking method, the injected mass or volume is represented by a group of particles, and each particle represents a physical mass/volume. These particles are migrated according to the velocity field (convection) and the dispersion/diffusion (Brownian motion). Particle distribution, instead of concentration/phase-saturation, is computed. Particle-tracking methods have been adopted successfully in hydrology/hydrogeology to simulate passive solute transport (Tompson and Gelhar 1990; Hassan and Mohamed, 2003) and reactive solute transport (Tompson and Gelhar, 1990) in single-phase flow. Tyagi et al. (2008) developed a novel stochastic particle method to model nonlinear immiscible multi-phase incompressible flow. Particle concentration or phase saturation is obtained by counting the number of particles over the control volume. However, large number of particles would be needed per grid block to avoid statistical bias; hence, computational efficiency of their proposed approach is compromised. Therefore, one of the objectives of this paper is to improve the accuracy of phase saturation estimation with dramatically fewer particles via the kernel methods.

Another issue commonly encountered in numerical transport modeling is that the model scale is generally much larger than the scale at which measurements are attained (e.g., logging measurements ~ decimeter scale; core measurements ~ centimeter scale). Generally speaking, transport modeling is often performed at a scale that is coarser than the finest resolution of heterogeneity. In this paper, two scales, in particular, are specified: (1) "Fine scale" describes a length scale over which detailed description about heterogeneity is available; (2) "Coarse scale" refers to the numerical transport modeling scale (e.g., 1-10 m). Many previous works have explored the topic of multi-phase flow upscaling. For flow-based upscaling, both steady-state and unsteady-state (dynamic) methods were proposed (Johnson et al. 1959; Saad et al. 1995; Pickup and Stephen 2000). A set of selection criteria of specific upscaling techniques for different heterogeneity characteristics and dominant forces can be found in Pickup et al. (2005).

These aforementioned techniques aim to identify an "equivalent" value such that the fine-scale response is reproduced. They are employed with the assumption that a single deterministic "upscaled" value would be obtained, which essentially neglects any uncertainty originated from the smoothening due to the averaging process. In the end, to construct a model at the coarse scale, it is important to account for the sub-scale variability that captures the smoothing of fine-scale heterogeneity and the associated uncertainties. There are two major approaches for analysing the scale-up of transport properties and the associated uncertainties: stochastic perturbation (or ensemble averaging) and the volume

187

averaging methods. Ensemble averaging considers the initial conditions, boundary conditions, pressure, flux, and transport parameters as random variables, and their ensemble or moment statistics are then used to obtain effective parameters at the coarse scale. This approach is applicable if the permeability distribution (e.g., covariance structure) can be well defined (Rubin et al. 1999). On the other hand, the volume averaging technique performs spatial averaging to the fine scale equations and formulates scaled-up equations that involve effective parameters. An example for two-phase flow can be found in Durlofsky (1998). Spatial average of the fine scale saturation equation to describe saturation distribution at the coarse scale; however, the complex formulation and assumptions may render the practical application of this approach challenging. An important requirement for the volume averaging is the separation of heterogeneity length scales. In other words, the size of a coarse-scale grid block should be larger than or equal to the representative elementary volume (REV) corresponding to the sub-grid heterogeneity (Leung and Srinivasan 2016). In theory, if the restriction on the heterogeneity length scale and the assumption of ergodicity are satisfied, both methods are equivalent (Wang and Kitanidis 1999).

In this work, a statistical workflow is devised to facilitate the quantification of uncertainty due to averaging in coarse-scale models. Though a similar workflow has been published in Vishal and Leung (2015; 2017), the technique has never been applied to scale up multi-phase flow functions. In order to isolate the impact of numerical dispersion, a particle-tracking transport model is employed to simulate immiscible flow. The method is formulated after Tyagi et

al. (2008), but new elements are incorporated to alleviate some of the existing limitations. For example, instead of employing a large number of particles (10,000-50,000 particles per grid) to minimize errors due to biases, the kernel method is proposed to reconstruct the concentration/saturation from particle distributions directly. The proposed approach is validated against analytical and conventional numerical simulation predictions. This particle-tracking tool is subsequently used to compute coarse-scale multi-phase flow functions, which can be considered readily as input to any commercial simulator. The main contribution of this work is that it offers a systematic workflow to compute multi-phase flow functions at any desired coarse/transport-modelling scale. Instead of deriving a deterministic upscaled value, conditional probability distributions of the multi-phase flow functions are calibrated, and a sampling procedure is utilized to properly quantify the uncertainty due to scale-up. The improved multi-phase particle-tracking formulation is also novel. It should be noted that, in this work, only the flow of two immiscible and incompressible fluids is considered, while the effect of gravity is neglected. The particle-tracking method, however, can be readily extended to incorporate gravity effect in the velocity computation. Although capillary pressure is assumed to be close to zero ($P_c \approx 0$) in the case study, the same scale-up workflow can be adopted to compute the coarse-scale capillary pressure function.

This chapter is organized as follows: first, mathematical detail of the particle-tracking formulation is summarized for both the single-phase miscible flow and multi-phase immiscible flow. Next, the proposed particle-tracking

method is validated against analytical solution, as well as with numerical simulation predictions. Finally, the method is integrated into a statistical scale-up procedure to model key reservoir properties, multi-phase flow functions (relative permeability and capillary pressure) at the coarse scale. In the end, a case study is presented, which is followed by discussions and conclusions.

6.2. Methodology

6.2.1 Random Walk Formulation for Single-phase and Multi-phase Flow

In this section, mathematical formulation of the particle-tracking technique is first presented for single-phase flow. Its analogy to the multi-phase immiscible flow formulation is then noted. Alternatives for estimating solute concentration or phase saturation from the ensuing particle distribution are also discussed.

6.2.1.1 Formulation for Single-Phase Miscible Flow

Mass balance corresponding to solute transport in a subsurface reservoir/aquifer is described by the classical Fickian-based ADE (Bear 1979), as shown in Eq. (6.1):

$$\frac{\partial C(X,t)}{\partial t} = \nabla \cdot (D(X,t) \cdot \nabla C(X,t)) - \nabla \cdot (V(X,t)C(X,t)), \qquad (6.1)$$

in which $C(X, t)$ is the volumetric local solute concentration at location X and time t, $V(X, t)$ is the pore velocity vector, and $D(X, t)$ denotes the dispersion tensor. The velocity field is calculated according to the continuity equation in Eq. (6.2) and the Darcy's law in Eq. (6.3) for incompressible flow conditions:

$$\nabla \cdot V(X,t) = 0. \qquad (6.2)$$

$$V(X,t) = -\frac{K(X)}{\phi(X)\mu}\nabla p(X,t).$$ (6.3)

p is the pressure, K is the absolute permeability tensor, ϕ is the porosity, and μ the fluid dynamic viscosity. In this work, an isotropic K is assumed (i.e., $K = k$), and it is empirically correlated with porosity (ϕ) according to Eq. (6.4) (Deutsch 2010):

$$\log_{10}(k) = \log_{10}(k_0) + a_1\phi + a_2\left(1 - e^{\frac{-3\phi}{\phi_c}}\right),$$ (6.4)

In the particle-tracking framework, solution of the ADE is approximated according to Eq. [5] (Delay et al. 2005):

$$X_p(t+\Delta t) = X_p(t) + \{V(X_p,t) + \nabla D(X_p,t)\}\Delta t + \{2D(X_p,t)\Delta t\}^{0.5}\xi(t).$$ (6.5)

$X_p(t)$ is the particle position at time t; ξ is an independent normally distributed random vector with a mean of zero and a standard deviation of one.

6.2.1.2 Formulation for Multi-Phase Flow

The mass balance equation for each fluid phase (subscript i) is mathematically analogous to Eq. (6.6) (Bear 1972 & 1979; Bolster et al. 2009):

$$\frac{\partial S_i(X,t)}{\partial t} + V_i\{X, S_i(X,t)\}\cdot\nabla S_i(X,t) - \nabla\cdot D\{X, S_i(X,t)\}\nabla S_i(X,t) = 0.$$ (6.6)

Despite its appeared similarity with the ADE equation, the above equation is highly nonlinear, since the drift $V\{X,S_i(X, t)\}$, as well as the dispersion coefficient $D\{X,S_i(X, t)\}$, are functions of phase saturation, $S_i(X, t)$. The velocity field is calculated by combining the continuity equation in Eq. (6.7) and the Darcy's law in Eqs. (6.8)- (6.9):

$$\phi(X)\frac{\partial S_i(X,t)}{\partial t} + \nabla \cdot \boldsymbol{u}_i(X,t) = 0; \tag{6.7}$$

$$\boldsymbol{u}_i(X,t) = -\frac{\boldsymbol{K}(X)k_{ri}(X,S_i)}{\mu_i}\nabla p_i(X,t) = -\boldsymbol{K}(X)\lambda_i(X,S_i)\nabla p_i(X,t); \tag{6.8}$$

$$V_i(X,t) = \frac{\boldsymbol{u}_i(X,t)}{\phi(X)S_i(X,t)}, \tag{6.9}$$

where $\boldsymbol{u}_i(X, t)$ and $p_i(X, t)$ are the superficial flow velocity and pressure of phase i; $k_{ri}(X, S_i)$ and $\boldsymbol{\lambda_i}(X, S_i)$ the relative permeability and mobility of phase i, respectively. Individual phase pressures, $p_i(X, t)$, are coupled as:

$$p_{c_{i-1}}(X,S_i) = p_{i-1}(X,S_{i-1}) - p_i(X,S_i), \tag{6.10}$$

under the following constraint regarding $S_i(X, t)$:

$$\sum_{i=1}^{n} S_i(X,t) = 1. \tag{6.11}$$

$p_c(X, S_i)$ is the capillary pressure, and n is the total number of phases. Each phase is represented by a large number of computational particles (Fig.6.1), and the particle's position at the new time level ($t+\Delta t$) can be obtained according to Eq. (6.12) (Tyagi et al. 2008):

$$X_p^i(t+\Delta t) = X_p^i(t) + \left\{V_i(X_p,t) + \nabla \cdot \boldsymbol{D}(X_p,t)\right\}\Delta t + \left\{2\boldsymbol{D}(X_p,t)\Delta t\right\}^{0.5}\xi(t), \tag{6.12}$$

where X_p^i represents the position of a given particle of phase i. A flow chart explaining the computational steps is shown in the Fig.2. In this work, Eq. (6.12) is implemented by modifying a popular random-walk particle-tracking formulation called RW3D-MRMT (Fernàndez-Garcia et al. 2005; Salamon et al.

2006a, 2006b; Fernàndez-Garcia and Sanchez-Vila 2011; Salamon et al. 2007; Riva et al. 2008), which was originally developed to model solute transport in single-phase flow systems. A few significant modifications must be made to the RW3D-MRMT code. Firstly, a kernel estimator is used to calculate phase saturation at the end of each time step. Next, the particle-tracking simulation, which represents the transport calculation, must be coupled with the flow calculation to compute the velocity field. An implicit-pressure explicit-saturation (IMPES) scheme is followed. Both phase saturation and velocity are updated after every time step. The resultant code is now suitable for modelling two-phase immiscible flow, and the results are validated against analytical solution and those obtained from conventional FD/FV schemes, as implemented in commercial simulators.

6.2.1.3 Construction of Concentration from Particle Distributions

Eq. (6.12) provides the discrete particle displacement (or position). To obtain the corresponding phase saturation, the collective positions of nearby particles must be considered. This is represented by the density of moving particles at a particular instance of time over the underlying computational grid from which the flow solution is obtained. Even though the particle-tracking simulation is grid free on its own, interpretation of concentration/phase-saturation of spatially distributed particles may invoke grid definitions or other smoothing methods, such as the Kernel functions.

The simplest way to construct concentration/saturation from particle distribution is the arithmetic averaging technique or the box kernel method (Fernàndez-Garcia and Sanchez-Vila 2011). In this method, the domain is discretized in space (for residual concentration) and/or time (for flux concentration); the number of particles corresponding a given support (cell) volume is counted. The residual concentration $C(X, t)$ in single-phase flow is defined as:

$$C(X,t) = \frac{N(X,t)m}{\phi V(X)},$$ (6.13)

where m is the mass associated with each particle, and N is the number of solute particles in the cell volume $V(X)$. An analogous expression for phase saturation in multi-phase flow is:

$$S^i(X,t) = \frac{N^i(X,t)v^i}{\phi V(X)},$$ (6.14)

where v^i is volume of the particle of phase i. It should be obvious that the accuracy of this approximation depends on the discretization scheme: limited number of particles in a small support volume would lead to noisy fluctuations, whereas oversized support would result in excessive smoothing. Fernàndez-Garcia and Sanchez-Vila (2011) proposed the use of Kernel density estimator f (u), which is based on a sample $\{u_1,\ldots,u_n\}$ in the form of:

$$f(u) = \frac{1}{nh} \sum_{i=1}^{n} K\left(\frac{u - u_i}{h}\right),$$ (6.15)

where K is the kernel function and h is a smoothing parameter and u is the point where density is to be estimated. The choice for K could be any kernel function

such as the Triangle, Eq. (6.16), and the Gaussian (Hong 2010), Eq. (6.17), models for optimal smoothing:

$$K(u) = (1 - |u|), |u| \leq 1;$$ (6.16)

$$K(u) = \frac{1}{\sqrt{2\pi}} \exp^{-\frac{1}{2}u^2},$$ (6.17)

Kernel density functions essentially establish the spatial distribution of concentration/saturation as a weighted average of discrete particle locations the associated mass/volume of each particle. The mass/volume of particle is a measure of its region of influence. Kernel functions are usually symmetric density functions, whose size and shape is parametrised on the basis of smoothing parameter h. It is worthwhile to note that kernel density estimation is a standard non-parametric technique of constructing histogram from unknown distributions. Because of its non-parametric nature, it is capable of producing multimode distributions. Moreover, it is also capable of producing non-Fickian nature of solute transport, such as the tailing characteristic.

6.2.2 Validation of Particle-Tracking Model in 1-D and 2-D

6.2.2.1 1-D model

In this section, we verify the simulation algorithm results against the analytical Buckley-Leverett (B-L) theory, which is based on the method of characteristics and a commercial numerical simulator (Eclipse black-oil 2011). To facilitate the comparison with the B-L solution, a 1-D domain [0, 20 m] with two phases (oil (o) and water (w)) is considered. The domain contains irreducible water saturation S_{wr} at $t = 0$:

$$S(X_1, t = 0) = S_{wr}. \tag{6.18}$$

Capillary pressure and the diffusion terms are assumed to be zero, and the following boundary condition is prescribed at the inlet:

$$S(X_1 = 0, t) = 1 - S_{or}, \tag{6.19}$$

where S_{or} is the irreducible oil saturation. To compute the total flux, water is injected at a constant rate of 0.216 m/day and a producer operating under constant pressure, same as reservoir pressure, is introduced. Other relevant model parameters and the relative permeability functions are summarized in Table 6.1 and Fig. 6.3, respectively. The resultant distributions of water and oil particles at t = 0 day, t = 10 day, and t = 20 day are shown in Fig. 6.4. The computed water phase saturation (S_w) after t = 10 days and t = 20 days obtained via the proposed particle-tracking method are compared against the B-Land simulator solutions in Fig. 6.5. It is clear that good agreement is obtained; despite that higher-order approximation schemes are implemented in the commercial flow simulators, numerical dispersion, as evidenced by spreading of the saturation front, is still obvious. On the contrary, the front's position and structure as predicted by the proposed particle-tracking formulation resembles the B-L computations more closely.

6.2.2.2 2-D model

A quarter-five-spot configuration of size 30 m × 30 m is considered. Same initial condition as in the above 1-D case is imposed. Once again, capillarity effect is neglected here. To compute the total flux, water is injected at a constant rate of

2.0 m/day at the bottom-left corner of the model, whereas a producer operating under constant pressure, same as the initial reservoir pressure, at the top-right corner of the model. The relative permeability functions are illustrated in Fig. 6.3. Initial ($t = 0$ day) distribution of oil and water particles is shown in Fig. 6.6.

First, a homogeneous domain is considered with absolute permeability of 100 mD and porosity of 0.2. The corresponding particle distributions of the oil and water phases after $t = 10$ days are shown in Fig. 6.7 (left). The computed water phase saturation (S_w) after $t = 10$ days (obtained via the kernel smoothing technique) is compared against the simulation predictions in Fig. 6.7 (right), which shows good consistency in the results.

Next, a heterogeneous domain is considered. Its porosity distribution is shown in Fig. 6.8. Permeability is empirically correlated with porosity by Eq. (6.4). The corresponding particle distributions of the oil and water phases after $t = 10$ days are demonstrated in Fig. 6.9. The computed S_w profiles obtained from the both particle-tracking method and the numerical simulation are compared in Fig. 6.10. Once again, good agreement with the numerical solution is observed.

6.2.3 Scale-up Methodology

Theory and mathematical formulation for constructing a multi-scale workflow are discussed. The workflow for constructing models of reservoir properties is presented, which is followed by the computation of effective, or 'pseudo', multi-phase flow functions, such as relative permeability and capillary pressure (p_c), at the transport modeling (coarse) scale.

6.2.3.1 Scale-up of Reservoir Attributes

Scale-up of reservoir static properties, such as porosity and permeability, is often performed because of disparity in scale among measured data from different sources, and volume support for the transport modeling scale is typically much larger than that of the measurement scale. These change in scale or volume support lead to additional uncertainty in the scaled-up models due to averaging of sub-scale heterogeneity. The variance of mean is a measure of the variability in spatial average over a volume support of V. Let Z be a continuous Gaussian random variable with a variance of σ^2; for given autocorrelation model ρ_{corr}, the variance of its linear average ($\overline{Z}$) can be computed according to Lake and Srinivasan (2004):

$$Var(\overline{Z}) = \frac{2\sigma^2}{V^2}\left(\iint\limits_{v\ \eta} \rho_{corr}(\eta)\,d\eta\,d\xi\right). \tag{6.20}$$

$Var(\overline{Z})$ approaches the mean of fine-scale Z in the limit of V becoming zero. The procedure presented in Leung and Srinivasan (2011) or Vishal and Leung (2015) is implemented to construct realizations of reservoir attributes at the transport modeling scale. For the sake of completeness, the steps are repeated here:

1. Calculate fine-scale variogram γ, which is directly related to ρ_{corr}.

2. Calculate $Var(\overline{Z})$ using Eq. (6.20).

3. Compute average variogram $\overline{\gamma}$ at the coarse scale using Eq. (6.21) (Journel and Hujbregts 1978):

$$\overline{\gamma}(V,V') = \frac{1}{VV'}\iint\limits_{V\ V'} \gamma(v,v')\,dv\,dv' \approx \frac{1}{nn'}\sum_{i=1}^{n}\sum_{j=1}^{n'}\gamma(\mathbf{h}_{ij}), \tag{6.21}$$

where n and n' refer to the numbers of regularly-spaced points in the two averaging volumes of V, V'.

4. Sample multiple sets of coarse-scale conditioning data values from distributions whose mean is the block-average of the actual measured values and the variance is $Var(\overline{Z})$.

5. For each sampled conditioning data set from step 4, perform conditional simulation at the coarse scale using $\overline{\gamma}$ and scaled-up histogram (mean = fine-scale global mean; variance = $Var(\overline{Z})$).

6. Repeat step 5 for remaining conditioning data sets.

In this chapter, the aforementioned procedure is used to compute scaled-up porosity values, which are assigned to individual grid blocks of the coarse-scale transport modeling mesh. Permeability is assumed to follow a log-normal distribution and can be related to the collocated porosity value as Eq. (6.4).

6.2.3.2 Scale-up of Multi-Phase Flow Functions

Power-law relationships are commonly adopted to parameterize the oil and water relative permeabilities. In this paper, the Brooks and Corey model, which are widely implemented in commercial simulators, is employed (Brooks and Corey 1964; Corey 1977, Wang et al. 2009):

$$K_{rw}(S_w) = K_{rwmax}\left(\frac{S_w - S_{wi}}{1 - S_{wi} - S_{oi}}\right)^{woexp}; \tag{6.22}$$

$$K_{ro}(S_w) = K_{romax}\left(\frac{1 - S_w - S_{oi}}{1 - S_{wi} - S_{oi}}\right)^{owexp}; \tag{6.23}$$

$$P_c = P_{cmin} - (P_{cmax} - P_{cmin})S_{wn3},$$ (6.24)

where S_{wn3} is defined as

$$S_{wn3} = \left(\frac{S_{wi}^{pcowexp}}{1 - S_{wi}^{pcowexp}} \right) \Bigg/ \left(\frac{S_{w}^{pcowexp}}{1 - S_{w}^{pcowexp}} \right).$$ (6.25)

Parameters, such as water relative permeability at residual oil saturation (K_{rwmax}), oil relative permeability at connate water saturation (K_{romax}), exponent of relative permeability curve of water (wo_{exp}), exponent of relative permeability curve of oil (ow_{exp}), exponent of capillary pressure ($pcow_{exp}$), critical, connate, or endpoint saturation of water (S_{wi}), and irreducible or end point saturation of oil (S_{oi}), are empirical parameters; they are tuned according to experimental measurements and can be used directly in the fine-scale models. To scale up these parameters to the coarse scale, a workflow previously presented in Vishal and Leung (2015), adopted. The previous work was applied successfully to scale up effective dispersivities for solute transport in single-phase flow. Therefore, this paper extends the procedure to compute coarse-scale transport parameters for multi-phase immiscible flow. The idea is to construct probability distributions of effective coarse-scale parameters (e.g., $\overline{K}_{rwmax}, \overline{K}_{romax}, \overline{ow}_{exp}, \overline{wo}_{exp}, \overline{pcow}_{exp}, \overline{S}_{wi}$, and $\overline{S}_{oi}$) that are conditional to $\overline{\phi}$ and $\overline{k}$ based on fine-scale simulation results that depict detailed sub-grid heterogeneity. The steps of the revised workflow are described as follow:

1. Divide the histogram of $\overline{\phi}$ into n_b bins.

2. For each bin, generate n_s unconditional sub-grid realizations of $\bar{\phi}$. In the case of Gaussian statistics, fine-scale variogram γ, together with a histogram consisting of mean $= \bar{\phi}_b$ and variance $= \sigma^2$, can be used. For each of the n_s sub-grid models, compute an equivalent homogeneous model via linear averaging.

3. Multi-phase particle-tracking simulation is performed on the detailed and averaged models generated in step 2.

4. Estimate $\bar{K}_{rwmax}$, $\bar{K}_{romax}$, $\overline{ow}_{exp}$, $\overline{wo}_{exp}$, $\overline{pcow}_{exp}$, $\bar{S}_{wi}$, and $\bar{S}_{oi}$ by minimizing the mismatch in effluent history between the two sets of models from step 3. A non-linear regression scheme with the following objective function (f) is implemented:

$$f(K_r, P_c) = \sum_{j=1}^{n} w(j) \sum_{N=1}^{T_{max}} w(j,N) \left(\frac{Sim_{j_N}^{fine} - Sim_{j_N}^{coarse}(K_r, P_c)}{\sigma_{j_N}} \right)^2, \ (6.26)$$

where j is data type (e.g., volumetric flow rate or pressure of each phase); N is time step, and $w(j, N)$ is a user-defined weight (the default value of $w = 1.0$) for the jth data type at time step N, and σ is the weight normalization factor. Several common options for σ are the standard deviation or a predefined percentage of the data mean (Wang et al. 2009).

5. Gather the results corresponding to bin i ($i = 1 \ldots n_b$) and construct

$P\{\bar{K}_{rwmax} | \bar{\phi}_i\}$, $P\{\bar{K}_{romax} | \bar{\phi}_i\}$, $P\{\overline{ow}_{exp} | \bar{\phi}_i\}$, $P\{\overline{wo}_{exp} | \bar{\phi}_i\}$, $P\{\overline{pcwo}_{exp} | \bar{\phi}_i\}$,

$P\{\bar{S}_{wi} | \bar{\phi}_i\}$, and $P\{\bar{S}_{oi} | \bar{\phi}_i\}$ for $i = 1, \ldots, n_b$. Repeat for all bins.

6. Use the conditional probability distributions derived from step 5 to assign coarse-scale values. At each location of the coarse grid, sample $\overline{K}_{rwmax}$, $\overline{K}_{romax}$, $\overline{ow}_{exp}$, $\overline{wo}_{exp}$, $\overline{pcow}_{exp}$, $\overline{S}_{wi}$, and $\overline{S}_{oi}$ from $P\{\overline{K}_{rwmax} \mid \overline{\phi}_i\}$, $P\{\overline{K}_{romax} \mid \overline{\phi}_i\}$, $P\{\overline{ow}_{exp} \mid \overline{\phi}_i\}$, $P\{\overline{wo}_{exp} \mid \overline{\phi}_i\}$, $P\{\overline{pcwo}_{exp} \mid \overline{\phi}_i\}$, $P\{\overline{S}_{wi} \mid \overline{\phi}_i\}$, and $P\{\overline{S}_{oi} \mid \overline{\phi}_i\}$, respectively.

A schematic of this scale-up procedure is shown in Fig. 6.11.

6.3. Case Study

A 2-D domain with 60 × 60 blocks ($\Delta x = \Delta y = 1$ m) and two wells as shown in Fig. 6.12 (A) is considered. For this synthetic example, it is assumed that the "true" fine-scale model 60 × 60 is also known here.

To construct scaled-up models of reservoir attributes, fine-scale porosity values at a resolution of 1 m × 1 m are extracted at the well locations; these are considered as fine-scale conditioning data. The corresponding histogram and anisotropic variogram model are shown in Fig. 6.13(A) and Fig. 6.14(A), respectively. Eq. (6.4) is used to populate k ($k_0 = 0.01$, $\phi_c = 0.35$, $a_1 = 3.667$, and $a_2 = 4.151$), whereas water- and oil- relative permeability functions are modelled using Eq. (6.21) and Eq. (6.22) ($K_{rwmax} = 0.2$, $K_{romax} = 0.8$, $wo_{exp} = ow_{exp} = 2.0$, $S_{wi} = S_{oi} = 0.2$), respectively. As mentioned previously, capillary pressure effect is neglected. Longitudinal dispersivity α_L is set to be 0.01 m, with transverse dispersivity $\alpha_T = 0.1 \times \alpha_L$ (Perkins and Johnston 1963; Gelhar et al. 1992).

Following the proposed method, a suite of coarse-scale 10 × 10 models with Δx = Δy = 6 m, as shown in Fig. 6.12(B), is constructed.

For the volume support of 6 m × 6 m, $Var(\bar{Z})$ is approximately 0.86. Results of scaled-up histogram and $\bar{\gamma}$ are shown in Fig. 6.13(B) and Fig. 6.14(B), respectively. Ten sets of coarse-scale conditioning data of ϕ are sampled at well locations, and conditional sequential Gaussian simulation (SGSIM), as implemented in GSLIB (Deutsch and Journel 1998). Ten realizations are simulated corresponding to each conditioning data set. Therefore, a total of 100 realizations of scaled-up porosity models are obtained, and a randomly-selected realization is presented in Fig. 6.15(B), which can be compared against the "true" fine-scale model in Fig. 6.15(A).

To obtain the effective relative permeability functions, the procedure detailed in section 6.2.3.2 is followed. First, a fine-scale sub-grid 6m× 6 m model with Δx = Δy = 1 m, as shown in Fig. 6.12(C), is considered. The histogram in Fig. 6.13(B) is divided into n_b = 3 bins corresponding to $\bar{\phi}$ = 0.1, 0.2, and 0.3. Fifty (n_s = 50) sub-grid porosity models are simulated by unconditional sequential Gaussian simulation for each bin; one of those realizations for $\bar{\phi}$ = 0.25 is shown in Fig. 6.15(C). As expected, the histogram for this sub-grid model, as shown in Fig. 6.13(C), should resemble that in Fig. 6.13(A). For each sub-grid model, an injector and a producer are placed diagonally across the domain. For the sake of brevity, in this study, only $\bar{K}_{rwmax}$, $\bar{K}_{romax}$ are considered, other parameters(i.e.,

$\overline{ow}_{exp}$, $\overline{wo}_{exp}$, $\overline{pcow}_{exp}$, $\bar{S}_{wi}$, and $\bar{S}_{oi}$) are assumed to be the same as the fine scale

values. The reduction in objective function Eq. (6.26) is shown in Fig. 6.16(B). The error is usually reduced below an acceptable tolerance level with fewer than 20 iterations when a very fast simulated annealing (VFSA) scheme is implemented (Li et al. 2004). Also shown in Fig. 6.16(A) is the comparison of water saturation profiles at the production well for one particular realization of the sub-grid model.

Bivariate distributions of $\overline{K}_{rwmax}$ and $\overline{K}_{romax}$ as functions of $\overline{\phi}$ are constructed. An example corresponding to $\overline{\phi} = 0.25$ are shown in Fig. 6.18. For each of the 100 coarse-scale models of porosity and permeability generated previously, a cloud transform procedure is adopted to sample values of $\overline{K}_{rw\max}$ and $\overline{K}_{ro\max}$ (Kolbjørnsen, and Abrahamsen 2005): a value of $\overline{K}_{rw\max}$ is drawn from $P\{\overline{K}_{rw\max} \mid \overline{\phi}_i\}$, and a value of $\overline{K}_{ro\max}$ is drawn $P\{\overline{K}_{ro\max} \mid \overline{\phi}_i\}$ conditioned to the drawn $\overline{K}_{rw\max}$ value. The effective relative permeability functions and the coarse-scale reservoir models are subjected to traditional numerical simulation. Predictions of oil and water rates at the production well are shown in Fig. 6.18. It is clear that the "true" fine-scale response is captured within the uncertainties exhibited by the coarse-scale models sufficiently.

6.4. Results and Discussions

As mentioned earlier, the objective of this study is to develop a particle-tracking model suitable for solving the saturation transport equation, which can be readily integrated in a statistical scale-up procedure to compute coarse-scale (i.e.,

effective) multi-phase flow functions. Though the particle-tracking method is primarily formulated after Tyagi et al. (2008), new elements are incorporated to enhance the computational efficiency. In particular, the kernel method is implemented to reconstruct the concentration/saturation from particle distributions directly, which alleviates the burden of utilizing an enormous amount of particles.

To estimate the kernel density at any specified locations, various non-parametric kernel functions are adopted. The Gaussian kernel function is incorporated for the 1-D example. For the 2-D case, an automatic and adaptive bivariate density estimator is incorporated based on the estimation of marginal and conditional densities (Simonoff 1995).This method has some advantages over the bivariate Gaussian kernel estimator, where the level of smoothing does not depend on the local features of the density distribution. Results in both 1-D and 2-D demonstrate the validity of the proposed particle-tracking model and its potential for removing artificial dispersion when estimating effective multi-phase flow functions.

6.5. Conclusions

1. A new particle-tracking method, where the kernel technique is implemented to reconstruct the concentration/saturation from particle distributions directly, is developed to solve the nonlinear transport equation of two immiscible phases. The method is coupled with the continuity equation in an IMPES (implicit pressure, explicit saturation) fashion to simulate phase saturation. The

proposed method has been validated against analytical and finite-difference predictions.

2. The phase concentration/saturation is constructed from the particles distribution using the non-parametric kernel estimator. The bivariate Gaussian kernel estimator, as well as an automatic and adaptive bivariate density estimator based on the estimation of marginal and conditional density distributions, have been adopted. The kernel technique helps to avoid statistical bias with a reduced number of particles. This aspect represents a significant improvement to the overall computational efficiency, when comparing to other existing formulations that entail the use of a large number of particles.

3. The particle-tracking model is integrated into a new workflow to scale up effective multi-phase flow functions. The main contribution is that this workflow takes into account the sub-scale variability explicitly. Conditional probability distributions of effective functions at the transport modeling scale are established; cloud transform and Monte Carlo simulation techniques are performed to sample from these distributions.

4. As shown in the case study, the uncertainties exhibited by the coarse-scale models, which are constructed in accordance to the proposed procedure, are consistent with the response obtained from the fine-scale model.

5. Extension to 3-D models and effect of gravity will be investigated in future work.

References

Bear, J. (1972). *Dynamics of fluids in porous media.* New York: Elsevier.

Bear, J. (1979). *Hydraulics of groundwater.* New York: McGraw-Hill.

Bolster, D., Dentz, M., & Carrera, J. (2009). Effective two-phase flow in heterogeneous media under temporal pressure fluctuations. *Water Resour Res*(45).

Brooks, R. J., & Corey, A. T. (1964). *Hydraulic properties of porous media.* Colorado State University: Hydrology and Water Resources Program.

Corey, A. T. (1977). *Mechanics of heterogeneous fluids in porous media.* Fort Collins, Colorado, USA: Water Resources Publications.

Delay, F., Ackerer, P., & Danquigny, C. (2005). Simulating solute transport in porous or fractured formations using random walk particle tracking. *Vadose Zone Journal, 4(2)*, (pp. 360-379).

Deutsch, C. V. (2010). Estimation of vertical permeability in the McMurray Formation. *Journal of Canadian Petroleum Technology, 49 (12)*, 10-18.

Deutsch, C. V., & Journel, A. G. (1998). *Geostatistical software library and users guide.* New York: Oxford university press.

Durlofsky, L. J. (1998). Coarse scale models of two phase flow in heterogeneous reservoirs: Volume averaged equations and their relationship to existing upscaling techniques. *Computat Geosci, 2 (2)*, 73-92.

Fernàndez-Garcia, D., & Sanchez-Vila, X. (2011). Optimal reconstruction of concentrations, gradients and reaction rates from particle distributions. *J Contam Hydrol, (120-121)*, (pp. 99-114).

Fernàndez-Garcia, D., Illangasekare, T. H., & Rajaram, H. (2005). Differences in the scale-dependence of dispersivity estimated from temporal and spatial moments in chemically and physically heterogeneous porous media. *Adv Water Resour, 28(7)*, (pp. 745-759).

Firoozabadi, A., & Hoteit, H. (2007). Numerical simulation of complex reservoir problems and the need for a different line of attack. *Society of Petroleum Engineers, 3 (03)*, 17-19.

Gelhar, L. W., Welty, C., & Rehfeldt, K. R. (1992). A critical review of data on field-scale dispersion in aquifers. *Water Resour Res, 28(7)*, (pp. 1955-1974).

Hassan, A. E., & Mohamed, M. M. (2003). On using particle tracking methods to simulate transport in single-continuum and dual continua porous media. *J Hydrol, 275(3)*, (pp. 242-260).

Hong, S. (2010). *Multivariate analysis of diverse data for improved geostatistical reservoir modeling.* Ph.D. Thesis, University of Alberta, Edmonton, Canada.

Johnson, E. F., Bossler , D. P., & Naumann, V. O. (1959). Calculation of relative permeability from displacement experiments. *SPE, Vol. 216*, 370-372.

Journel, A. G., & Huijbregts, C. J. (1978). *Mining geostatistics.* London: Academic press.

Kolbjørnsen, O., & Abrahamsen, P. (2005). Theory of the cloud transform for applications. *Geostatistics Banff 2004*, 45-54.

Lake, L. W., & Srinivasan, S. (2004). Statistical scale-up of reservoir properties: Concepts and applications. *J Pet Sci Eng, 44(1)*, (pp. 27-39).

Leung, J. Y., & Srinivasan, S. (2011). Analysis of uncertainty introduced by scaleup of reservoir attributes and flow response in heterogeneous reservoirs. *SPE J, 16(3)*, (pp. 713-724).

Leung, J. Y., & Srinivasan, S. (2016). Effects of reservoir heterogeneity on scaling of effective mass transfer coefficient for solute transport. *J Contam Hydrol, 192*, (pp.181-193).

Li, X., Koike, T., & Pathmathevan, M. (2004). A very fast simulated re-annealing (VFSA) approach for land data assimilation. *Comput Geosci, 30(3)*, (pp. 239-248).

Perkins, T. K., & Johnston, O. C. (1963). A review of diffusion and dispersion in porous media. *SPE J, 3(01)*, (pp. 70-84).

Pickup, G. E., & Stephen, K. D. (2000). An assessment of steady-state scale-up for small-scale geological models. *Pet Geosci, 6 (3)*, 203-210.

Pickup, G. E., Stephen, K. D., Ma, J., Zhang, P., & Clark, J. D. (2005). Multi-stage upscaling: Selection of suitable methods. *Transport Porous Med, 58 (1-2)*, 191-216.

Riva, M., Guadagnini, A., Fernandez-Garcia, D., Sanchez-Vila, X., & Ptak, T. (2008). Relative importance of geostatistical and transport models in describing heavily tailed breakthrough curves at the Lauswiesen site. *J Contam Hydrol, 101(1)*, (pp. 1-13).

Rubin, Y., Sun, A., Maxwell, R., & Bellin, A. (1999). The concept of block-effective macrodispersivity and a unified approach for grid-scale-and plume-scale-dependent transport. *Journal of Fluid Mechanics, 395*, 161-180.

Saad, N., Cullick, A. S., & Honarpour, M. M. (1995). Effective relative permeability in scale-up and simulation. *In Low Permeability Reservoirs Symposium* (pp. 451-464). Denver, Colorado: Society of Petroleum Engineers.

Salamon, P., Fernàndez-Garcia, D., & Gómez-Hernández, J. J. (2006a). A review and numerical assessment of the random walk particle tracking method. *Journal of contaminant hydrology, 87(3)*, (pp. 277-305).

Salamon, P., Fernàndez-Garcia, D., & Gómez-Hernández, J. J. (2006b). Modeling mass transfer processes using random walk particle tracking. *Water Resour Res, 42(11)*.

Salamon, P., Fernandez-Garcia, D., & Gómez-Hernández, J. J. (2007). Modeling tracer transport at the MADE site: the importance of heterogeneity. *Water resources research, 43(8)*.

Schlumberger Information Solutions. (2011). *Eclipse reservoir simulator:Reference manual and technical description.*

Simonoff, J. S. (1995). A simple, automatic and adaptive bivariate density estimator based on conditional densities. *Statistics and Computing, 5 (3)*, 245-252.

Tompson, A. F., & Gelhar, L. W. (1990). Numerical simulation of solute transport in three-dimensional, randomly heterogeneous porous media. *Water Resour Res, 26(10)*, (pp. 2541-2562).

Tyagi, M., Jenny, P., & Tchelepi, H. A. (2008). A Lagrangian, stochastic modeling framework for multi-phase flow in porous media. *J Comput Phys, 227(13)*, 6696-6714.

Vishal, V., & Leung, J. Y. (2015). Modeling impacts of subscale heterogeneities on dispersive solute transport in subsurface systems. *Journal of contaminant hydrology, 182*, (pp. 63-77).

Vishal, V., & Leung, J. Y. (2017). Statistical scale-up of dispersive transport in heterogeneous reservoir. In *In Geostatistics Valencia 2016* (pp. 733-743). Springer International Publishing.

Wang, J., & Kitanidis, P. K. (1999). Analysis of macrodispersion through volume averaging: comparison with stochastic theory. *Environmental Research and Risk Assessment, 13(1-2)*, 66-84.

Wang, K., Killough, J. E., & Sepehrnoori, K. (2009). A new upscaling method of relative permeability curves for reservoir simulation. *SPE Annual Technical Conference and Exhibition.* Orleans, Louisiana: Society of Petroleum Engineers.

Zheng, C., & Bennett, G. D. (2002). *Applied contaminant transport modeling* (Vol. 2). New York: Wiley-Interscience.

Table 6.1: Parameters used for the particle-tracking model validation

General parameters	Value	Unit
Independent intrinsic permeability (K)	1.00E-13	m^2
Porosity (ϕ)	1.0	
Irreducible oil saturation (S_{oi})	0.2	
Irreducible water saturation (S_{wi})	0.2	
Oil relative permeability (K_{ro})	Fig. 3	
Water relative permeability (K_{rw})	Fig. 3	
Non-wetting fluid (oil) viscosity (μ_o)	0.0005	Pa*s
Wetting fluid (water) viscosity(μ_w)	0.001	Pa*s
Reservoir initial pressure	2.00E+07	Pa
Capillary pressure (P_c)	0.00E+00	Pa
Water injection rate	0.216	m/day
Eclipse parameters		
Number of grid cell in X direction	100	
Grid cell size in X direction	0.2	m
Grid cell size in Y direction	1.0	m
Particle tracking parameters		
Number of grid cell in X direction	20.0	
Grid cell size in X direction	1.0	m
Grid cell size in Y direction	1.0	m
Time step size	1.0	day
Number of oil particles per grid cell (uniformly)	100	
Number of water particle injected per time step	100	
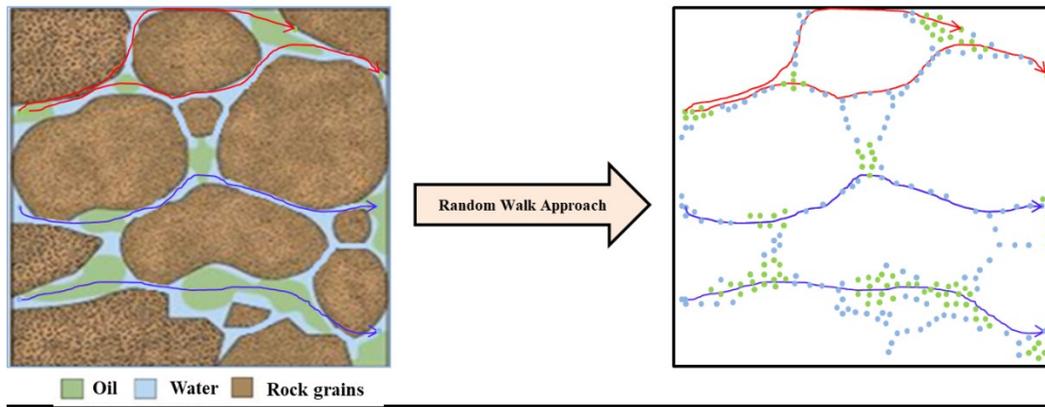
Figure 6.1: Particle representation of a system with two phases: oil (green) and water (blue).
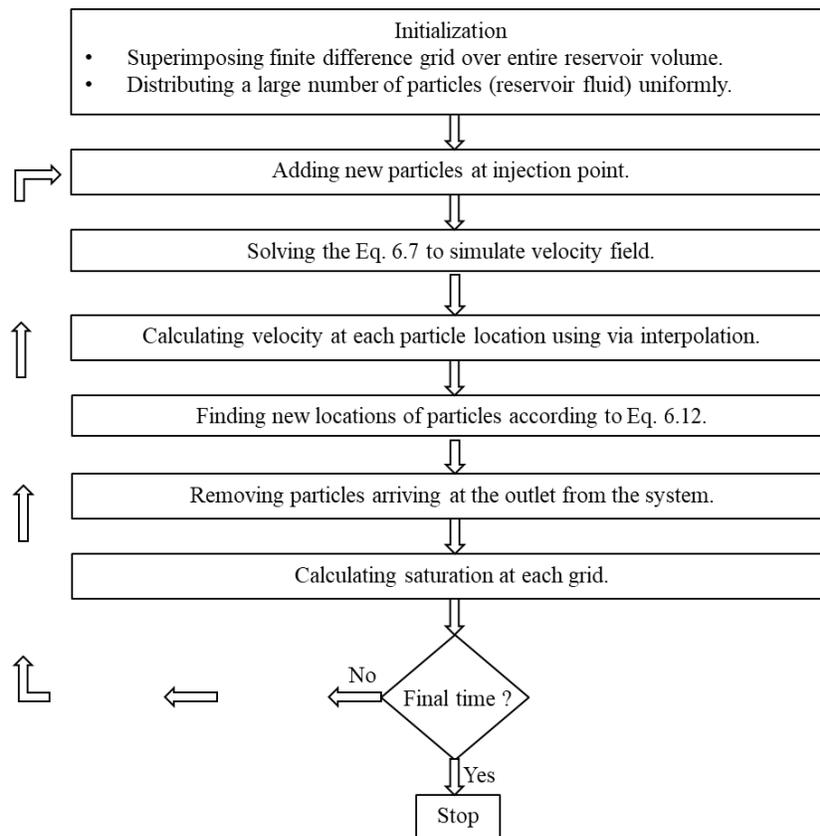
Figure 6.2: Flow chart of the particle-tracking scheme for modeling two-phase immiscible flow.
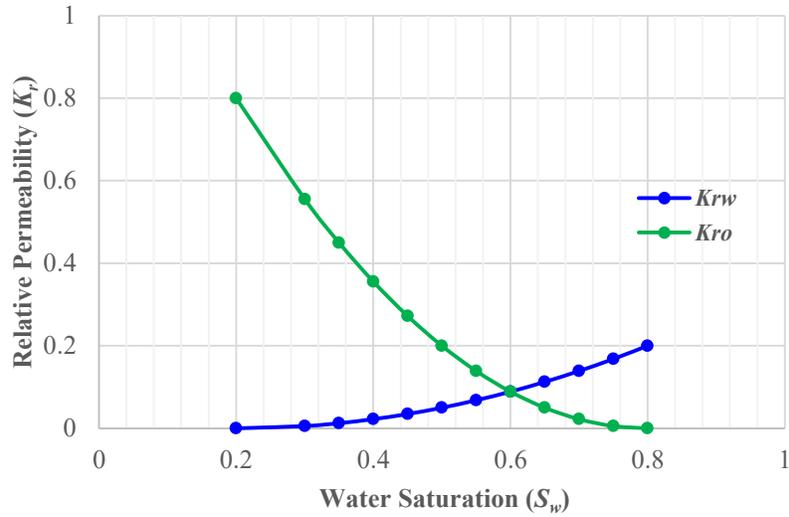
Figure 6.3: Water-oil relative permeability functions used for the particle-tracking model validation.
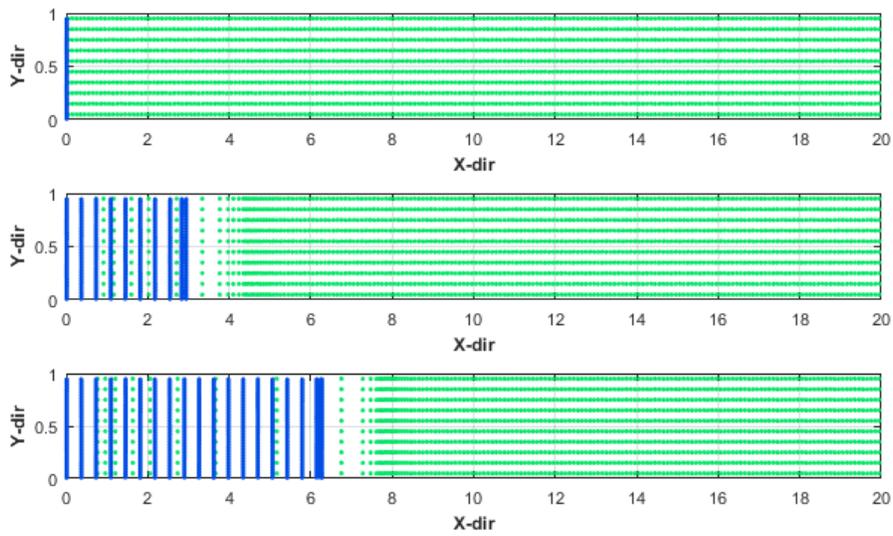
Figure 6.4: 1-D Validation: Distribution of water (blue) and oil (green) particles at $t = 0$ day (top), $t = 10$ days (middle), and $t = 20$ day (bottom).
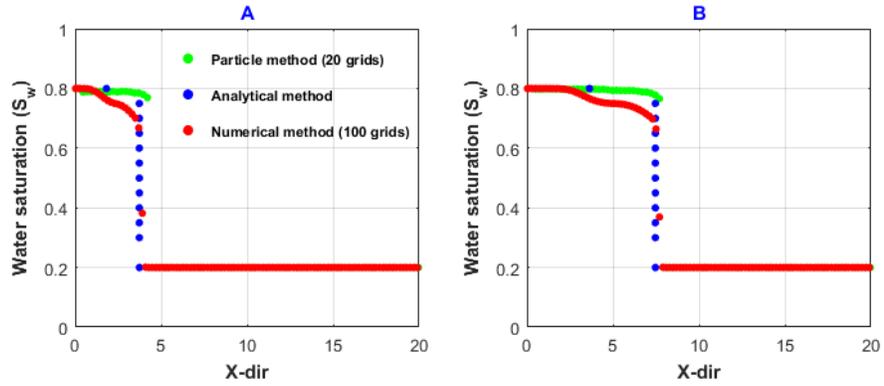
Figure 6.5: 1-D Validation: Water saturation profile at: (A) $t = 10$ day and (B) $t = 20$ day.
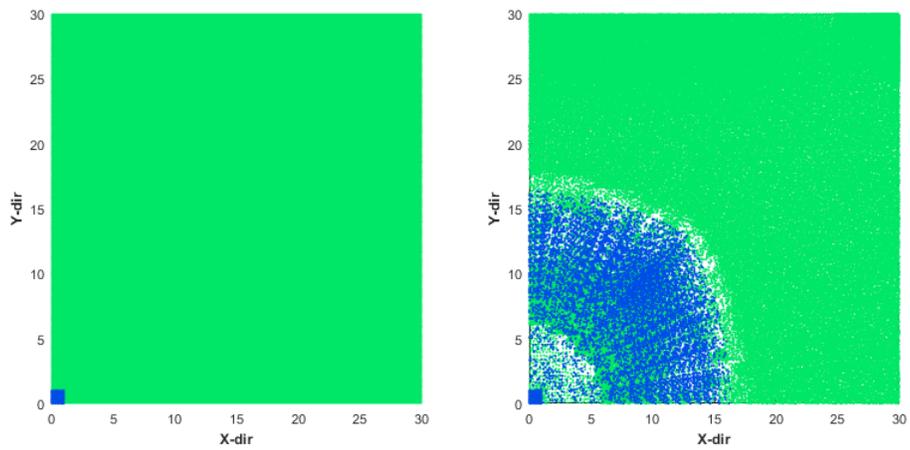
Figure 6.6: 2-D Validation for Homogeneous Reservoir: Distribution of water (blue) and oil (green) particles at $t = 0$ day (left), $t = 10$ days (right).
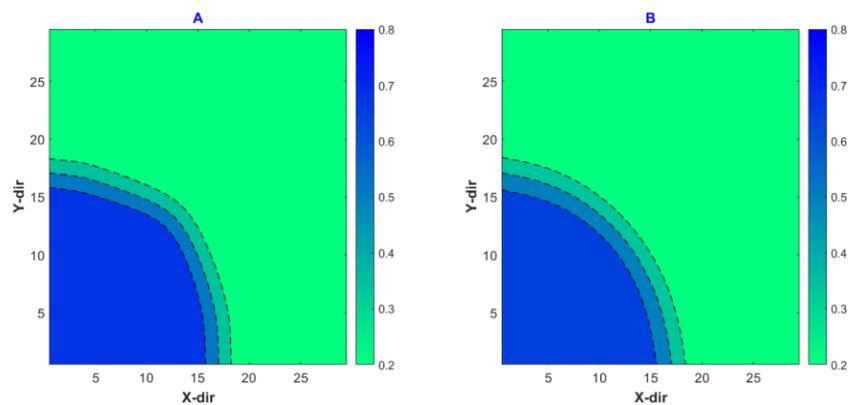
Figure 6.7: 2-D Validation for Homogeneous Reservoir: Water saturation profile by (A) particle method and (B) numerical simulation at $t = 10$ day.
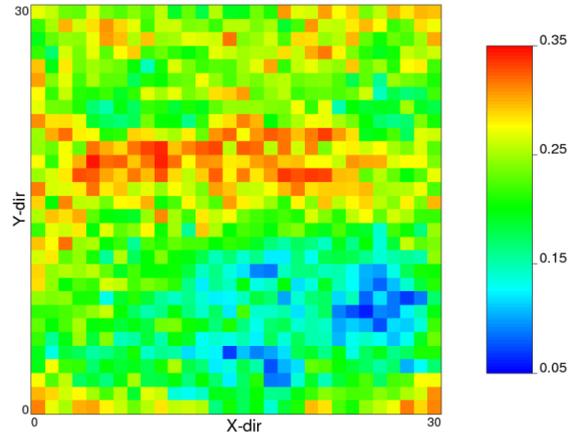
Figure 6.8: 2-D Validation for Heterogeneous Reservoir: Porosity distribution.
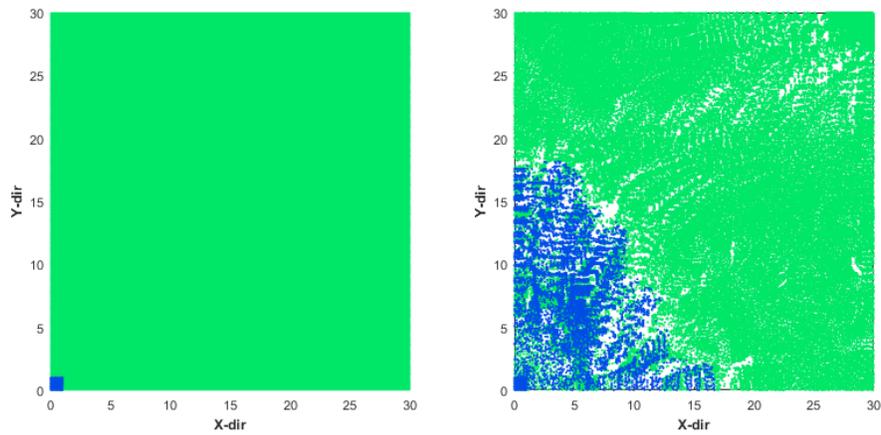
Figure 6.9: 2-D Validation for Heterogeneous Reservoir: Distribution of water (blue) and oil (green) particles at $t = 0$ day (left) and $t = 10$ day (right).
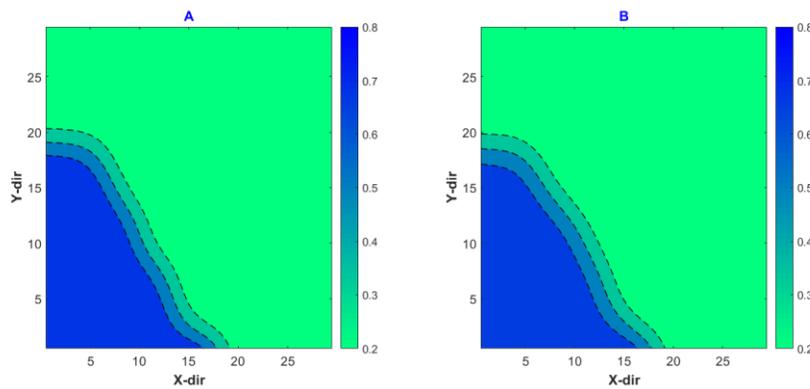
Figure 6.10: 2-D Validation for Heterogeneous Reservoir: Comparison of water saturation profiles at $t = 10$ day obtained by (A) proposed particle-tracking method and (B) numerical simulation.

217
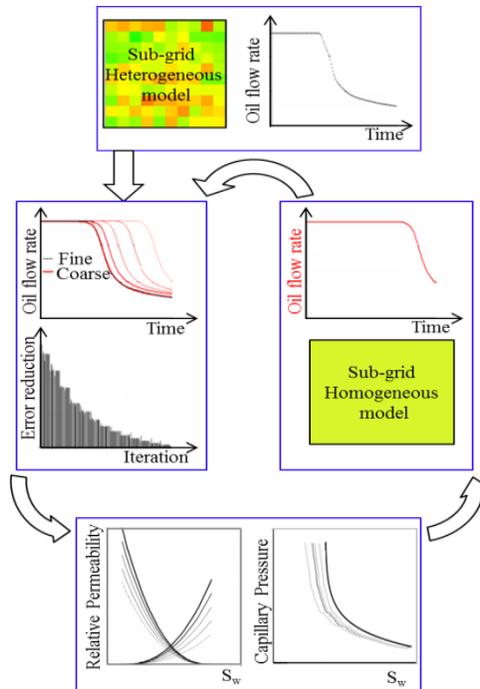
Figure 6.11: Schematic of the optimization procedure.
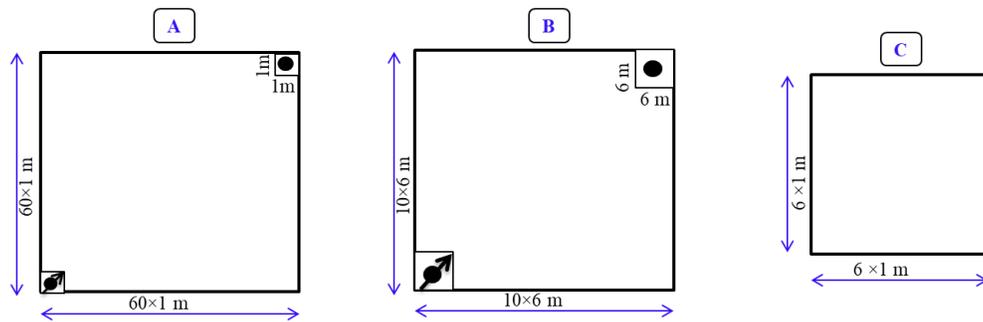
Figure 6.12: Model setup for (A) fine-scale, (B) coarse-scale, and (C) sub-grid.
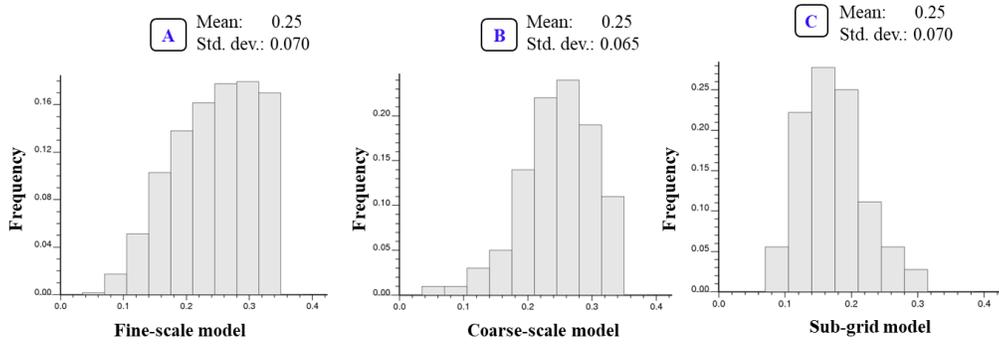
Figure 6.13: Histogram of porosity of (A) fine-scale model, (B) coarse-scale model, and (C) sub-grid model.
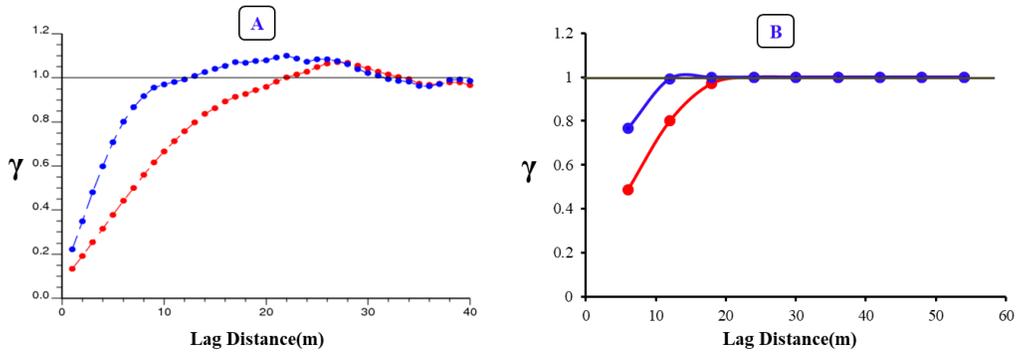
Figure 6.14: Variogram of porosity for (A) fine-scale model and (B) coarse-scale model. Red: direction of maximum anisotropy; blue: direction of minimum anisotropy.
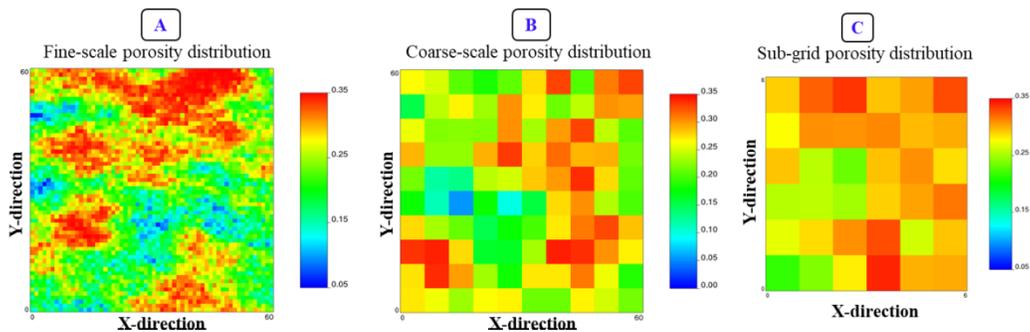
Figure 6.15: Distribution of porosity: (A) fine-scale model, (B) coarse-scale model, and (C) sub-grid model.
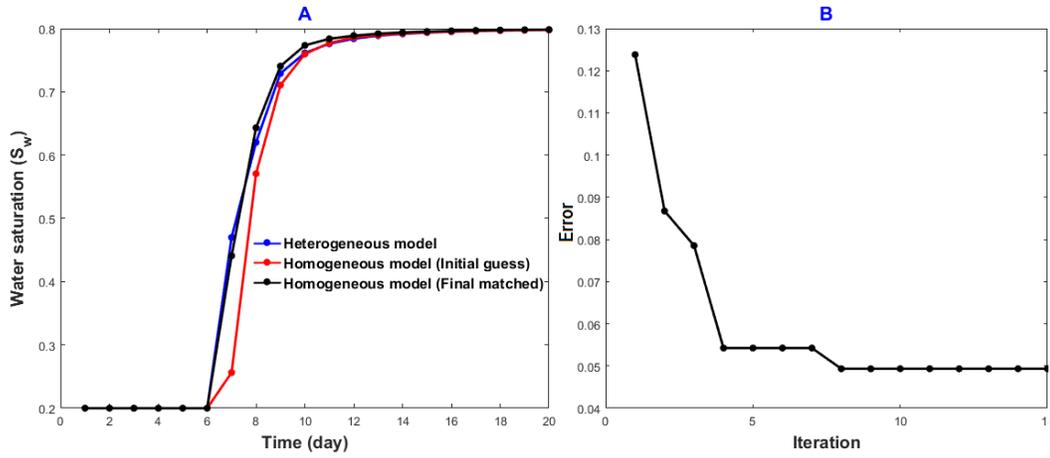
Figure 6.16: (A) Water saturation profile at producer in the sub-grid model and (B) reduction in objective function according to Eq. (6.26).
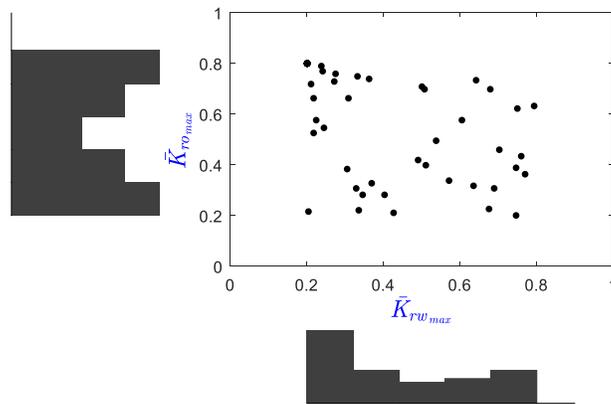
Figure 6.17: Histograms of $\overline{K}_{rw_{\max}}$ and $\overline{K}_{ro_{\max}}$ corresponding to $\overline{\phi} = 0.25$.
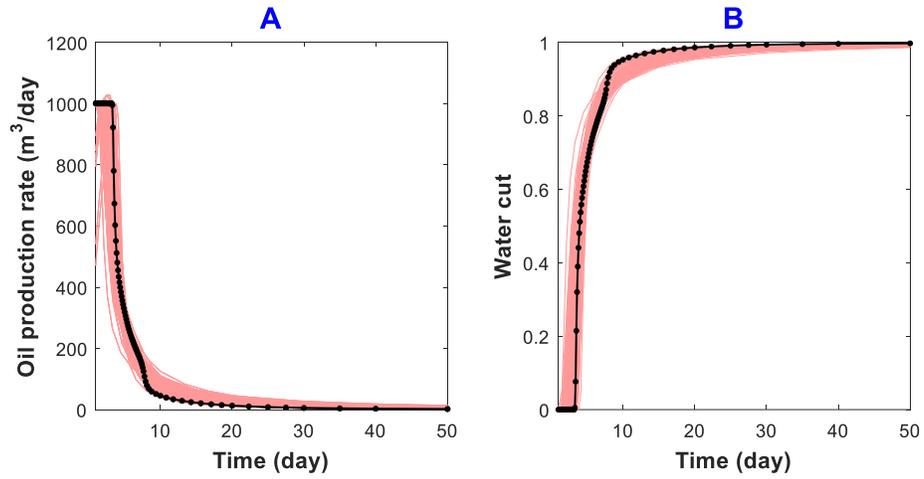
Figure 6.18: (A) Oil production rate and (B) water cut at the production well of the "true" fine-scale model (black) and coarse-scale models (orange).

Chapter 7: Conclusions & Recommendations for Future Work

7.1 Conclusions

- Particle-tracking based techniques, which are free of numerical dispersion, is an appropriate tool for studying scaling of dynamic transport-related properties.

- As opposed to the scaling characteristics of static properties such as porosity, dynamic transport-/flow-related properties may increase with scale, and the associated uncertainties may increase or decrease with scale, depending on the underlying heterogeneity distribution.

- Ignoring the spatial variability in scaled-up effective dispersivities could not properly capture the effects of sub-scale variability, causing the overall uncertainty in the final recovery response to be overestimated. Apart from the sub-scale heterogeneity, the large-scale and sub-fine-scale (sub-grid) heterogeneity also play an important role in both flow-transport modeling and scale-up because the non-Fickian features such as heavy-tailed multi-peaked effluent history and early breakthrough are dramatically more pronounced.

- The purposed particle tracking algorithm to model non-Gaussian transport behavior shows good agreement with the analytical solution.

- Also, the purposed particle tracking algorithm to model multi-phase immiscible flow shows good agreement with the analytical and finite-difference predictions.

7.2 Contributions

- A new framework is proposed to scale-up dispersivities for single phase flow as well as multiphase function for multiphase immiscible flow using particle tracking transport. Combining statistical scale-up with particle-tracking transport modeling for flow-based upscaling is novel. The proposed method allows uncertainty due to sub-scale variability, large-scale variability, and variability below the fine-scale variability to be captured.

- In comparison to other existing scale-up procedures, three key novelties of this work are: (1) effects of numerical dispersion is controlled or eliminated; (2) steady-state assumptions are not required; (3) the method is flexible to handle a wide range of multivariate distribution of heterogeneous variables.

- A new stochastic particle-tracking transport modeling tool is developed. It facilitates the modeling of solute and phase transport in single- and multiple-phase flows. It is flexible to handle continuous injection, multiple sources and non-Fickian behavior.

7.3 Recommendations for Future Work

The particle-tracking method is a more accurate way to model transport phenomenon alternative to the numerical methods because it is free from numerical dispersion and does not require discretization. Moreover, incorporation of this method in scale-up procedure gives additional benefit. There are a number of suggestions on which further research is recommended:

- The particle-tracking method can be easily extended to model transport in fractured porous media in single-phase flow.

- The particle-tracking method can also be easily extended to model miscible displacement process in heterogeneous porous media as well as in fractured porous media.

- The particle-tracking method should be extended to model transport in transient flow.

- Convolution technique can be incorporated with particle-tracking method to model continuous injection process as well as the multi-injection point process.

- The presented particle-tracking approach to model multi-phase immiscible flow ignores the capillary pressure effect. Its addition to the approach would be great improvement to the particle-tracking method.

- Upscaling of transport using particle tracking in facies scale-up would be good study to address real field problem.

- The particle-tracking method could be used in subsurface reservoir characterization.

Bibliography

Adepoju, O. O., Lake, L. W., & Johns, R. T. (2013). Investigation of anisotropic mixing in miscible displacements. *SPE Reservoir Evaluation & Engineering, 16(01)*, 85-96.

Aronofsky, J. S., & Heller, J. P. (1957). A diffusion model to explain mixing of flowing miscible fluids in porous media. *Trans AIME, 210(12)*, (pp. 345-349).

Arya, A., Hewett, T. A., Larson, R. L., & Lake, L. W. (1988). Dispersion and reservoir heterogeneity. *SPE Reservoir Eng, 3(1)*, (pp. 139-148).

Barker, J. W., & Fayers, F. J. (1994). Transport coefficients for compositional simulation with coarse grids in heterogeneous media. *SPE Adv Technol Ser, 2(2)*, 103-112.

Bear, J. (1972). *Dynamics of fluids in porous media.* New York: Elsevier.

Bear, J. (1979). *Hydraulics of groundwater.* New York: McGraw-Hill.

Becker, M. W., & Shapiro, A. M. (2003). Interpreting tracer breakthrough tailing from different forced-gradient tracer experiment configurations in fractured bedrock. *Water Resour Res, 39(1)*, 1024.

Benson, D. A., Aquino, T., Bolster, D., Engdahl, N., Henri, C. V., & Fernàndez-Garcia, D. (2017). A comparison of Eulerian and Lagrangian transport and non-linear reaction algorithms. *Advances in Water Resources, 99*, 15-37.

Benson, D. A., Wheatcraft, S. W., & Meerschaert, M. M. (2000). Application of a fractional advection-dispersion equation. *Water Resources Research, 36(6)*, 1403-1412.

Berentsen, C. W., Van Kruijsdijk, C. P., & Verlaan, M. L. (2007). Upscaling, relaxation and reversibility of dispersive flow in stratified porous media. *Transport Porous Med, 68(2)*, (pp. 187-218).

Berkowitz, B., & Scher, H. (1995). On characterization of anomalous dispersion in porous and fractured media. *Water Resour. Res., 31(6)*, 1461–1466.

Berkowitz, B., & Scher, H. (1997). Anomalous transport in random fracture networks. *Physical review letters, 79*, 4038–4041.

Berkowitz, B., Cortis, A., Dentz, M., & Scher, H. (2006). Modeling non-Fickian transport in geological formations as a continuous time random walk. *Reviews of Geophysics, 44(2)*.

Berkowitz, B., Klafter, J., Metzler, R., & Scher, H. (2002). Physical pictures of transport in heterogeneous media: Advection-dispersion, random-walk, and fractional derivative formulations. *Water Resources Research, 38(10)*.

Berkowitz, B., Scher, H., & Silliman, S. E. (2000). Anomalous transport in laboratory-scale, heterogeneous porous media. *Water Resour Res, 36(1)*, (pp. 149-158).

Bijeljic, B., Raeini, A., Mostaghimi, P., & Blunt, M. J. (2013). Predictions of non-Fickian solute transport in different classes of porous media using direct simulation on pore-scale images. *Physical Review E, 87(1)*, 013011.

Binning, P., & Celia, M. A. (2002). A forward particle tracking Eulerian–Lagrangian localized adjoint method for solution of the contaminant transport equation in three dimensions. *Adv Water Resour, 25(2)*, (pp. 147-157).

Bird, R. B., Stewart, W. E., & Lightfoot, E. N. (1960). *Transport phenomena.* Madison, USA: John Wiley & Sons.

Bolster, D., Dentz, M., & Carrera, J. (2009). Effective two-phase flow in heterogeneous media under temporal pressure fluctuations. *Water Resour Res*(45).

Boso, F., Bellin, A., & Dumbser, M. (2013). Numerical simulations of solute transport in highly heterogeneous formations: A comparison of alternative numerical schemes. *Advances in Water Resources, 52*, 178-189.

Brooks, R. J., & Corey, A. T. (1964). *Hydraulic properties of porous media.* Colorado State University: Hydrology and Water Resources Program.

Carrera, J., Sánchez-Vila, X., Benet, I., Medina, A., Galarza, G., & Guimerà, J. (1998). On matrix diffusion: formulations, solution methods and qualitative effects. *Hydrogeology Journal, 6(1)*, 178-190.

Christie, M. A. (2001). Flow in porous media — scale up of multiphase flow. *Current Opinion in Colloid & Interface Science, 6(3)*, (pp. 236-241).

Corey, A. T. (1977). *Mechanics of heterogeneous fluids in porous media.* Fort Collins, Colorado, USA: Water Resources Publications.

Cortis, A., & Berkowitz, B. (2005). Computing "anomalous" contaminant transport in porous media: the CTRW MATLAB toolbox. *Ground Water, 43(6)*, (pp. 947-950).

Cortis, A., & Berkowitz, B. (2005). Computing "anomalous" contaminant transport in porous media: The CTRW MATLAB toolbox. *Ground Water, 43 (6)*, 947-950.

Cortis, A., Emmanuel, S., Rubin, S., Willbrand, K., & Berkowitz, B. (2010). *The CTRW Matlab toolbox v3.1: a practical user's guide*. Retrieved from http://www.weizmann.ac.il/ESER/People/Brian/CTRW.

Cortis, A., Gallo, C., Scher, H., & Berkowitz, B. (2004). Numerical simulation of non-Fickian transport in geological formations with multiple-scale heterogeneities. *Water Resour Res, 40(4)*.

Dagan, G. (1982). Stochastic modeling of groundwater flow by unconditional and conditional probabilities: 1. Conditional simulation and the direct problem. *Water Resources Research, 18(4)*, 813-833.

Dagan, G. (1984). Solute transport in heterogeneous porous formations. *Journal of fluid mechanics, 145*, 151-177.

Dagan, G. (1987). Theory of solute transport by groundwater. *Annual review of fluid mechanics, 19 (1)*, 183-213.

Dagan, G. (1989). *Flow and transport in porous formations.* New-York: Springer-Verlag.

Delay, F., Ackerer, P., & Danquigny, C. (2005). Simulating solute transport in porous or fractured formations using random walk particle tracking. *Vadose Zone Journal, 4(2)*, (pp. 360-379).

Dentz, M., Cortis, A., Scher, H., & Berkowitz, B. (2004). Time behavior of solute transport in heterogeneous media: transition from anomalous to normal transport. *Advances in Water Resources, 27(2)*, (pp. 155-173).

Deutsch, C. V. (2010). Estimation of vertical permeability in the McMurray Formation. *Journal of Canadian Petroleum Technology, 49 (12)*, 10-18.

Deutsch, C. V., & Journel, A. G. (1998). *Geostatistical software library and users guide.* New York: Oxford university press.

Di Donato, G., Obi, E. O., & Blunt, M. J. (2003). nomalous transport in heterogeneous media demonstrated by streamline-based simulation. *Geophys. Res. Lett., 30(12)*.

Dullien, F. A. (2012). *Porous media: fluid transport and pore structure.* New York : Academic press.

Durlofsky, L. J. (1998). Coarse scale models of two phase flow in heterogeneous reservoirs: Volume averaged equations and their relationship to existing upscaling techniques. *Computat Geosci, 2 (2)*, 73-92.

Efendiev, Y., Durlofsky, L. J., & Lee, S. H. (2000). Modeling of subgrid effects in coarse-scale simulations of transport in heterogeneous porous media. *Water Resour Res, 36(8)*, (pp. 2031-2041).

Fanchi, J. R. (1983). Multidimensional numerical dispersion. *SPE J, 23(1)*, (pp. 143-151).

Fernàndez-Garcia, D., & Sanchez-Vila, X. (2011). Optimal reconstruction of concentrations, gradients and reaction rates from particle distributions. *J Contam Hydrol, (120-121)*, (pp. 99-114).

Fernàndez-Garcia, D., Illangasekare, T. H., & Rajaram, H. (2005). Differences in the scale-dependence of dispersivity estimated from temporal and spatial moments in chemically and physically heterogeneous porous media. *Adv Water Resour, 28(7)*, (pp. 745-759).

Fernàndez-Garcia, D., Llerar-Meza, G., & Gómez-Hernández, J. J. (2009). Upscaling transport with mass transfer models: Mean behavior and propagation of uncertainty. *Water Resour Res, 45(10)*.

Ferreira, J. A., & Pinto, L. (2014). Non-Fickian tracer transport in porous media. *Proceedings of the 14th International Conference on Computational and Mathematical Methods in Science and Engineering* (pp. 543-554). Rota (Cádiz), Spain: CMMSE.

Ferreira, J. A., & Pinto, L. (2015). An integro-differential model for non-Fickian tracer transport in porous media: validation and numerical simulation. *Mathematical Methods in the Applied Sciences*.

Fetter, C. W. (2000). *Applied hydrogeology.* Prentice hall.

Field, M. S., & Leij, F. J. (2012). Solute transport in solution conduits exhibiting multi-peaked breakthrough curves. *Journal of hydrology, 440*, 26-35.

Field, M. S., & Pinsky, P. F. (2000). A two-region nonequilibrium model for solute transport in solution conduits in karstic aquifers. *Journal of Contaminant Hydrology, 44 (3)*, 329-351.

Firoozabadi, A., & Hoteit, H. (2007). Numerical simulation of complex reservoir problems and the need for a different line of attack. *Society of Petroleum Engineers, 3 (03)*, 17-19.

Fleurant, C., & Van Der Lee, J. (2001). A stochastic model of transport in three-dimensional porous media. *Math Geol, 33(4)*, (pp. 449-474).

Fogedby, H. C. (1994). Langevin equations for continuous time Lévy flights. *Physical Review E, 50, 1657*.

Gao, G., Zhan, H., Feng, S., Huang, G., & Mao, X. (2009). Comparison of alternative models for simulating anomalous solute transport in a large heterogeneous soil column. *Journal of hydrology, 377(3)*, (pp. 391-404).

Geiger, S., Cortis, A., & Birkholzer, J. T. (2010). Upscaling solute transport in naturally fractured porous media with the continuous time random walk method. *Water Resources Research, 46(12)*.

Gelhar, L. W. (1986). Stochastic subsurface hydrology from theory to applications. *Water Resources Research, 22(9s)*, 135S–145S.

Gelhar, L. W., & Axness, C. L. (1983). Three-dimensional stochastic analysis of macrodispersion in aquifers. *Water Resour.Res, 19 (1)*, 161-180.

Gelhar, L. W., Gutjahr, A. L., & Naff, R. L. (1979). Stochastic analysis of macrodispersion in a stratified aquifer. *Water Resources Research, 15(6)*, 1387-1397.

Gelhar, L. W., Welty, C., & Rehfeldt, K. R. (1992). A critical review of data on field-scale dispersion in aquifers. *Water Resour Res, 28(7)*, (pp. 1955-1974).

Gouze, P., Le Borgne, T., Leprovost, R., Lods, G., Poidras, T., & Pezard, P. (2008). Non-Fickian dispersion in porous media: 1. multiscale measurements using single-well injection withdrawal tracer tests. *Water Resour Res, 44(6)*.

Gylling, B., Moreno, L., & Neretnieks, I. (1999). The channel network model—A tool for transport simulations in fractured media. *Ground Water, 37(3)*, (pp. 367-375).

Haajizadeh, M., Fayers, F. J., Cockin, A. P., Roffey, M., & Bond, D. J. (1999). On the importance of dispersion and heterogeneity in the compositional simulation of miscible gas processes. *In SPE Asia Pacific Improved Oil Recovery Conference.* Kuala Lumpur, Malaysia: Society of Petroleum Engineers.

Haggerty, R., & Gorelick, S. M. (1995). Multiple-rate mass transfer for modeling diffusion and surface reactions in media with pore-scale heterogeneity. *Water Resources Research, 31(10)*, 2383-2400.

Hassan, A. E., & Mohamed, M. M. (2003). On using particle tracking methods to simulate transport in single-continuum and dual continua porous media. *J Hydrol, 275(3)*, (pp. 242-260).

Hoffman, F., Ronen, D., & Pearl, Z. (1996). Evaluation of flow characteristics of a sand column using magnetic resonance imaging. *J Contam Hydrol, 22(1)*, 95-107.

Hong, S. (2010). *Multivariate analysis of diverse data for improved geostatistical reservoir modeling.* Ph.D. Thesis, University of Alberta, Edmonton, Canada.

Hoteit, H., Mose, R., Younes, A., Lehmann, F., & Ackerer, P. (2002). Three-dimensional modeling of mass transfer in porous media using the mixed hybrid finite elements and the random-walk methods. *Math Geol, 34(4)*, 435-456.

Itô, K. (1951). *On stochastic differential equations* (Vol. 4). Rhode Island, Rhode Island: Mem. Am. Math Soc.

Jha, R. K., Bryant, S., & Lake, L. W. (2011). Effect of diffusion on dispersion. *SPE J, 16(1)*, (pp. 65-77).

Jha, R. K., John, A., Bryant, S. L., & Lake, L. W. (2009). Flow reversal and mixing. *SPE J, 14(1)*, (pp. 41-49).

John, A. K. (2008). *Dispersion in Large Scale Permeable Media (Dissertation).* University of Texas at Austin.

John, A. K., Lake, L. W., Bryant, S., & Jennings, J. W. (2010). Investigation of mixing in field-scale miscible displacements using particle-tracking simulations of tracer floods with flow reversal. *SPE J, 15(3)*, (pp. 598-609).

Johnson, E. F., Bossler , D. P., & Naumann, V. O. (1959). Calculation of relative permeability from displacement experiments. *SPE, Vol. 216*, 370-372.

Journel, A. G., & Huijbregts, C. J. (1978). *Mining geostatistics.* London: Academic press.

Käss, W. (1998). *Tracing Technique in Geohydrology.* Rotterdam, The Netherlands: A.A. Balkema.

Kenkre, V. M., Montroll, E. W., & Shlesinger, M. F. (1973). Generalized master equations for continuous-time random walks. *ournal of Statistical Physics, 9(1)*, 45-50.

Kinzelbach, W. (1986). *Groundwater modelling: an introduction with sample programs in BASIC* (Vol. 25). New York: Elsevier.

Kinzelbach, W., & Uffink, G. (1991). The random walk method and extensions in groundwater modelling. In J. Bear, & M. Y. Corapcioglu, *Transport*

Processes in Porous Media (pp. 761-787). The Netherlands: Kluwer Academic Publishers.

Kitanidis, P. K. (1988). Prediction by the method of moments of transport in a heterogeneous formation. *Journal of Hydrology, 102(1)*, 453-473.

Kitanidis, P. K. (1988). Prediction by the method of moments of transport in a heterogeneous formation. *Journal of Hydrology, 102(1)*, 453-473.

Kitanidis, P. K. (1992). Analysis of macrodispersion through volume-averaging: Moment equations. *Stochastic Hydrology and Hydraulics, 6(1)*, 5-25.

Kleinhans, D., & Friedrich, R. (2007). Continuous-time random walks: Simulation of continuous trajectories. *Physical Review E, 76, 061102/1–6.*

Kolbjørnsen, O., & Abrahamsen, P. (2005). Theory of the cloud transform for applications. *Geostatistics Banff 2004*, 45-54.

Kreft, A., & Zuber, A. (1978). On the physical meaning of the dispersion equation and its solutions for different initial and boundary conditions. *Chemical Engineering Science*(33(11)), 1471-1480.

Kreft, A., & Zuber, A. (1978). On the physical meaning of the dispersion equation and its solutions for different initial and boundary conditions. *Chemical Engineering Science, 33(11)*, (pp. 1471-1480).

LaBolle, E. M., Fogg, G. E., & Tompson, A. F. (1996). Random-walk simulation of transport in heterogeneous porous media: Local mass-conservation problem and implementation methods. *Water Resour Res, 32(3)*, (pp. 583-593).

Lake, L. W. (1989). *Enhanced oil recovery.* New Jersey: Prentice Hall.

Lake, L. W., & Srinivasan, S. (2004). Statistical scale-up of reservoir properties: Concepts and applications. *J Pet Sci Eng, 44(1)*, (pp. 27-39).

Lantz, R. B. (1971). Quantitative evaluation of numerical diffusion (truncation error). *Society of Petroleum Engineers Journal, 11(03)*, (pp. 315-320).

Le Borgne, T., & Gouze, P. (2008). Non-Fickian dispersion in porous media: 2. Model validation from measurements at different scales. *Water Resour Res, 44(6)*.

Leibundgut, C., Maloszewski, P., & Külls, C. (2011). *Tracers in hydrology.* Chichester, U. K: Wiley-Blackwell.

Leij, F. J., Toride, N., Field, M. S., & Sciortino, A. (2012). Solute transport in dual-permeability porous media. *Water Resources Research, 48(4)*.

Leung, J. Y., & Srinivasan, S. (2011). Analysis of uncertainty introduced by scaleup of reservoir attributes and flow response in heterogeneous reservoirs. *SPE J, 16(3)*, (pp. 713-724).

Leung, J. Y., & Srinivasan, S. (2012). Scale-up of mass transfer and recovery performance in heterogeneous reservoirs. *J Pet Sci Eng, (86-87)*, (pp. 71-86).

Leung, J. Y., & Srinivasan, S. (2016). Effects of reservoir heterogeneity on scaling of effective mass transfer coefficient for solute transport. *J Contam Hydrol, 192*, (pp.181-193).

Levy, M., & Berkowitz, B. (2003). Measurement and analysis of non-fickian dispersion in heterogeneous porous media. *J Contam Hydrol, 64(3)*, (pp. 203-226).

Li, L., Zhou, H., & Gómez-Hernández, J. J. (2011). A comparative study of three-dimensional hydraulic conductivity upscaling at the macro-dispersion experiment (MADE) site, Columbus Air Force Base, Mississippi (USA). *Journal of Hydrology, 404(3)*, (pp. 278-293).

Li, L., Zhou, H., & Gómez-Hernández, J. J. (2011). A comparative study of three-dimensional hydraulic conductivity upscaling at the macro-dispersion experiment (MADE) site, Columbus Air Force Base, Mississippi (USA). *J Hydrol, 404(3)*, (pp. 278-293).

Li, X., Koike, T., & Pathmathevan, M. (2004). A very fast simulated re-annealing (VFSA) approach for land data assimilation. *Comput Geosci, 30(3)*, (pp. 239-248).

Lichtner, P. C., & Kang, Q. (2007). Upscaling pore-scale reactive transport equations using a multiscale continuum formulation. *Water Resour. Res, 43*, W12S15.

Lichtner, P. C., Kelkar, S., & Robinson, B. (2002). New form of dispersion tensor for axisymmetric porous media with implementation in particle tracking. *Water Resources Research, 38(8)*.

Mahadevan, J., Lake, L. W., & Johns, R. T. (2003). Estimation of true dispersivity in field-scale permeable media. *SPE J, 8(3)*, (pp. 272-279).

Margolin, G., Dentz, M., & Berkowitz, B. (2003). Continuous time random walk and multirate mass transfer modeling of sorption. *Chemical physics, 295(1)*, (pp. 71-80).

Metzler, R., & Klafter, J. (2000). The random walk's guide to anomalous diffusion: a fractional dynamics approach. *Physics Reports, 339*, 1–77.

Nash, J., & Sutcliffe, J. V. (1970). River flow forecasting through conceptual models part I—A discussion of principles. *Journal of hydrology, 10(3)*, (pp. 282-290).

Neretnieks, I., Eriksen, T., & Tähtinen, P. (1982). Tracer movement in a single fissure in granitic rock: Some experimental results and their interpretation. *Water resources research, 18(4)*, 849-858.

Neuman, S. P. (1994). Generalized scaling of permeabilities: Validation and effect of support scale. *Geophysical Research Letters, 21(5)*, (pp. 349-352).

Neuman, S. P., & Tartakovsky, D. M. (2009). Perspective on theories of non-Fickian transport in heterogeneous media. *Advances in Water Resources, 32(5)*, 670-680.

Neuman, S. P., & Zhang, Y. K. (1990). A quasi-linear theory of non-Fickian and Fickian subsurface dispersion: 1. Theoretical analysis with application to isotropic media. *Water Resources Research, 26(5)*, 887-902.

Neuman, S. P., Winter, C. L., & Newman, C. M. (1987). Stochastic theory of field-scale Fickian dispersion in anisotropic porous media. *Water Resources Research, 23(3)*, 453-466.

Oswald, S., Kinzelbach, W., Greiner, A., & Brix, G. (1997). Observation of flow and transport processes in artificial porous media via magnetic resonance imaging in three dimensions. *Geoderma, 80(3)*, 417-429.

Parker, J. C. (1984). Analysis of solute transport in column tracer studies. *Soil Science Society of America Journal*(48(4)), 719-724.

Parker, J. C., & Genuchten, M. T. (1984). Flux-averaged and volume-averaged concentrations in continuum approaches to solute transport. *Water Resources Research*(20(7)), 866-872.

Pedretti, D., & Fernàndez-Garcia, D. (2013). An automatic locally-adaptive method to estimate heavily-tailed breakthrough curves from particle distributions. *Advances in Water Resources, 59*, 52-65.

Pedretti, D., Fernàndez-Garcia, D., Sanchez-Vila, X., Bolster, D., & Benson, D. A. (2014). Apparent directional mass-transfer capacity coefficients in three-dimensional anisotropic heterogeneous aquifers under radial convergent transport. *Water Resour Res, 50(2)*, (pp. 1205-1224).

Perkins, T. K., & Johnston, O. C. (1963). A review of diffusion and dispersion in porous media. *SPE J, 3(01)*, (pp. 70-84).

Pickens, J. F., & Grisak, G. E. (1981a). Scale-dependent dispersion in a stratified granular aquifer. *Water Resources Research, 17(4)*, 1191-1211.

Pickens, J. F., & Grisak, G. E. (1981b). Modeling of scale-dependent dispersion in hydrogeologic systems. *Water Resources Research, 17(6)*, 1701-1711.

Pickup, G. E., & Stephen, K. D. (2000). An assessment of steady-state scale-up for small-scale geological models. *Pet Geosci, 6 (3)*, 203-210.

Pickup, G. E., Stephen, K. D., Ma, J., Zhang, P., & Clark, J. D. (2005). Multi-stage upscaling: Selection of suitable methods. *Transport Porous Med, 58 (1-2)*, 191-216.

Pulloor Kuttanikkad, S. (2009). *Pore-scale Direct Numerical Simulation of Flow and Transport in Porous Media (Dissertation).* Heidelberg University, Germany.

Pyrcz, M. J., & Deutsch, C. V. (2014). *Geostatistical reservoir modeling.* New York: Oxford university press.

Riva, M., Guadagnini, A., Fernandez-Garcia, D., Sanchez-Vila, X., & Ptak, T. (2008). Relative importance of geostatistical and transport models in describing heavily tailed breakthrough curves at the Lauswiesen site. *J Contam Hydrol, 101(1)*, (pp. 1-13).

Rubin, Y. (2003). *Applied stochastic hydrogeology.* Oxford University Press, Oxford: UK.

Rubin, Y., Sun, A., Maxwell, R., & Bellin, A. (1999). The concept of block-effective macrodispersivity and a unified approach for grid-scale-and plume-scale-dependent transport. *Journal of Fluid Mechanics, 395*, 161-180.

Saad, N., Cullick, A. S., & Honarpour, M. M. (1995). Effective relative permeability in scale-up and simulation. *In Low Permeability Reservoirs Symposium* (pp. 451-464). Denver, Colorado: Society of Petroleum Engineers.

Saaltink, M. W., Ayora, C., & Carrera, J. (1998). A mathematical formulation for reactive transport that eliminates mineral concentrations. *Water Resour. Res, 34 (7)*, 1649–1657.

Salamon, P., Fernàndez-Garcia, D., & Gómez-Hernández, J. J. (2006). A review and numerical assessment of the random walk particle tracking method. *Journal of contaminant hydrology, 87(3)*, (pp. 277-305).

Salamon, P., Fernàndez-Garcia, D., & Gómez-Hernández, J. J. (2006a). A review and numerical assessment of the random walk particle tracking method. *Journal of contaminant hydrology, 87(3)*, (pp. 277-305).

Salamon, P., Fernàndez-Garcia, D., & Gómez-Hernández, J. J. (2006b). Modeling mass transfer processes using random walk particle tracking. *Water Resour Res, 42(11)*.

Salamon, P., Fernandez-Garcia, D., & Gómez-Hernández, J. J. (2007). Modeling tracer transport at the MADE site: the importance of heterogeneity. *Water resources research, 43(8)*.

Scheidegger, A. E. (1959). An evaluation of the accuracy of the diffusivity equation for describing miscible displacement in porous media. *Proc. Theory Fluid Flow Porous Media Conf*, (pp. 101-116).

Schlumberger Information Solutions. (2011). *Eclipse reservoir simulator:Reference manual and technical description.*

Schulze-Makuch, D., & Cherkauer, D. S. (1998). Variations in hydraulic conductivity with scale of measurement during aquifer tests in heterogeneous, porous carbonate rocks. *Hydrogeology Journal, 6(2)*, (pp. 204-215).

Schulze-Makuch, D., Carlson, D. A., Cherkauer, D. S., & Malik, P. (1999). Scale dependency of hydraulic conductivity in heterogeneous media. *Ground Water, 37(6)*, (pp. 904-919).

Simonoff, J. S. (1995). A simple, automatic and adaptive bivariate density estimator based on conditional densities. *Statistics and Computing, 5 (3)*, 245-252.

Srinivasan, G., Tartakovsky, D. M., Dentz, M., Viswanathan, H., Berkowitz, B., & Robinson, B. A. (2010). Random walk particle tracking simulations of non-Fickian transport in heterogeneous media. *Journal of Computational Physics, 229(11)*, (pp. 4304-4314).

Taylor, G. (1953). Dispersion of soluble matter in solvent flowing slowly through a tube. *In Proceedings of the Royal Society of London A: Mathematical, Physical and Engineering Sciences*, (pp. 186-203).

Tompson, A. F., & Gelhar, L. W. (1990). Numerical simulation of solute transport in three-dimensional, randomly heterogeneous porous media. *Water Resour Res, 26(10)*, (pp. 2541-2562).

Toride, N., Leij, F. J., & Genuchten, M. T. (1993). A comprehensive set of analytical solutions for nonequilibrium solute transport with first-order decay and zero-order production. *Water Resources Research, 29 (7)*, 2167-2182.

Tyagi, M., Jenny, P., & Tchelepi, H. A. (2008). A Lagrangian, stochastic modeling framework for multi-phase flow in porous media. *J Comput Phys, 227(13)*, 6696-6714.

Vishal, V., & Leung, J. Y. (2017). Statistical Scale-Up of Dispersive Transport in Heterogeneous Reservoir. *In Geostatistics Valencia 2016*, (pp. 733-743). Springer International Publishing.

Vishal, V., & Leung, J. Y. (2015). Modeling impacts of subscale heterogeneities on dispersive solute transport in subsurface systems. *Journal of contaminant hydrology, 182*, (pp. 63-77).

Vishal, V., & Leung, J. Y. (2017). Statistical scale-up of dispersive transport in heterogeneous reservoir. In *In Geostatistics Valencia 2016* (pp. 733-743). Springer International Publishing.

Wang, J., & Kitanidis, P. K. (1999). Analysis of macrodispersion through volume averaging: comparison with stochastic theory. *Environmental Research and Risk Assessment, 13(1-2)*, 66-84.

Wang, K., Killough, J. E., & Sepehrnoori, K. (2009). A new upscaling method of relative permeability curves for reservoir simulation. *SPE Annual Technical Conference and Exhibition.* Orleans, Louisiana: Society of Petroleum Engineers.

Zheng, C., & Bennett, G. D. (2002). *Applied contaminant transport modeling* (Vol. 2). New York: Wiley-Interscience.